Office of Energy Efficiency & Renewable Energy
Award #: DE-EE0008476

FINAL TECHNICAL/SCIENTIFIC REPORT

HYBRID HEAVY DUTY DIESEL POWERTRAIN FOR OFF-ROAD APPLICATIONS

PI: Dr. Robert McDavid

Recipient Organization: Caterpillar Inc.

Project/Grant Period: 01/01/2019 –9/30/2022
Reporting Period End Date: 09/30/2022
Submission Date: 01/28/2023

Table of Contents

Executive Summary

In this program, a heavy-duty hybrid powersystem, consisting of a 30% downsized diesel engine and a front-end accessory drive (FEAD) incorporating a high-speed flywheel (HSFW) energy storage system, a mechanical-drive turbocharger (SuperTurbo), and motor-generator units (MGU) was developed and demonstrated. The high efficiency core 13L engine coupled with the hybrid elements was physically validated across various off-road machine and transient work cycles with the ultimate goal of demonstrating 17% efficiency improvement with equivalent transient response as the 18L diesel engine this concept powersystem would replace. The project culminated in a physical demonstration of the high-efficiency powersystem in a high-capability test cell with the engine, all the hybrid devices, controls, and required performance and emissions measurements.

Table 1 summarizes the efficiency contributions from key hybrid system components and subsystems against various transient cycles. As a reminder the ranges show in the table are reflective of the three different machine applications examined. Additionally, for some subsystems, only simulation results are shown – the reduced cooling system parasitic was out-of-scope for the program, and the other two items were not physically validated due to time and resources constraints. However, in each of these cases simulations that were calibrated against available physical validation data were used.

Table 1: Final quantification of high-level efficiency contributions over the baseline 18L engine powersystem

Duty Cycle	Test or Final Validation Result	Sim. Prediction	Component
Machine Cycles	**10.3 – 13.8%**	9.0-12.6%	13L Concept engine
		0.3-1.1%	SuperTurbo Turbo-compounding
		0.5-2.0%	Thermal Barrier Coatings (TBC)
NRTC Cycles	**11.8 -16.1%**	12.4-15.9%	All Engine-Only Components*
Machine & NRTC Cycles	Assist Only Mode: **(-2.4) – (-0.7)%** With Regeneration: **0.0% – 3.0% ****	0.5-1.9%	High-Speed Flywheel (HSFW) & 48V MGU
Machine Cycles	**0.6% – 3.5% ****	0.6-3.5%	Start/stop implementation
Machine Cycles	**0% ****	0%	Advanced Engine Controls
Machine Cycles	**2.0% – 3.0% ****	2.0-3.0%	Reduced Cooling Parasitic
Machine & NRTC Cycles	***Final Possible Range: 10.5 – 25.6%*** ***Midpoint : 17.9%***	*13.5 – 24.1%*	***Program Total***

***Includes 13L Concept Engine, SuperTurbo, and TBC**

****Simulation Only and Not Tested in Final Validation**

Based on the combination of physical validation and rigorous system simulation, the following program conclusions may be drawn:

- The developed hybrid H2D2 powersystem demonstrated a range of efficiency improvement of 10.5 - 25.6%, with a midpoint of 17.9%
  - This result met the program goal of 17%±2 efficiency improvement.
- Transient load response on the order of ~1-1.5 second response times from 800 - 1800rpm was validated.
- The HSFW system was validated to achieve peak assisting of 110kW at 12,000 Nm/sec ramp rates.
- The powersystem was validated to be capable of meeting U.S. EPA Tier 4 Final off-road emissions through transient NRTC testing
- As required for Go/No-Go Milestone #2, the durability of the concept 13L engine was validated through structural and thermofluid simulations to be acceptable for continuous operation in the 30% downsized applications.

- A Total Cost of Ownership (TCO) analysis and found that the core 13L engine would pay back immediately.
    - Adoption of start/stop would pay back in less than one year, and
        - The full hybrid system payback was three years.

Section I – Accomplishments

1. Introduction

Driven by the need for sustainability and economic value, the heavy-duty off-road industry greatly values R&D towards increases in fuel efficiency. Total cost of ownership (TCO) is a primary metric for heavy-duty products, and the off-road sector is no exception. Fuel consumption can be a large factor and even the dominant factor when calculating the TCO for a given off-road product. If significant enough in magnitude, reductions in fuel consumption can therefore justify financial investment and acceptable payback periods, if significant enough in magnitude. Sustainability may also be a stronger driver for reduced fuel consumption, and efficiency improvements at the off-road machine/product level may be required to meet site-level metrics, such as allowable greenhouse gas (GHG) emissions. Caterpillar has a long history of addressing efficiency and fuel consumption with a first level of powertrain and machine technologies, centered on optimizing and right-sizing the system. Examples of this are the hydraulic-hybrid excavators, which were introduced in 2012[1], and the subsequent electric-drive dozers[2,3] and large wheel loaders[4].

Continuing to be motivated by these economic and sustainability forces, the present Hybrid Heavy Duty Diesel (H2D2) project aimed to research and develop additional and differentiated technologies applicable for off-road powersystems which could make a significant efficiency impact. The performance targets for this project were:

- 17 (+/-2) % more fuel efficient than current Tier 4 diesel engine
- Equivalent transient response vs. baseline diesel engine
- Tier 4-Final exhaust emissions levels

If these performance targets can be achieved, the proposed improvements applied to Caterpillar's off-road product range would save more than twenty-five million barrels of oil over ten years, contributing to the critical sustainability and TCO improvements required.

The result of this R&D effort was the design of a high-efficiency powersystem with a 13L concept engine – downsized from 18L – for use in off-road machine applications. The 18L to 13L downsizing was selected due to a wide application opportunity and for understanding of how hybridization may help with this difficult ~30% downsizing magnitude. The powersystem had hybrid elements and a front-end accessory drive (FEAD) that incorporated:

- High-Speed Flywheel (HSFW)
- Mechanical-drive Turbocharger (SuperTurbo)
- Motor-Generator Unit (MGU)

A unique aspect of off-road applications and this project was the concept of a powersystem as opposed to a powertrain. Figure 1 attempts to draw the boundary diagram demarking the difference between a powertrain and a powersystem. A powersystem is unique because it delivers power to some boundary condition, like the flywheel-transmission interface, which is not the final destination for useful

[1] Cat® 336E H Hybrid Excavator Press Release October 2012, https://www.cat.com/en_US/news/machine-press-releases/cat-sup-174-sup-336ehhydraulichybridexcavatordeliversnocompromis.html
[2] Cat® D7E Dozer Press Release November 2014, https://www.cat.com/en_US/news/machine-press-releases/updated-cat-d7e-featuresadvancedtechnologytoboostproductivityand.html
[3] Cat® D6 XE Electric Drive Dozer Press Release November 2018, https://www.cat.com/en_US/news/machine-press-releases/new-cat-d6-debuts-worlds-first-high-drive-electric-drive-dozer.html
[4] Cat® 988K XE Electric Drive Wheel Loader Press Release August 2017, https://www.cat.com/en_US/news/machine-press-releases/new-electric-drive-cat-988kxe-wheel-loader-offers.html

work. The hybrid elements of this program are contained within the powersystem boundary, while the resulting off-road machine performance is outside of the boundary. Therefore, the goal of the powersystem is to match the current machine performance with increased efficiency without knowledge or alteration to the upper machine system level.

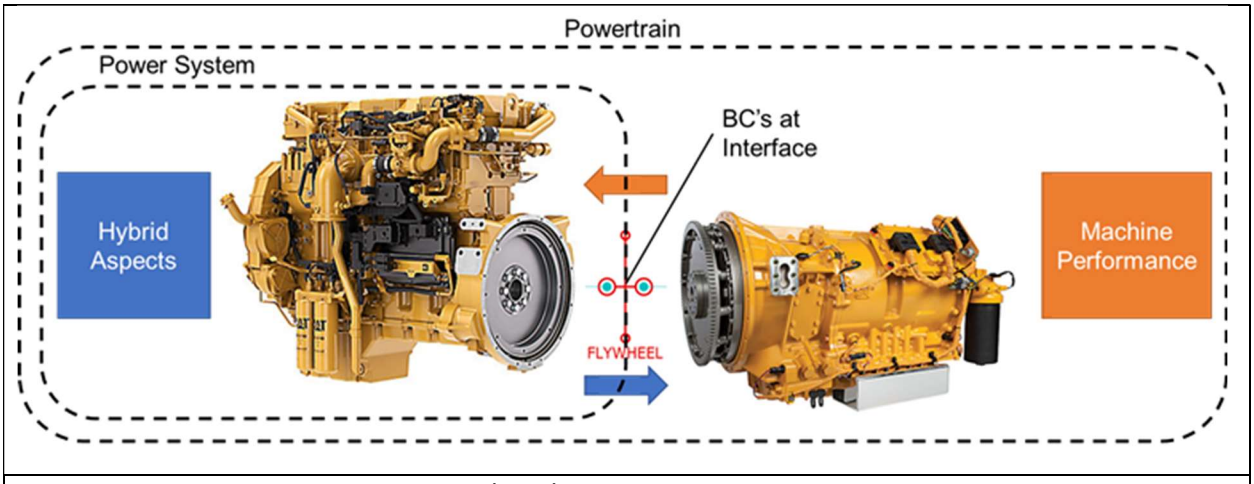

Figure 1: Boundary diagram powersystem vs Powertrain

The three key off-road machine application selected for this R&D project were the 988K large wheel loader (LWL), the 390F hydraulic excavator (HEX), and the 745 articulated truck (AT), Figure 2. These represent some of the major off-road construction machine types, each with different powertrains, uses, needs, and constraints. In Figure 2 the representative work cycle engine speed/ torque 2D histograms highlight where each of the three key machine applications operate. A common theme is one of high load and high power, which is not unexpected from heavy-duty equipment. The powertrains produce different operation histograms and only one application, the 745AT, has recoverable energy at the powersystem boundary. This regeneration opportunity stems from the existing engine compression release brake used to retard the truck. The data and transient work cycles behind these histograms were the target for the hybrid concept simulations and definition. These histograms do not include significant engine idle periods which do exist in real applications, and a separate start/stop analysis was conducted for this aspect. At present all three of the Tier 4 Final key off-road machines are powered by a Cat® C18 ACERT™ diesel engine. The developed hybrid powersystem will shift to the concept 13L engine, which represents a significant (and difficult) 30% increase in power density.

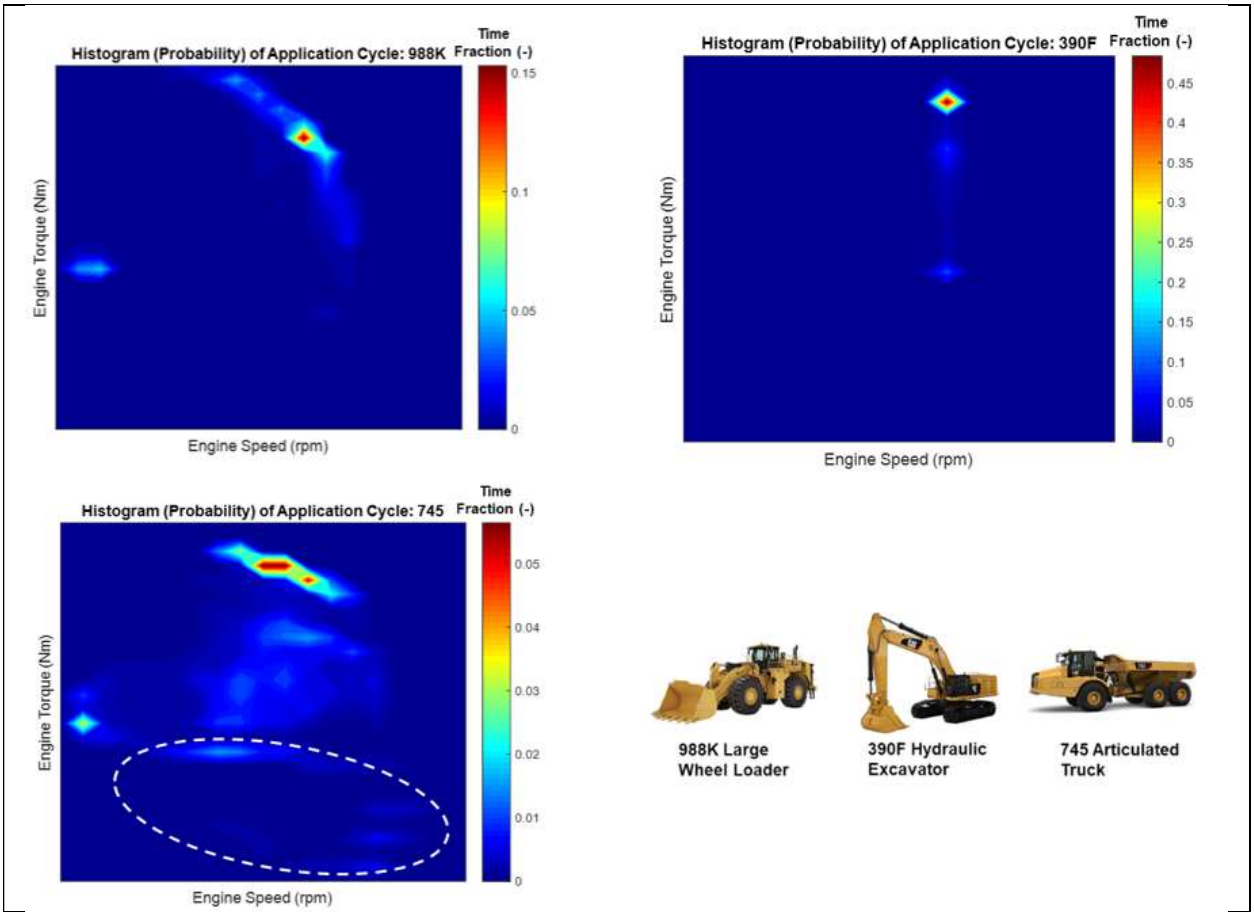

Figure 2: Key machine representative work cycle engine speed/torque 2D histograms showing where operation occurs. The white circle is where brake energy recovery is possible.

2. Summary of Milestones

Figure 3 summarizes how the program progressed through key milestones. Out of the 11 program milestones (of which the SOPO Milestones were a subset), 82% were either completed on time or early. Critically, the two key SOPO Go/No-Go milestones were completed on schedule (Table 2), and provided confidence in the overall program timeline.

However, as discussed in Section 3.4.4, there were significant prototype hardware failures which occurred during the physical validation stage of the program. While these failures were ultimately resolved, they resulted in a total of 117 calendar days of delay. Thus, a 3-month, no-cost extension was applied for and granted. This additional quarter was Q16 (see Figure 3), and therefore the final validation milestone (#11) was achieved a quarter late.

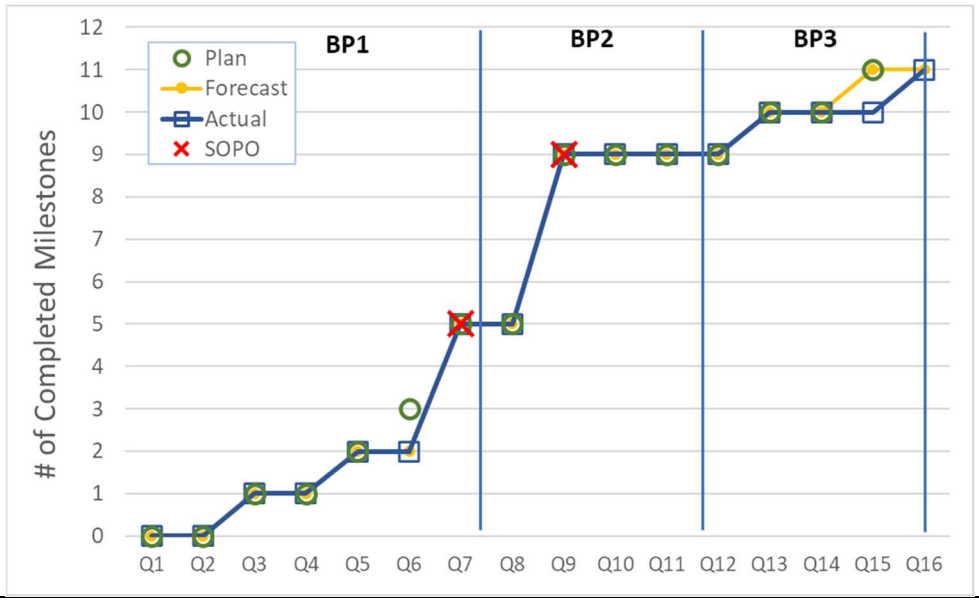

Figure 3: Final Milestone Progress Chart

Table 2: Go/No-Go Program Milestones Achieved

SOPO ID #	Item Title	Item Description	Completion Date	Status
GNG-1	**Go/No-Go #1 Decision Point**	IF 1D system level simulation validates that the target total fuel consumption reduction AND Tier IV Final emissions AND the powersystem can be packaged in to target off-road machines; THEN proceed to Task 3.	6/30/2020	Complete - Proposed "Go"
GNG-2	**Go/No-Go #2 Decision Point**	IF the structural, dynamics simulations show that the target 12,000 hour durability can be achieved AND the subsystems demonstrate required performance on bench tests; THEN proceed to ST-3.1	12/31/2020	Complete - Proposed "Go"

3. Technical Discussion

3.1. Concept Definition

3.1.1. Hybrid Concept Validation

SOPO ID #	Item Title	Item Description	Start Date	End Date	Status
Task 1.1.	**Hybrid Concept Validation**	Develop/refine 1D models to predict hybrid powersystem fuel consumption reduction against 3 off-road machine duty cycles.	6/1/2019	12/31/2019	100% Complete

DYNASTY™ H2D2 System Level Model Overview

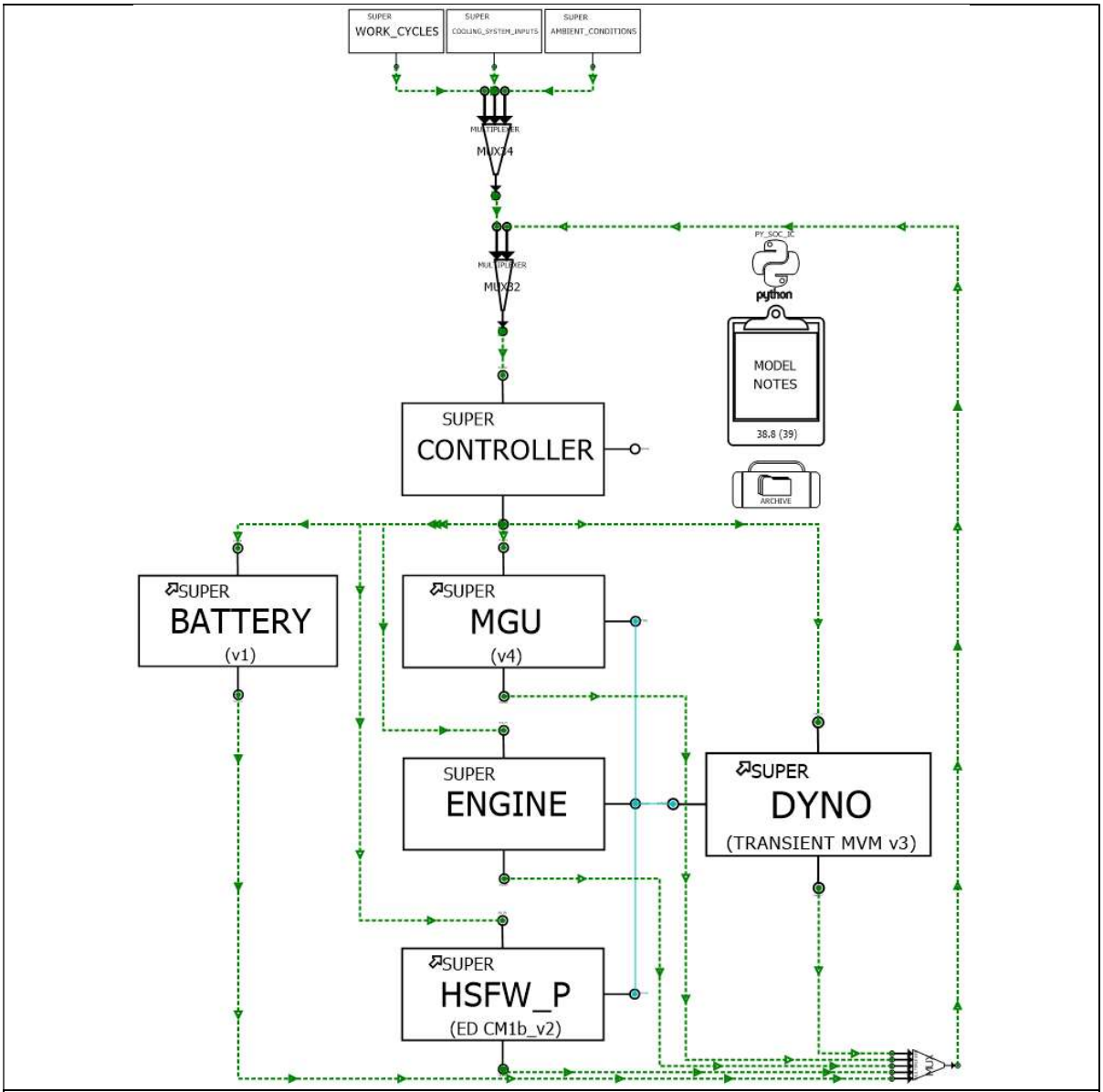

Figure 4: H2D2 System Level Model – Top Level View

Caterpillar has extensive experience in evaluating the efficiency and productivity benefits associated with various levels of hybridization. Due to the extremely wide range of off-road machine applications,

duty cycles and hardware configurations, 1D simulation tools are used extensively in the development process – from concept definition all the way to prototype and production performance validation. The H2D2 System Level Model (Figure 4) is one of the main performance assessment and development tools employed by the H2D2 team throughout the duration of the H2D2 project[5].

The H2D2 System Level Model has employed a Modular Model Architecture which enables the simulation of multiple powersystem hardware configurations with varying levels of fidelity. This architecture provided the necessary flexibility and robustness to meet the evolving project requirements using a single 1D simulation model. Some of the main model features are summarized below:

- Transient and Steady-State capability
- Capability to simulate a wide range of transient cycles - machine cycles, application-specific Non-Road Transient Cycles (NRTC), Constant Speed Load Acceptance (CSLA), Lug curve and user-defined cycles)
- Ability to simulate the C18 baseline powersystem
- Ability to simulate various 13L hardware configurations
  (H2D2 CVT SuperTurbo, H2D2 13L MGU SuperTurbo, 13L VGT)
- L4 (engine level) and L5 (powersystem level) controls fully integrated with the plant models and ability to use both compiled code and co-simulation for controls development

The H2D2 System Level Model includes the following major subsystems / Supercomponents:

❖ **Controller**

Figure 5 shows the Controller subsystem in more detail. This subsystem contains all the controllers used by the H2D2 System Level Model for performing transient simulations.

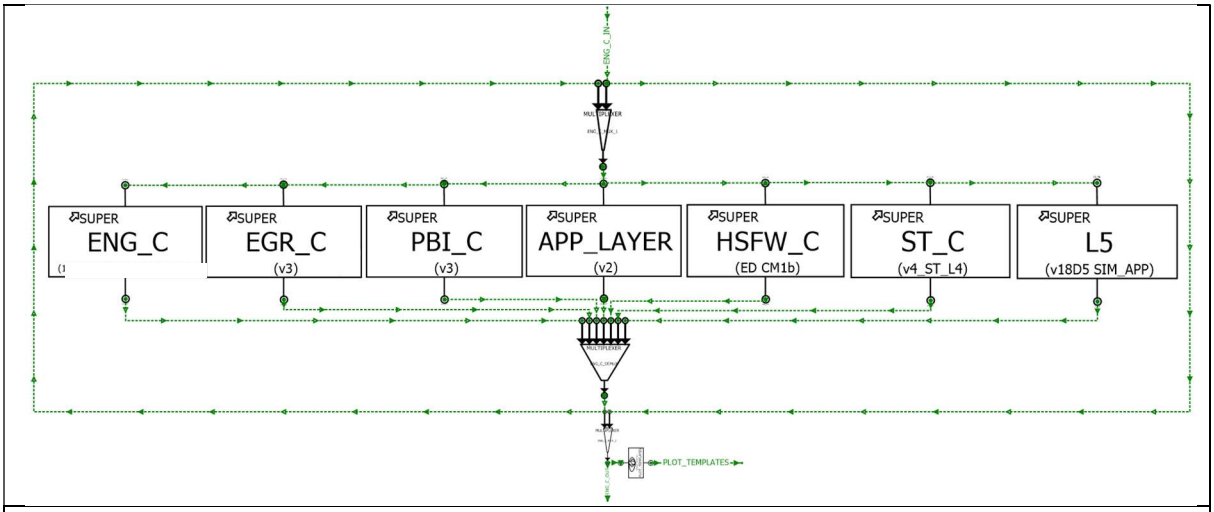

Figure 5: H2D2 System Level Model – CONTROLLER Supercomponent

- ENG_C – contains engine controllers for the various engine plant models, including 13L VGT, C18 and 13L H2D2 traditional controllers, as well as multiple versions of the H2D2 Advanced Controller software.

[5] Koci, C., Steffen, J., Kruiswyk, R., Guo, F. et al., "A Hybrid Heavy-Duty Diesel powersystem for Off-Road Applications - Concept Definition," SAE Technical Paper 2021-01-0449, 2021, https://doi.org/10.4271/2021-01-0449.

- EGR_C – contains EGR controller software for use in conjunction with the various traditional controllers. The H2D2 Advanced Controller has its own, EGR flow estimator-based controller built in.
- PBI_C – contains Physics-based Injector controller. This controller is only required in simulation and serves as an interface between the Engine controller and Engine plant subsystems.
- APP_LAYER – contains a simplified version of application layer software usually used for interfacing with machine-level L5 controllers. Although the H2D2 System Level Model is powersystem model and not Machine level model, some application layer controller functionality was still required and utilized for the transient simulations.
- HSFW_C – contains the L4 High-Speed Flywheel controller. This controller receives the feedback signals from the HSFW plant virtual sensors in order to estimate the maximum power available for charging and discharging and broadcasts those channels to the L5 controller.
- ST_C – contains the L4 SuperTurbo controller. Throughout the project, two distinctive versions of the L4 SuperTurbo controller were used:
    - Simplified DYNASTY controller

      This controller was used at the early stages of the project when the "production" L4 SuperTurbo controller was not available. A PID control logic was used in order to match the Desired SuperTurbo power requested by the L5 controller to the actual SuperTurbo shaft power measured in the DYNASTY model by adjusting the SuperTurbo CVT ratio.
    - SuperTurbo L4 controller

      This controller was provided by the SuperTurbo Technologies Inc. team in the form of compiled, "black-box" software for use in Simulation. This is the same L4 controller used on engine during the testing. Unlike the Simplified DYNASTY controller, the SuperTurbo L4 controller is targeting desired intake manifold absolute pressure (IMAP) instead of power with the desired IMAP command coming from the Advanced Controller Engine Software.
- L5 – contains the L5 Supervisory controller software. This controller is tasked with managing the power split between the Engine, HSFW and MGU while meeting the desired Cycle Power. In practice, the controller needs to generate Desired HSFW and MGU power requests and send them to the respective L4 controllers based on a number of factors, including HSFW and MGU L4 level power limits, Battery and HSFW State of Charge (SOC), Engine, HSFW and MGU operational state, etc. More details about the L5 controller can be found in the **3.2.4 Realtime Optimizer Control** section of this report.

❖ **Engine**

Figure 6 shows the Engine subsystem in more detail. It contains the Engine plant and all the additional engine-related subsystems.

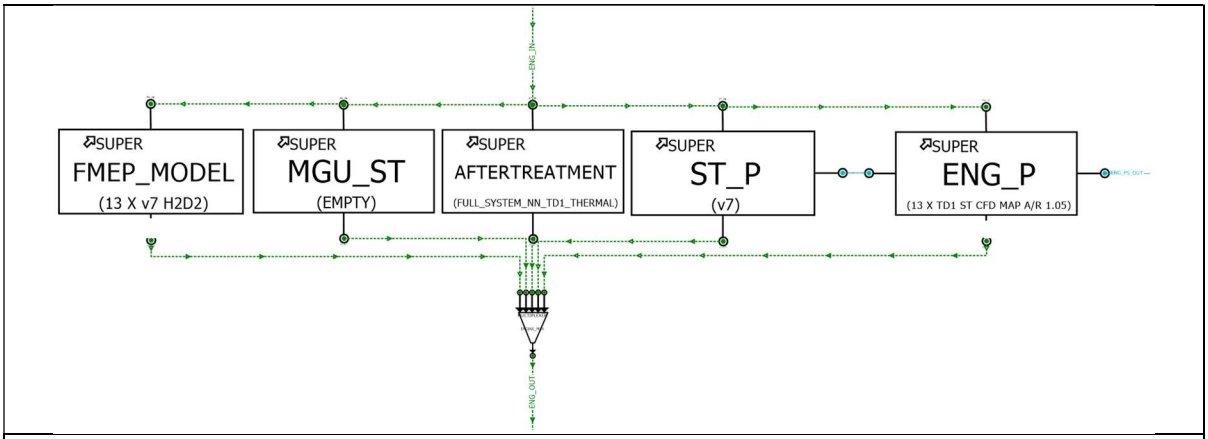

Figure 6: H2D2 System Level Model – ENGINE Supercomponent

- FMEP_MODEL – contains high-fidelity FMEP model. This model consists of several sub-models (Fuel System, Coolant Pump, Oil Pump, Valvetrain, Bearings and PRL) which calculate the different contributions to the engine FMEP based on a combination of predictive and test data-based approaches. The FMEP model uses a combination of engine geometry (number of cylinders, bore, stroke, connecting rod length, main and big end bearing geometry, number of bearings, etc.) and engine operational parameters (engine speed, cylinder pressure, fuel rail pressure, fuel mass flow Rate, etc.) in order provide more accurate FMEP predictions.
- MGU_ST – contains SuperTurbo MGU plant and controller models. This subsystem was utilized for the evaluation of some hybrid powersystem concepts which featured an electrical power "transmission" between the SuperTurbo and the engine crank. Please, refer to Figure 10, Concept 3a for a schematic of this concept).
- AFTERTREATMENT – contains neural-net based engine emissions and aftertreatment sub models. multiple versions of this subsystem were implemented, and they reflect various improvements enabled by test data availability.
- ST_P – contains the SuperTurbo plant model. It consists of engine crankshaft side / PTO gearbox, CVT / High Speed Traction Drive model and turbine shaft interface. The SuperTurbo plant model illustrated on Figure 7 was bult based on CVT, drivetrain and traction drive specification provided by SuperTurbo Technologies Inc.

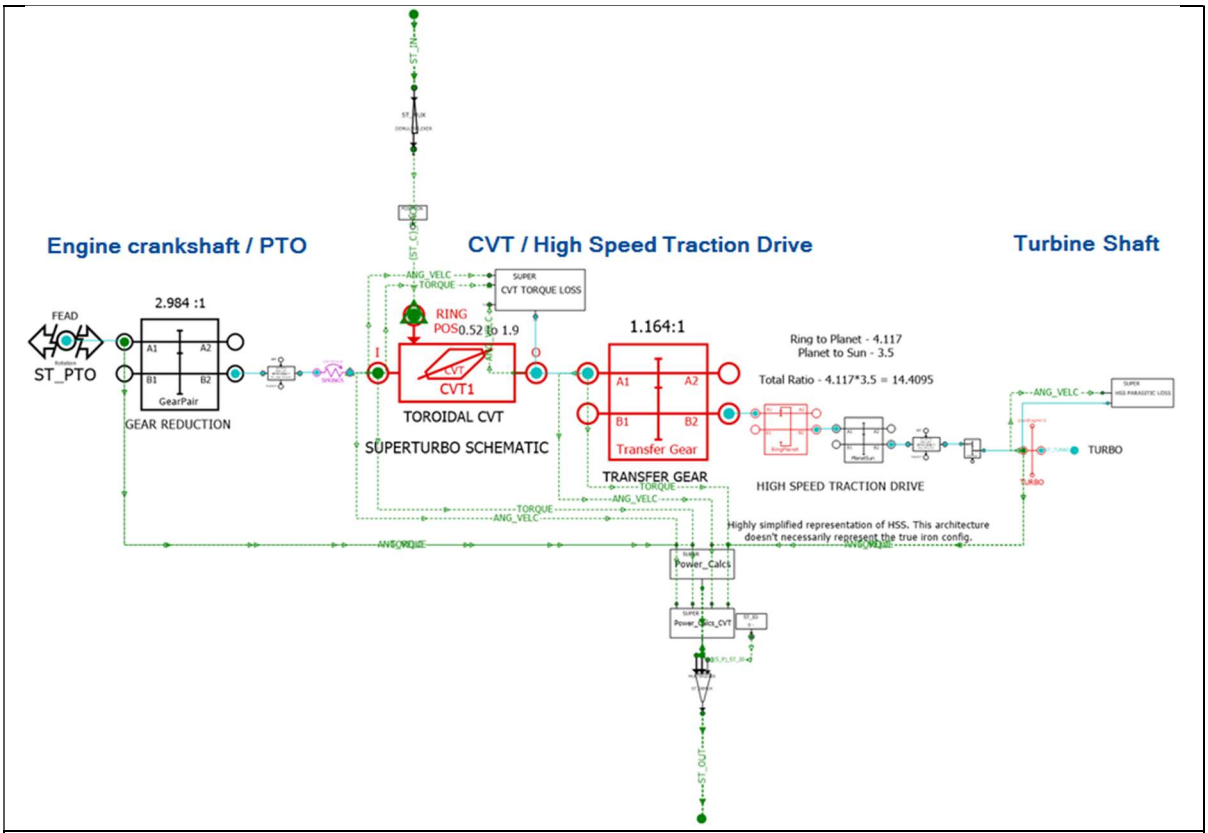

Figure 7: H2D2 System Level Model – SuperTurbo Plant Model

- ENG_P – contains the engine plant model. For the needs of this project, over 10 different engine plant models were implemented and utilized. Those models range from fast-running Mean Value Models (MVM) used for rapid controls development, to high-fidelity DYNASTY Engine models. The latter are able to accurately predict engine performance by employing full crank-angle resolved engine cycle simulation approach and utilize physics-based fuel injection, combustion, and emissions sub-models.

Figure 8 illustrates the final version of the H2D2 13L High-Fidelity Engine Plant Model used for validation against both steady-state and transient cycle test data. The model features high-fidelity air system geometry, including finely discretized exhaust manifold geometry, capable of capturing the pressure pulsation effects upstream of the turbine and EGR loop. This is critical for accurately predicting both the turbine performance and the EGR flow rate and enables the model to be used for SuperTurbo and EGR controller calibration. In addition, the engine plant model also features physics-based fuel injector and combustion sub-models, which are able to accurately predict engine performance without needing extensive test data in advance. As a result, the H2D2 13L High-Fidelity Engine Plant Model has been used as one of the main engine performance development tools from the very early stages of the project up until the final validation.

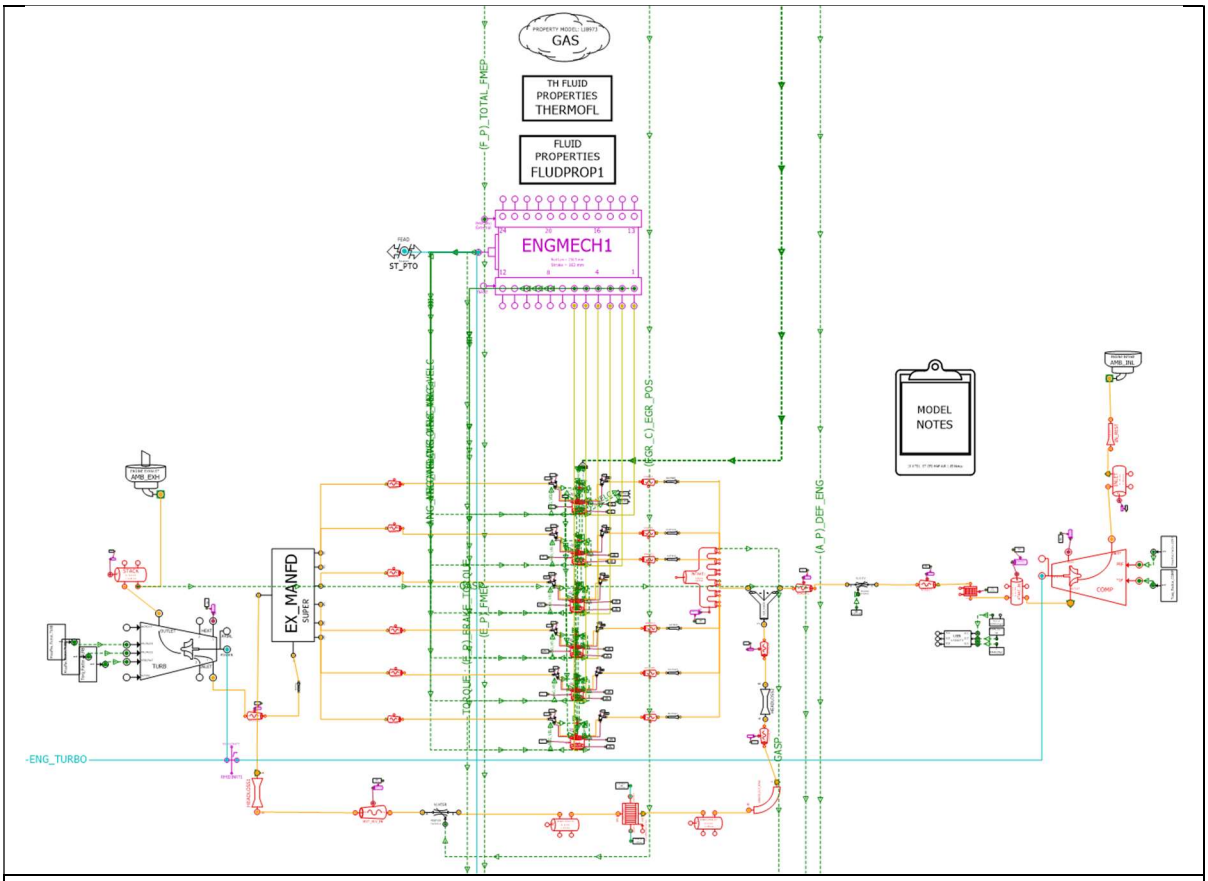

Figure 8: H2D2 System Level Model – H2D2 13L High-Fidelity Engine Plant Model

- HSFW_P – contains the High-Speed Flywheel plant model. The HSFW is one of the subsystems which changed significantly between the initial Hybrid Concepts (Figure 10, Concepts 1, 2 and 3) and the final two concepts (Figure 10, Concepts 2a and 3a) which were benchmarked against each other over all 19 Machine Application Cycles.

Figure 9 contains the schematics for the two different HSFW transmission concepts – mechanical CVT and e-CVT. The mechanical CVT option uses a planetary gear set coupled with a metal belt drive type variator to change the speed ratio between the engine crank and the High-Speed Flywheel (Figure 9, top). The electric drive CVT option an MGU connected to the engine and another MGU connected to the high-speed flywheel transfer power through a common DC bus. This concept is referred to as e-CVT (Figure 9, bottom)

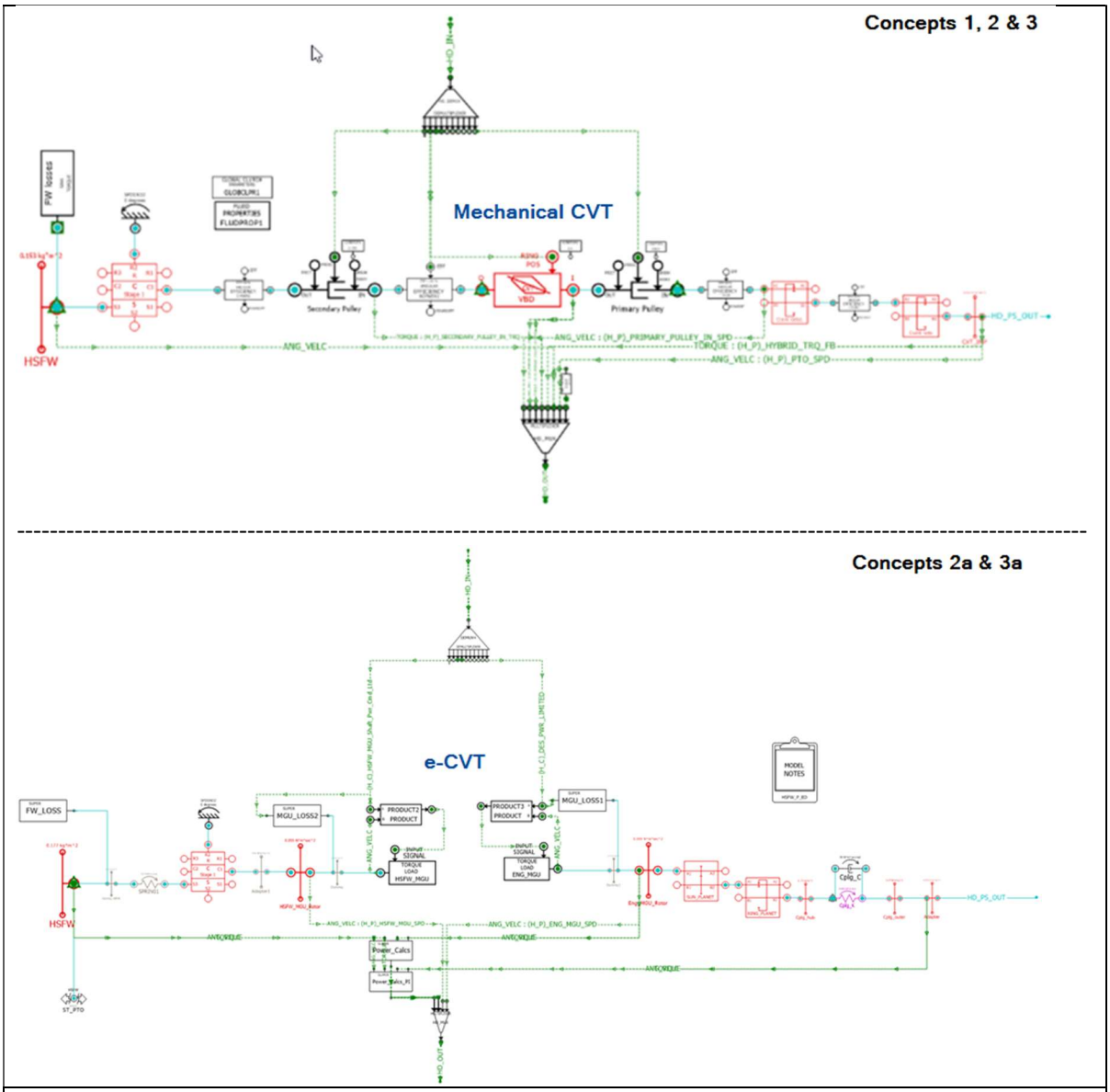

Figure 9: H2D2 System Level Model – High-Speed Flywheel Plant Model

Hybrid Powersystem Concept Evaluation

The availability of 3 unique Hybrid services (HSFW, MGU and SuperTurbo) all of which able to either assist the engine during transient events or recover otherwise wasted energy, enables multiple different arrangements to be made depending on how these devices are connected to each other and/or to the Engine. These arrangements, or concepts, can result in different overall powersystem performance and one of the main tasks for the H2D2 System Level Model was to evaluate the feasibility and performance implications of the different Hybrid powersystem concepts over the relevant Machine application cycles.

Figure 10 provides an overview of the Hybrid powersystem Concepts evaluated as part of this project, and additional discussion can also be referenced in a publication part way through the program.

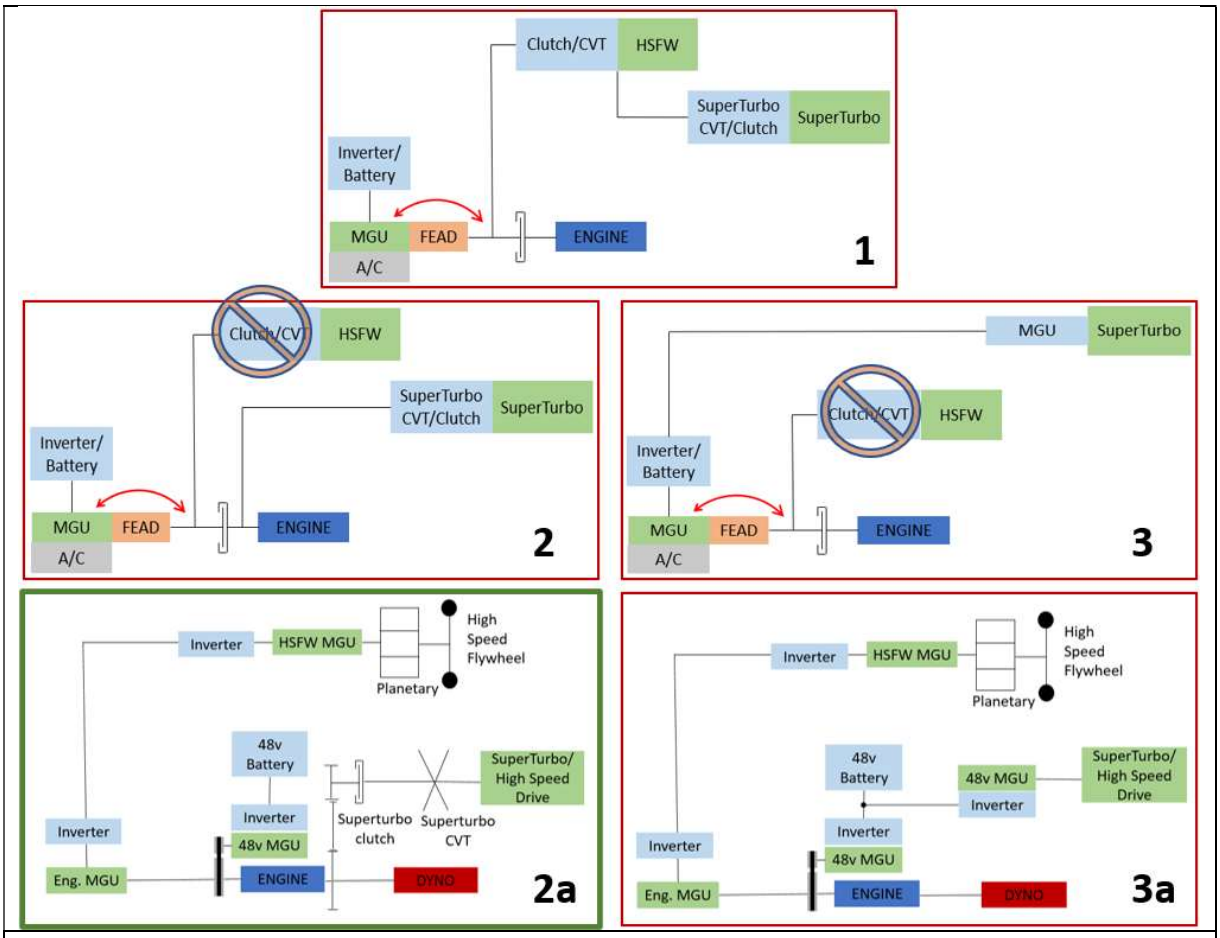

Figure 10: Hybrid Powersystem Concepts – Overview

❖ Concept 1

The main distinguishing feature of Concept 1 compared to all other concepts is the direct mechanical connection between the HSFW and the SuperTurbo via their respective CVTs. However, this concept was dismissed early in the development process for the following reasons:

- Unresolvable packaging design interference between the mechanical connection from the SuperTurbo to the HSFW and the core engine architecture (please, refer to the **3.2.1 Variable FEAD Design & Simulation** section of this report for more details)
- Smaller than required speed range coverage from the two CVT drives of the SuperTurbo and HSFW, such that the turbo speed range, HSFW speed range, and engine speed range cannot be fulfilled (please, refer to the **3.2.1 Variable FEAD Design & Simulation** section of this report for more details)
- Increased transmission power losses when turbo-compounding with the SuperTurbo, as power needs to flow through the SuperTurbo CVT drive system (70-80% efficient) and then through the HSFW CVT drive system (70-80%)
- Significantly increased HSFW and SuperTurbo controls complexity to track three (engine, HSFW, SuperTurbo) speed ranges simultaneously

❖ Concept 2

With Concept 2 the HSFW is connected directly to the engine crank via a mechanical CVT transmission and is completely independent of the SuperTurbo, which is also connected to the engine via a mechanical CVT transmission. Such arrangement enables more efficient turbo-compounding via the SuperTurbo and allows the L5 supervisory controller to choose optimal control strategy for each hybrid device without the additional constraints present with Concept 1.

❖ Concept 3

The difference between Concept 3 and Concept 2 is related to the way the SuperTurbo transfers power to and from the engine crank. The CVT from Concept 2 has been replaced with an electric drive (MGU + Inverter) which would enable the SuperTurbo to utilize the 48V battery for energy storage. As a result, the energy recovered by the SuperTurbo during turbo-compounding wouldn't need to be used immediately for assisting the engine, but the L5 supervisory controller can decide when to use the stored energy and in theory achieve better overall system efficiency. Another advantage of this concept is that when the SuperTurbo is requested to assist the engine during a transient event, the required power can be drawn from the battery instead of the engine crank, which in turn will result in higher engine brake power during the transient event.

The main purpose of the HSFW device is to directly assist the engine during transient events by transferring kinetic energy stored in the flywheel to the engine crank. When a CVT transmission is used to connect the HSFW and the engine crank, the rate of energy transfer (power) between the HSFW and the engine is proportional to the rate of CVT ratio change. If the ratio response of the HSFW CVT transmission is not fast enough, instead of assisting the engine, the HSFW operation can result in un-commanded loads on the engine crank during the transient event, especially in cases where the engine speed also increases fast during the transient event. During the performance evaluation of Concepts 2 and 3, the deficiencies described above were identified with the initial HSFW CVT transmission concept. As a result, the transient response and assist requirements of the powersystem could not be met due to the combination of the insufficient CVT ratio response rate, but also – due to the insufficient overall power capability of the CVT transmission.

This led to the exploration of alternative HSFW transmission systems, during which an electric drive (e-CVT) concept was selected as it demonstrated the best response rate of all the options

which were evaluated. This was enabled by complete decoupling of engine speed and flywheel speed. The ratio range constraint of other CVT transmission concepts was also eliminated as the two MGU units are capable of changing speed very rapidly and independently from the engine speed. The e-CVT HSFW transmission replaced the mechanical CVT option in Concepts 2 and 3, resulting in the creation of Concepts 2a and 3a (Figure 10).

❖ Concept 2a

In summary, Concept 2a incorporates:

- E-Drive HSFW connected directly to the engine crank
- 48V Battery and MGU connected directly to the engine crank
- SuperTurbo connected directly to the engine crank via a mechanical CVT transmission Due to packaging concerns and multiple other connections with the front of the engine, the SuperTurbo connection was moved to the rear PTO of the engine instead of the FEAD

❖ Concept 3a

In summary, Concept 3a incorporates:

- E-Drive HSFW connected directly to the engine crank
- 48V Battery and MGU connected directly to the engine crank
- SuperTurbo connected to the 48V Battery via an additional MGU

Concepts 2a and 3a were the final H2D2 concepts which were benchmarked against each other. In order to evaluate their performance for the three key machine applications (745 articulated truck (AT), 390F hydraulic excavator (HEX) and 988K large wheel loader (LWL)), a total of 19 representative work cycles were identified and made available for transient simulation in the H2D2 System Level Model. The total length of the down-selected cycles is over 5 hours real time. Each individual cycle is based on real-world data collected on different customer machines operating in the field. The off-highway / heavy-duty applications are much more diverse and even the same machine can be subjected to very different operating conditions depending on customer's site location, characteristics and productivity targets.

Figure 11 illustrates the performance differences between concepts 2a and 3a relative to the C18 baseline performance. All the results shown are H2D2 System Level Model predictions and the positive values indicate that Concepts 2a and 3a demonstrate better efficiency when compared to the C18 baseline.

When summarizing the results by application (top bar chart) it is evident that the 745 articulated truck (AT) application cycles (1-9 in Figure 11) are more favorable when it comes to efficiency improvement opportunities. Those cycles comprise of relatively steady-state operating conditions which enable good turbo-compounding gains. In addition, by using the MGU and to a lesser extent – the HSFW during portions of the cycles where retarding is required, additional energy can be recovered and stored in the battery instead of being transformed into heat and lost to the environment when using the engine compression release brake. This recovered and stored energy can be used later during the cycle to offset some of the engine fuel energy depending on the L5 supervisory logic.

The 390F hydraulic excavator (HEX) and 988K large wheel loader (LWL) cycles (10-19 in Figure 11) are much more transient by nature. They are characterized by frequent transitions in engine operating conditions from relatively low load to high/rated load (Figure 2) with almost no recoverable energy available at the powersystem boundary (Figure 1). This reduces the predicted

benefit not only because almost no energy can be recovered and stored in the battery during those cycles, but also because the HSFW, MGU and SuperTurbo need to assist the engine during a significantly increased number of transient events. Under those operating conditions the energy required to power the additional hybrid devices is drawn mainly from the engine crank, thereby reducing the efficiency improvement over the C18 baseline.

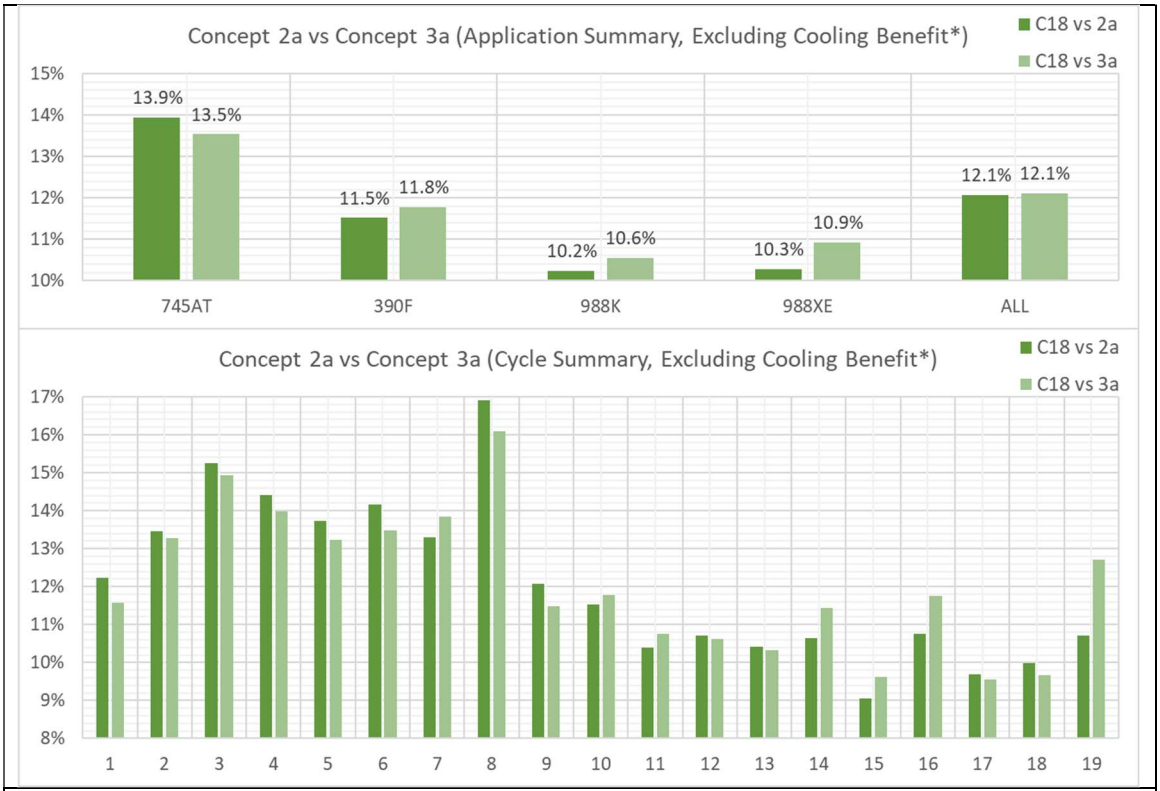

Figure 11: Hybrid powersystem Concepts – 2a vs 3a – Predicted BSFC Benefit vs C18 Baseline

When it comes to the relative performance of Concept 2a versus Concept 3a, the differences are very slim, irrespective of the application cycle. This indicates that both the mechanically driven SuperTurbo (Concept 2a) and the alternative electrically driven SuperTurbo (Concept 3a) options demonstrated very comparable efficiencies. In addition, the perceived advantage of Concept 3a to be able to store the recovered energy in the battery as opposed to using it immediately to offset engine fuel did not impact the efficiency improvement predictions with the exception of a few 988K large wheel loader (LWL) cycles (14, 16 and 19 in Figure 11).

Ultimately Concept 2a was selected over Concept 3a for the following reasons:

- Simpler design with more mature mechanical prototype experience by SuperTurbo
- Simple controls requirements with less 48V batter power management complexity
- Very similar cycle efficiencies between 2a and 3a that are within the range of uncertainty

All simulation results presented in this report from this point onwards will be using Concept 2a for the H2D2 powersystem hardware configuration unless otherwise specified.

In order to better illustrate the interactions between the hybrid devices and the engine, Figure 12 presents timeseries simulation results from the H2D2 System Level Model over 745 articulated truck (AT) application Cycle 5:

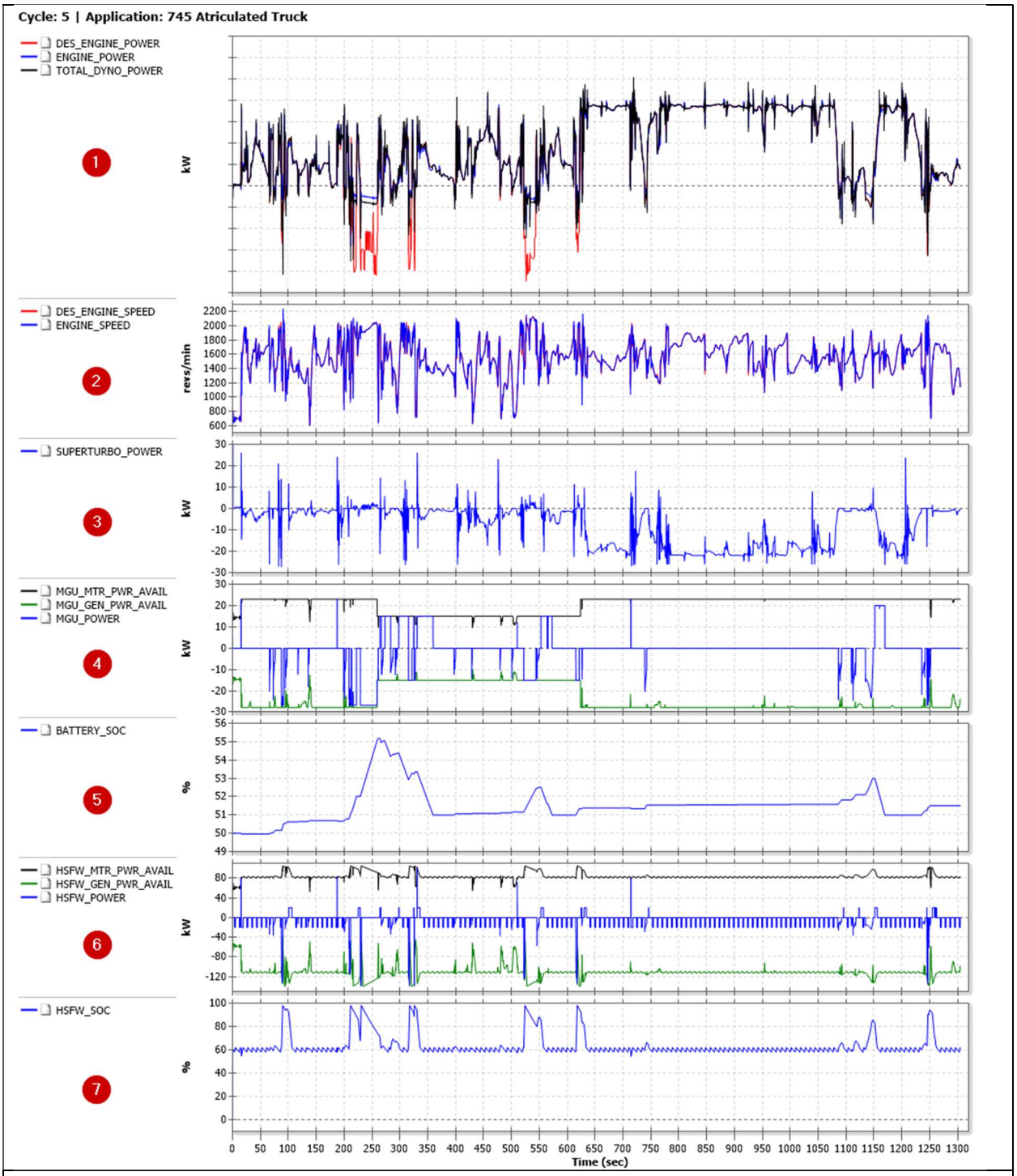

Figure 12: H2D2 System Level Model Results – Cycle: 5 | Application: 745 Articulated Truck
Hybrid Device Power Signs: Positive = Assist | Negative = Regen

Cycle 5 is based on real-world customer data with a length of just over 1300 seconds and demonstrates some typical articulated truck cycle features: relatively steady-state operating conditions (Figure 12, 625s-1025s) combined with portions where extra retarding power from the engine compression release brake equipped C18 is available for recovery (Figure 12, 200s-270s, 320s-350s, 530s-550s, 640s-650s).

The simulated 2a powersystem concept targets the same power/torque and engine speed as the compression release brake equipped C18 baseline (Figure 12, plots 1 and 2). Where the negative power of the C18 baseline (DES_ENGINE_POWER) is lower than the 13L engine motoring curve, additional energy can be recovered by the MGU and HSFW devices when they are switched into regen mode.

The SuperTurbo is tasked with assisting the engine during acceleration events by providing additional power to the turbo shaft (Figure 12, plot 3). This results in increased turbo speed, boost pressure and consecutively – AFR limit, allowing more fuel to be injected during the transient event. In addition, during prolonged operation at high load conditions (Figure 12, 625s-1025s), the SuperTurbo harvests the extra energy from the exhaust gasses which would have otherwise been lost due to wastegate operation during those operating conditions.

The MGU and the Battery are two of the devices in the powersystem which enable the recovery, storage and reuse of the recoverable energy available (Figure 12, plots 4 and 5). Since the Battery has much greater storage capacity than the HSFW, it stores most of the recoverable energy. It also enables the MGU to assist the engine when the L5 controller decides to convert some of the energy stored in the battery into MGU assist power, thus reducing the engine fueling. The MGU itself also has a secondary task of assisting the SuperTurbo during transient events. Since the power ratings of the MGU and SuperTurbo are well matched, when there is a case of simultaneous assist event from the SuperTurbo and the MGU, no additional power is drawn from the engine crank and the energy stored in the battery is used instead.

Since many off-road applications undergo heavy and frequent transient events, the maximum power rating of the MGU/Battery constrained by the 48V architecture (~30kW) is often not sufficient to assist the engine during a sudden load increase. On the other hand, achieving higher electrical power levels by using higher power MGU and more importantly – larger capacity battery with sufficiently high C-rating would pose a significant challenge on the powersystem approach from packaging and cost considerations. Under these circumstances the HSFW provides a good solution for off-road applications in combination with a 48V based MGU/Battery system.

The HSFW allows much higher assist and regen powers to be achieved compared to the 48V MGU. Even with the limited HSFW energy storage capacity compared to the battery, the HSFW is particularly suitable for transient assist events where the duration of those assist events is quite short, thus not requiring a lot of energy per assist event.

The HSFW operation is illustrated in Figure 12, plots 6 and 7. High power bursts can be observed during the frequent assist events throughout the cycle. In addition, the HSFW can also recover energy in addition to the MGU and store it as kinetic energy using the e-CVT transmission (Figure 10, Concept 2a). Once the HSFW has reached maximum state of charge (SOC), the HSFW Controller limits the available regen power.

The HSFW also has some distinguishing features when compared to the MGU/Battery combination. In Figure 12, plot 6 the reader can note that the maximum available assist and regen power (HSFW_MTR_PWR_AVAIL and HSFW_GEN_PWR_AVAIL) are a function of the HSFW SOC (Figure 12, plot 7). At higher HSFW SOC conditions the HSFW can reach higher assist and regen powers. In practice only the higher assist power can be realized as there is not much headroom for capturing extra energy using the HSFW when the HSFW SOC is almost at its maximum. Another HSFW specific feature is the fact that the HSFW loses charge over time due to friction losses in the flywheel mechanism. This necessitates the initiation of numerous micro-charge commands which keep the HSFW at a predefined minimum SOC level. It is desirable to set the minimum SOC level at the lowest

possible setting in order to minimize the HSFW charge loss over time and reduce the frequency of the micro-charge commands. In practice the minimum SOC level is determined by the minimum HSFW assist power requirement for a typical transient event and can be adjusted as needed depending on the application.

The HSFW is best suited for transient cycles with frequent transitions in engine operating conditions (390F hydraulic excavator (HEX) and 988K large wheel loader (LWL)) as they lack prolonged steady-state operating conditions. Nevertheless, the HSFW is also helpful in most 745 articulated truck (AT) application cycles as its transient assist capabilities generally outweigh the energy lost to maintain the minimum SOC during the steady-state portions of the AT cycles.

Illustrating and quantifying the impact of improved transient performance enabled by the HSFW, SuperTurbo and MGU is not straightforward when using powersystem level models. The reason is the boundary diagram (Figure 1) and how the desired engine speed and torque are taken from the C18 baseline and used as boundary conditions for the H2D2 powersystem to follow. Even if the H2D2 powersystem has superior transient performance compared to the C18 baseline, this will not be obvious in the transient cycle results as the target would always be the C18 performance. Therefore, the expected productivity benefit associated with improved transient performance needs to be evaluated using a full machine simulation model.

In order to demonstrate the improved transient performance enabled by the Hybrid devices in the H2D2 powersystem, industry-standard transient load step tests such as the Constant Speed Load Acceptance (CSLA) test can be used and replicated in simulation using the H2D2 System Level Model. The CSLA test is done by holding the engine speed constant at low load initially and then requesting maximum torque from the engine by increasing the dyno throttle to 100%. This test evaluates the transient performance capability of the engine using metrics such as time to 85% load, snap torque and boost/torque raise rate.

Figure 13 illustrates the transient performance advantage of the full H2D2 Hybrid powersystem as predicted by the H2D2 System Level Model. Three sets of simulation data are compared – the C18 baseline, a downsized 13L equipped with Variable Geometry Turbocharger (VGT) and the full H2D2 Hybrid powersystem which includes the SuperTurbo, HSFW and MGU. During the test the desired engine speed (Figure 13, Plot 1) is kept constant at 1400rpm. At t=1s maximum torque / power is requested by setting the dyno command to 100% load.

The Engine Only Power traces for the three powersystems (Figure 13, Plot 4) can be characterized with fast initial torque / power increase, followed by a slower increase rate until the desired torque is reached. The fast initial torque increase is proportional to the amount of fuel which can be injected before a predetermined Air-Fuel Ratio (AFR) limit is reached. Since the C18 baseline would have much higher air mass flow rate compared to the 13L engines at a given engine speed, more fuel can be injected before the C18 becomes AFR limited, which in turn results in higher initial torque / power peak. This peak is referred to as snap torque and is an important transient performance metric for many off-highway, heavy-duty applications.

After the snap torque is reached, the engines become AFR-limited, and the rate of torque / power increase is proportional to the rate of intake manifold pressure / boost increase. Figure 13, Plot 4 also highlights the superior performance of the SuperTurbo compared to a conventional VGT. The SuperTurbo is able to increase the boost much faster compared to the VGT, which results in ~40% reduction in the time to 85% load metric (the gray dashed line represents the 85% load in Figure 13).

When looking at the Total System Torque (Figure 13, Plot 2) and Total System Power (Figure 13, Plot 2) metrics it becomes clear how the HSFW and MGU enable the H2D2 Hybrid powersystem to

achieve or even improve the C18 levels of transient performance. The reduced snap torque capability from downsizing is being compensated by the HSFW which in this example is able to provide additional 80kW of power almost instantaneously at the start of the transient even and then sustain this power until the target load is reached (Figure 13, Plot 5). At the same time the 48V MGU is also assisting the engine and even though the power contribution is much lower compared to the HSFW, it is still sufficient to offset the power draw caused by the SuperTurbo during the transient event. It is also worth noting that at lower engine speeds the H2D2 Hybrid powersystem will have even more substantial transient performance advantage compared to the C18 baseline due to the decreased air mass flow rate at lower engine speeds. However, the 1400rpm speed is more relevant for the machine applications chosen for the project.

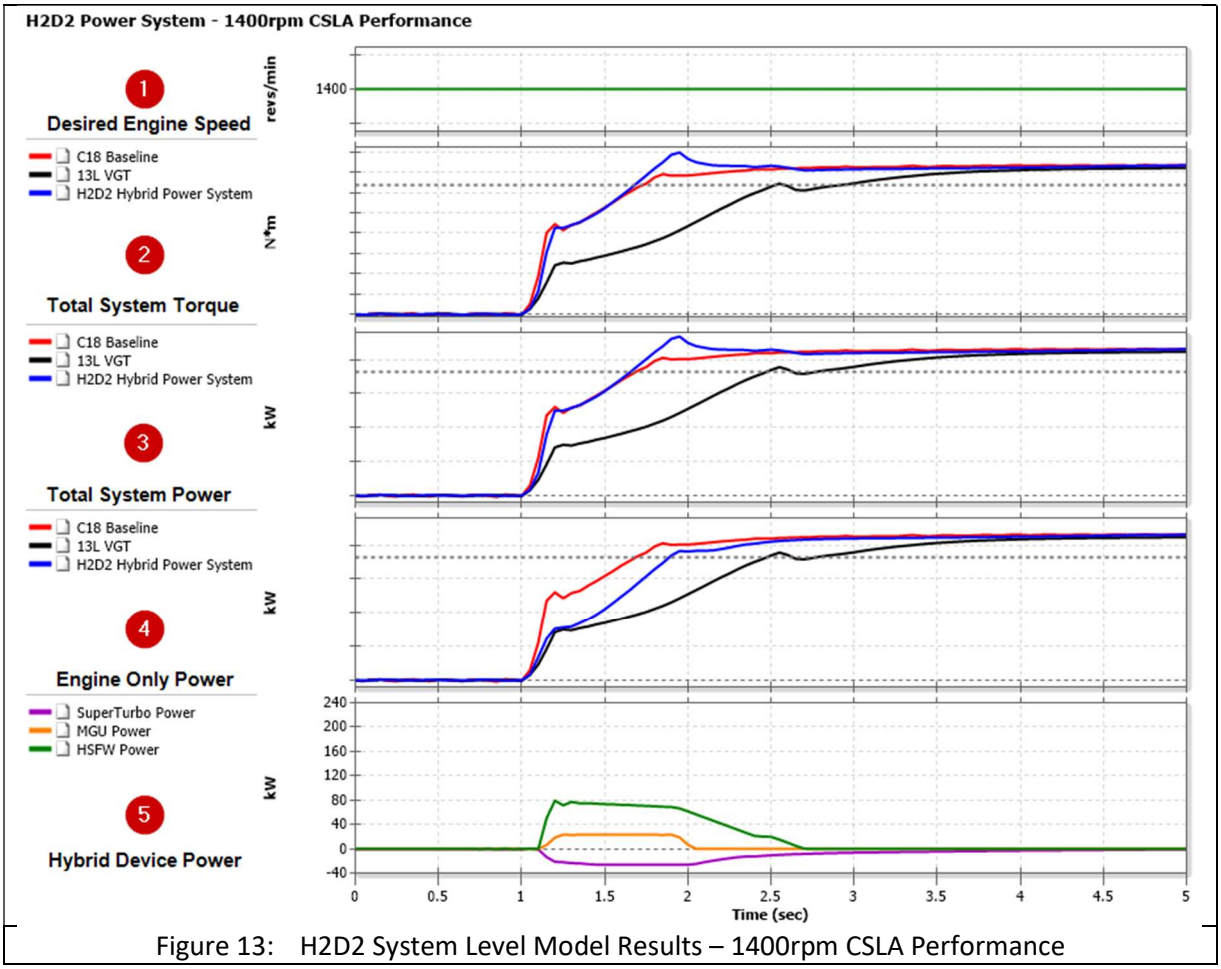

Figure 13: H2D2 System Level Model Results – 1400rpm CSLA Performance

A secondary, but significant, core engine benefit was found in the area of the off-road machine cooling system. As a result of using the powersystem paradigm for analyzing the powersystem performance and imposing the C18 baseline torque and speed as targets at the powersystem boundary means that some benefits of using a more efficient downsized engine may not become apparent from the transient simulations and need to be accounted for separately.

Such is the case with the power requirement for the cooling system. Most off-highway machine applications are stationary or near-stationary and can't depend on air flow through the radiators / heat exchangers purely as a result of the relative speed between the vehicle and the environment. Therefore, in order to provide sufficient cooling performance, the off-highway cooling systems must

rely on larger heat exchangers and forced air flow provided by additional high-power fans. The more efficient 13L engines will also have reduced heat rejection. Cascading the reduced heat rejection requirement downstream to the radiators, heat exchanges, cooling fans, and fan drives can result in a notable reduction in cooling power requirements as illustrated in Figure 14.

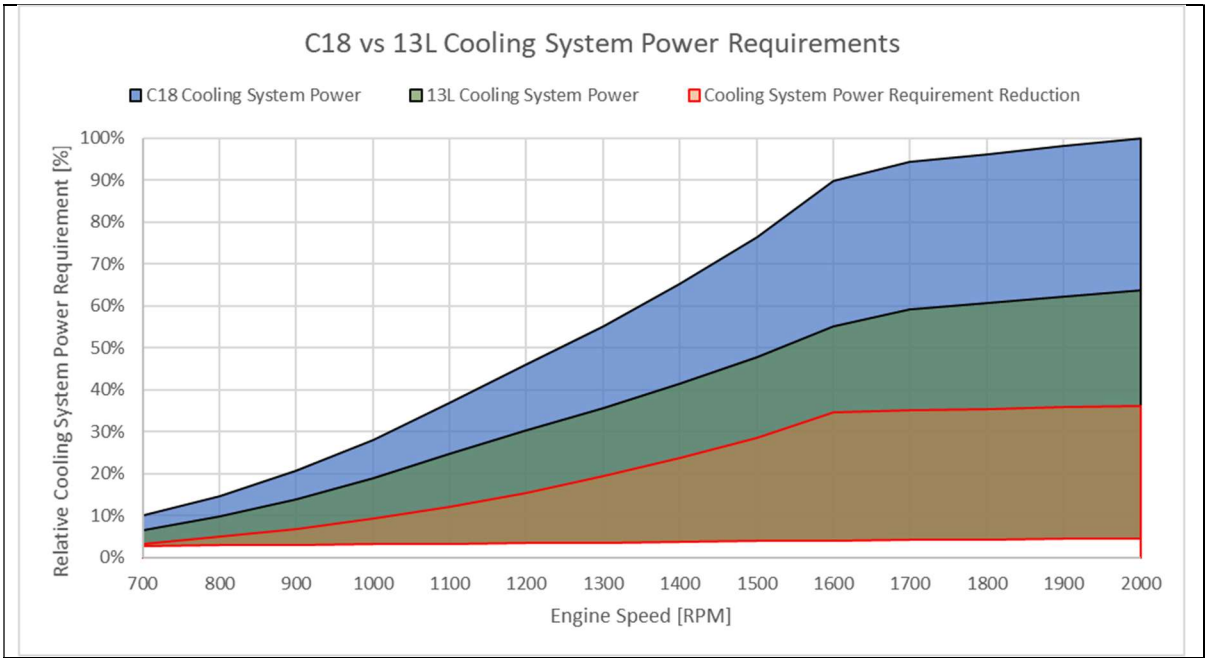

Figure 14: Cooling System Power Requirement Reduction – C18 vs 13L

The cooling system power requirement reduction is minimal at low engine speeds but increases to a maximum of 35% at engine speeds >=1600rpm, which is well suited for the H2D2 machine applications which spend significant time in the 1400-1800rpm region. With the information from Figure 14 the C18 desired torque can be reduced and the H2D2 application cycles re-run in order to estimate the fuel efficiency benefit associated with the Cooling System Power Requirement Reduction.

Figure 15 shows an example result for one of the 745AT Machine Application Cycles (Cycle 5) and the results confirm that the cooling parasitic requirement of slow/non-moving off-road machines without a free stream of cooling air can be quite substantial. The 35% difference in Figure 14 translates to ~2.5% efficiency at the engine and powersystem boundary. This power requirement reduction cannot be realized simply by running the C18 cooling system at lower speed. In order to get the full extent of the benefit, the cooling system has to be re-sized and re-designed with new components operating at or close to their peak efficiency. This analysis is for the engine-only heat rejection and the accounting for increased heat rejection from the hybrid elements, namely the HSFW and MGU systems, is expected to erode this ~2.5% efficiency benefit. Additionally, no impact of Thermal Barrier Coatings (TBC) were included in this benefit prediction, so further heat rejection reductions from TBC adoption (discussed in **Thermal Barrier Coatings** section) may help to offset the hybrid element heat rejection increase.

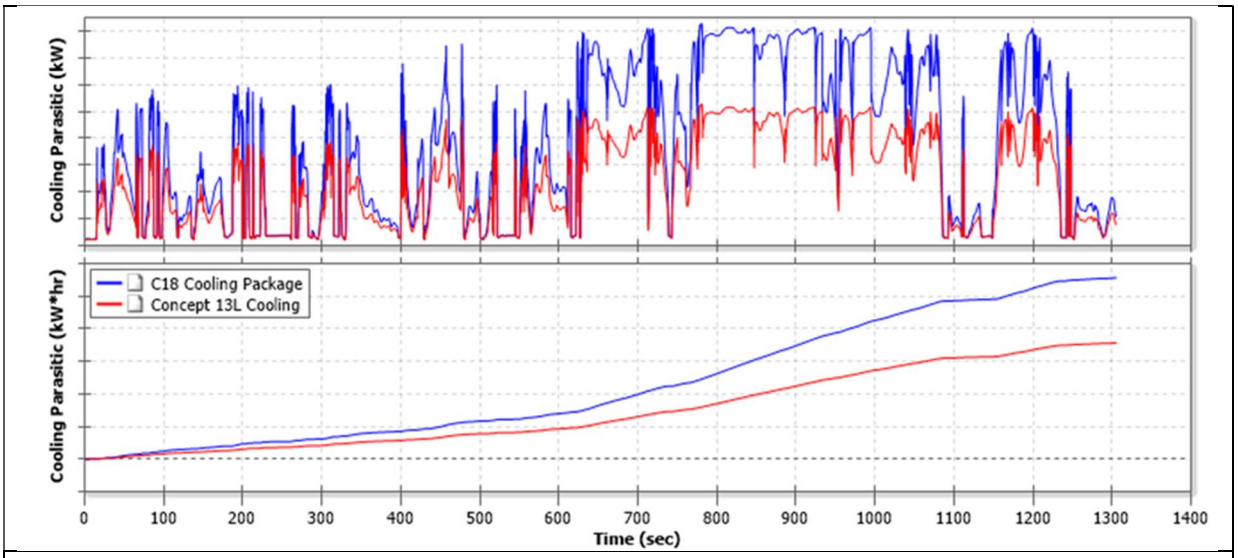

Figure 15: Reduced machine level cooling due to the lower heat rejection of the concept engine

Continuous H2D2 System Level Model Development

Even after the completion of the Hybrid Concept Definition task, the H2D2 System Level Model remained one of the main performance assessment and development tools employed by program. This section highlights some of the main model development areas which enabled the model to be effectively used during the validation phase:

❖ Aftertreatment Sub model Development

An important model update was the development and integration of high-fidelity aftertreatment models aimed at helping the H2D2 team with develop engine calibrations which included more accurate emissions constraints. The program advanced the integration of two different versions of the aftertreatment system – **F**ull **F**idelity DYNASTY Aftertreatment Model (**FF**) and Fast Running **N**eural **N**et Aftertreatment Model (**NN**). Both of those models are illustrated in Figure 16.

The **F**ull **F**idelity DYNASTY Aftertreatment Model (**FF**) was based on native DYNASTY aftertreatment components utilizing Advanced Chemistry gas properties. The model contains DOC, DPF, SCR and AMOX components and was parametrized to represent the actual H2D2 13L aftertreatment system.
This model was the most complete Aftertreatment model currently available for the H2D2 13L engine but had the disadvantage of running relatively slowly and therefore was used for specific aftertreatment-focused simulation runs. It was also used to generate data which was then used to train fast running aftertreatment models which were then used directly for transient simulations, such as the Fast-Running **N**eural **N**et Aftertreatment Model (**NN**).

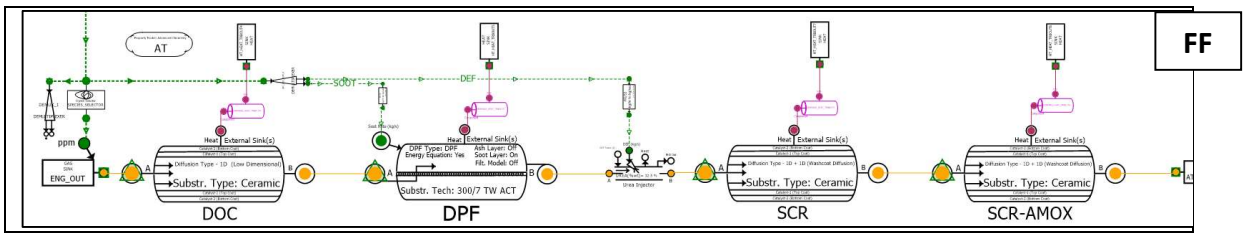

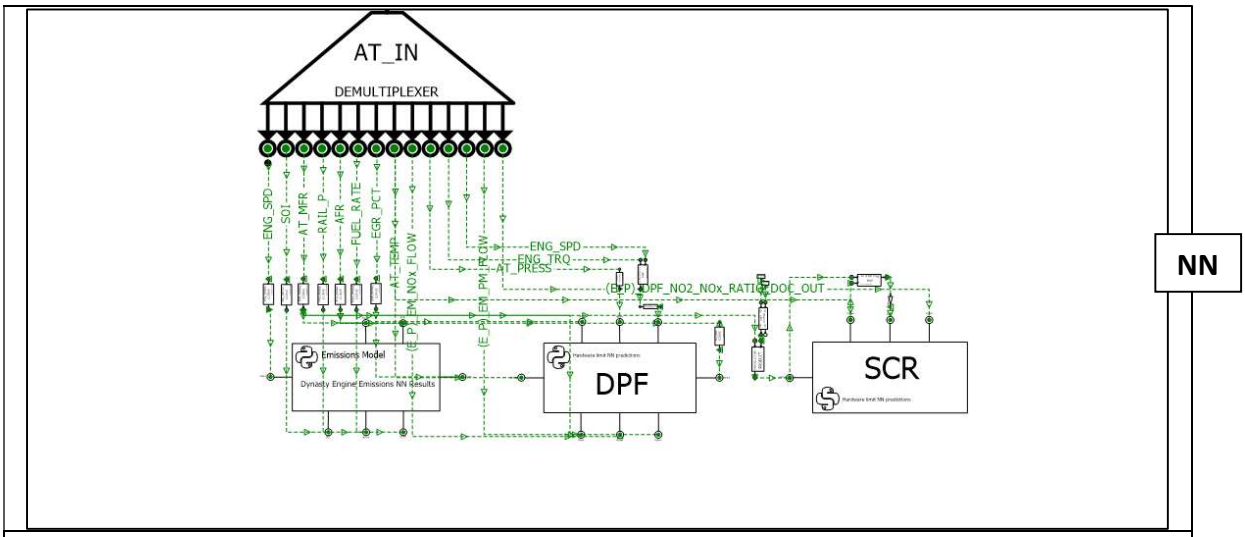

Figure 16: H2D2 System Level Model – Aftertreatment – **F**ull **F**idelity (**FF**) and **N**eural **N**et (**NN)**

The Fast-Running **N**eural **N**et Aftertreatment Model (**NN**) had 3 main components:

- Emissions – predicted the engine-out emissions. The model was trained using test data obtained from the 13L Phase 1 engine over an operating range which was wide enough for the needs of the H2D2 13L Phase 2 engine calibration
- DPF – simplified DOC/DPF component trained using data obtained from running the **F**ull **F**idelity DYNASTY Aftertreatment Model (**FF**)
- SCR – simplified SCR/AMOX component trained using data obtained from running the **F**ull **F**idelity DYNASTY Aftertreatment Model (**FF**)

The purpose of the Fast-Running **N**eural **N**et Aftertreatment Model (**NN**) was to provide similar levels of predictiveness as the **F**ull **F**idelity DYNASTY Aftertreatment Model (**FF**), but at much lower computational cost. This model was the main Aftertreatment model used for predicting the H2D2 System Level Model engine out and tailpipe emissions.

❖ <u>SuperTurbo L4 Controls Integration and Calibration</u>

Another important model update was the adoption, integration, and calibration of the SuperTurbo supplied L4 controller. This controller version was also used during testing, so having it available in the H2D2 System Level Model much earlier enabled the team to debug and optimize its performance when working in conjunction with the Engine Advanced Control Software and the Supervisory L5 controller.

Figure 17 below shows example results from the SuperTurbo L4 Controller calibration work completed using the H2D2 System Level Model prior to the engine testing:

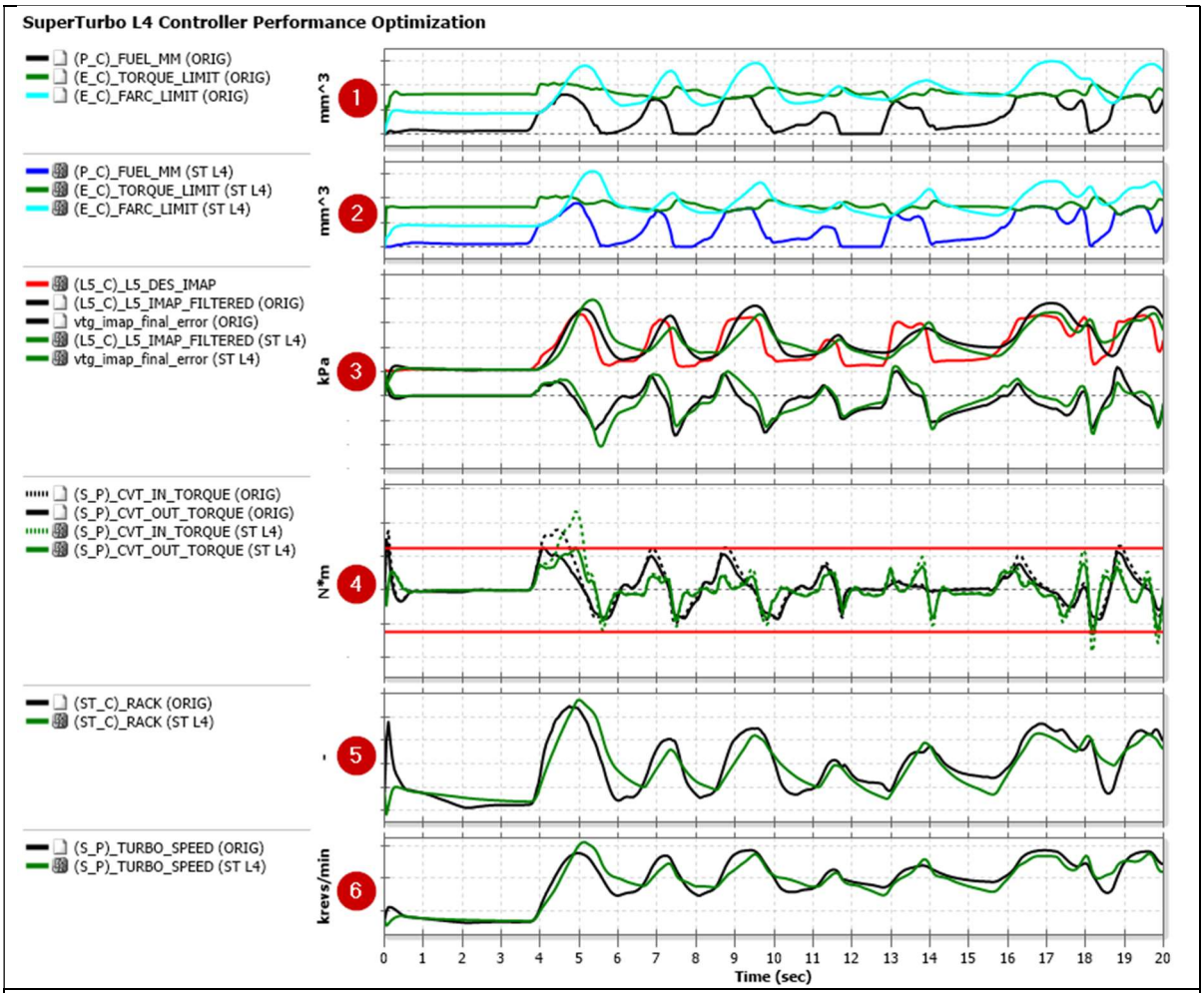

Figure 17: H2D2 System Level Model – SuperTurbo L4 Controller Optimization

The results shown above compare the performance of the Original SuperTurbo L4 controller (black) and the New SuperTurbo L4 Controller (green) over a short test cycle which represents a 20s portion of Cycle 19 (988XE Application). In this example the original controller performed better than the production controller when it comes to the IMAP following as it was able to follow the IMAP target more closely (3). Since the Original controller used the turbocharger shaft power predicted in DYNASTY as a direct feedback signal, it was able to go to the maximum assist effort very quickly without exceeding the CVT torque values (4). This performance trend can be seen even more clearly when looking at the Rack / CVT Commander position (5) and Turbocharger shaft speed (6) plots. However, when comparing the FARC limits observed when using the Original SuperTurbo L4 controller (1) and New SuperTurbo L4 Controller (2), it is clear that despite being tuned a bit more conservatively, the New controller did not cause the engine to become FARC limited throughout this particular test cycle.

- Implementation of additional Test Cycles to support testing and validation – NRTC cycles plot:

  Another focus area has been the addition of application specific NRTC cycles to the list of standard cycles. The NRTC cycles are used routinely as part of the Controls Development and are also part of the transient cycles ran in the test cell. Since the H2D2 powersystem concept is aiming to replace the C18 over a range of different applications (745AT, 390F and 988K/XE), multiple implementations of the NRTC cycle are required as illustrated in Figure 18below:

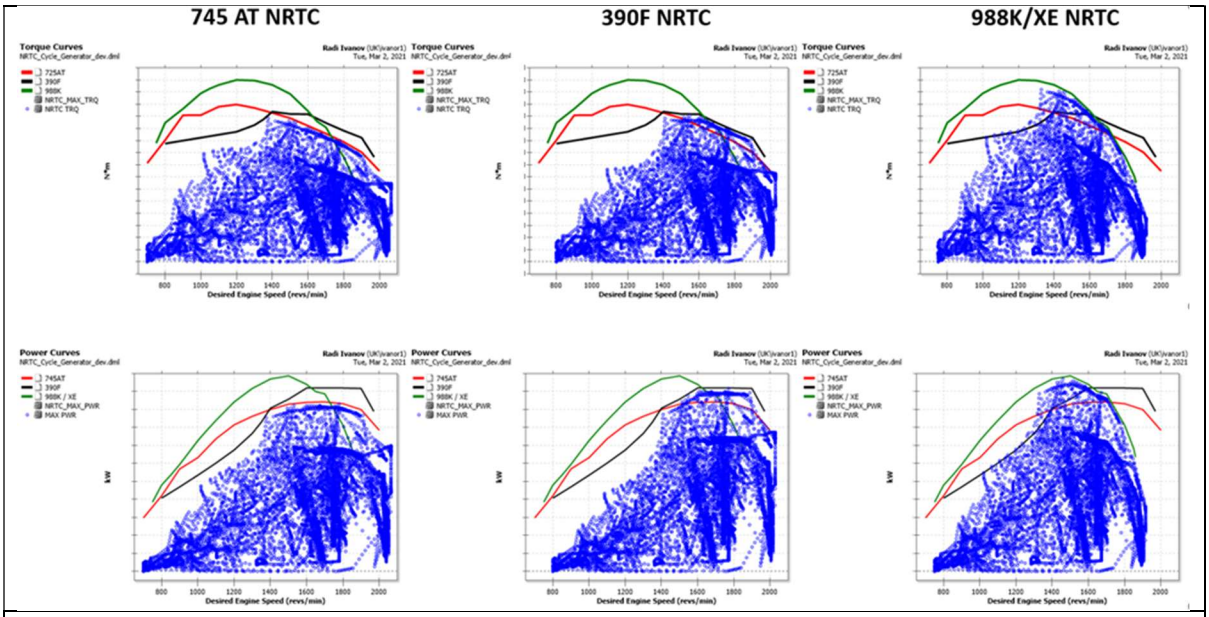

Figure 18: H2D2 System Level Model – Additional Application Specific NRTC Cycles

❖ <u>L5 Controller Logic Development</u>

The performance of the H2D2 Hybrid powersystem over highly transient cycles where very limited opportunities for energy recovery is more challenging and represents an opportunity for improvement. The H2D2 System Level Model has been used to evaluate numerous alternative control strategies which may be better suited for highly transient operation of the Hybrid powersystem.

One of the investigated and implemented strategies is the Hybrid Assist Power Trim Strategy. This strategy gradually reduces the Assist Power during the transient event so that the Hybrid powersystem doesn't overshoot the target power value. Overshoots are generally undesired as they use more energy to increase the hybrid powersystem power to undesirably high levels which exceed the needs of the cycle.

Figure 19 illustrates the intention behind the Hybrid Assist Power Trim strategy during an idealized Accel event over a Constant Speed Load Acceptance (CSLA) cycle. During this cycle the target engine speed ❷ is kept constant (at 1200rpm in this example) while the target torque/power is stepped up from 0 to the maximum torque/power which the engine is capable of at the given engine speed (❶ and ❸). During the transient event the engine and the hybrid devices are aiming to increase the powersystem torque/power as quickly as possible until the target torque/power is reached. During this time the engine would normally be FARC limited ❹. The transient event duration is also indicated by the Accel Flag ❺ and with the **Default Strategy** the Accel Flag drives the MGU + HSFW Power Request ❻. In addition, this Power Request is only limited by the maximum assist power available from the MGU and HSFW ❻. This often results in the powersystem torque/power overshooting the desired torque/power towards the end of the transient event (❶ and ❸).

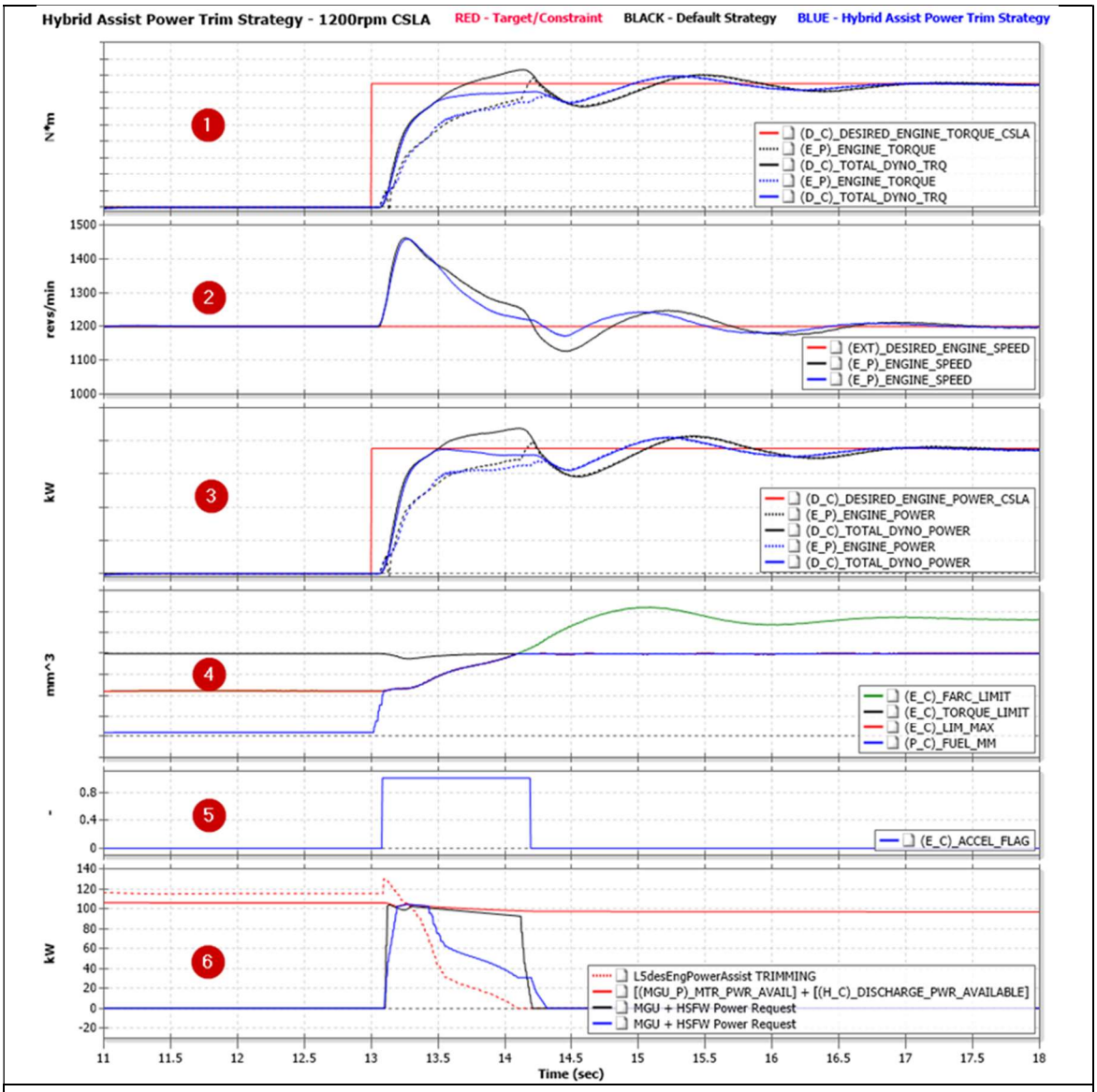

Figure 19: H2D2 System Level Model – Hybrid Assist Power Trim Strategy – 1200rpm CSLA cycle

In contrast, the **3.4.1 Hybrid Assist Power Trim Strategy** aims to gradually reduce the desired MGU and HSFW target Assist Power after the initial part of the transient event as seen in 6. At the beginning of the transient event (between 13s and 13.5s - Figure 19) the assist power is kept at the maximum assist power available from the MGU and HSFW 6 in order to assist the engine as much as possible until the target torque/power is reached. However, the gradual reduction of the desired MGU and HSFW target Assist Power results in the elimination of the powersystem torque/power overshoot towards the end of the transient event (1 and 3). In conclusion – both strategies enable the target power to be reached at the same time (13.5s – Figure 19) which in turn indicates that the transient performance should remain the same while the overall powersystem efficiency will be increased as less Hybrid assist energy will be required for each transient event.

❖ HSFW Plant Updates

The HSFW plant and controller models have been under continuous development throughout the project with 3 main model revisions used in the H2D2 System Level Model being:

- Initial HSFW model: The first HSFW plant model was developed using supplier-provided performance and efficiency data. This initial model was characterized with better performance and higher efficiency compared to later revisions validated against available test data.
- HSFW model validated against Standalone Hybrid Test Data: During the Standalone Hybrid Testing the team had the opportunity to collect HSFW performance data which was then used to validate the HSFW plant model. More details about the Standalone Hybrid Testing can be found in the **Hybrid-Only Validation** section of this report.
- HSFW model validated against Full Hybrid Test Data: In order to make sure the HSFW plant model performance is still representative of the HSFW hardware, an additional validation exercise was performed when test data became available from the full H2D2 Hybrid powersystem testing.

Figure 20 shows the results from the HSFW validation exercise using the final H2D2 Hybrid powersystem test data:

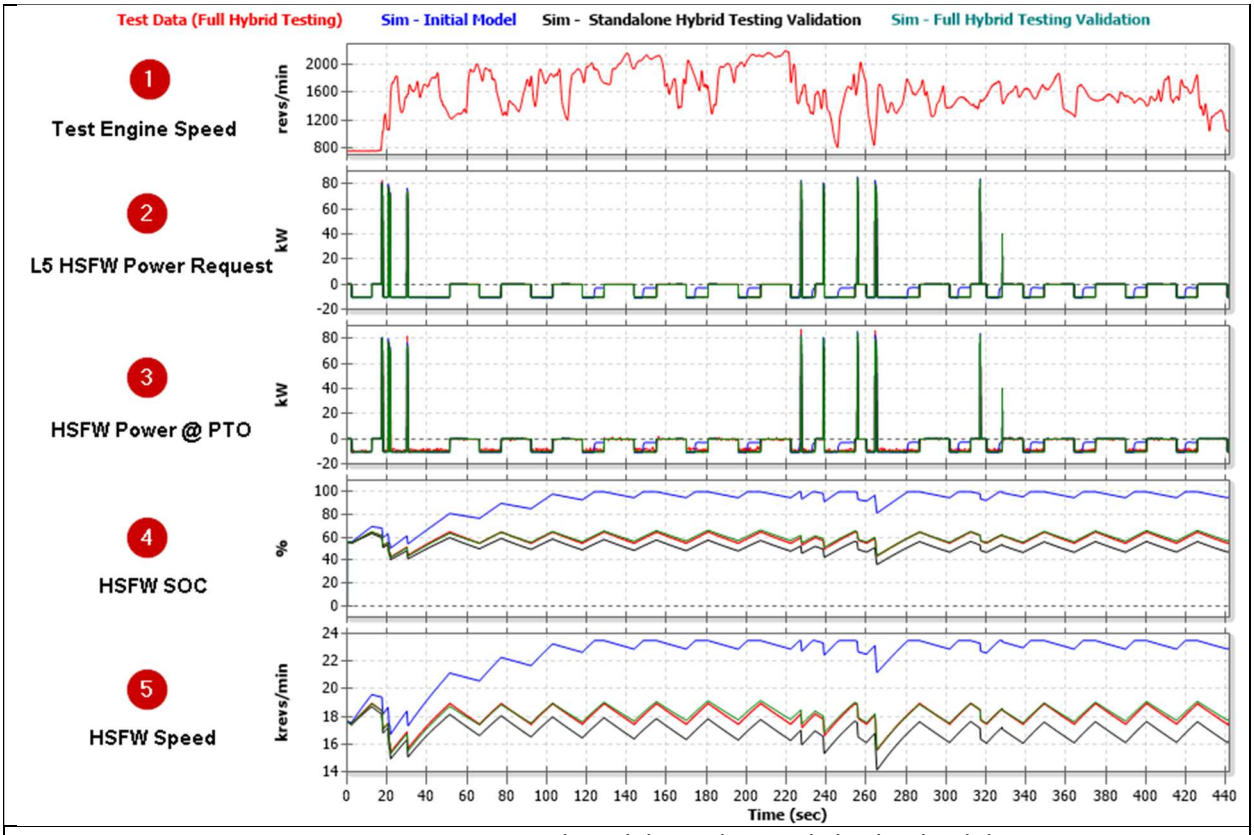

Figure 20: H2D2 System Level Model – High Speed Flywheel Validation

In order to isolate the HSFW performance from the rest of the H2D2 powersystem, a boundary diagram was established around the HSFW plant and Controller. This was achieved by using the test engine speed ❶ as a boundary condition at the HSFW PTO and the test L5 HSFW Power Request an input to the HSFW L4 controller ❷. The HSFW power at the PTO ❸, HSFW SOC ❹ and HSFW speed ❺ were then used as the performance parameters based on which the model vs test match quality can be assessed.

As seen from the results in Figure 20, the **Initial Model** predicted much higher HSFW SOC 4 and HSFW Speed 5, which indicates lower losses compared to the test data. **The HSFW model validated against Standalone Hybrid Test Data** showed much improved performance compared to the Initial model and was able to get much closer to the test data. However, the HSFW losses set in this model revision were a bit higher than necessary in order to get a good match with the test data and as a result – the predicted HSFW SOC 4 and HSFW Speed 5 were lower than their respective test values. Finally, the HSFW losses in the HSFW plant model were reduced slightly compared to the **HSFW model validated against Standalone Hybrid Test Data** in order to get a good match with the test data for the HSFW SOC 4 and HSFW Speed 5. The resulting **HSFW model validated against Full Hybrid Test Data** set was used in the H2D2 System Level Model when generating the simulation results used for the final H2D2 powersystem validation.

Validation Results

Accurately predicting the performance of all Engine (C18 baseline, 13L VGT) and powersystem (H2D2 SuperTurbo Only, H2D2 Full Hybrid) configurations is a crucial requirement for the H2D2 System Level Model. Even though a number of validation exercises were completed, and model enhancements implemented throughout the project, the improvements made should ultimately result in good predictive capability.
The final validation results can be separated into the following groups:

❖ Steady-State Validation

The steady-state validation is an important step towards the development of a predictive transient model and gives information about how well the H2D2 System Level Model matches the test data during steady-state operating conditions.

Figure 21 shows a BSFC comparison between the H2D2 System Level Model predictions and the Test Data. The values shown in the bubble plot are the % differences between the simulation value and the Test value for each operating point (% Delta = $\frac{Simulation - Test}{Test} * 100\%$). The blue bubbles show positive values and indicate that the simulation model is overpredicting while the white bubbles show negative values and indicate that the simulation model is underpredicting. The BSFC results, which account for the SuperTurbo power and the Engine Power, indicate a good match between the simulation model and the test data. Some notable exceptions are the low load points where the simulation model underpredicts the BSFC, and the delta is larger in general. However, in the 1400rpm to 1600 rpm medium to high load operating region, which is most relevant for the 3 machine applications (Figure 2), the H2D2 System Level Model predicts the BSFC with very high accuracy.

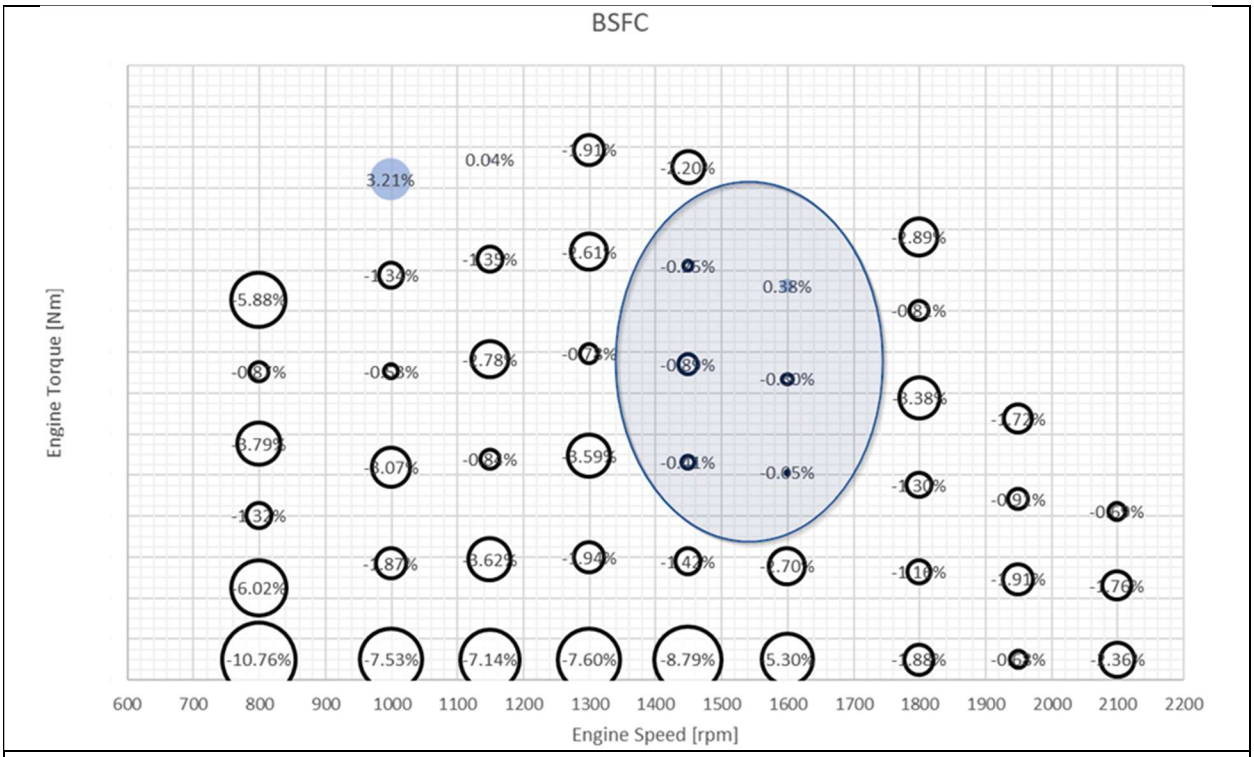

Figure 21: H2D2 System Level Model Results – BSFC Predictions vs Test Data (48 PCOpt Points)

❖ C18 Baseline Transient Performance Validation

The H2D2 System Level Model, when configured to represent the C18 baseline, can be used to generate simulation data over the same set of transient cycles used for predicting the H2D2 powersystem performance. This enables clear back-to-back comparisons between the Baseline C18 powersystem and the H2D2 powersystem to be made. However, since C18 test data is only available for a limited set of NRTC cycles, the only way to validate the C18 Baseline transient performance prediction is to compare the model predictions with C18 test data over the same set of NRTC cycles.

H2D2 System Level Model was used to produce simulation data for comparison to available C18 and H2D2 NRTC transient test data for the 3 key applications (745AT, 390F and 988K/XE). Figure 22 presents the results for the 745AT NRTC cycle.

The C18 Simulation predictions (**BLUE**) match the two C18 NRTC data sets (**RED** and **BLACK**) very well for all 3 application cycles. The difference between the Test BSFC and Simulation BSFC is in the range between -0.65% (390F NRTC) and 0.04% (988K/XE NRTC) with the 745AT NRTC cycle illustrated on Figure 22 showing -0.49% difference.

These results reaffirm the team's confidence that the H2D2 System Level Model, when configured to represent the C18 baseline, is able to predict the performance of the C18 baseline powersystem over transient operating cycles remarkably well. This predictive accuracy in turn enables the project team to use the H2D2 System Level Model to predict the baseline C18 powersystem performance over all Machine Application Cycles for which there is no existing C18 baseline test data.

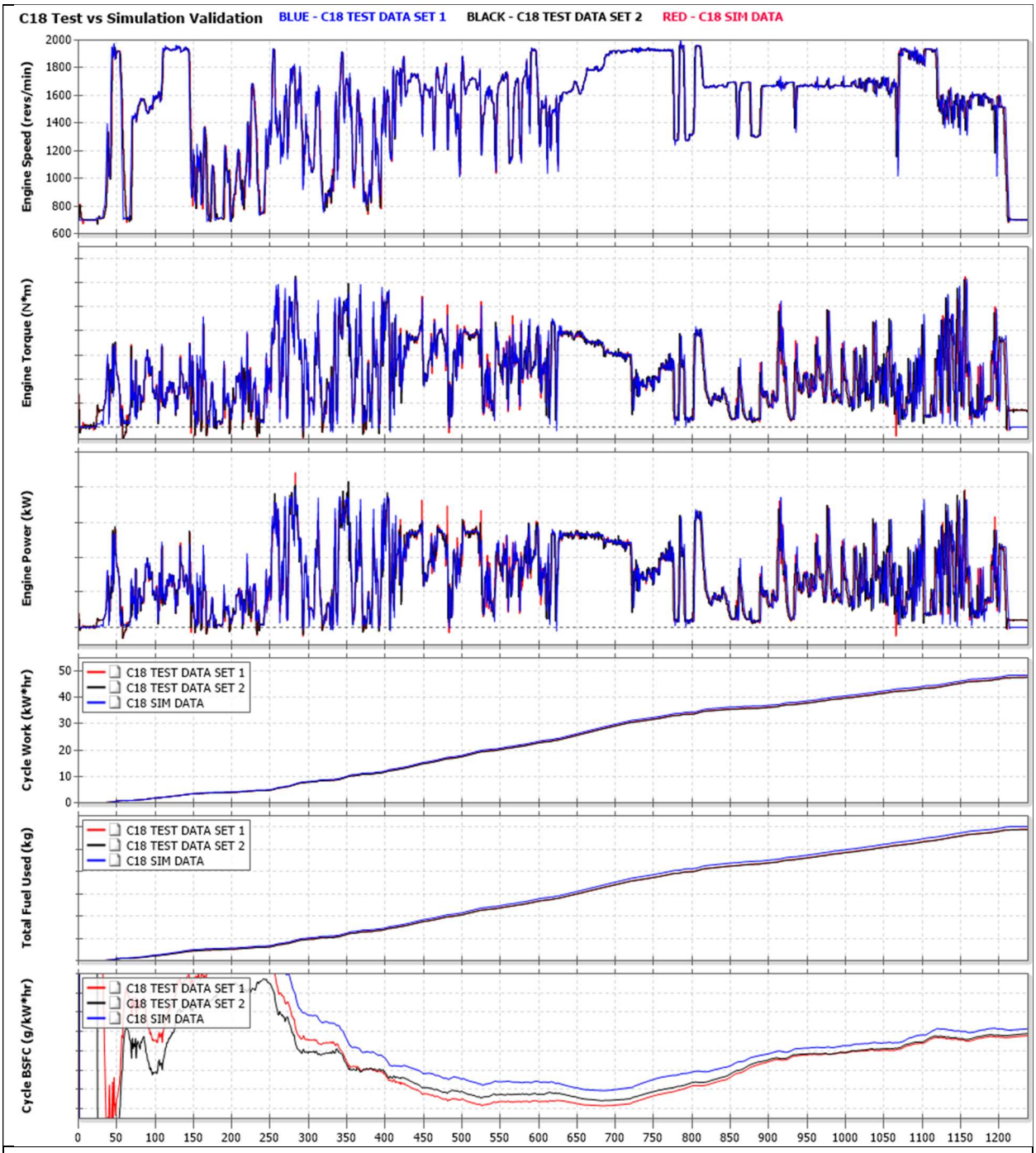

Figure 22: C18 Model Validation – 745AT NRTC Cycle – C18 Test vs C18 Simulation

❖ <u>H2D2 Powersystem Validation (Engine + Aftertreatment)</u>

The engine + aftertreatment validation was performed following the **3.4.1 Hybrid-Only Validation** and was aimed at evaluating the performance of the 13L engine, SuperTurbo and aftertreatment systems over a range of transient application cycles. In addition, this was the first time the advanced controls software was used on engine for running transient cycles. This was a significant shift in the SuperTurbo control strategy as the SuperTurbo target was changed from Power to IMAP and the IMAP

target signal was generated by the advanced controls software as opposed to the L5 Supervisory controller.

Figure 23 shows a comparison between the H2D2 System Level Model predictions and test data over the 745AT NRTC cycle:

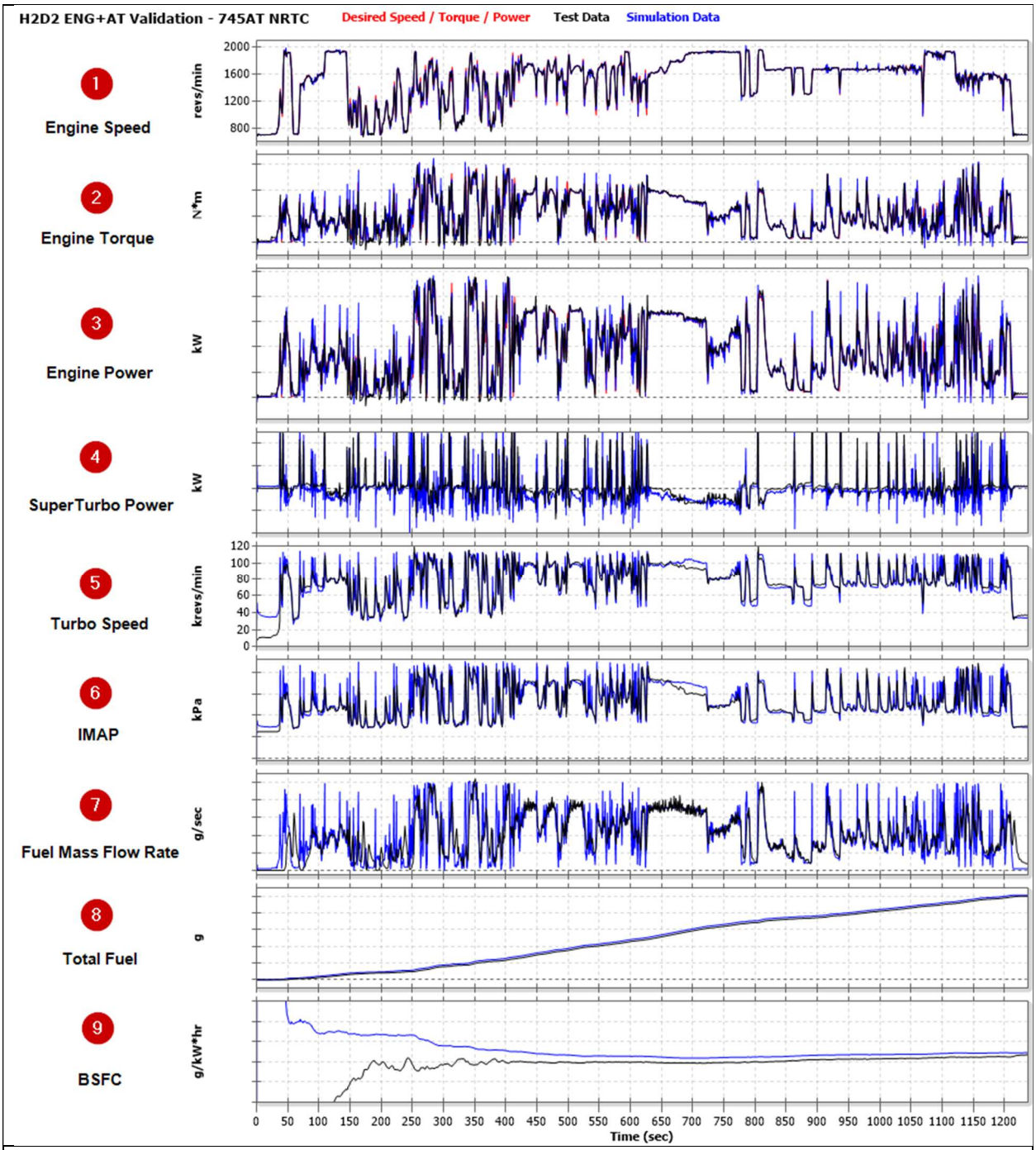

Figure 23: H2D2 System Level Model Results – H2D2 Engine + AT – 745AT NRTC Cycle

In general, the model demonstrates a very correlation with the test data throughout the duration of the cycle. The Engine Speed 1, Engine Torque 2 and Engine Power 3 all match well, which indicates that both the H2D2 System Level Model and the Test Cell Engine are able to track the desired cycle well. The Turbo Speed 5 and IMAP 6 are also in a good agreement throughout most of the

cycle. The two exceptions are the idle period at the beginning of the cycle (0-30s) and a short section between 670s and 730s which are likely due to slight differences in the Advanced Controls map lookup resulting in slightly higher IMAP targets for the H2D2 System Level Model during parts of the cycle.

Finally, when it comes to the Total Fuel 8 and Cycle BSFC 9, the model is able to predict the performance of the test engine very well (<1% difference).

The tabulated validation results for all application cycles can be found in Figure 25 with the Engine + Aftertreatment correlation between Test and Simulation summarized in row 4.

❖ H2D2 powersystem Validation (Full Hybrid System)

The Full Hybrid System validation was performed following the Engine + Aftertreatment validation and was aimed at evaluating the performance of the full H2D2 powersystem (Engine, SuperTurbo, Aftertreatment, HSFW and MGU) over a range of transient application cycles. However, due to differences between the desired L5 strategy used in simulation and the L5 strategy used during testing, no direct comparison between the two could be made. In the test data the L5 strategy was not optimum and did not switch to regen mode when it was expected to do so, therefore it did not take full advantage of any recoverable energy during some of the transient application cycles.

In order to overcome the issue and validate the H2D2 System Level Model against Full Hybrid System test data, it was decided to use the H2D2 System Level Model to replicate the sub-optimal L5 strategy used during testing. This was achieved by taking the HSFW and MGU L5 commands from the test data and using them directly in simulation, thus ensuring consistency in how the Hybrid System operates. Figure 24 shows a comparison between the H2D2 System Level Model predictions and test data over the 745AT NRTC cycle. Just like with the Engine + Aftertreatment validation the Engine Speed 1, Engine Torque 2 and Engine Power 3 all match well, which indicates that both the H2D2 System Level Model and the Test Cell Engine are able to track the desired cycle well. The Turbo Speed 4 and IMAP 10 are also in a good agreement with the same few exceptions observed in the Engine + Aftertreatment validation.

When it comes to the Hybrid Device Performance, the MGU Power 5 is only being used for assisting during transient events due to the sub-optimal L5 strategy as explained earlier. As a result, the Relative Battery Energy 6 is negative throughout the duration of the cycle. For this parameter the H2D2 System Level Model predicts slightly higher energy used over the duration of the cycle, however, that difference is only about 0.014kWh, which compared to the total cycle positive work of a bout 50kWh is a negligeable difference.

The HSFW Power 7 is also being used for assisting during transient events (at a much higher power), but unlike the MGU, the HSFW SOC 9 is being kept at around 60% by employing relatively frequent micro-charge events. This enables the HSFW to have enough charge to assist the engine with sufficiently high power on one hand, but on the other hand keep the HSFW spin down losses down to more manageable levels. In addition, as a result of the HSFW plant validation, the HSFW Speed 8 is matching very well between Test and Sim, indicating the HSFW plant model provides accurate spin down losses estimation.

Finally, when it comes to the Total Fuel 12 and Cycle BSFC 13, the model is able to predict the performance of the test engine very well (~ 0.13 % difference). The tabulated validation results for all application cycles can be found in Figure 25 with the Full Hybrid System correlation between Test and Simulation summarized in row 5.

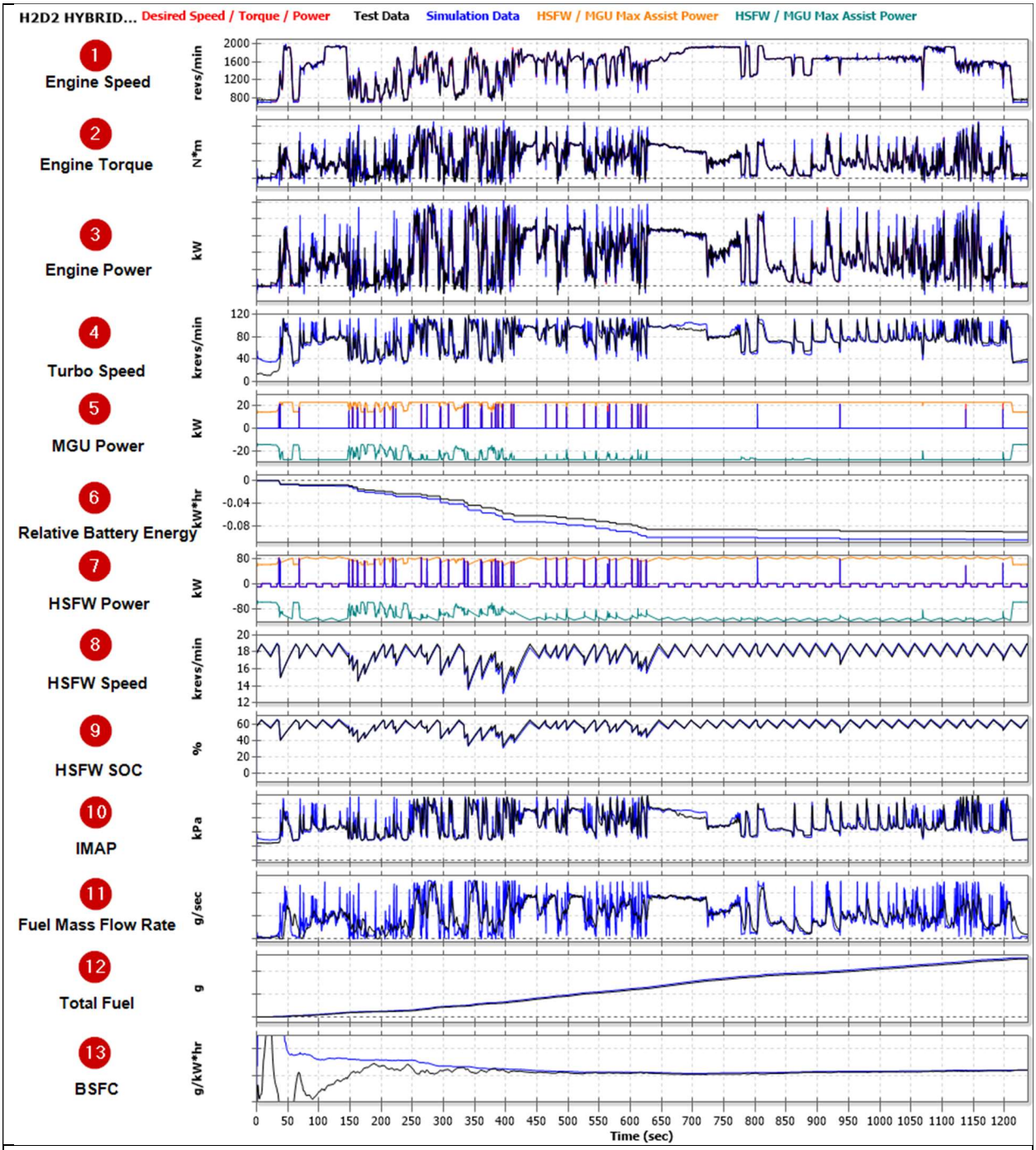

Figure 24: H2D2 System Level Model Results – H2D2 Hybrid powersystem – 745AT NRTC Cycle

Despite the reduced number of transient cycles used for the Full Hybrid System validation, the correlation between the H2D2 System Level Model and the test data is consistently good. This gives the team confidence that the H2D2 Hybrid powersystem efficiency benefits vs the C18 Baseline, predicted using the validated H2D2 System Level Model (Figure 25, 2), accurately and objectively represent the performance advantage of the H2D2 powersystem.

❖ Summary

The transient H2D2 powersystem validation results from the Engine + Aftertreatment only and the Full Hybrid System validation exercised are summarized in Figure 25:

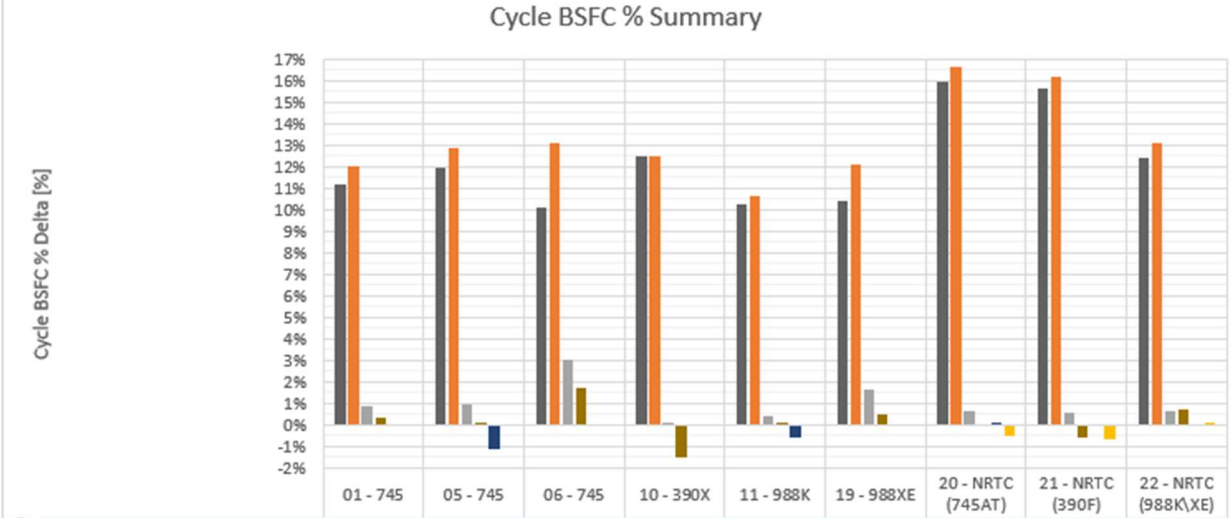

	01 - 745	05 - 745	06 - 745	10 - 390X	11 - 988K	19 - 988XE	20 - NRTC (745AT)	21 - NRTC (390F)	22 - NRTC (988K\XE)
❶ C18 SIM vs H2D2 SIM (ENG+AT)	11.16%	11.93%	10.10%	12.52%	10.25%	10.41%	15.94%	15.64%	12.43%
❷ C18 SIM vs H2D2 SIM (HYBRID)	12.05%	12.86%	13.11%	12.53%	10.64%	12.10%	16.63%	16.22%	13.10%
❸ HYBRID BENEFIT	0.89%	0.93%	3.01%	0.01%	0.39%	1.69%	0.69%	0.58%	0.67%
❹ H2D2 TEST vs H2D2 SIM (ENG+AT)	0.36%	0.15%	1.71%	-1.52%	0.10%	0.52%	-0.07%	-0.55%	0.71%
❺ H2D2 TEST vs H2D2SIM (HYBRID*)		-1.10%			-0.58%		0.13%		
❻ C18 TEST vs C18 SIM							-0.49%	-0.65%	0.04%

Figure 25: BSFC Benefit Summary Table – NRTC and Machine Cycles

❶ Shows the % BSFC benefit of the H2D2 powersystem (Engine + Aftertreatment) vs the C18 Baseline

❷ Shows the % BSFC benefit of the H2D2 powersystem (Full Hybrid System) vs the C18 Baseline

Please, note that the Optimal L5 strategy, which takes advantage of recoverable energy during some of the application cycles, was used by the H2D2 System Level Model to generate this data

❸ Shows the % BSFC associated with the addition of the HSFW and MGU (❸ = ❷ - ❶)

The additional benefit from the Hybrid devices (HSFW & MGU) is higher for cycles which have significant recoverable energy available.

❹ H2D2 System Level Model (Engine + Aftertreatment) validation results vs H2D2 Test data

❺ H2D2 System Level Model (Full Hybrid System) validation results vs H2D2 Test data

Please, note that sub-optimal L5 strategy, which does not take advantage of recoverable energy, was used by the test H2D2 powersystem to generate this data

❻ H2D2 System Level Model (C18 Baseline configuration) validation results vs C18 Test data

3.1.2. Core Engine Development

SOPO ID #	Item Title	Item Description	Start Date	End Date	Status
Task 1.2	**Core Engine Development**	Computer Aided Design, performance, thermofluid and structural simulations	4/1/2019	3/31/2020	100% Complete

An upgrade to the core engine is a foundational part of the improved engine performance achieved in this program. The core engine was developed in 2 phases: a relatively quick build phase 1 engine to enable test-based down selection of the performance recipe and a fully designed phase 2 engine that enabled the full demonstration of the H2D2 program goals.

Phase 1 Engine

The phase 1 engine was used for performance testing on an engine that includes the main core capabilities but not all the friction reduction improvements and overall design enhancements. This engine will enable the team to verify the performance improvements and provide input into the performance recipe down selection on an adequate timeline to ensure that fully vetted decisions are made prior to the ultimate (phase 2) efficiency improvement demonstration. If the program had waited until a full demonstration engine design to be completed, an adequate test program would have pushed beyond the project timeline, so the phase 1 engine enabled earlier selection and calibration of the engine system recipe.

The test platform for phase 1 testing was a "mule" multi-cylinder engine based on a current Caterpillar Tier 4 C13 engine with modifications to enable combustion and air system performance similar to the final H2D2 phase 2 demonstrator (including upgraded PCP capability, increased stroke, larger valve size, increased port flow, and new fuel system). This engine was designed and procured on a much shorter timeline than the major re-design that was under development for the final H2D2 demonstration. However, the full re-design was required to enable acceptable durability, robustness, noise, and friction reduction. The phase 1 engine shown below was designed, procured, and tested. This testing went through multiple test campaigns and provided significant knowledge to improve the final H2D2 demonstration, including baselining and measurement accuracy, friction measurements, piston bowl comparisons, fuel injection system comparisons, and turbo comparisons for the different applications under consideration under this program.

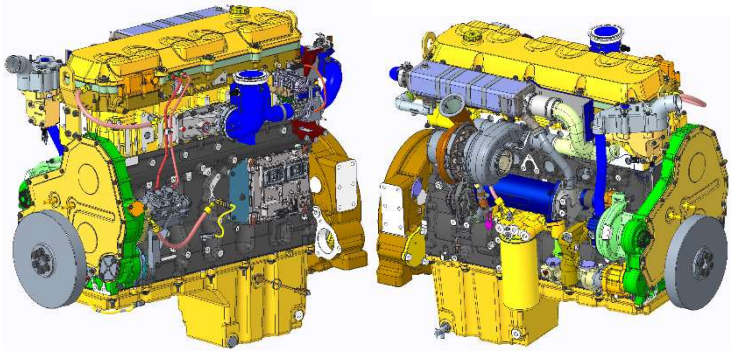

Figure 26: Design of "mule" engine that will serve a performance downselect and verification test platform.

Phase 2 Core Engine Architecture

The phase 2 engine underwent an exhaustive design process to provide a high performing but cost-effective design. The high-level design requirements for the core engine were determined by using

performance analysis so that the correct designs could be developed to meet the performance and durability targets. The overall development path was chosen to be the stroked and upgraded 13L platform which maintained cylinder spacing to minimize capital requirements, and a path to meeting the program targets for fuel efficiency was laid out. This path to efficiency improvement in the engine system includes reduced friction, increased peak cylinder pressure (PCP), compression ratio change, reduced aftertreatment backpressure, improved combustion, better breathing, and improved air system as shown in Figure 27. This section of the report will look at the design and simulation advancements in the core engine and the performance recipe to meet this efficiency improvement path.

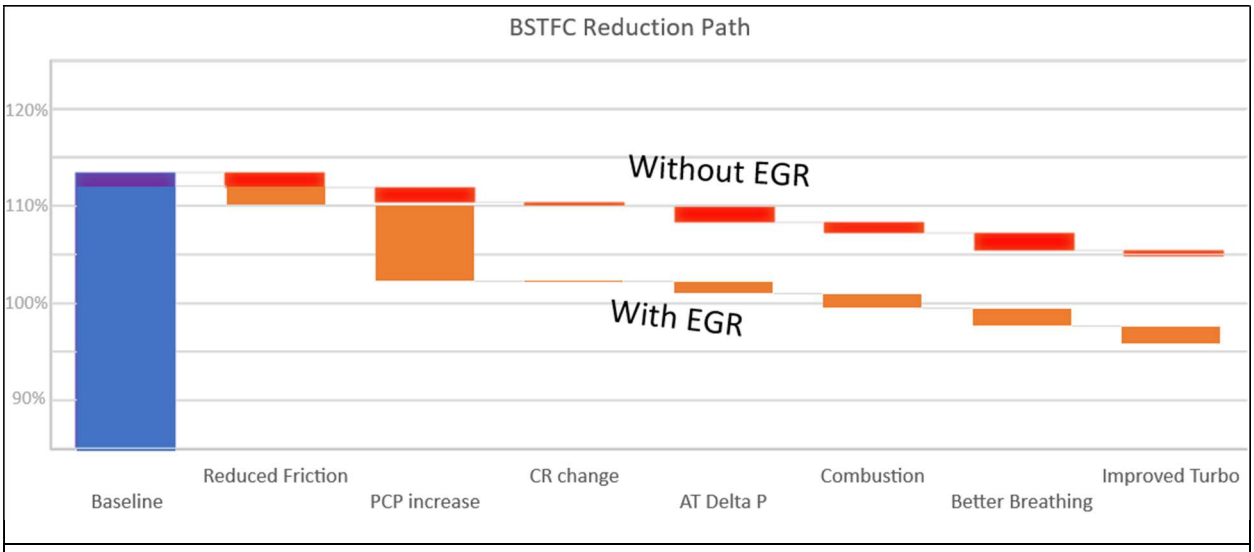

Figure 27: Path to core engine efficiency (steady state DYNASTY simulations)

Simulation-led design and development efforts on the core demonstrator engine progressed from parametric analyses to determine the general design specifications to more in-depth simulations on specific concepts and geometries. The core engine components will be discussed in the bulleted list below to further illustrate the final design refinements:

- A top-flange liner design showed lowest bore distortion characteristics - the foundation to reducing friction, oil consumption and blowby. It was determined that a robust design could not be achieved for the current bore size in the current bore spacing of the engine, so with input from the manufacturing analysis, the team decided to revise the bore spacing to enable this significant low friction, low BSFC building block. Collaboration sessions regarding liner coatings to help reduce friction were held with potential suppliers. The liner support and cooling gallery design was iterated to minimize cavitation, provide uniform temperatures, and minimize distortion.
- With the increase in cylinder spacing, the team performed crankshaft parametric DoE simulation and explored concepts for reduced number of counterweights to minimize weight and cost along with surface crowning and surface finish refinements to enable durability and smaller sizes.
- There were many iterations to cylinder head design to create multiple concept designs, working through trade-offs of cam number, cam location, valve size and spacing, head bolt layout, water jacket shape, and port geometry towards a finalized concept. Ultimately, the design achieved significant flow improvement while meeting the heat transfer and durability requirements.
- Improvements to the cooling system layout created a more compact design while also improving flow distribution. An oil thermostat cooler bypass was implemented to reduce friction via consistent oil viscosity. Water jacket designs with top-down cooling scheme and a dedicated top

channel liner coolant passage enabled the system to achieve low pressure drop and uniform cooling. Simulations highlighted areas to address stagnant flow regions and reduce system restrictions. A fluids module concept was implemented that enables part consolidation. Ultimately, the cooling system design enables the water pump to consume less power to circulate coolant through the engine.

- A variable displacement oil pump was selected as the prime path design for feeding the lubrication system to reduce overall parasitic load on the engine as a means of reducing BSFC.
- An engine architecture with an offset crankshaft has been evaluated for this demonstrator engine as a building block to reducing BSFC. The improvements have been estimated through simulations and considered against design implications, ultimately leading to the removal of the offset crankshaft from design consideration on this engine.
- Investigated valve lift profiles, including the inclusion of piston pockets in the valve to enable increased valve overlap with 1D and 3D simulations and single cylinder tests.
- Used CFD and historical data to identify target swirl ratio for reduced heat transfer, good breathing, and fast combustion.
- Explored the common rail rate-shaping capabilities of the fuel injector, and identified rate shape with best emissions performance.
- Evaluated traditional piston bowl shapes and thermal barrier coatings using combustion CFD and single cylinder tests to identify best piston candidates. Some of this will be highlighted in the next section.

As indicated from the activities above, friction reduction is a consideration in much of the core engine design. Therefore, significant effort was put into outlining the potential fiction reduction technologies and evaluating their cost-benefit trade-off so that the most effective technologies can be incorporated into the core design. The following list shows technologies that were considered to create the roadmap to the engine goal of 20% friction reduction. Ultimately, the bottom three items of the list were left off of the final concept based on cost-benefit analysis.

- Oil thermostat for maintaining consistent oil viscosity
- Increased rod length to reduce rod angularity
- Reduced bore distortion through liner flange design and form honing
- Optimization of ring tension, height, and coating
- Optimized piston skirt profile
- Cooling jacket design to increase mid-stroke temperature and lower oil viscosity in that region
- Cooling and lube system flow optimization to minimize restrictions
- Crowned crank journals
- Bearing materials including polymer overlay
- Variable oil pump
- Clutched water pump
- Variable piston cooling jets
- Low viscosity oils
- Liner surface treatments such as thermal spray with mirror finish or honing stratification
- Offset crankshaft
- Rolling element bearing on geartrain and camshaft
- Rollerized cranktrain

Piston Designs and Thermal Barrier Coatings

The most critical, and most flexible, mixing-controlled combustion aspect is the geometric design of the piston bowl and the interaction with the fuel jets. Both conventional bowl shapes and innovative non-axisymmetric pistons geometries were generated and CFD simulations were performed. The simulations consisted of open-cycle breathing simulations and closed-cycle combustion simulations to capture effects of charge motion as well as combustion. Detailed soot modeling was employed for the most accurate emissions trade-off possible. The main goal of the innovative piston development is to gain an efficiency increase for the same or lower level of NOx and soot emissions. This gain will come from a shortened burn duration and a lower in-cylinder heat transfer. Examples of the innovative non-axisymmetric geometries that were simulated is shown in Figure 28.

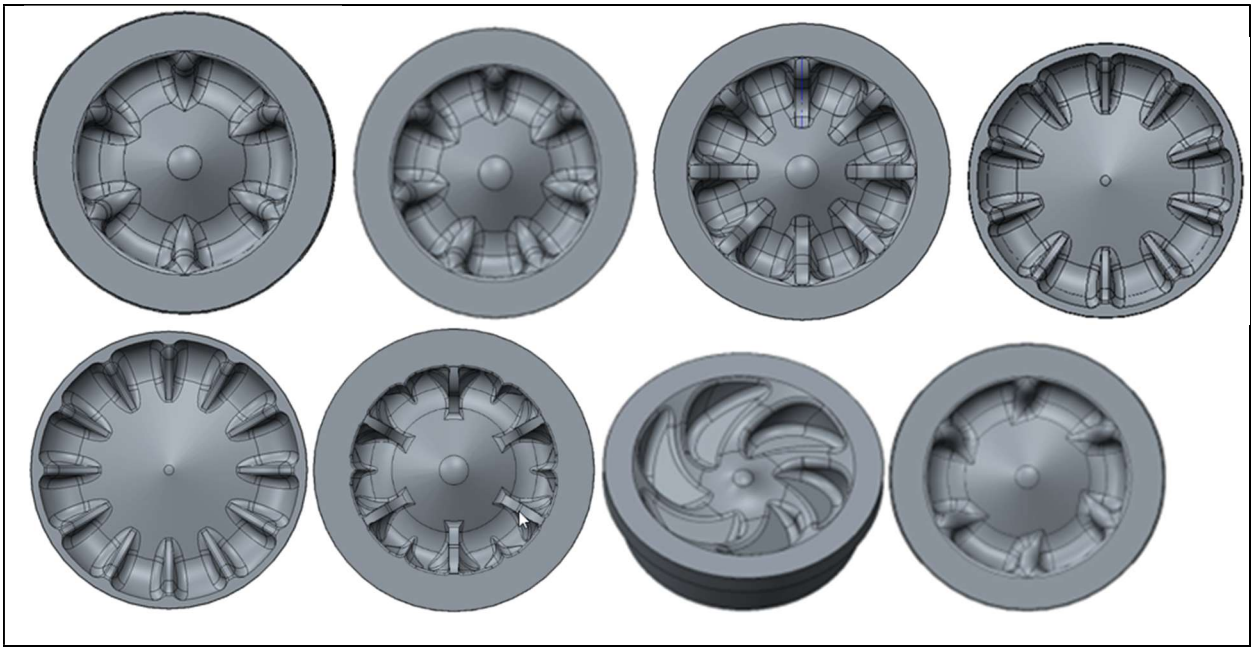

Figure 28: Example images of the innovative non-axisymmetric piston geometries that underwent CFD evaluation

Four innovative pistons and one axisymmetric piston were finalized for prototype procurement and testing. These pistons exhibited beneficial characteristics, from CFD simulations, predominantly in particulate matter (PM) and efficiency metrics relative to baseline piston geometries. Due to the unconventional geometry, structural FEA was completed and identified a ring-pinching issue. This issue was resolved by increasing the ring groove height for safe testing. The five pistons procured were tested in one of Caterpillar's heavy-duty single cylinder test engines (SCTE) over eight different speed and fueling conditions, with and without EGR, and with different levels of injection pressure, injection timing, and injection shot mode. Figure 29 shows the the top-view picture of the selected pistons prior to testing. The engine load range was from 1000kPa to 2600kPa IMEPn.

Figure 29: The five procured innovative pistons predicted to have benefits in PM and efficiency

Figure 30 and Figure 31 show a selection of the key emissions and efficiency tradeoff curve results, generated by sweeping start of injection, for the relevant operation condition of the H2D2 machine applications. The emissions and BSFC are raw and uncorrected single cylinder data, so they should be treated as useful relative comparisons. Caterpillar's Tier 4 Final "T4F" combustion system is plotted as the baseline and can be seen to be the lowest BSFC in Figure 30. The soot response of the innovative pistons can be lower in Figure 31, but at the expense of ~1% efficiency. For clarity, the "6R-2 Step" and "2 Step" bowls are not shown, as both exhibited higher soot levels than the other options under consideration.

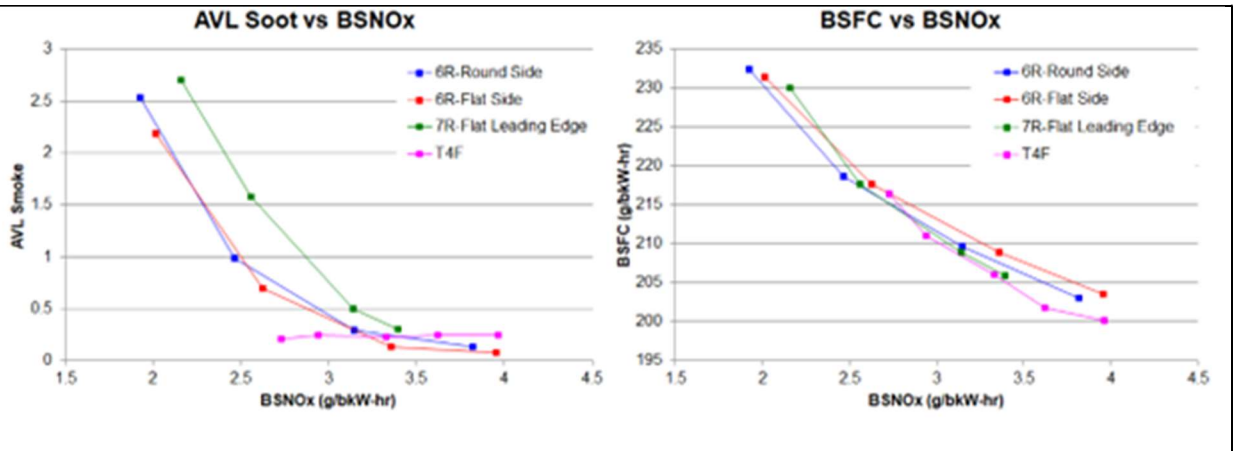

Figure 30: Innovative piston SCTE emissions and fuel consumption tradeoff curve results for 1425rpm, 265g/min (2550kPa IMEPn) fueling, 14% EGR and 160MPa rail pressure.

The high EGR condition of Figure 31 illuminates the combustion system differences by being lower NOx and higher soot than would actually be run with the H2D2 high-NOx conversion aftertreatment system. At this condition it again can be seen that the T4F combustion system is the most efficient but followed closely by the "6R-Round" and "7R-Flat Leading Edge" pistons. The 6R innovative pistons reduce soot significantly, which successfully confirms one of the design intents. The 7R piston moves to higher soot, indicating that it is a candidate that is not good for the H2D2 applications (which will have EGR).

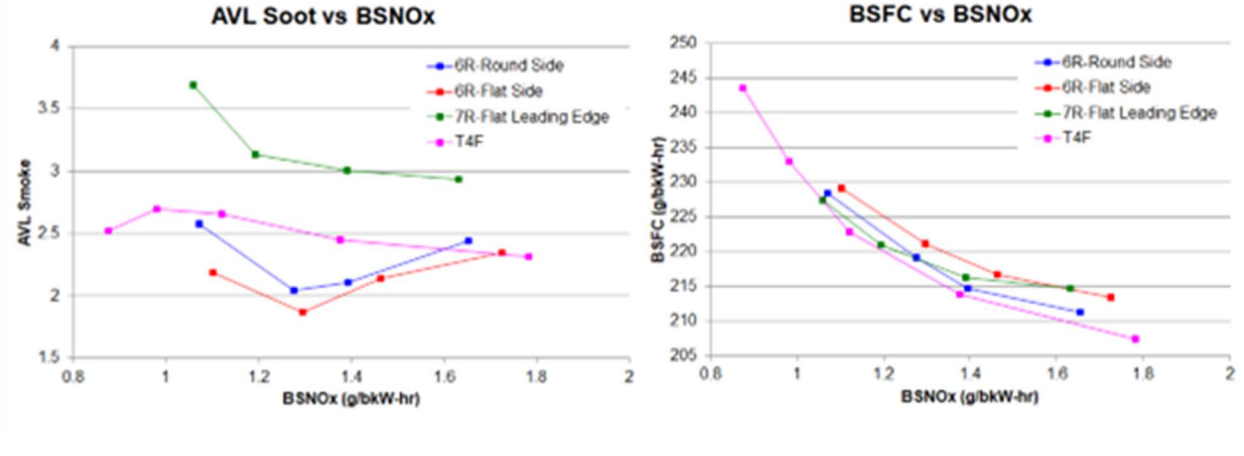

Figure 31: Innovative piston SCTE emissions and fuel consumption tradeoff curve results for 2100rpm, 317g/min (2000kPa IMEPn) fueling, 23% EGR and 220MPa rail pressure.

The innovative piston testing pointed toward limited to no efficiency benefit beyond the baseline T4F piston and combustion system. However, the efficiency data is closely grouped for the T4F and 6R-Round Side pistons with a slight soot advantage for the 6R-Round side. At the present time, the non-axisymmetric 6R-Round is believed to be too complicated for Thermal Barrier Coating (TBC) processing. Based on these results, the final demonstration did not include any non-axisymmetric pistons.

Thermal Barrier Coatings

TBC samples were received from suppliers early on in the program, with two sets of ceramic thermal spray TBC samples seen in Figure 32. The samples were a circular steel substrate with varying coating property, thickness, and surface roughness. These samples were utilized for physical coating property understanding and bench testing.

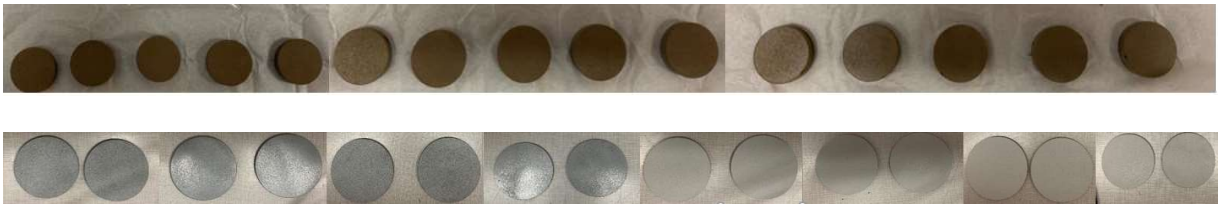

Figure 32: TBC samples received from two different suppliers

Using the property information of the TBC's in the expected manufactured state, 1D DYNASTY engine-only simulations were completed. DYNASTY has the ability to model the different thermo-physical properties of the combustion chamber surfaces, and a model was built where the TBC properties could

be applied and varied. The model simplifies each surface as a uniform boundary but captures the temporal heat convection/conduction in a continuous manner. Figure 33 illustrates this temporal behavior for the piston surface temperature and heat transfer rate for three different conditions. The speed/load evaluation points and full engine map is also shown.

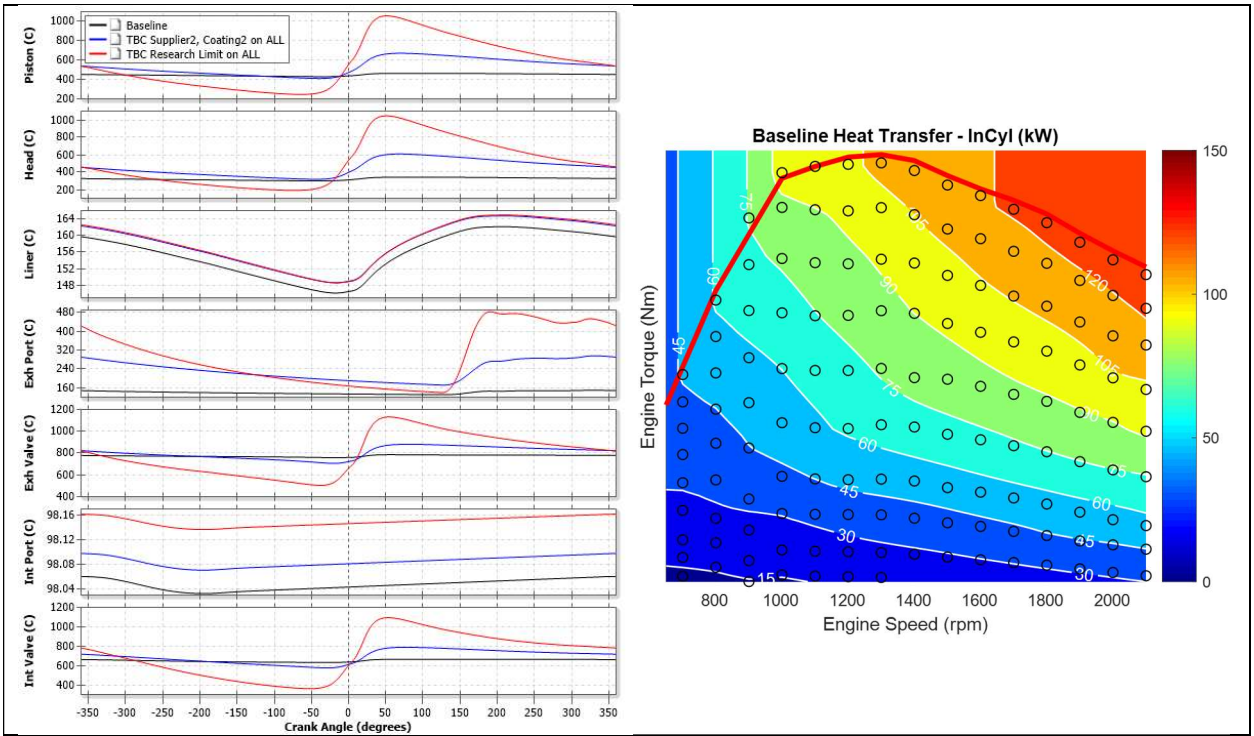

Figure 33: 1D DYNASTY engine simulations of TBC's showing the temporal surface temperature behavior (Left) and the entire speed/load map evaluated (Right)

Efficiency, or BSFC, results are presented in Figure 34 and Figure 35 as percent differences between the baseline engine model with normal components and the model setup with TBC surfaces. The reader should disregard the contour plot noise at the low loads. 1.0 to 2.0% benefit can be seen from coating all of the combustion chamber surfaces with supplier #2's second TBC variant. A theoretical far-term research TBC limit is presented for comparison using property information gathered from recent literature[6]. Supplier #1 and #2 TBC coatings of the piston-only are predicted to be very similar and in the range of 0.5 to +1.0%. It should be noted that the impact of TBC's is surprisingly predicted to be uniform across the speed/load map due to a simultaneous offsetting of heat transfer reduction with heat transfer apportionment of fuel energy, i.e. TBC's reduce the heat transfer more at times when heat transfer is naturally a lower amount of fuel energy loss.

[6] Schaedler, T., Hughes Research Laboratories., "Temperature Following Thermal Barrier Coatings for High Efficiency Engines," U.S. Department of Energy Vehicle Technologies Office 2020 Annual Merit Review and Peer Evaluation Meeting, June 1-4, 2020.

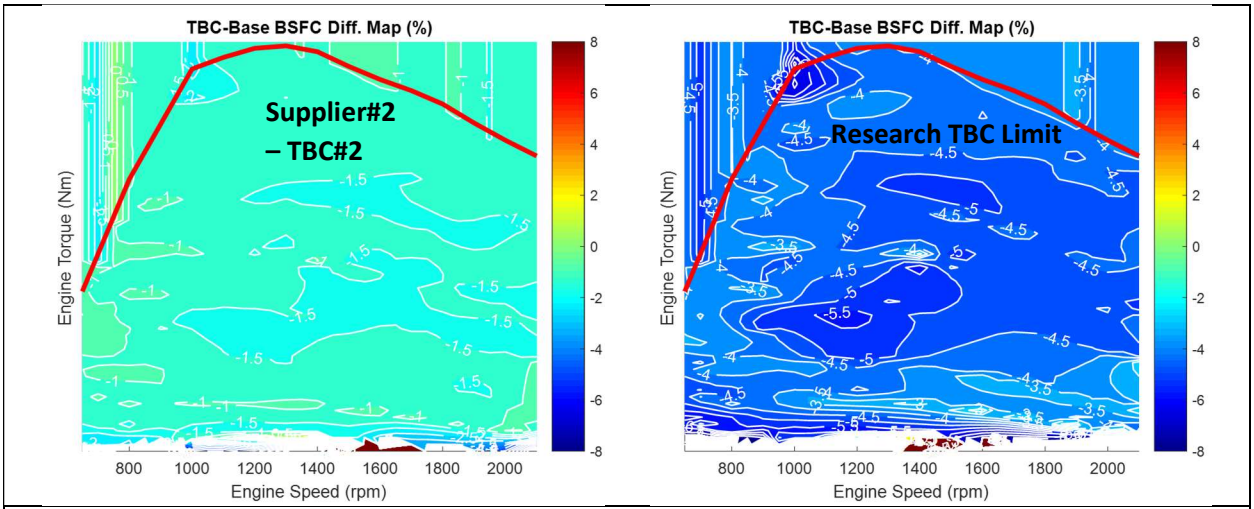

Figure 34: BSFC benefit ("-"%) predictions for the different TBC coatings applied to: all combustion chamber surfaces except the cylinder liner, and the exhaust port

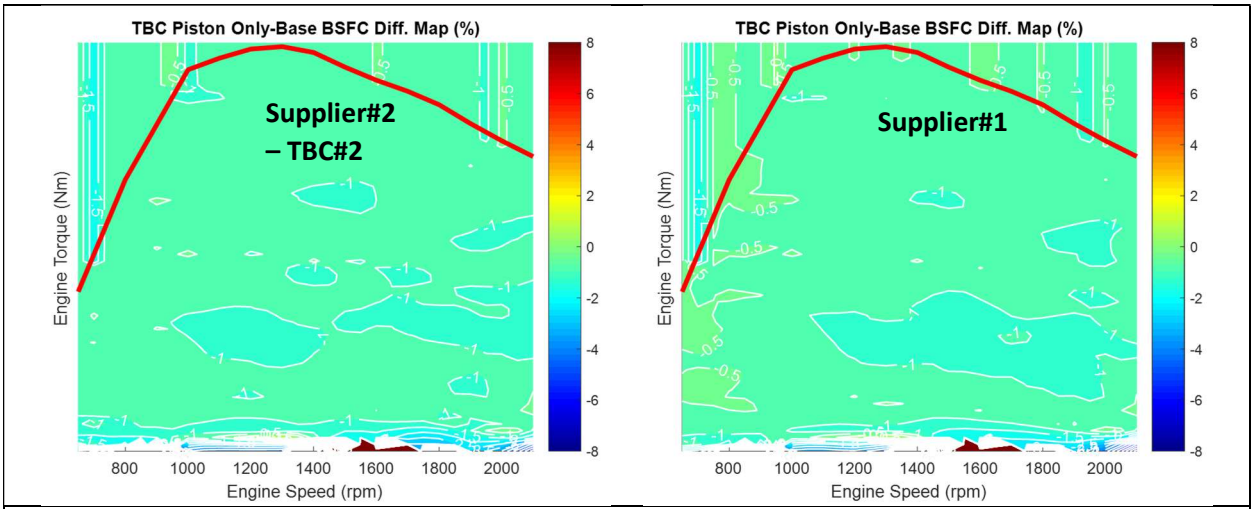

Figure 35: BSFC benefit ("-"%) predictions for the different TBC coatings applied to: piston crown only

To aid in the analytical understanding, full-cycle CFD was completed for Supplier #1 and Supplier #2 TBC coatings. Two consecutive engine cycles were simulated to allow for a reasonable convergence (temporal history) of the surface temperatures. Piston, valve, cylinder head, and exhaust port surface boundaries were applied with TBC properties in the CFD code, Figure 36. Three different combinations of coating locations were simulated: piston only, piston and valve faces, and all. Additionally, three different thickness were simulated, and some work did investigate simulating the impact of surface roughness differences between the TBC's and baseline materials. The conclusions and direction from the 3D simulation effort were as follows and agreed with the general efficiency range as predicted by the 1D simulations.

- 7 to 23% in-cylinder heat transfer reduction range
- 0.4 to 1.7% ISFCn improvement range
- Supplier #2 Coating #2 shows more ISFCn benefit than Coating #1
- Piston and valve face coating are ~2/3 of the ISFCn benefit range and should be pursued

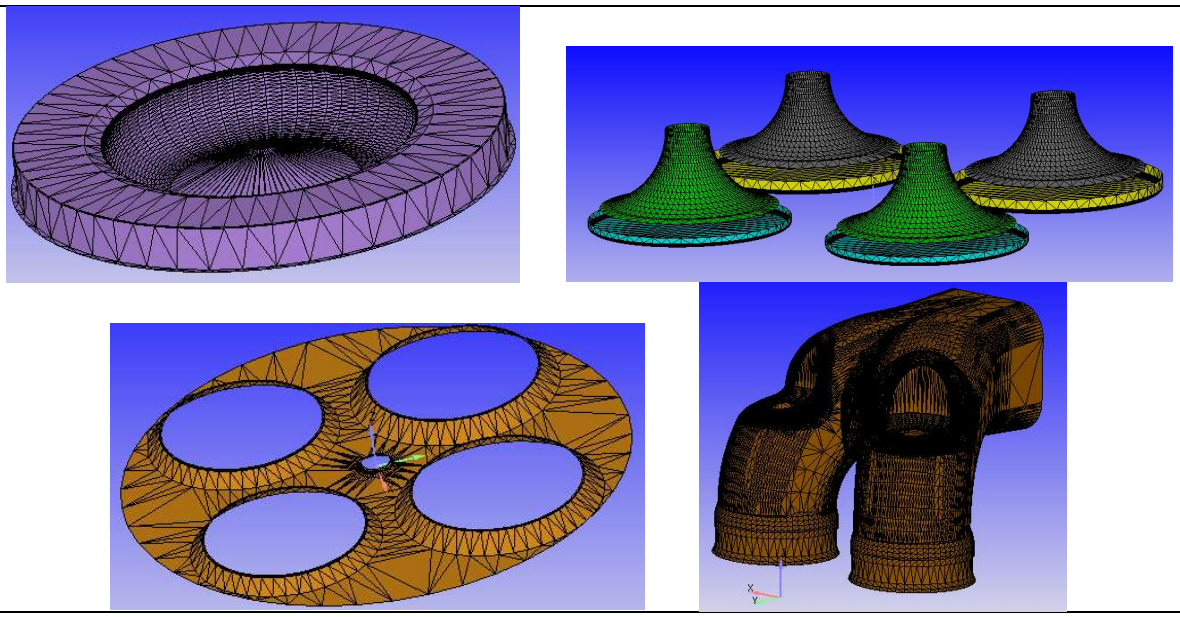

Figure 36: CFD surfaces where TBC properties were applied: Piston, valves, cylinder head, exhaust port.

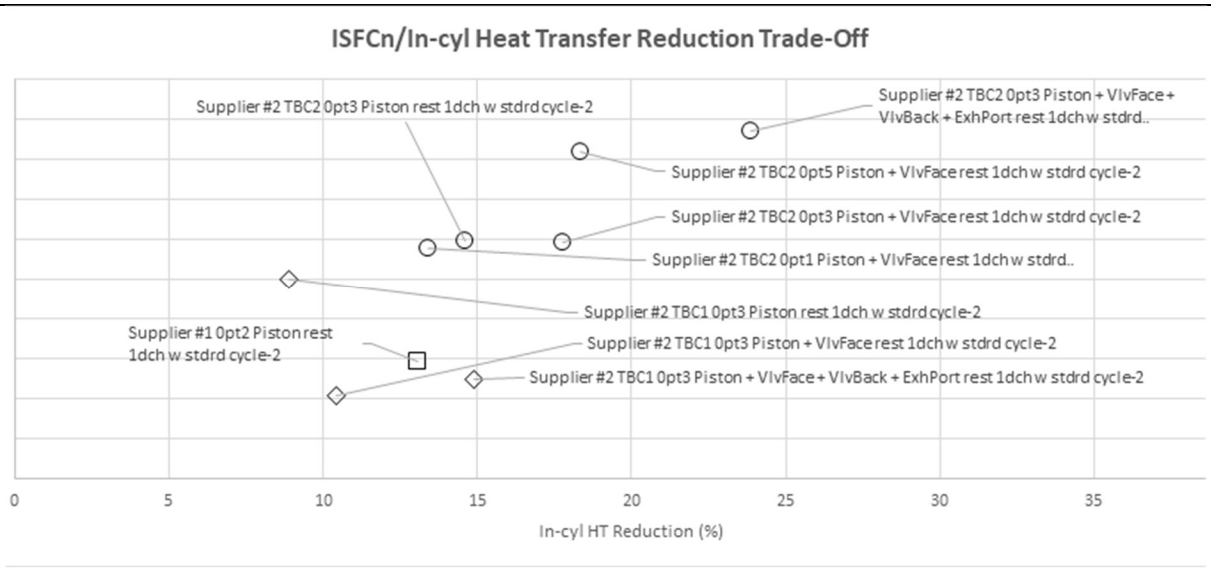

Figure 37: CFD predictions of TBC impact on heat transfer and ISFCn reduction (+Y Axis Direction).

Moving beyond the simulations, TBC component testing was conducted within the early phases of the program utilizing the same heavy-duty single cylinder test engine as the aforementioned piston design work. Similar engine configurations and experimental boundary conditions were used, and over 20 different operating conditions were screened with injection timing sweeps. Multiple sets of pistons from the multiple suppliers were evaluated over the course of the work, and included repeat data sets and iterations on geometry, material, and surface roughness. An example of the TBC pistons after being tested is shown in Figure 38 and includes an example of a piston TBC which exhibited coating delamination; however, the testing did have samples with successful durability results.

Figure 38: Tested TBC pistons in the SCTE showing soot deposits, successful coating adhesion, and coating delamination (right piston)

The overall performance and efficiency impact was one of limited success and confounding results. Indicated and brake measurements were used to compare efficiency and performance results, along with measurements of heat rejection from the oil and coolant systems. Comparisons between steel pistons and TBC coated pistons targeting the same geometry only found limited times of outright efficiency benefit. Figure 39 demonstrates one of the limited times of observed benefit, and efficiency numbers are not applicable to the concept 13L as the SCTE was not correlated, so again they should be treated as useful relative comparisons. This data shows a clear reduction in BSFC for a constant NOx and combustion phasing, just as the simulation and theory would predict. However, this was a limited example of a clear efficiency benefit and Figure 40 better describes the macroscopic efficiency trend from the many sets of data. In aggregate there is no distinct shift in efficiency in Figure 40 and there was found to be difficulty in repeating the conditions where efficiency benefits were observed – the recent literature contains similar such conclusions and experiences[7]. The role of natural engine variability from assembly and reassembly, data acquisition, and deposits on the combustion chamber surfaces are believed to add noise to system and make the problem confounded.

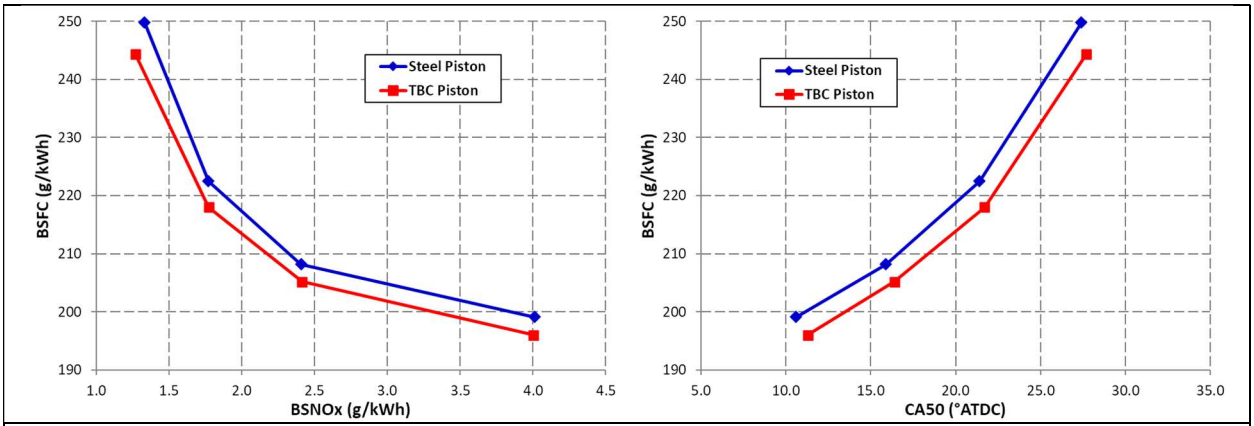

Figure 39: A example of an observed high load brake efficiency benefit in both NOx and combustion phasing space - 1800rpm, 1700kP BMEP

[7] Somhorst, J., Oevermann, M., Bovo, M., and Denbratt, I., "Evaluation of Thermal Barrier Coatings and Surface Roughness in a Single-Cylinder Light-Duty Diesel Engine" International Journal of Engine Research, October 2019, https://doi.org/10.1177/1468087419875837.

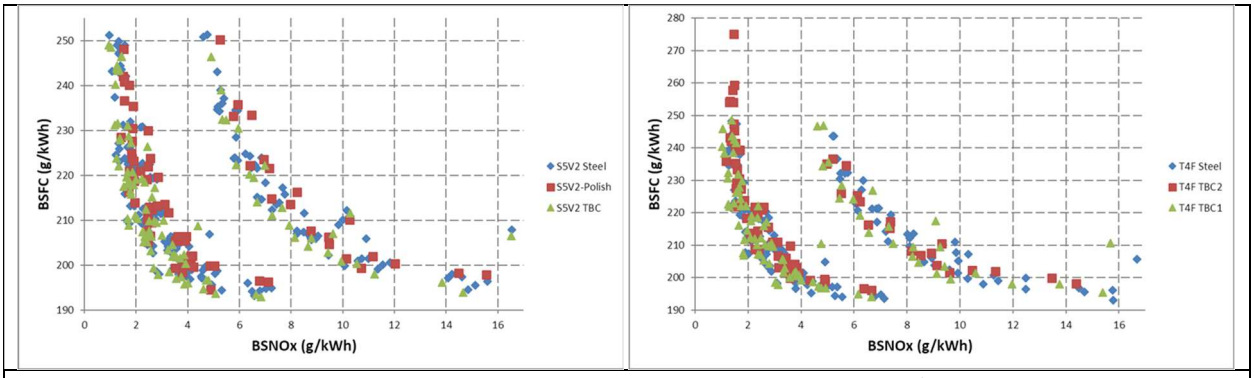

Figure 40: Tested TBC pistons in the SCTE showing macroscopic efficiency/NOx trade-off over all of the operating points evaluated

To understand the TBC intrusiveness to the heavy duty diesel combustion system (with significant jet-wall interaction) a detailed investigation was performed interrogating the net piston bowl shape accuracy, and surface roughness on combustion and engine performance. The investigation used optical diagnostics in conjunction with the obtained SCTE data and should be referenced for extended information[8]. The conclusions for the H2D2 program from the testing phases of the TBC work were:

- Coatings with sufficient durability were identified for prototype multicylinder testing with duration limits of 500-1000 hours
- Limited sets of operating conditions show consistent improvements in brake efficiency
- The improvement or change in efficiency is within the variability of testing and rebuilding the engine, which confounds deterministic comparisons
- The accuracy of the net piston bowl shape is paramount and small (~0.1mm) deviations in critical areas can negatively impact the fuel-air mixing energy and speed of heat release
- The surface roughness in the ranges investigated (1-10 µm) has a secondary impact on fuel-air mixing relative to the piston bowl shape accuracy
- TBC pistons and components with high geometric accuracy should be included in the Phase 2 hybrid engine demonstration despite the difficulty in isolating direct efficiency benefits – any reduced heat transfer can also be beneficial to the system via turbocharging and turbocompounding

[8] Koci, C., Svensson, K., Martin, G., Kim, C., et al., "Optical Imaging for Understanding of Thermal Barrier Coated Piston Engine Performance," presented at THIESEL 2022 Conference on Thermo- and Fluid Dynamics of Clean propulsion Powerplants 2022, Spain, September 13-16, 2022.

3.2. Major Subsystem Analysis & Specification

3.2.1. Variable FEAD Design & Simulation

SOPO ID #	Item Title	Item Description	Start Date	End Date	Status
Task 1.3	**Variable FEAD Design & Simulation**	Clutch and variable front-end accessory drive design, analysis, simulation and subsystem controls development	7/1/2019	1/31/2021	100% Complete

The variable FEAD integration design was focused on several different concepts on how the Superturbo was driven. The main areas of concern for concept selection were packaging, performance, and efficiency. Leading concepts were high-speed flywheel (HSFW) driven, crankshaft/belt driven, and electrically/MGU driven. For the HSFW driven configuration, interference issues were found with the engine. The combination of the SuperTurbo turbine inlet placed near the exhaust manifold and HSFW transmission placement in relation to the crankshaft resulted in few options to work around the interference, Figure 41.

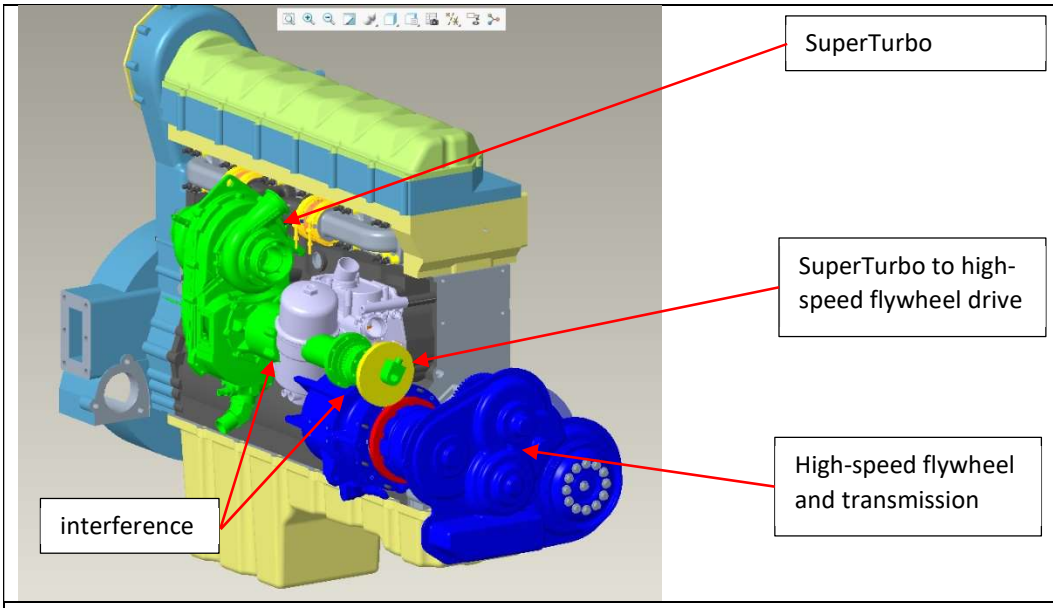

Figure 41: SuperTurbo and HSFW interference with engine

In terms of performance, it was found that the HSFW driven SuperTurbo concept would result in either limited HSFW speed range or turbo-shaft speed range, Figure 42. For the HSFW desired speed range, the SuperTurbo CVT ratio spread was not large enough to cover the desired turbo speeds for all operating conditions. At higher flywheel speeds, the minimum attainable turbo speed is higher than desired which would add losses due to over-boost or waste gating. At lower flywheel speeds, the maximum attainable turbo speed is lower than desired which would cause performance deficiencies. Controls complexity would also be added due to the coupling of the devices. Due to the performance and packaging concerns the HSFW driven SuperTurbo concept was eliminated as an option.

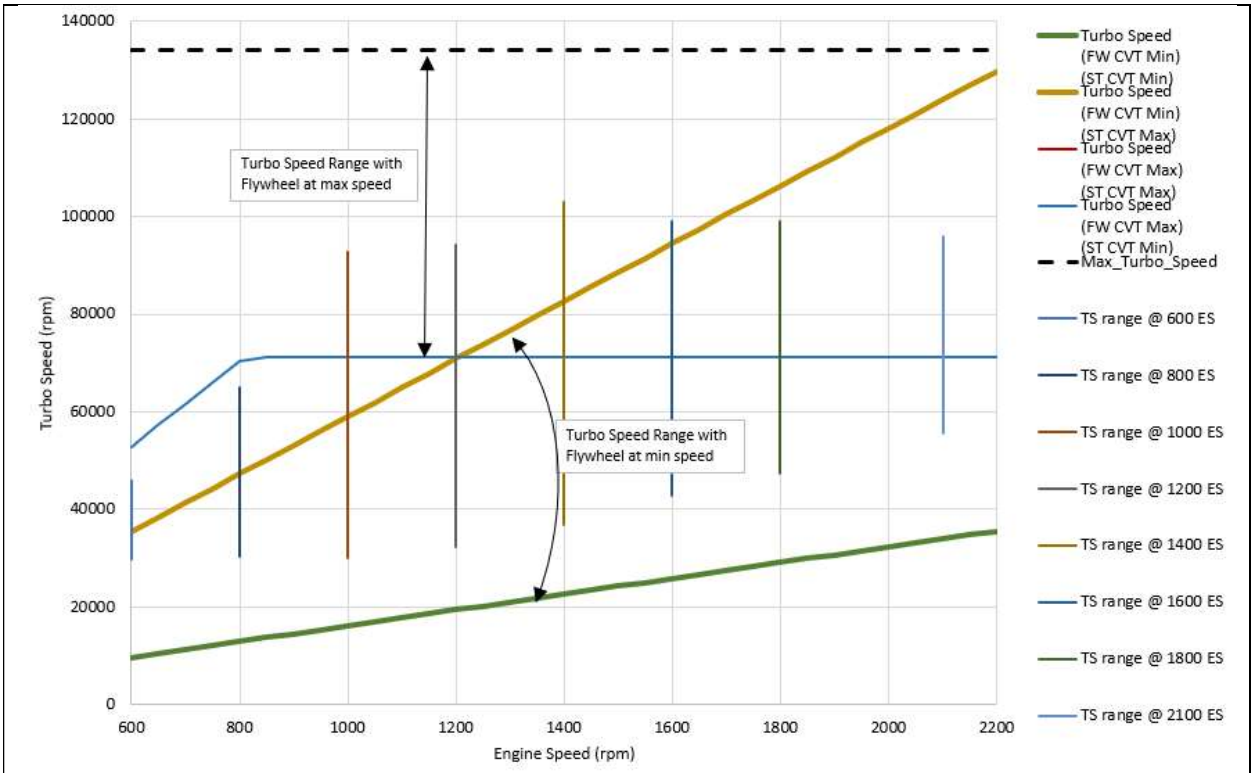

Figure 42: SuperTurbo turbo speeds when driven by high-speed flywheel (HSFW). When HSFW is at higher speeds, desired turbo speeds (vertical lines) are not attainable on the lower end. When HSFW is at lower speeds, desired turbo speeds are not attainable on the upper end.

Packaging analysis for the crankshaft/belt driven and electrically/MGU driven concepts found either was acceptable. For the crankshaft driven concept, the leading design was to drive off the rear geartrain of the engine to not interfere with the HSFW or FEAD components. The MGU driven variation would just replace the belt drive and shaft with an MGU and be connected to the 48V battery system. Additional activities were performed with most of the work involving DYNASTY simulations to evaluate the efficiency, maximum power, and response differences between the concepts. Initial steady state analysis showed an average of 3% efficiency advantage with the mechanical CVT vs. the MGU driven concept for turbo-compounding. See the Figure 43 efficiency plot showing both concepts at varying power levels. Based on this, and implementation efficiency, the rear geartrain mechanical CVT concept was selected.

From concept selection, detailed integration design work was completed involving the PTO integration, belt drive, and mounting. The integration design went through several iterations in conjunction with the core engine, flywheel housing and test stand design, Figure 44. Additional bosses were added to the engine block to allow for the most durable structure. Many belt tensioner concepts were evaluated for packaging and shaft loading. Design concepts were created, evaluated, and selected for the compressor inlet and turbine outlet and their connections to the test facility.

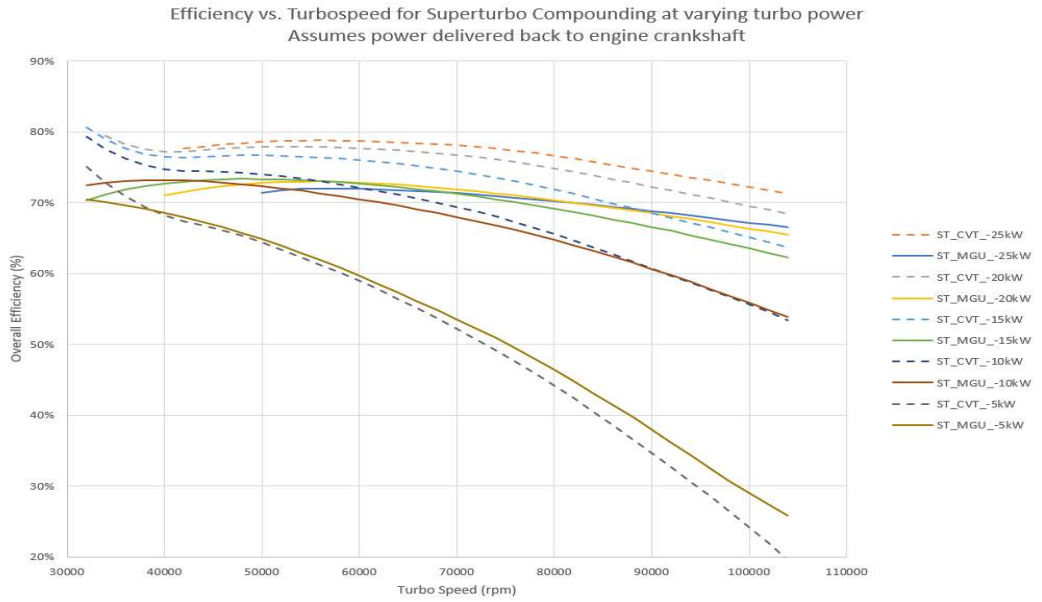

Figure 43: Steady state analysis of mechanical CVT driven SuperTurbo vs. MGU driven

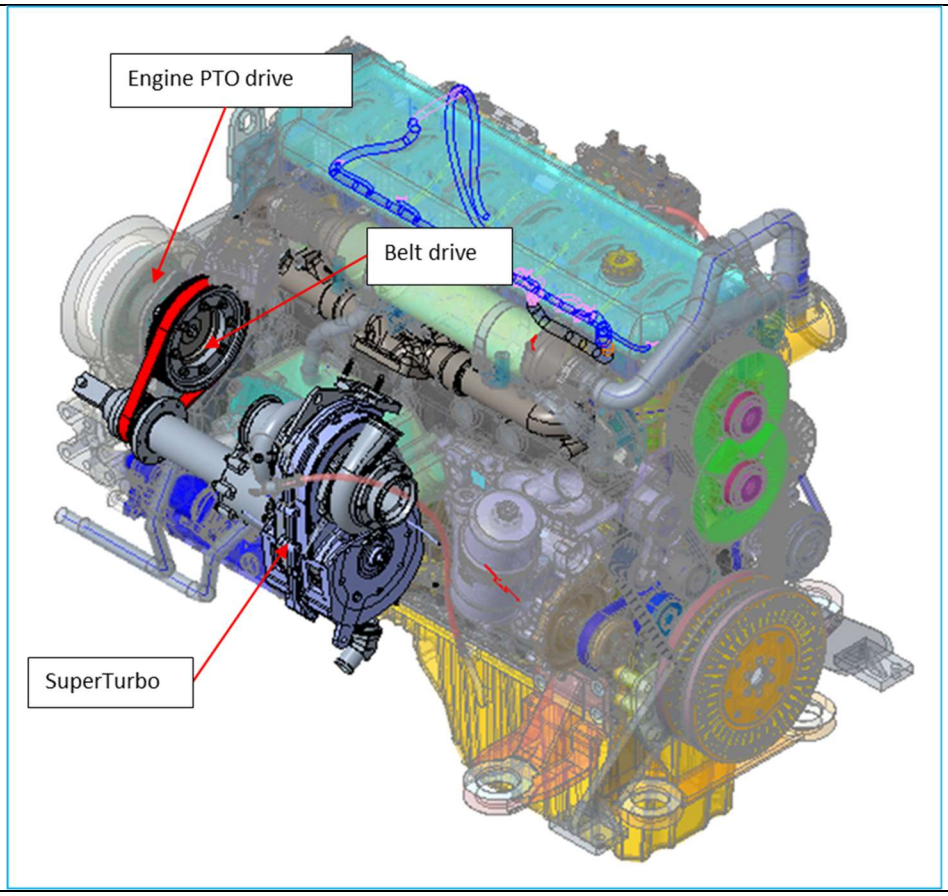

Figure 44: Initial SuperTurbo integration onto concept engine

One of the major changes involving the design was the integration with the engine PTO. In an effort to reduce prototype cost and parts, a gearbox was internally designed to allow the use of the simpler "Industrial" PTO housing instead of the original, unnecessarily strong and longer lead-time, "Heavy Duty" PTO. The SuperTurbo was changed to be driven off the rear face of the industrial PTO instead of the front face of the Heavy Duty PTO which was originally planned. From the output of the gearbox, a stock sized Gates pulley and belt were used to integrate with the SuperTurbo. This setup allowed for a ratio of 3.133 to the SuperTurbo and demonstrated to Caterpillar how the SuperTurbo drive may be highly configurable to different PTO arrangements through gearbox and pulley drive solutions.

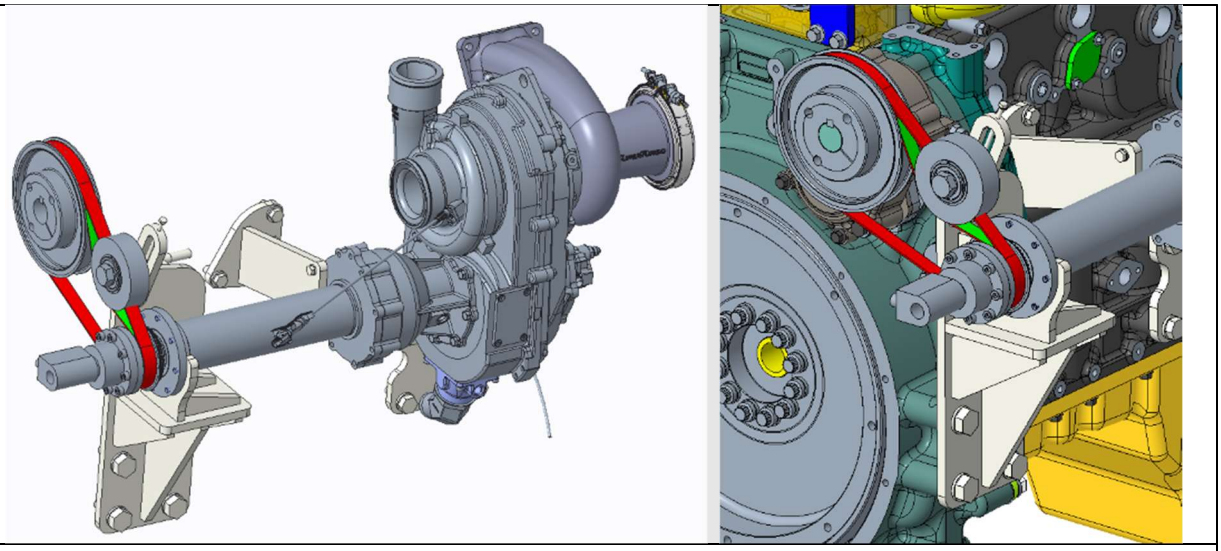

Figure 45: SuperTurbo integration design to PTO.

Figure 46: Assembled PTO Gearbox

The SuperTurbo mounting scheme consists of bolting a bracket group to the flywheel housing and two locations on the engine block. Each bracket supported a different section including the input shaft, clutch housing, and main housing.

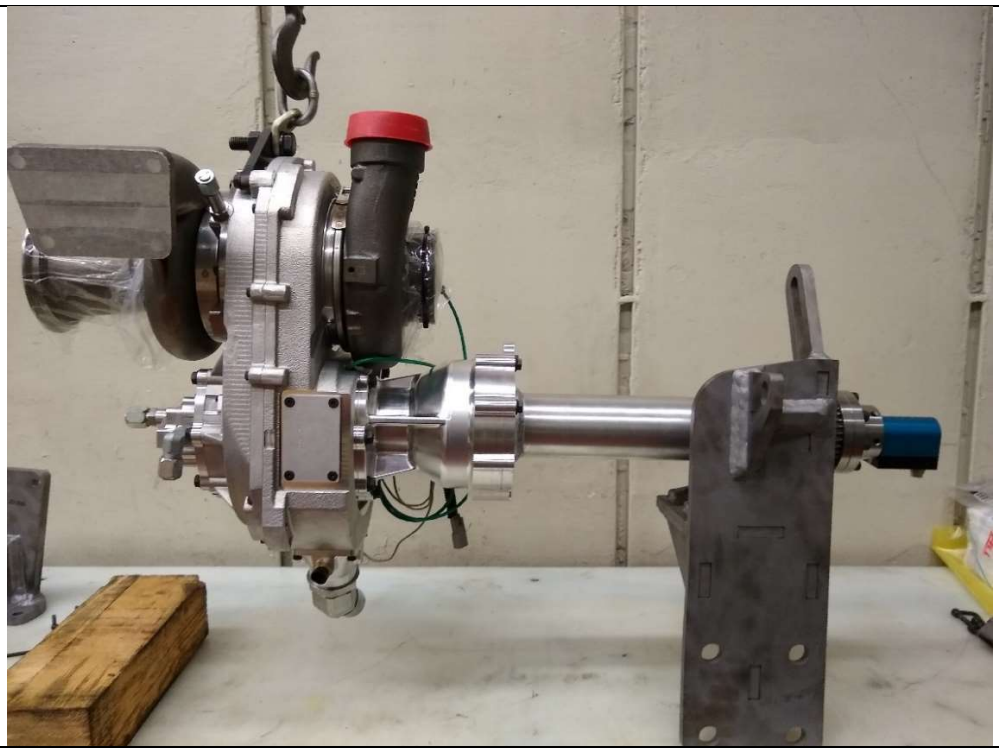

Figure 47: Initial PTO housing bracket fit up to SuperTurbo

After the drive configuration was finalized, brackets were designed and modified through several FEA simulations to reach the highest vibration levels within the time constraints. The mounting system for the SuperTurbo resulted in a lowest natural frequency of 228 Hz with the target greater than or equal to two times the maximum engine firing frequency, or 240 Hz. This capacity is judged sufficient for the limited hour testing for this project and given the fact that the vast majority of testing will occur at engine speeds below the maximum firing frequency. Modal analysis is shown as Figure 48.

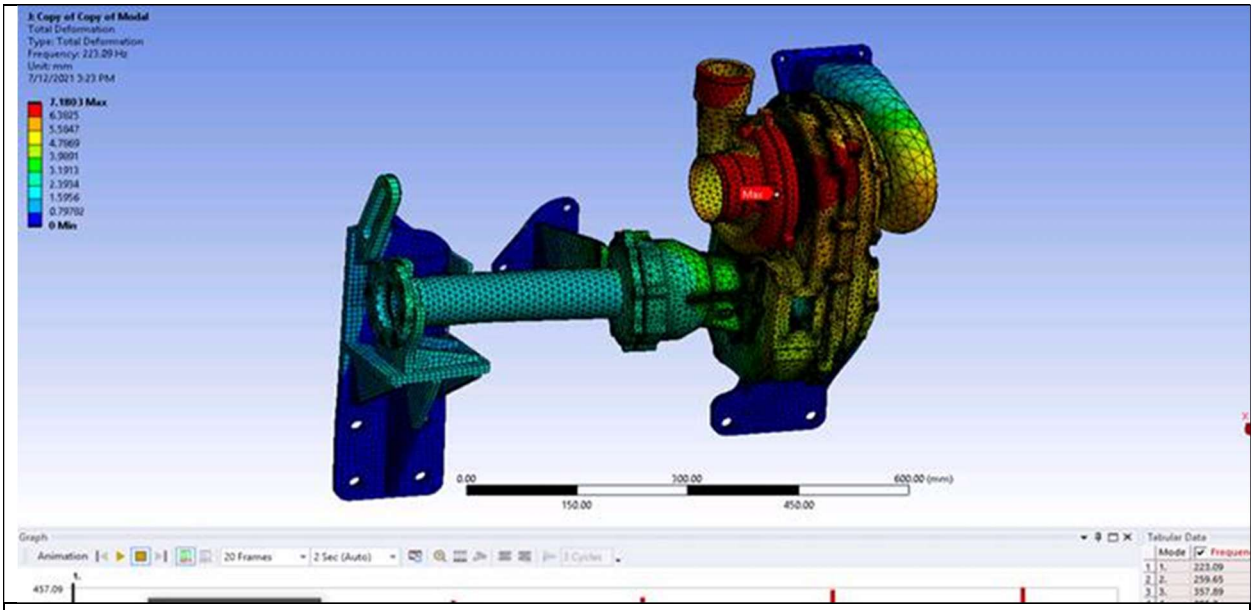

Figure 48: SuperTurbo Support Structure FEA Modal Analysis

The 48V MGU was integrated on the front of the engine separate from the SuperTurbo. The design considered many factors including packaging, torsional vibration, and drive system. For easier implementation for the testbed, the MGU was integrated on a separate belt drive system whereas on a machine application the intention would be to replace the alternator and exist on the main belt drive. The available space claim and engine torsional data were provided to the belt drive supplier and a tensioner and crankshaft decoupler drive pulley for our application was designed. The belt tensioner was designed to provide correct belt tension with the MGU either motoring or generating power. The decoupler pulley was recommended to isolate the belt drive system from the torsional dynamics of the engine.

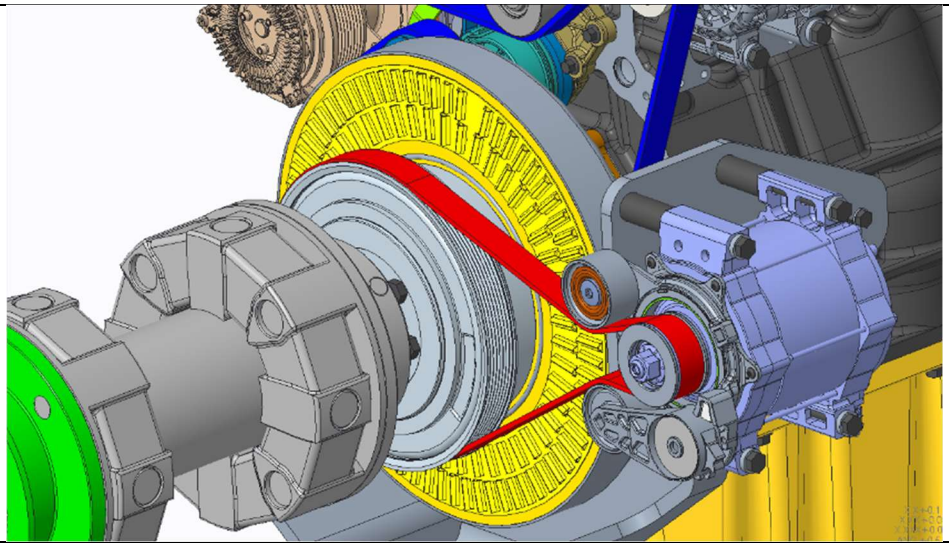

Figure 49: 48V MGU, bracket, decoupler, and tensioner

Start/Stop Analysis

As part of the FEAD analysis and simulation, controls were developed, and simulations were performed involving engine stop-start. The requirements specified for start/stop were 120 seconds maximum off-time and required power of 4 kW to support air conditioning and electrical loads. When an engine stop is triggered, the control first charges the HSFW and/or battery depending on their state of charge and maximum charge time allowed. After the engine is stopped and disconnect clutch is opened, the MGU controls speed while the HSFW is discharged to supply the needed power. After the HSFW power is exhausted or minimum threshold is reached, the battery is then discharged.

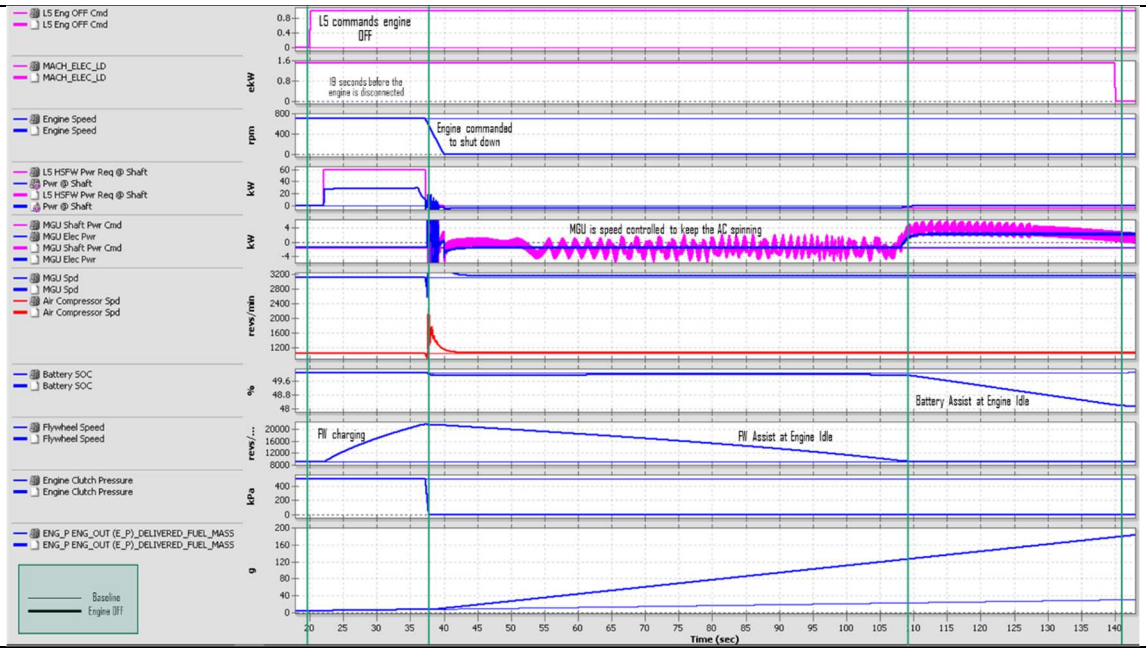

Figure 50: Start/stop simulation results

Another part of the stop-start analysis involved the quantification of possible fuel savings. The start/stop analysis process is documented in Figure 51 and involves accessing Caterpillar's machine telematics database (SC2). Suitable machines were found for the three key project applications and data was processed to understand the fuel consumption opportunity during machine idle periods. For each of the three applications, five to ten machines were analyzed over an entire calendar year. The range of operation hours was from hundreds to thousands during this period, varying by machine and machine location. The idle speed for the 745AT was 675-725rpm, for the 988K it was 700-800rpm, and for the 390F it was 975-1075rpm. Generally, these machines idle for 10-35% of the operation time.

A simple fuel savings fraction (FSF) formula was generated with two reduction factors which deteriorate the savings, Equation 1. Here FRi is the idle fuel rate, FRw is the working fuel rate, and xi is the idle time fraction. The first factor (k1) accounts for debounce time (the time required to wait until the engine can be turned off once idle is detected), a less than infinite engine-off time, and the energy required to restart the engine. The second deterioration factor (k2) accounts for the recovery of energy required to power the hotel load during the engine-off idle time.

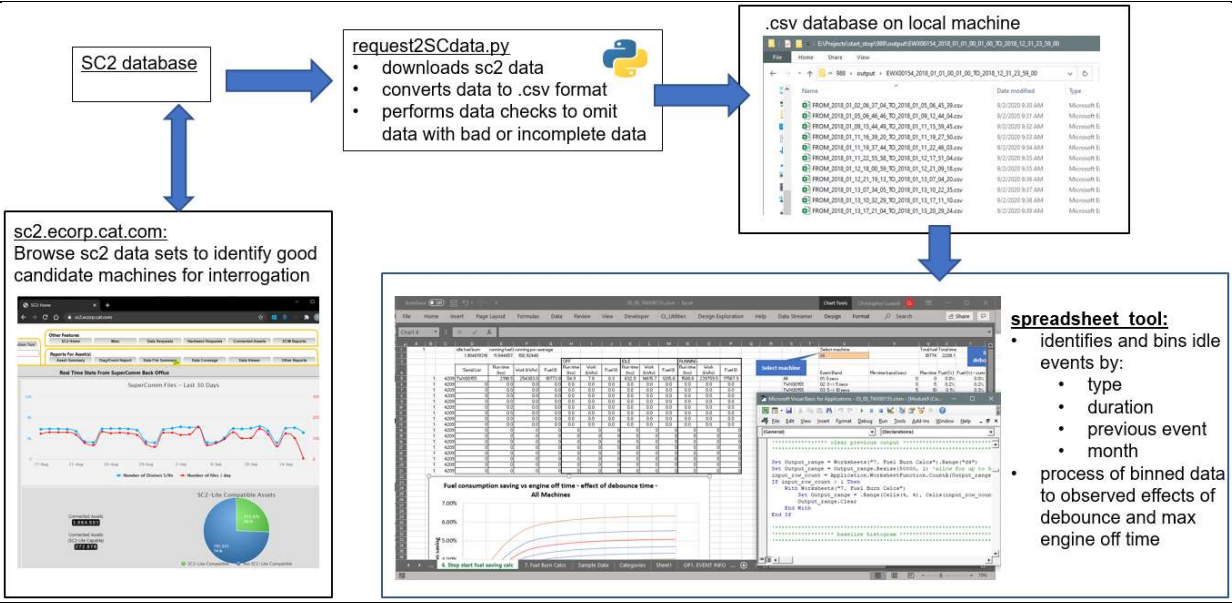

Figure 51: Machine start/stop analysis process using the Caterpillar Super Comm 2 (SC2) machine telematics database.

$$FSF = x_i * \frac{FR_i}{x_i * FR_i + (1 - x_i) * FR_w} * k_1 * k_2 \qquad \text{Equation (1)}$$

Figure 52 shows the magnitude of k1 for reasonable settings (debounce of 10 seconds and maximum engine off time of 300 seconds) and how the engine restart energy further lowers k1. The calculations use average machine PDF's of the idle opportunity time from the SC2 database.

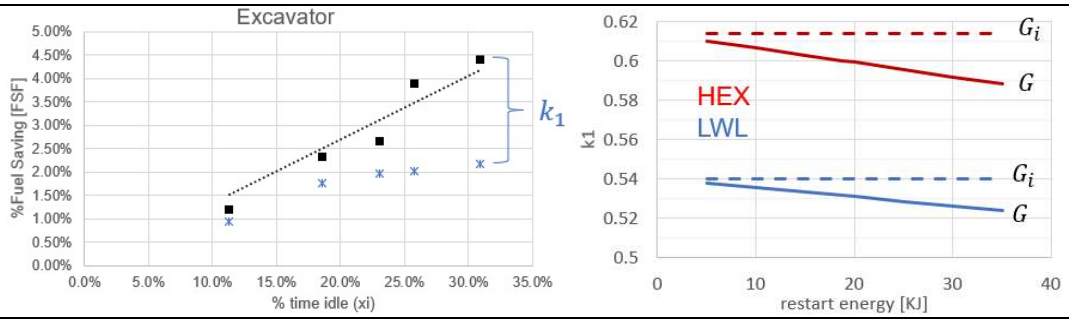

Figure 52: Left – k1 deterioration factor fuel savings reduction example, Right – restart energy impact on k1

The influence of the idle efficiency, or BSFC, on the k2 deterioration factor can be seen Figure 53 as a function of the ratio of the hotel power to the total idle power (friction + hotel). The final details of the summary of the analysis are in Figure 54, where a k1 factor of ~0.6-0.7 and a k2 factor of ~0.7-0.8 were found. Details about the idle load, hotel power, and modeled savings can also be viewed.

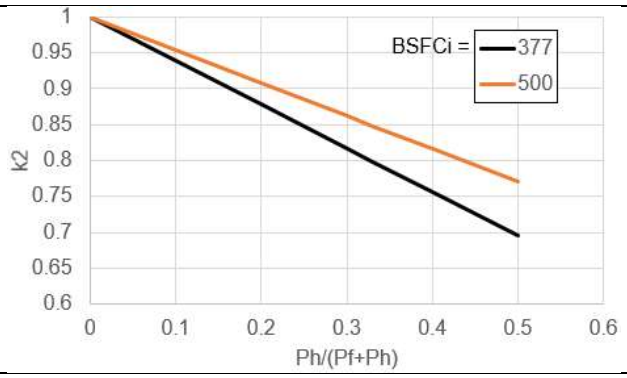

Figure 53: k2 deterioration factor change with idle BSFC and hotel/friction power factor (X-axis).

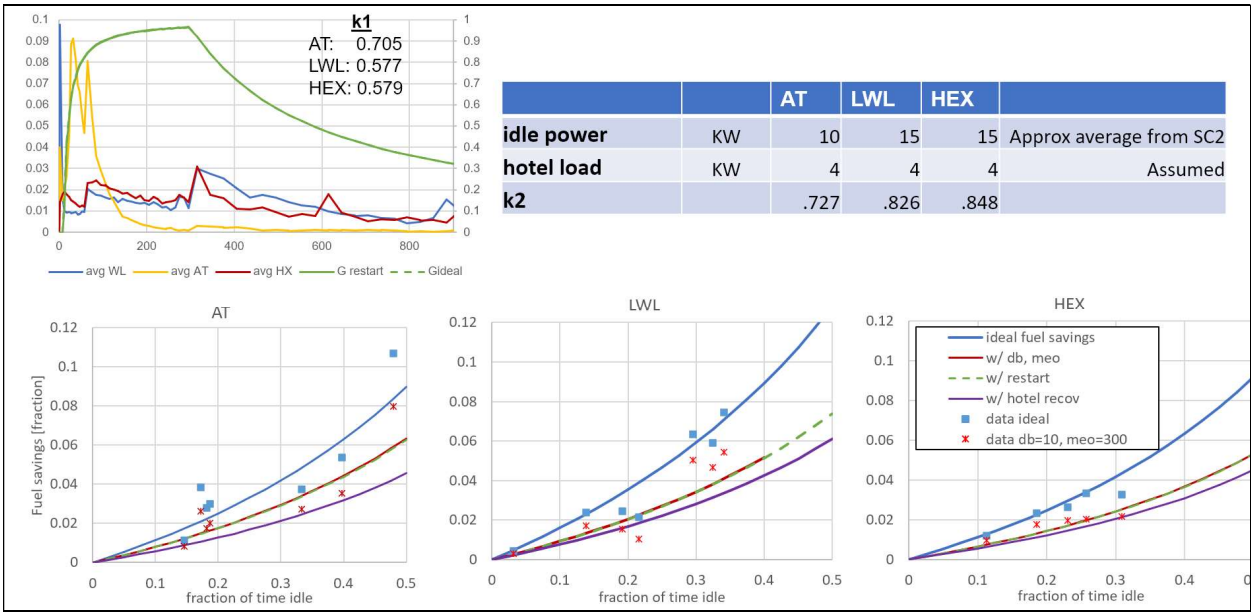

		AT	LWL	HEX	
idle power	KW	10	15	15	Approx average from SC2
hotel load	KW	4	4	4	Assumed
k2		.727	.826	.848	

Figure 54: Start/stop summary showing ideal, modeled and actual SC2 data fuel savings.

The final summary of the analysis found the following start/stop fuel savings for the three key machine applications, using the assumption that the machines will remain unchanged and only the hybrid powersystem will be installed:

Table 3: Summary of Fuel Savings due to Start-Stop	
745AT:	0.6 – 2.6%
988K:	0.8 – 3.5%
390F:	0.6 – 2.8%

This range stems from applying the 10-35% idle time range to the FSF model (purple line in Figure **54**) which has a 10 second debounce, 300 second maximum engine off time and 4kW hotel load recovery accounted for.

3.2.2. SuperTurbo and Turbocompound Development

SOPO ID #	Item Title	Item Description	Start Date	End Date	Status
Task 1.4	**Turbocompound Development**	Analysis and decision for electrical vs. mechanical turbocompound. Design specification and engagement of vendor	3/1/19	12/31/2020	100% Complete

With the project goal of demonstrating 17±2% improvement in fuel consumption, partially through aggressive 30% engine downsizing, a necessary technology building block is a turbocharger with *power access to the turbo shaft*. This means a mechanism for adding power to the turbo shaft during transient events to assist turbo and engine response (so that the 13L engine can be as productive as an 18L engine), and a mechanism for removing power from the turbo shaft at full load to recover excess exhaust energy and convert it into fuel consumption benefit via turbocompounding. This access to turbo shaft power can be achieved either electrically, by putting an electric motor-generator on the turbo shaft, or mechanically, with a mechanical drive and speed reduction system. For this demonstration project, the mechanical system was selected for the following reasons:

1. A mechanical energy storage system in the form of a high-speed flywheel was already planned as part of the powersystem solution, so a mechanical shaft-access turbo kept open the possibility of direct mechanical interaction between the turbo and the high-speed flywheel, see Concept 1 in Figure 10 (though this specific system configuration of a direct coupling between turbo and flywheel was ultimately rejected for packaging and speed-compatibility reasons, see Figure 42).
2. There were concerns that an electric turbo based on a 48V system would not have sufficient continuous power capability to deliver the turbocompound levels required to maximize waste heat recovery over a heavy-duty high load-factor machine application cycle. Compounding power levels approaching 30kW were expected to be required for optimum system performance.
3. SuperTurbo Technologies has been developing and demonstrating their mechanical shaft-access turbocharger (or “driven turbocharger”) for heavy-duty applications and could readily supply a customized demonstrator unit for this project.

The SuperTurbo uses a high-speed traction drive system on the turbo shaft and a continuously variable transmission to deliver power to or from the turbocharger shaft as required. This system enables the SuperTurbo to move seamlessly between turbo assist, free-floating, and turbocompound operation. The SuperTurbo that was delivered to Caterpillar for the demonstration is shown in Figure 55. A belt-drive at the end of the shaft on the right in the figure connects the SuperTurbo to the engine crankshaft via the rear geartrain.

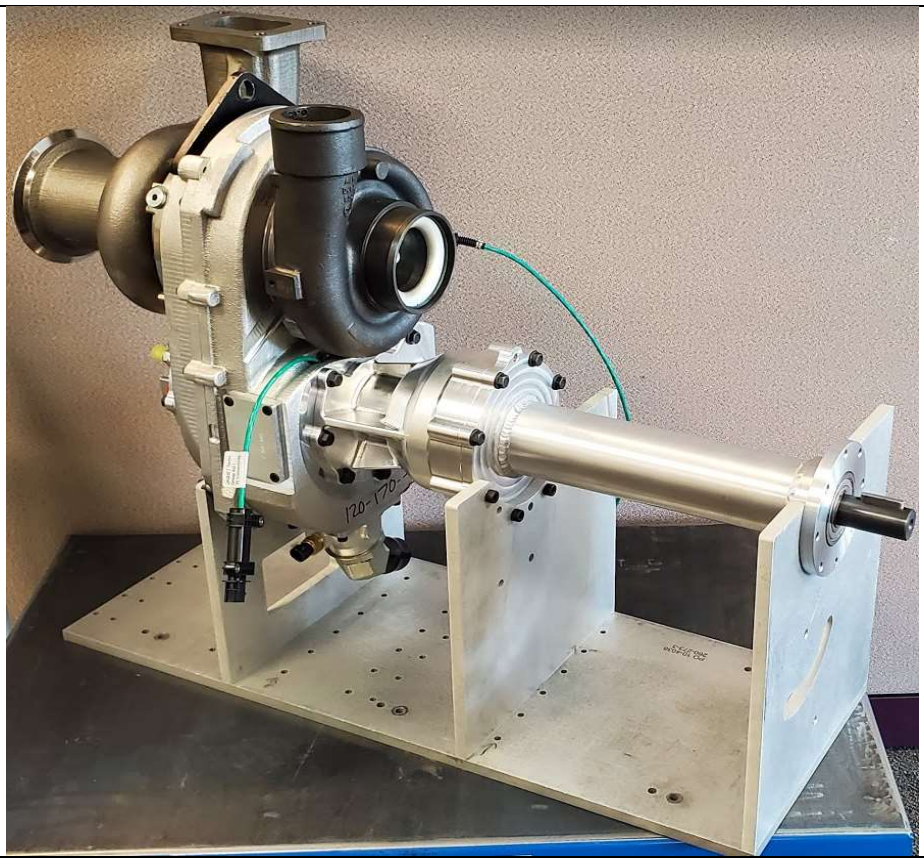

Figure 55: SuperTurbo Turbocharger Delivered for H2D2 Demonstration

Properly matching a turbocharger for turbocompound operation is a balance between maximizing compounding power while minimizing engine pumping work in order to minimize engine fuel consumption. On an engine with high-pressure loop EGR, the turbine sizing also impacts EGR-driving capability and therefore urea dosing requirements and total specific fluid consumption (TSFC). With these tradeoffs in mind, selection of the optimum turbine stage flow capacity requires careful engine system simulation over a range of key operating conditions. The SuperTurbo turbocharger and drivetrain were modeled in Caterpillar's in-house 1D system simulation software DYNASTY, using technical specifications provided by SuperTurbo Technologies. Data provided by SuperTurbo Technologies included turbine performance/map data, drivetrain gear/ring gear ratios, CVT efficiencies, auxiliary power consumption, inertias, constraints etc. A view of the SuperTurbo subcomponent in the DYNASTY system simulation model is shown in Figure 7.

An example of the turbine flow capacity optimization exercise is shown in Figure 56 for the 745AT and 988WL applications. In these graphs the plotted TSFC numbers are weighted-averages over key steady-state operating points. A turbine flow capacity increase benefits engine pumping work but decreases turbocompound power and EGR driving capability, and vice versa as the flow capacity is decreased. In the examples shown in the Figure, the optimum turbine flow capacity is at a Turbine Area Factor (flow capacity multiplier) of approximately 1.05; with this flow capacity, the SuperTurbo is predicted to deliver a TSFC benefit of 1.5-2% versus the baseline VGT turbocharger for both applications.

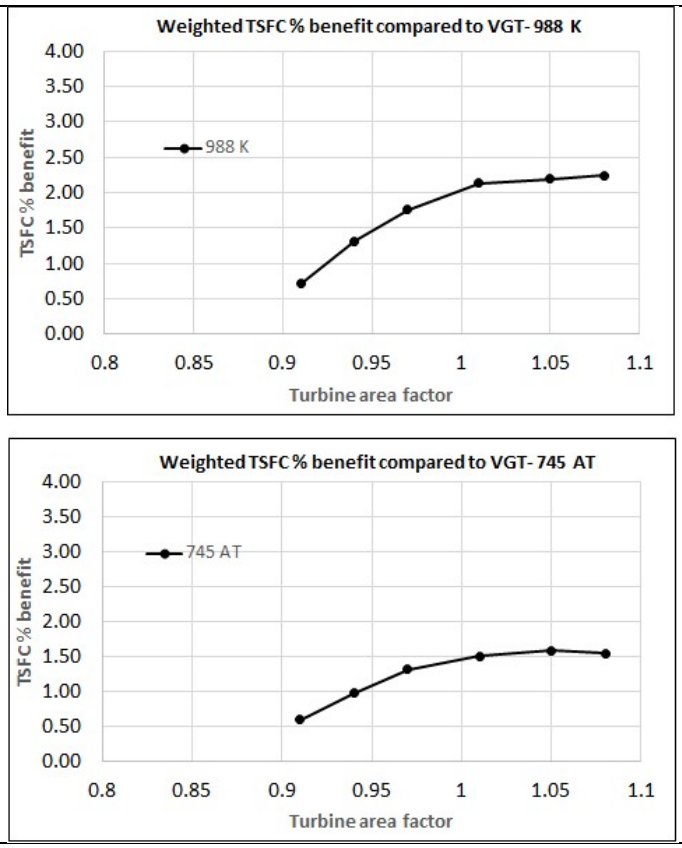

Figure 56: Turbine Flow Capacity Optimization via System Simulation

An 88 mm compressor available in the Caterpillar compressor inventory was selected for the SuperTurbo as the engine operating points were centered in the high efficiency region of the compressor map (see Figure 60). A bespoke 90mm turbine was designed to provide maximum efficiency over the critical range of operating conditions for these off-road applications. A nozzled turbine design was selected to enable multiple nozzle staggers to be procured to enable the turbine flow capacity to be dialed-in for optimum SuperTurbo performance on-engine. A view of the final wheel, nozzle, and stage designs are shown in Figure 57.

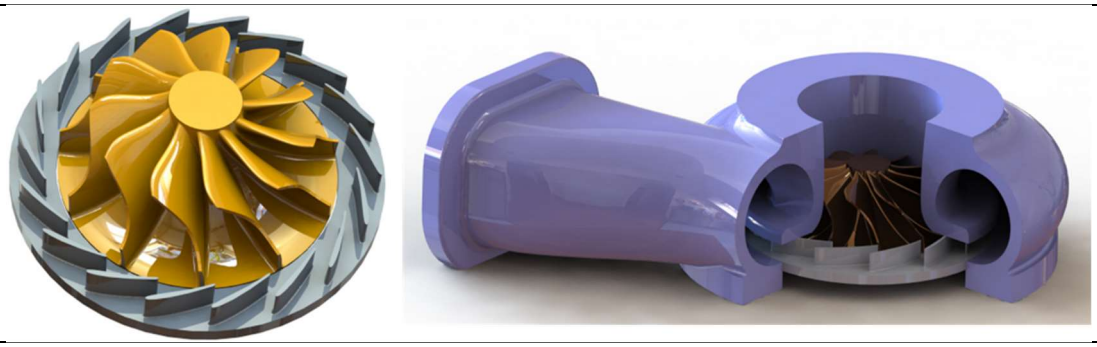

Figure 57: Final Turbine Wheel, Nozzle, and Stage Design

Structural analysis of the new turbine wheel design indicated that all operational stresses are below the targeted 85% of yield strength except in the turbine bore, where the stress reaches 88% of yield strength when the turbine is at 10,000ft altitude conditions. This peak stress is contained in the bore and does not pose significant risk. No natural frequency resonances are predicted within the normal operating

range of this turbine. The final turbine wheel design and structural analysis results are shown in Figure 58.

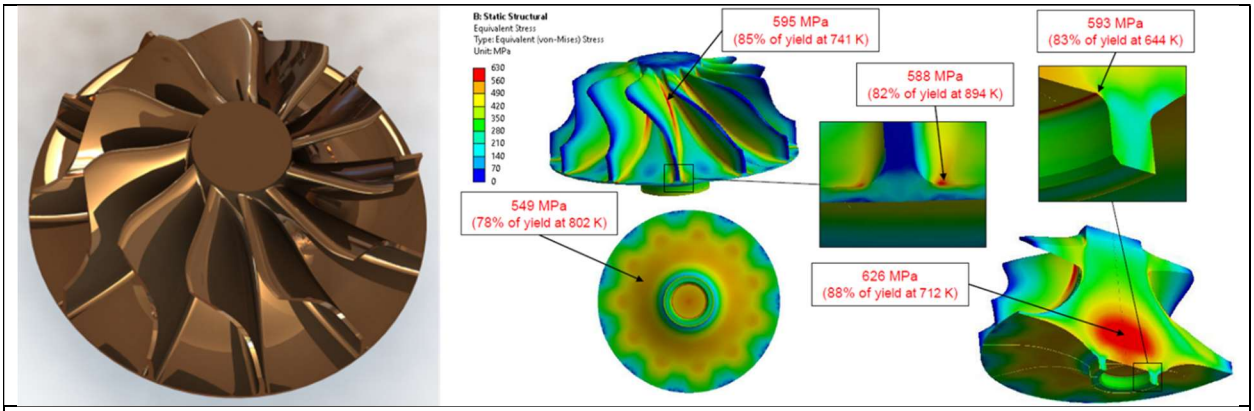

Figure 58: Structural Analysis of Bespoke Turbine Wheel Design for SuperTurbo

SuperTurbo Durability Assessment

The SuperTurbo hardware provided for this hybrid diesel demonstration was designed and developed for on-highway and lower power off-highway applications; it was expected to be sufficiently durable for the test demonstrations planned and scheduled for this project, but would not meet the long-life requirements for typical off-road heavy-duty applications. Durability calculations were performed on several design options to assess the ability of the SuperTurbo and CVT to meet the 12,000-hour life target for the HD applications under consideration in this program.

The durability of the SuperTurbo was calculated using simulation results over each of the 19 application work cycles representing field operation of the 745 Articulated Truck, 390F Hydraulic Excavator, and 988K Large Wheel Loader. Simulation time histories of SuperTurbo and CVT speeds and torques over each of these 19 cycles were used to create duty-cycles, which were then fed into life calculators for the critical components of the SuperTurbo and CVT. These life calculators use a linear damage rule backed by durability testing of the SuperTurbo traction drive components and the CVT at high speed / high load conditions. Life is calculated as L10 life, the theoretical life that 90% of the component population should meet or exceed without failure.

For the fixed ratio high-speed planetary of the SuperTurbo, with an optimized traction geometry, the average calculated life over the 19 application work cycles was 19,081 hours. For the current CVT design with upgraded materials, the average calculated life over the 19 application work cycles was 6,924 hours, short of the target. When a slightly larger design was considered for the CVT, the average calculated life over the 19 cycles was 12,661 hours when using standard materials and 44,315 hours when using upgraded materials.

Given the diversity of the off-road heavy-duty applications, it is expected that the difficulty of meeting the life targets will vary by application. Table 4 shows the calculated L10 life for each of the SuperTurbo/CVT design options considered, separated by machine application. While the high speed planetary and some form of the CVT design can both meet the 12,000-hour life target for the 745AT and 988K LWL, further upgrades to the high speed planetary will be required to meet the life target for the 390F HEX.

Table 4: Calculated L10 life in hours, SuperTurbo high speed planetary and CVT

	HSP	B1X+	PL1	PL1+
745AT	26,416	10,751	19,659	68,805
390F	7,192	2,818	5,152	18,032
988K	12,881	3,364	6,150	21,526

HSP = Fixed Ratio High Speed Planetary
B1X+ = Current CVT design w/ upgraded materials
PL1 = Larger CVT design w/ standard materials
PL1+ = Larger CVT design w/ upgraded materials

A few SuperTurbo hardware issues did arise during the H2D2 test program. The most common and serious issues were failures of the rubber coupler that sat between the belt-drive and the CVT in the SuperTurbo drivetrain, see Figure 59. The purpose of the rubber coupler is to provide torsional damping and isolate the elements of the SuperTurbo high speed drive from potentially damaging engine torsional vibrations. Failure #1 in Figure 59 occurred after approximately 250hrs of testing and was due to excess heat in the coupler housing, leading to melting and breakage of the coupler. Failure #2 in Figure 59 occurred after only 30hrs of testing and was found to be due to an assembly error. It should be noted that the SuperTurbo units that were tested for this project are now considered 'legacy' designs; the latest SuperTurbo designs do not include the rubber coupler in the drivetrain, and extensive testing at SuperTurbo Technologies without this coupler has shown no adverse effects to date.

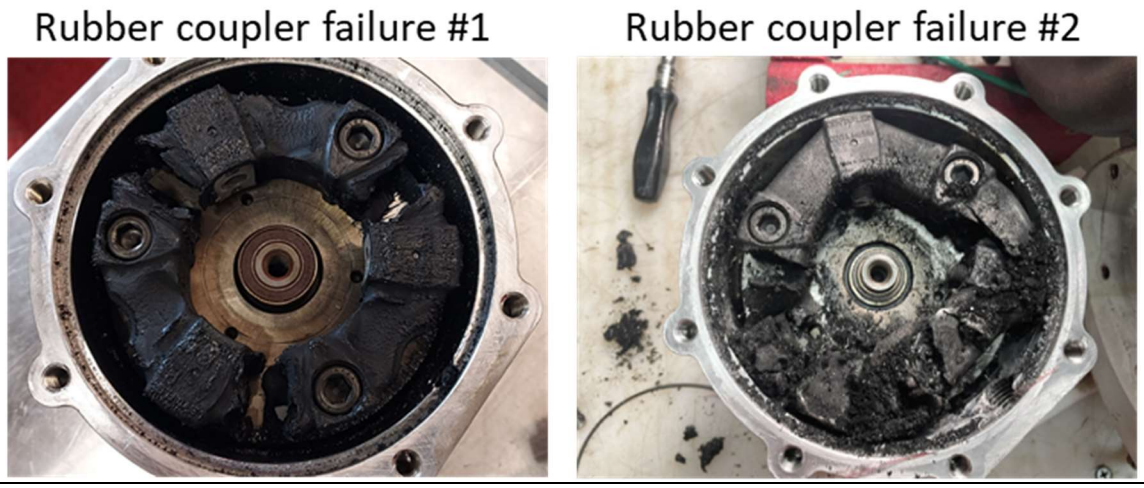

Figure 59: SuperTurbo Coupler Failures

From a performance standpoint the SuperTurbo behaved exactly as expected during engine testing. Figure 60 shows the simulated and measured SuperTurbo performance on the compressor map, demonstrating excellent agreement between the predicted and demonstrated behavior.

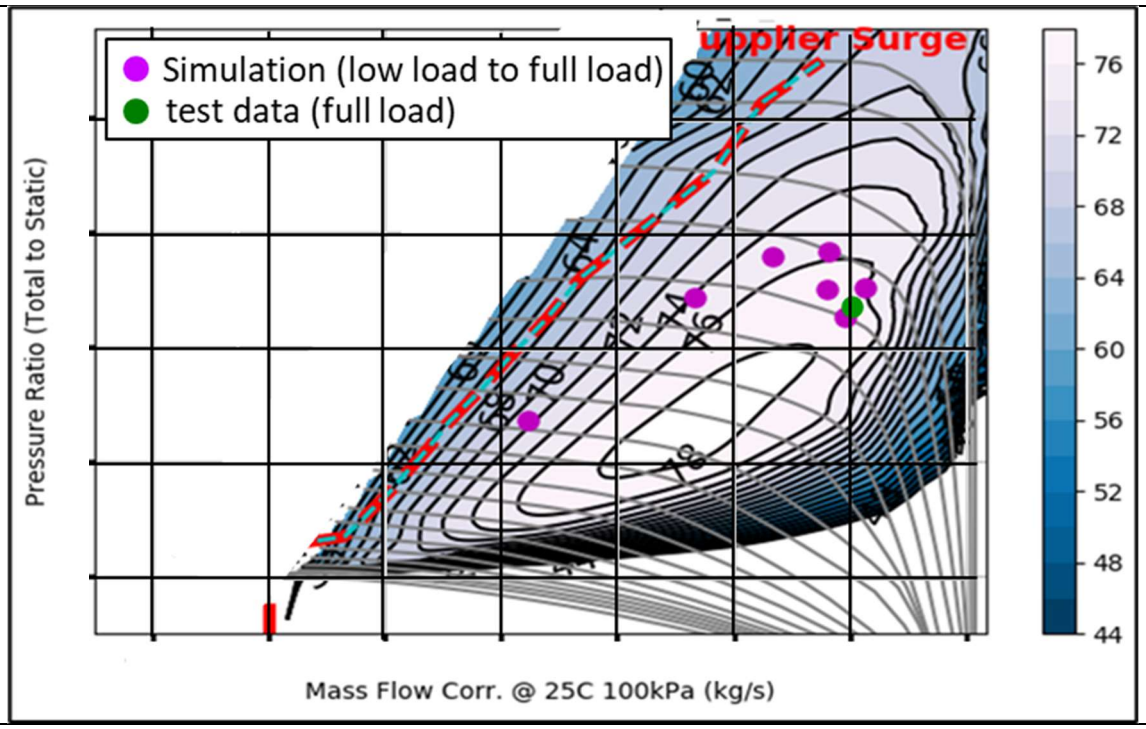

Figure 60: SuperTurbo Performance on Compressor Map

3.2.3. Variable Valve Actuation System

SOPO ID #	Item Title	Item Description	Start Date	End Date	Status
Task 1.5	**Variable Valve Actuation System**	Evaluation of multiple VVA concepts with the goal of achieving variable valve lift in a cost-effective package. Demonstrate (in simulation) target fuel consumption reduction.	6/1/2019	9/30/2020	100% Complete

Variable valve actuation (VVA) concepts were explored for integration in the H2D2 engine. Variable valve events were investigated on their ability to provide two main possible engine performance benefits: improved efficiency directly from optimizing valve lift profiles for different conditions throughout the engine operating range; and thermal management capability to provide the ability to warm the catalysts above their activation temperature, regenerate the diesel particulate filter, and desulfate the selective catalytic reduction (SCR) system. These performance benefits were examined with respect to the expected system-level costs of the various potential variable valve actuation systems, and a down selection of potential technologies to include in the demonstration was completed.

Two main concepts for improving efficiency directly from optimizing valve lift profiles for the specific operating condition emerged as the most beneficial and most straightforward to implement. The first is using independent cam phasers on the exhaust and/or intake shift the valve lift profile based on speed and/or load for efficiency improvement. This was explored through thermodynamic cycle simulation as discussed in previous sections, and Figure 61 below shows the optimum phasing for each of the operating points. As can be seen, the phasing shift is relatively small over the operating range. In general, the benefits over the operating space of from shifting the cam phasing versus holding the phasing in the single overall optimized position provides an average 0.3% fluid consumption benefit at a given operating point. Because of the relatively small speed range and the unthrottled nature of the base engine, variable valve timing provides very modest benefits.

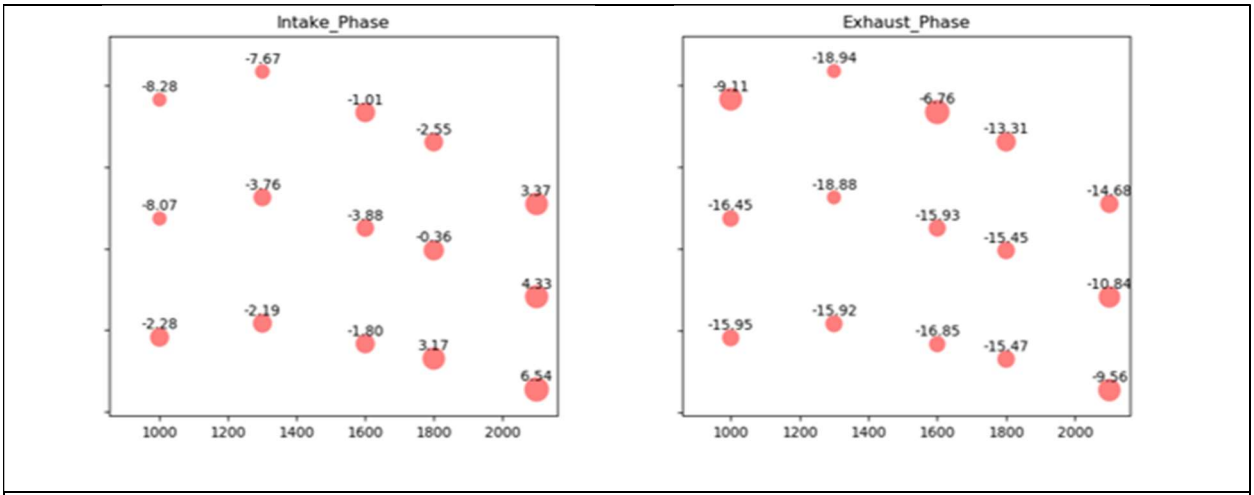

Figure 61: Cam phasing map for maximum efficiency

The second concept that shows promise is the use of variable valve actuation to provide Miller cycle operation. This concept has been shown to enable high effective expansion ratios with controlled peak cylinder pressure, and it is in production on the current nonroad Caterpillar C18 engine, known as Intake Valve Actuation (IVA). For this engine, both the production-like variable valve system that extends the

intake valve event and alternative VVA systems were considered, so the analysis was not restricted to the current production system. The total fluid consumption benefits of implementing the IVA system on the H2D2 engine are shown in Figure 62 at full load and three different speeds as simulated using DYNASTY cycle simulation analysis. As can be seen in Figure 62, at 1300 rpm and 1800 rpm, almost no benefit can be observed. At 2100 rpm, a more significant benefit can be observed, and that benefit increases with altitude. These benefits are generally only present near the full load location. However, for the applications considered as part of the H2D2 program (and overall machine operation in general) operation above 1800 rpm represents a relatively small portion of the operating range, and thus the effective improvement is modest. The main reason that IVA is less effective than other engine applications is that this engine includes significant cylinder pressure capability upgrades, and thus can already have acceptable effective expansion ratio at most conditions through a high base compression ratio. In addition, because of the power density requirements of this application, decreasing the effective breathing capacity of the engine with Miller cycle operation would push the requirements for the air system beyond current system capabilities to be effective.

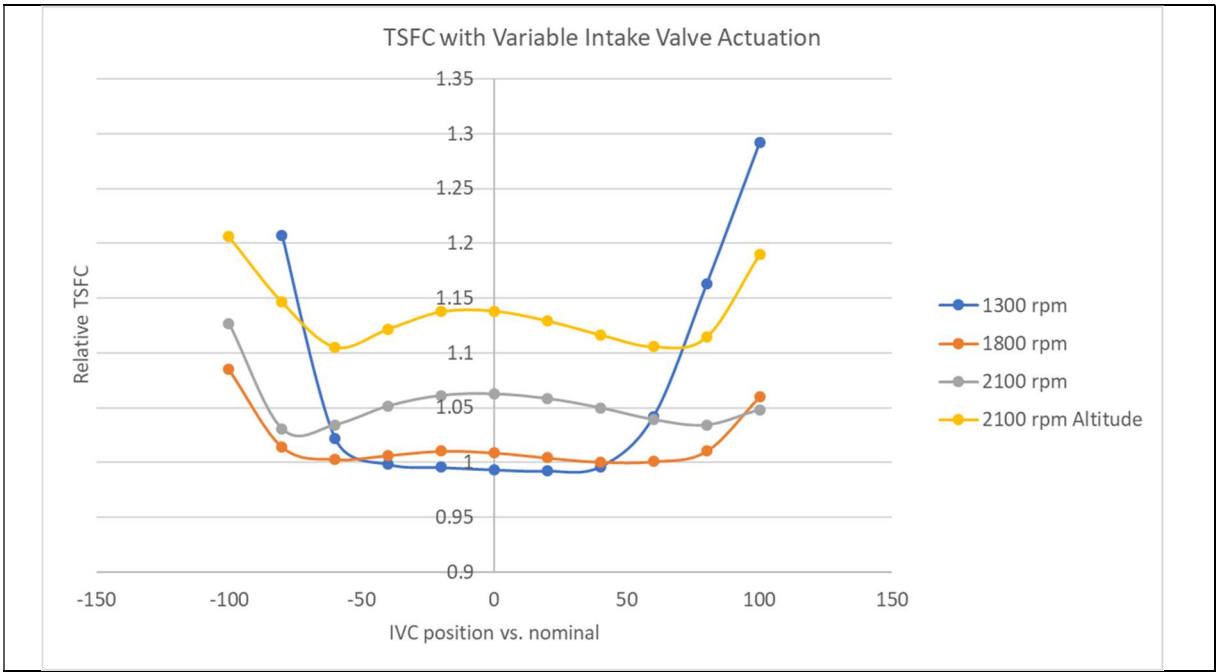

Figure 62: Impact on IVA on fuel consumption along the lug curve.

Because the fuel consumption benefits of both phasing and IVA look to be modest, variable valve actuation was explored for thermal management capability to provide the ability to warm the catalysts above their activation temperature, regenerate the diesel particulate filter, and de-sulfate the selective catalytic reduction (SCR) system. The performance benefits were examined with respect to the expected system-level costs of the various potential variable valve actuation systems, and a down selection of potential technologies to possibly include in the demonstration was completed.

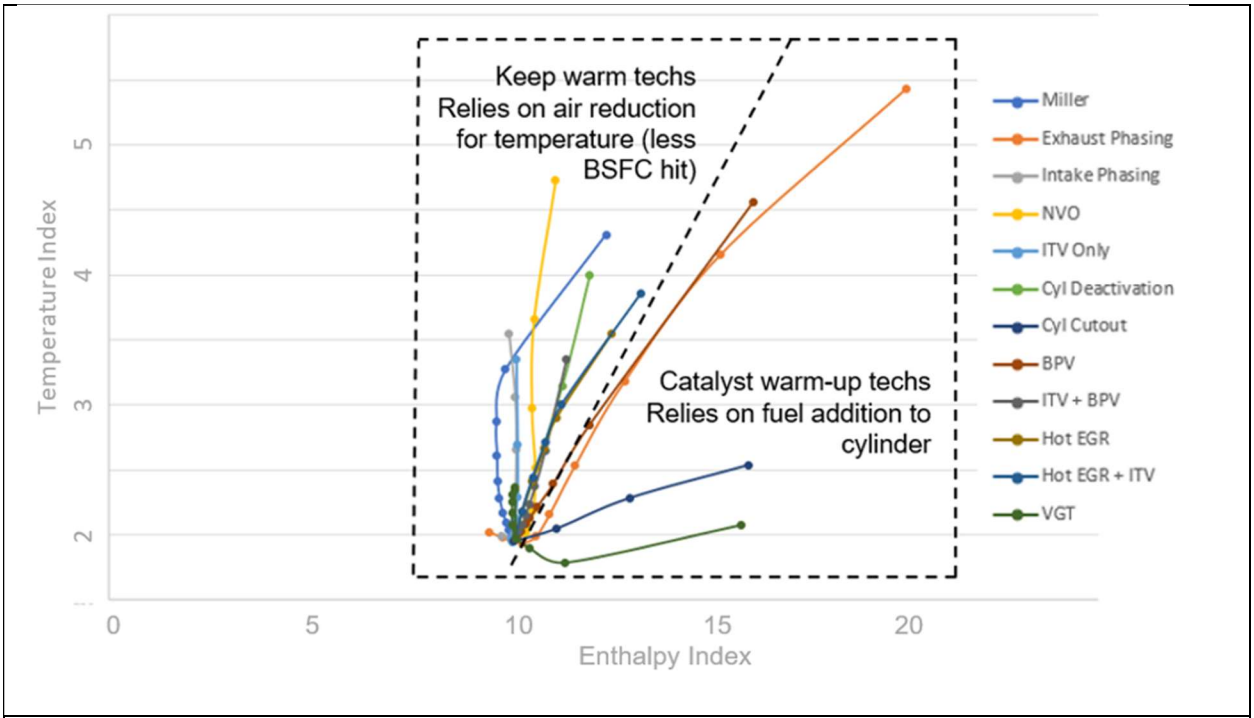

Figure 63: Temperature capability vs. enthalpy capability of various thermal management options.

Figure 63 shows the results of thermodynamic cycle simulation of different thermal management strategies. The plot is divided into technologies that primarily reduce the air flow through the engine to elevate temperature, which can keep the engine warm and can be used to light off catalysts given enough time but are not effective at warming up the aftertreatment quickly, and technologies that increase the overall exhaust energy by increasing the fuel usage and thus provide more capability to warm up catalysts for faster aftertreatment effectiveness in starting situations. The former represents the minimum thermal management requirement to meet regulations and protect the system (ability to de-sulfate the SCR system, regenerate the DPF, etc.), while the latter provide more capability to reduce emissions at start-up, which is a potential requirement for future low emissions regulations. The list includes variable valve actuation strategies (Miller cycle, phasing the exhaust lobe, phasing the intake lobe, phasing both lobes away from each other for negative valve overlap (NVO), and cylinder deactivation when valves do not actuate) and external systems technologies (intake throttle valve (ITV), cylinder cutout where fuel is cut to certain cylinders, back pressure valve (BPV), a combination of both intake throttle and backpressure valves (ITV+BPV), hot exhaust gas recirculation, and adjusting the variable geometry turbocharger (VTG). As can be seen in the plot, the external valves (ITV and/or BPV) provide as much thermal management capability as the variable valve actuation strategies, and the most recent design estimates of the costs to incorporate the VVA systems is considerably more than the external valve strategies. Based on this analysis, the thermal management benefits by themselves do not justify the expense of adding VVA to the engine.

3.2.4. Realtime Optimizer Control

SOPO ID #	Item Title	Item Description	Start Date	End Date	Status
Task 1.6	**Realtime Optimizer Control**	Engine + Variable FEAD + high speed flywheel energy storage (HSFW) + turbocompound system-level controller development	9/1/2019	12/31/2020	100% Complete

To begin the control of the complex powersystem with multiple devices providing and absorbing power, an L5 control structure and controller were developed. L5 is the Caterpillar designation for the level of the entire powersystem, and lower numbers proceed down the system and component level. The functional requirement definition at the L5 system level was started while considering L4 subsystem level capability (Engine, HSFW, SuperTurbo, MGU, etc.). The requirements for meeting engine performance while minimizing fluid consumption drove the L5 system level control functionality as follows:

- At each engine operating condition, categorization of the energy flow state based on the machine-level energy demand and L4 level subsystem energy storage limit and availability;
- Modeling power requests at each state and tuning/adjusting controller(s) to meet engine performance requirements (transient capability) while harvesting energy (SuperTurbo compounding, braking power) to minimize fluid consumption efficiency (BSFC, TSFC).

L4 System Energy State

The L5 supervisory controller monitored the L4 system health condition or energy state, and this facilitated the supervisory controller to make decisions on which L4 components were available for energy flow path optimization.

L5 System Level State Vector

The energy flow pattern [EngStat, SuperTurboStat, HSFCStat, MGUStat] was defined in more than one way for each of the engine operating conditions and is listed in Figure 64. The structure enabled exploration of which hybrid flow paths were most beneficial throughout the simulation phases of the project.

The information from the L5 health monitor / machine level energy demand is necessary to create two energy nodes: one that needs power, the other one that can provide power. The connection of these two nodes forms an energy flow path. A unique set of energy flow paths were defined based on the pre-determined feasible paths w.r.t the hybrid hardware concept configuration. The combination of any one or more energy flow paths were then explored and implemented in the control block of the L5 states through state flow modeling. This modeling covers four typical engine operation conditions: start, stop/braking, normal running, and acceleration. The simplified example of the L5 states are listed in the rows of Table 5, where the SuperTurbo could provide turbo compounding power to Engine (row 1), or where the engine provides shaft power to SuperTurbo to maintain optimal air fuel ratio (row 2), the HSFW and MGU both provide power with combined total value equivalent to what SuperTurbo needs during transient event (row 3), or harvest what is available as free energy during a braking event (row 4). The power split ratio “r” between the HSFW and MGU is optimized considering each device’s respective L5 energy level constraint set.

L5_State_vector	L5_State	Eng_State	Super Turbo_State	HSFW_State	MGU_State	Eng_Mode	Eng_Mode description
[0 0 0 0]	1	0	0	0	0	1,2,0,-1	
[2 1 0 0]	2	2	1	0	0	2	Running_nonaccel
[2 -1 0 0]	3	2	-1	0	0	2	Running_nonaccel
[2 0 1 0]	4	2	0	1	0	2	Running_nonaccel
[2 0 -1 0]	5	2	0	-1	0	2	Running_nonaccel
[2 0 0 1]	6	2	0	0	1	2	Running_nonaccel
[2 1 1 0]	7	2	1	1	0	2	Running_nonaccel
[2 1 -1 0]	8	2	1	-1	0	2	Running_nonaccel
[2 -1 1 0]	9	2	-1	1	0	2	Running_nonaccel
[2 -1 -1 0]	10	2	-1	-1	0	2	Running_nonaccel
[2 1 0 1]	11	2	1	0	1	2	Running_nonaccel
[2 -1 0 1]	12	2	-1	0	1	2	Running_nonaccel
[2 0 1 1]	13	2	0	1	1	2	Running_nonaccel
[2 1 1 1]	14	2	1	1	1	2	Running_nonaccel
[2 -1 1 1]	15	2	-1	1	1	2	Running_nonaccel
[2 0 -1 1]	16	2	0	-1	1	2	Running_nonaccel
[2 1 -1 1]	17	2	1	-1	1	2	Running_nonaccel
[2 -1 -1 1]	18	2	-1	-1	1	2	Running_nonaccel
[0 1 -1 0]	19	0	1	-1	0	3	Running_accel
[0 1 0 -1]	20	0	1	0	-1	3	Running_accel
[-1 1 0 0]	21	-1	1	0	0	3	Running_accel
[0 1 -1 -1]	22	0	1	r	1-r	3	Running_accel
[1 0 -1 0]	23	1	0	-1	0	1	Start
[1 0 0 -1]	24	1	0	0	-1	1	Start
[-1 0 1 0]	25	-1	0	1	0	0	Brake
[-1 0 0 1]	26	-1	0	0	1	0	Brake
[-1 0 1 0]	27	-1	0	1	0	-1	Stop
[-1 0 0 1]	28	-1	0	0	1	-1	Stop

Figure 64: L5 system level controller state vector

Table 5: Example of the L5 Powersystem States

	Engine State	SuperTurbo State	HSFW State	MGU State
Engine Normal Running	1	-1	0	0
Engine Normal Running	-1	1	0	0
Engine Accelerating	0	1	-r	-1+r
Engine Braking	-1	0	r	1-r

L5 Power Request Vector

For each L4 system (Eng., SuperTurbo, HSFW, MGU) the L5 power request was calculated for each state vector using a closed-loop PI controller with the potential for simplification to an open-loop controller under certain engine conditions. During accel(eration) and nonaccel(eration) engine modes, the PI controller used IMAP error as its input to calculate how much turbo power needs to be harvested (turbo compounding) or how much power needed to be drawn from other systems to assist the turbo. This IMAP error-based PI structure allowed assisting during transient accel events while still closely matching desired air-fuel ratios in nonaccel engine modes. During braking and start/stop modes, the PI controller used engine speed error as input to calculate how much braking or start/stop power was available for use. Positive and negative speed errors indicate braking or startup power needs, respectively.

L4 Power Limiting

Limiting conditions were defined based on each L4 system hardware constraints. These power limits were used to constrain the L5 power request before they were used in L4 to drive the energy transfer. An overview of the model structure is shown in block diagram form can be seen in Figure 65.

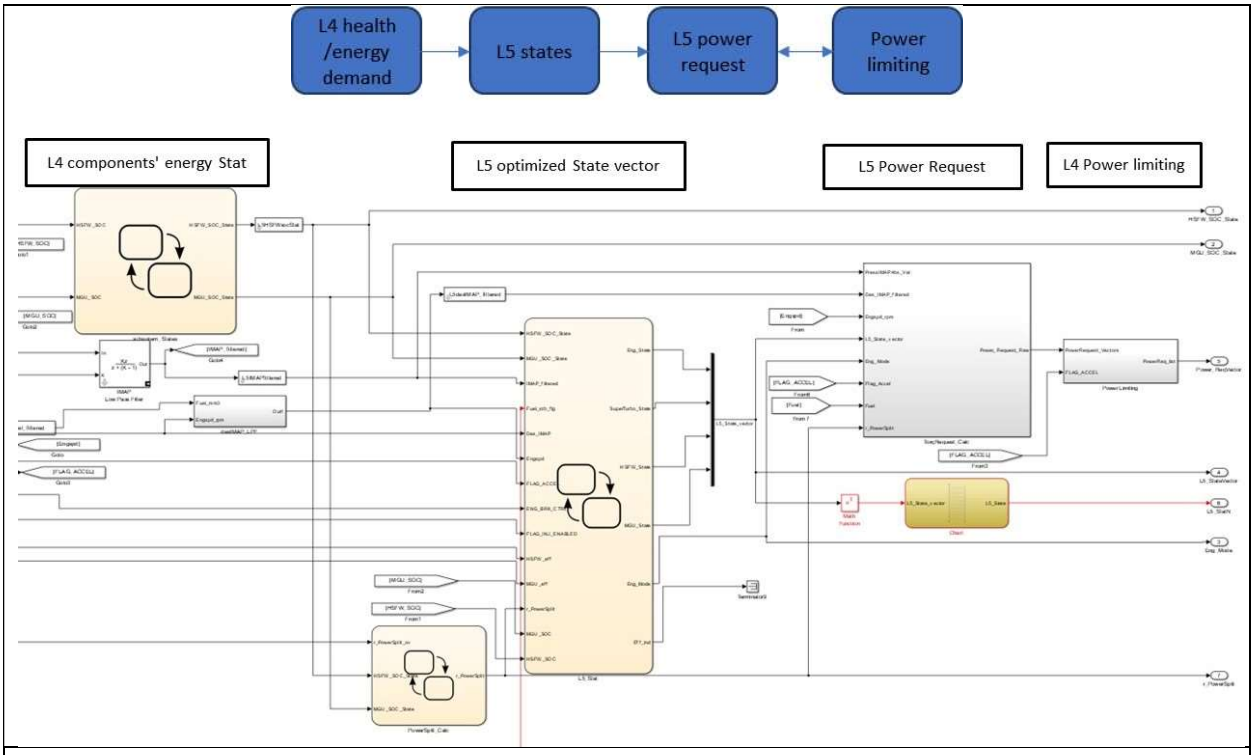

Figure 65: L5 supervisory controller key elements

L5 Integration, Tuning, and DoE

The L5 supervisory controller was integrated in the H2D2 DYNASTY system level model with the L4 system plant models and lower level controls. Full system DYNASTY model base calibration tuning / hardware limits / constraints for the SuperTurbo intake manifold absolute pressure (IMAP) based PID controller, the L5 controller and the L4 hybrid devices was completed to define the desired performance. Additional Design of Experiment (DoE) simulations were executed to explore the calibration space for the best fuel consumption (and/or system level TSFC) while meeting the transient response capability, for each of the main hybrid hardware configuration layouts (#2, 3, 2a, 3a). In addition, a secondary control effort surrounded converting the full system model for compatibility with the Advanced Engine Control software (with Realtime Optimization), was conducted so that the optimization of engine control settings with respect to the H2D2 hybrid elements could be evaluated.

A total of 17 base control parameters and 21 non-DoE related hardware constraints / limits / characteristic maps, Figure 66, were tuned to allow the system level simulation to run with a reasonable calibration setting.

- Hardware limits for hybrid devices were defined with Caterpillar and supplier input.
- Desired IMAP and SuperTurbo power request open loop maps were defined to drive the lowest BSFC.

- Some inputs to the L5 controller were pre-processed (IMAP, fuel) and IMAP closed-loop PI controller gain / multiplier map were tuned for the simulation stability and convergence requirements.
- Closed-loop controls and SuperTurbo power open-loop controls were tuned to allow smooth transitions.

Tune name	unit / range	Value	base control tuning list	non DOE, just check
ts_L5	sec	0.01	x	
ENGOnRPM	rpm	600		x
EngOffRPM	rpm	300		x
Des_Start_Engspd	rpm	600		x
Des_Brake_Engspd	rpm	600		x
Des_Stop_Engspd	rpm	600		x
HSFW_SOC_min	percent	5		x
HSFW_SOC_max	percent	95		x
MGU_SOC_min	percent	5		x
MGU_SOC_max	percent	95		x
IMAP_filterFact		1	x	
Fuel_filter_TC		25	x	
DesIMAP_filterFact_Dec		0.5	x	
DesIMAP_filterFact		0.5	x	
L5_Des_IMAP_map		2D		x
L5_Engspd_rpm_Colm	rpm	2D		x
L5_Fuel_mm3_Row	mm3	2D		x
L5_Des_IMAP_mapout	kPa	2D		x
HSFW_powerlim	kW	25		x
MGU_powerlim	kW	26		x
MGU_accelpowerlim	kW	26		x
superTurbo_powerlim	kW	26		x
STpower_min_rt_change	kW/sec	-40		x
STpower_max_rt_change	kW/sec	40		x
STpower_min_rt_change_accel	kW/sec	-40		x
STpower_max_rt_change_accel	kW/sec	40		x

Figure 66: Base and non-DoE controller parameter list

A total of 16 parameters were selected for the DoE list to represent the storage level and energy transition criteria, specifically for exploration of the tradeoff between fuel consumption and transient capability. The key DoE settings were defined (as highlighted in Figure 67) to conduct an initial DoE runs of just the 745AT cycle 1 for all hardware configurations (Configuration Layout #2, 3, 2a, 3a) and the DoE result shows that the batch 4 column had best tradeoff. The detailed analysis of this batch 4 parameter list showed faster energy charging and discharging without transient capability sacrifice. However, the HSFW state of charge (SOC) is dependent on the engine speed and it is favorable if its calibration is set at the batch 2 settings, because these give enough margin to support transient assisting for other application cycles beyond the 745AT cycle 1. Hybrid concept layout 2a provided best system level TSFC and BSFC compared to all other configurations, as discussed in the Concept Definition portion of the report.

		Lowest energy stored	highest energy stored for transient event	mid level	discharging at different fuel min threshold		
DOE list narrow down	range	Batch1	Batch2	Batch3	Batch4	Batch5	Batch6
HSFW_constEnergyFlow	[2 10 20]	10	10	10	20	20	20
MGU_constEnergyFlow	[2 10 20]	10	10	10	20	20	20
HSFW_offset	[2 5 10]	5	5	5	5	5	5
HSFW_nonaccel_offset	[2 5 10]	5	5	5	5	5	5
HSFW_SOC_min_mid	**[8 15 30], use 8 as default for all.**	**8**	**8**	**8**	8	8	8
HSFW_SOC_accel_mid	**[15 30 50]**	15	25	25	15	15	15
HSFW_SOC_nonaccel_mid	**[30 50 70]**	**30**	**70**	**50**	**30**	**30**	**30**
HSFW_SOC_mid_max	**[40 65 85]**	40	85	65	40	40	40
MGU_offset	[2 5 10]	5	5	5	5	5	5
MGU_nonaccel_offset	[2 5 10]	5	5	5	5	5	5
MGU_SOC_min_mid	[8 15 30]	**8**	**30**	**15**	**8**	**8**	**8**
MGU_SOC_accel_mid	**[15 30 50]**	15	45	30	15	15	15
MGU_SOC_nonaccel_mid	**[30 50 70]**	**30**	**70**	**50**	**30**	**30**	**30**
MGU_SOC_mid_max	**[40 65 85], [30 50 70],**	36	76	56	36	76	56
L5in_r_Power_Split_ov	auto_calculated	IC = 0.5	same	same	IC = 0.5	same	same
DischgAllowed_Fuel_min	[20, 50, 80, 150]	20	20	20	50	80	150

Figure 67: Controller DoE parameter list with key settings highlighted in yellow

From the DoE simulations the following were some key control strategy findings for this powersystem:

- Perform fast, but not too fast energy recovery
- Reduce overactive recovery/assist swings
- Bias HSFW state of charge to upper range for superior acceleration assisting

Engine Realtime Optimizer Advanced Control

For core engine controls and optimizer development, fast running mean value models (MVM) of the engine plant were modeled using Caterpillar's existing library components. Calibration and alteration of the library MVM models for the SuperTurbo and other unique concept engine aspects was performed, and this was based on the higher-fidelity DYNASTY engine physics model. Caterpillar's SimApp build and execution platform was used for engine plant DLL creation and communication with the engine control DLL and other subsystems in DYNASTY. The intent was to utilize the SimApp platform as a bridge to migrate the full version of the Realtime Optimizer advanced control software and MVM plant model into the DYNASTY environment. This had to be done virtually to have enough time to validate the various H2D2 hardware and software requirements. The end result was that a highly modular DYNASTY systems model was created, where multiple types of controllers and engine plants could be seamlessly switched between during development (Figure 68 Engine plant & Integrated system level). A notable result was that the DYNASTY system simulation was able to run production ECM software and calibrations for the most physics-accurate transient performance and fuel consumption predictions, and could provide significant help in troubleshooting problems throughout the program.

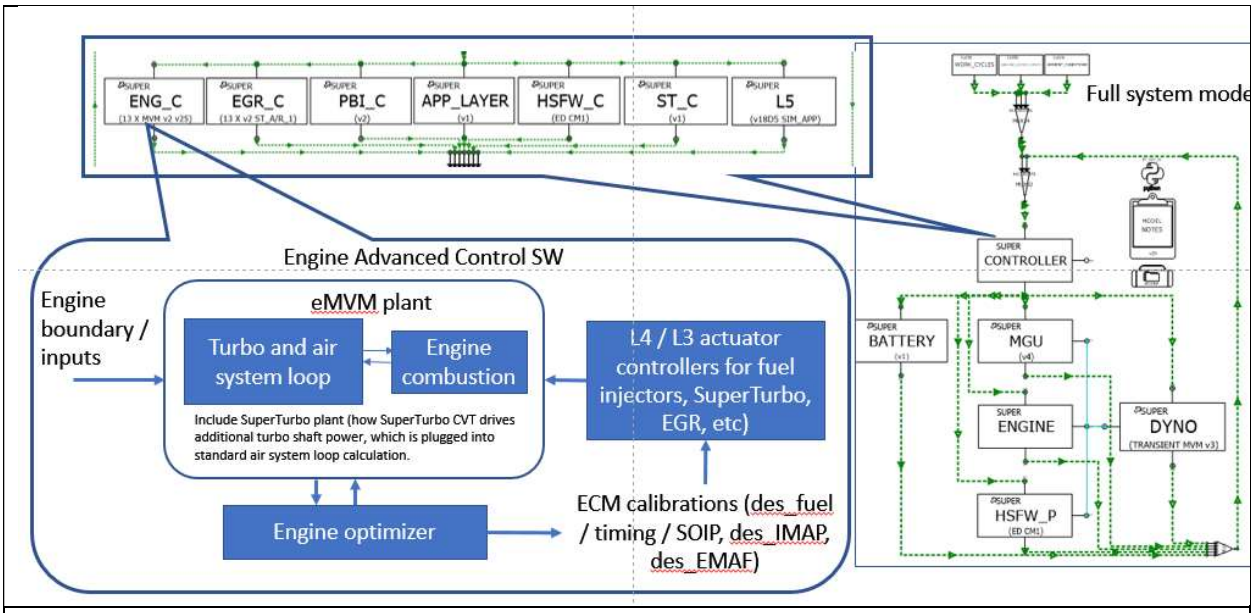

Figure 68: H2D2 engine plant and Engine ctrl DLLs (fully integrated into system level model with config#2a), Engine Advanced control SW is to be implemented (illustrated above)

The Realtime Optimizer engine advanced control software utilized an embedded version of the aforementioned MVM plant model and an online optimizer to do real-time optimization for combustion key settings (such as Start of Injection Timing, Fuel, Start of Injection Pressure) and air system parameters such as desired intake manifold pressure, and desired EGR flow. The L3/L4 actuator controls (such as fuel system injectors / EGR system EGR valve, SuperTurbo CVT, etc.) then drove their component level devices to achieve the desired settings such that the overall engine performance meets hardware constraints and emission regulations while trying to achieve efficiency benefits. Advanced controls did not alter boundaries above the engine level, so the L5 control and hybrid devices were not impacted.

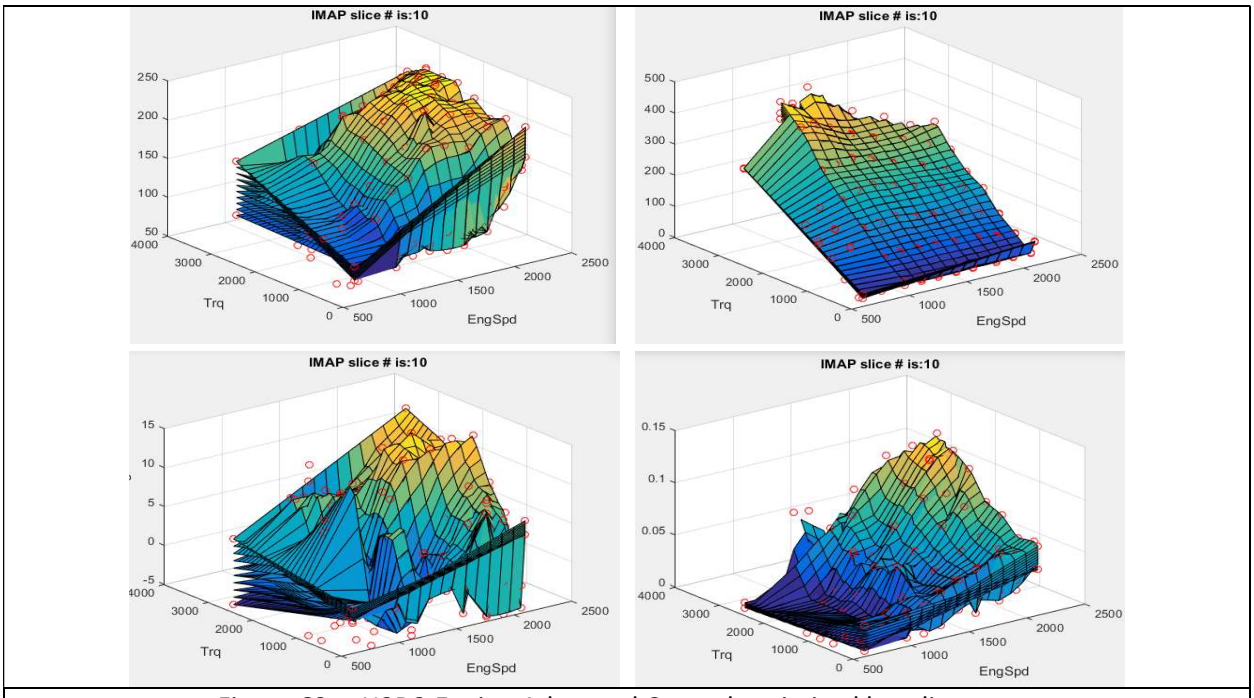

Figure 69: H2D2 Engine Advanced Control optimized baseline maps

The Realtime Optimizer controller was exercised offline in a PC environment to generate the optimized base calibration maps for the concept engine. Extensive debugging and troubleshooting were completed in these offline efforts to enable production level ECM calibrations and software. An example of the types of optimized calibration maps/surfaces in Figure 69 illustrates the regions of adjustment, and non-linearity that come from the system interaction trade-offs.

The controls task had to prioritize finishing the final software of the L5 powersystem for validation testing due to untimely controls engineering staff departures. The L5 Supervisory controller was completed and successfully used for the validation testing, but with the following deliverable outcome for the Realtime Optimizer aspect:

- Reduced Realtime Optimizer evaluation and validation
    - No real-world testing of the Realtime Optimizer on the Phase 2 engine
    - Simulation-only evaluation of the Realtime Optimizer on the Phase 2 engine with VGT

The Realtime Optimizer was able to be evaluated for efficiency impacts in simulation. Since the optimizer was used offline to generate the H2D2 concept engine calibration it did not produce any confident efficiency improvement, and therefore the contribution was set to zero in the high-level efficiency summary for the program. This is a conservative view as the Advanced Controls does provide a 3-5% efficiency improvement over traditional controls structures (based on prior Caterpillar work), as it is already included in the engine performance measurements. The Realtime Optimizer is focusing on other aspects of engine operation, like emissions and durability, while maintaining the base calibration level of efficiency. An example of these functions is the improved tailpipe NOx emissions when the Realtime Optimizer is enabled, Figure 70.

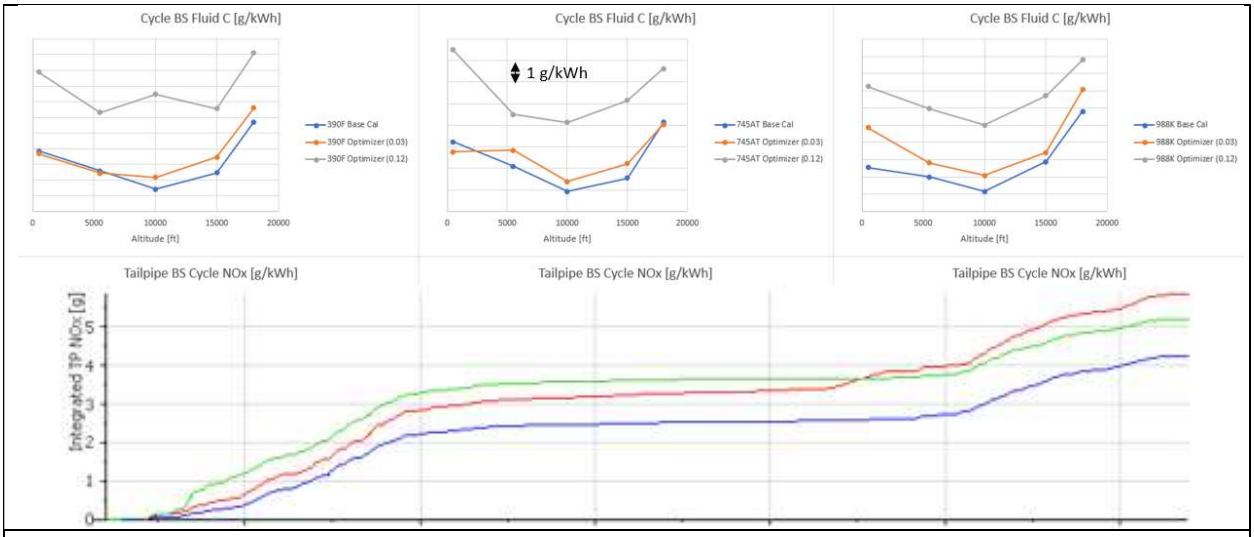

Figure 70: Optimizer impact on fluid consumption and reducing tailpipe NOx over a transient cycle. Lower Plot: Red = Base Calibration, Green = Optimizer 0.12, Blue = Optimizer 0.03

3.2.5. Flywheel Energy Storage Development

SOPO ID #	Item Title	Item Description	Start Date	End Date	Status
Task 1.7	**Flywheel Energy Storage Development**	Initial flywheel trade-off studies will be performed. A detailed engineering design of the flywheel concept, followed by prototype fabrication and limited testing will be conducted. A cost-effective vacuum system and bearing mounting will be designed.	9/1/2019	12/31/2020	100% Complete

The University of Texas at Austin, Center for Electromechanics conducted research of flywheel designs and trade-off studies involving sizing, materials, windage losses, and bearings. Initial requirements for the flywheel were 250 mm maximum diameter, 200 mm maximum length, 30-50 krpm operating speed, and 1 MJ (0.28 kW-hr) minimum stored energy. Several concepts matching these requirements were evaluated including the concept below with a steel hub and composite bands.

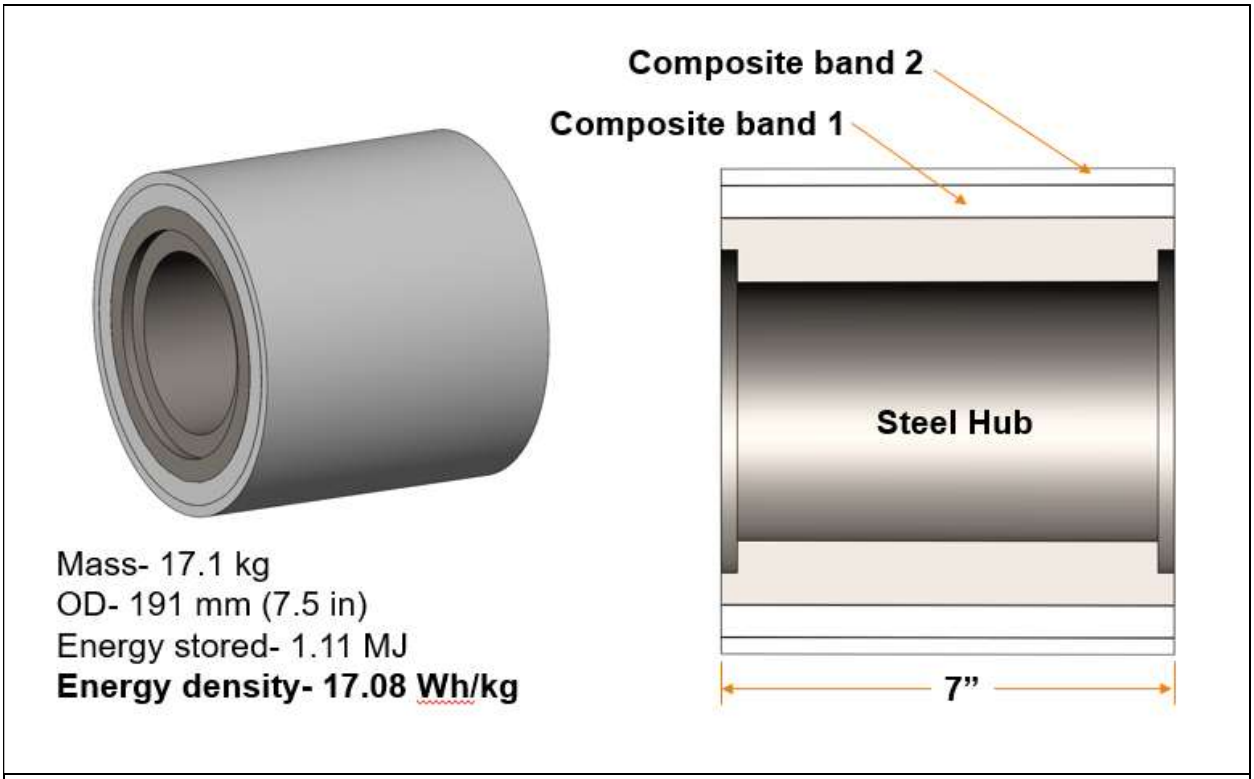

Figure 71: Conceptual steel and composite flywheel shown without rotor shaft

Windage analysis was performed for the concepts to better understand the windage loss as a function of operating speed and vacuum level. The windage losses for the first flywheel concept at 50,000 rpm was 5.6 W or 51.1 W loss (1 mtorr and 20 mtorr respectively). For this design a feasible sealing solution was not found so a second slower composite flywheel design was developed. The design had the same 1.1 MJ stored energy and flywheel rim length but more composite bandings and a larger, 0.237m diameter. The flywheel operating speed was 37,500 rpm but the design was able to store the same amount of energy because of the larger OD. The windage loss at 20mtorr and 37.5 krpm were 57.6 W. Bearing designs were evaluated for the different concepts. Typically, high speed flywheels use magnetic bearings to minimize losses but also add cost, complexity, and development time. Due to the drawbacks,

the project focused on mechanical bearing designs. Barden 208H angular contact bearings were found that can operate up to 37,500 rpm with oil lubrication. For similar bearings rated to 50,000 rpm the maximum shaft size may be too small to allow connection to the drive system. Bearing losses were also shown to be a concern even with the lower speed flywheel.

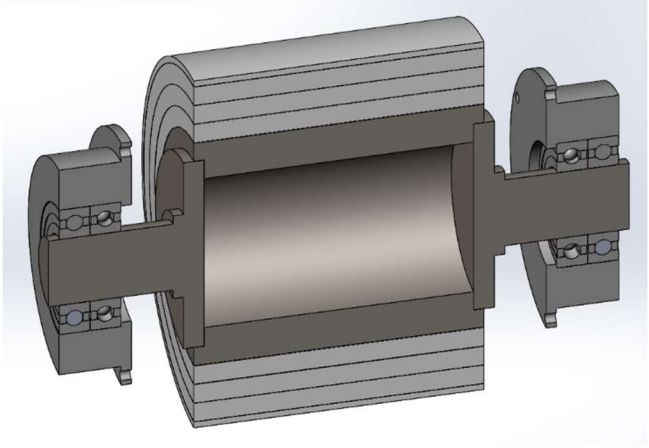

Figure 72: 37,500 rpm flywheel with mechanical bearings

Testbed Flywheel Sizing and Design

For the testbed, a flywheel module was designed by a supplier per requirements with an all-steel rotor and low-cost containment system while still meeting life targets. The design parameters and views of the module are below. As part of the design process, analysis was done to evaluate the effect of a vacuum system on the performance of the module. The CFD results showed a significant drop in aerodynamic drag between atmospheric pressure and partial vacuum. In order to create partial vacuum, vacuum seals were added in the design. The partial vacuum system was further analyzed using several off-highway machine duty cycles to understand the effect of the flywheel parasitic losses on the system performance. The results showed that running the flywheel in partial vacuum significantly improves the system performance in various applications.

Table 5: Flywheel Key Parameters	
Parameter	**Value**
Outside diameter	210 mm
Width	121.5 mm
Inertia	0.177 kg.m^2
Mass	33.1 kg
Speed	23,500 rpm

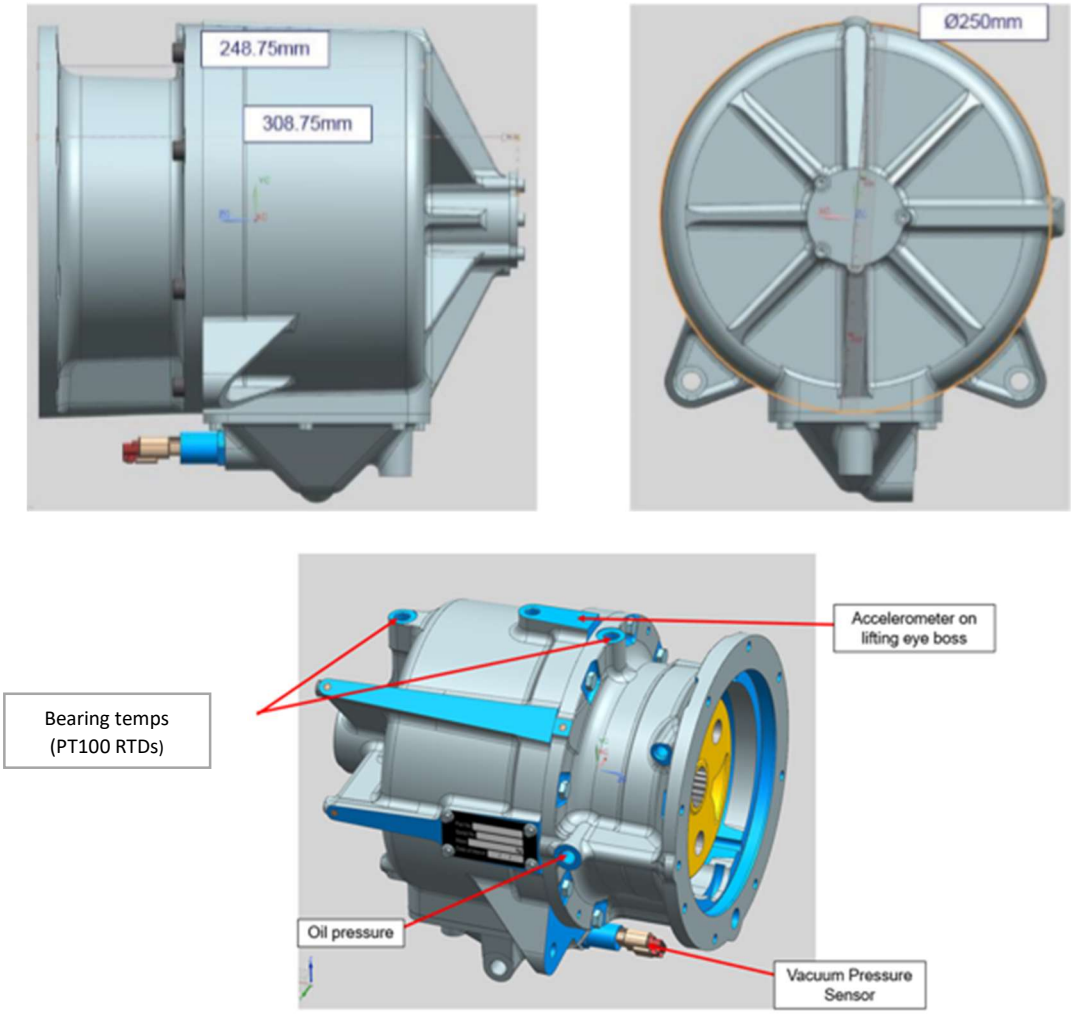

Figure 73: High Speed Flywheel Design

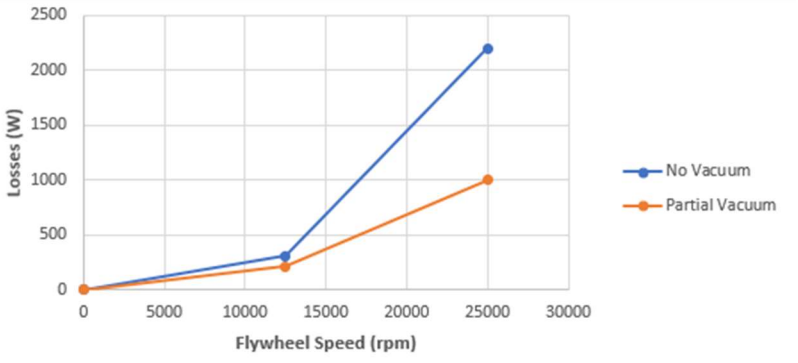

Figure 74: Aerodynamic drag loss comparison – No Vacuum vs Partial Vacuum

3.2.6. Variable FEAD Development

SOPO ID #	Item Title	Item Description	Start Date	End Date	Status
Task 1.8	**Variable FEAD Development**	Design and development of belt-drive system to connect HSFW and engine and integrate with FEAD	6/1/2019	12/31/2020	100% Complete

The initial concept and design for the HSFW connection to the engine was a belt-drive system. It consisted of a clutch for startup isolation, countershaft and planetary gearing, and a metal belt drive. Subsequent requirements and constraints drove the need to explore additional concepts for high-speed flywheel power conveyance. In addition to design and packaging concerns, simulation results showed the mechanical CVT response time and control had difficulty meeting the requirements of this application. The final design selected for the high-speed flywheel drive was an electrical CVT with an MGU connected to the engine and an MGU connected to the high-speed flywheel with power transferred through a common DC bus. The e-CVT advantages included fast response time and insensitivity to engine transients due to engine/HSFW mechanical decoupling. DYNASTY plant models and controls were created for the design and were integrated into the full system simulation. Simulation results showed improved torque accuracy and more capability than the mechanical CVT.

Further analysis work was done to investigate the power requirements needed for the HSFW drive. Transient assist requirements were evaluated using engine performance simulations at different HSFW assist values and comparison to the current production engine. This analysis is covered in other sections. For energy capture, a Matlab analysis routine was used on 745AT data to investigate the sensitivity to HSFW power and energy capability on BSFC benefit. See Figure 75.

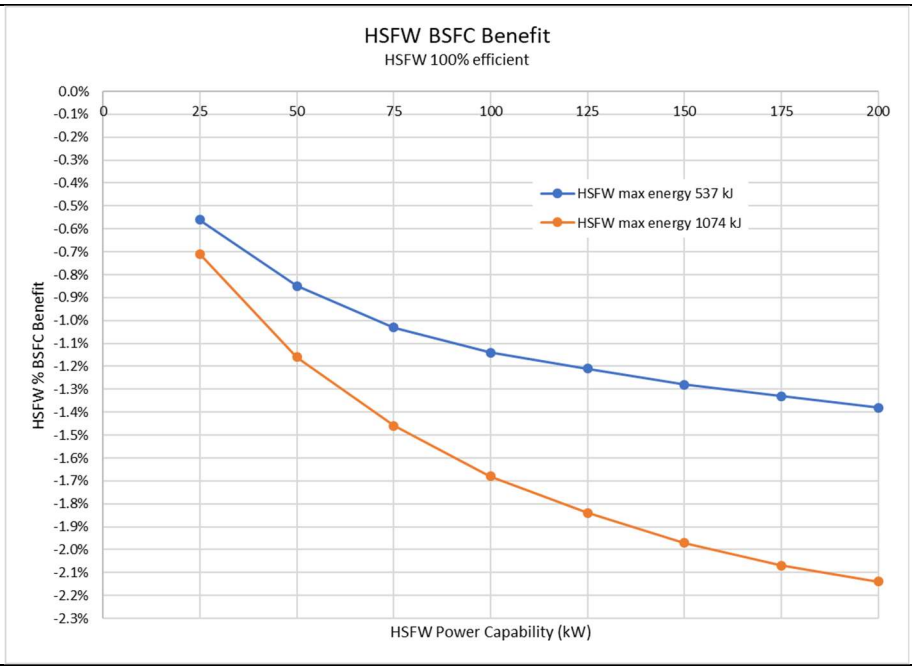

Figure 75: 745 articulated truck high-speed flywheel power and energy capability vs. BSFC

Key takeaways:

- Diminishing returns on power capability with a particular energy size.

- BSFC benefit with a 1074 kJ max energy flywheel with 50 kW max power is similar to 537 kJ max energy flywheel with 100 kW max power.
- BSFC benefit for HSFW alone is small, main function is to support engine downsize with transient assist. Should focus more on minimum hybrid device size to support engine response instead of stand-alone BSFC benefit.

745AT application has the most negative "free" energy while 988 and 390 have much less. BSFC benefit of HSFW alone could be negative for these applications. As the e-CVT concept progressed, several different MGU variations were analyzed using DYNASTY full system simulation and CREO. Options were compared based on performance, packaging, and cost.

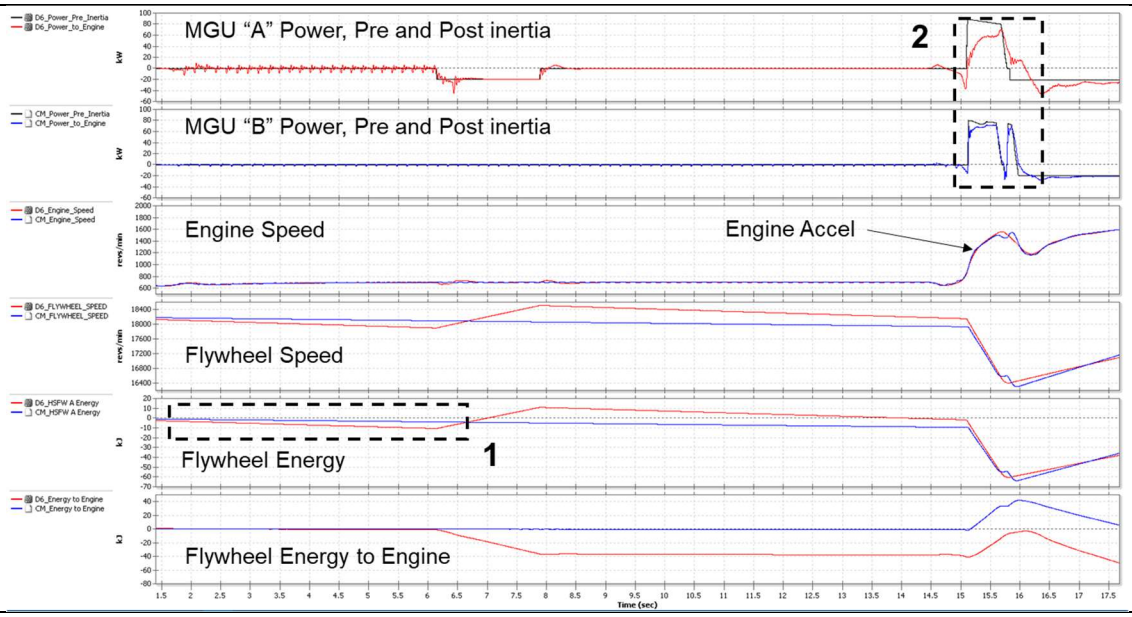

Figure 76: DYNASTY analysis results showing differences between 2 different MGU options. Highlighted area #1 shows a performance difference due to no-load losses and #2 shows a performance difference due to MGU inertia.

Final hardware selection and configuration was made along with detailed component design, engine and test cell facility integration design, and torsional vibration analysis.

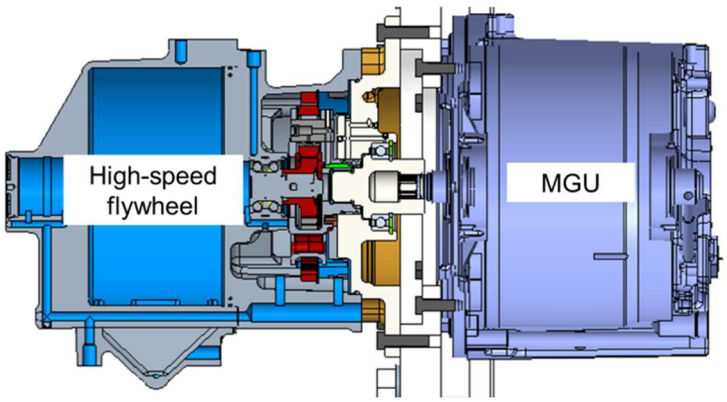

Figure 77: High-speed flywheel module coupled to an MGU

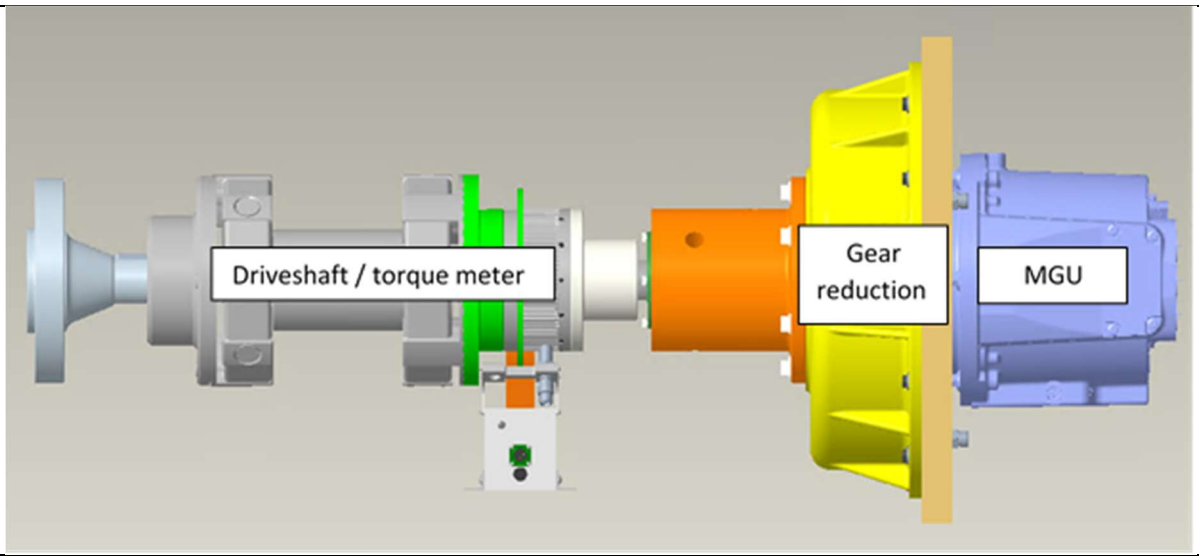

Figure 78: High-speed flywheel system engine integration

Durability analysis was performed on the high-speed flywheel drive system using histograms created from simulated machine cycles. The histograms were input into Romax analysis software and showed bearing life and stress to be acceptable to meet the 12,000-hour target. The histograms were also used to evaluate gear life in Caterpillar's gear analysis software. Gear life and stress were also found to be acceptable. Durability analysis and testing was also done by the high-speed flywheel supplier for the flywheel module itself. Extensive fatigue analysis was done to verify the target of 600,000 full charge and discharge cycles could be met. Bench tests were also done on a similar design to validate the inputs of the analysis including material testing and stress validation. Bearing life calculations were performed by the bearing supplier and predicted 20,000 + hours of life based on a generic off-road duty cycle and vibration levels.

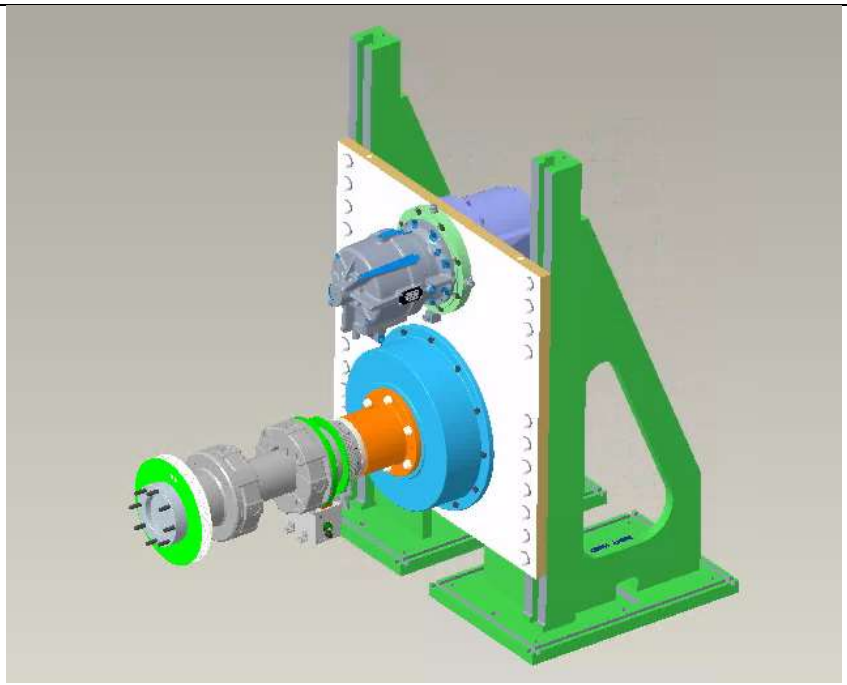

Figure 79: High-speed flywheel hybrid system

3.2.7. MGU Specification & Procurement

SOPO ID #	Item Title	Item Description	Start Date	End Date	Status
Task 1.9	**MGU Specification & Procurement**	Motor Generator Unit for vehicle stop-start will be specified based on 1D simulation in ST1.1	6/1/2019	9/30/2020	100% Completed

A 48V MGU supplier and model were identified and procured along with a compatible inverter. The 48V MGU had a continuous power rating of 15 kW and peak power of 23 kW. Once the motor was selected, the integration design of the MGU onto the engine FEAD was developed. This included a belt-drive system with a tensioner and torsional decoupler pulley along with bracketry. With data from the MGU supplier, a plant model was created for use in DYNASTY along with an initial battery model. An MGU controller was also created in Simulink and together with the plant model were integrated into the full H2D2 system model. Simulations were completed to develop the L5 and MGU controls and determine its most efficient use. For test cell integration reasons, a battery emulator was chosen instead of a battery and the battery parameters were simulated.

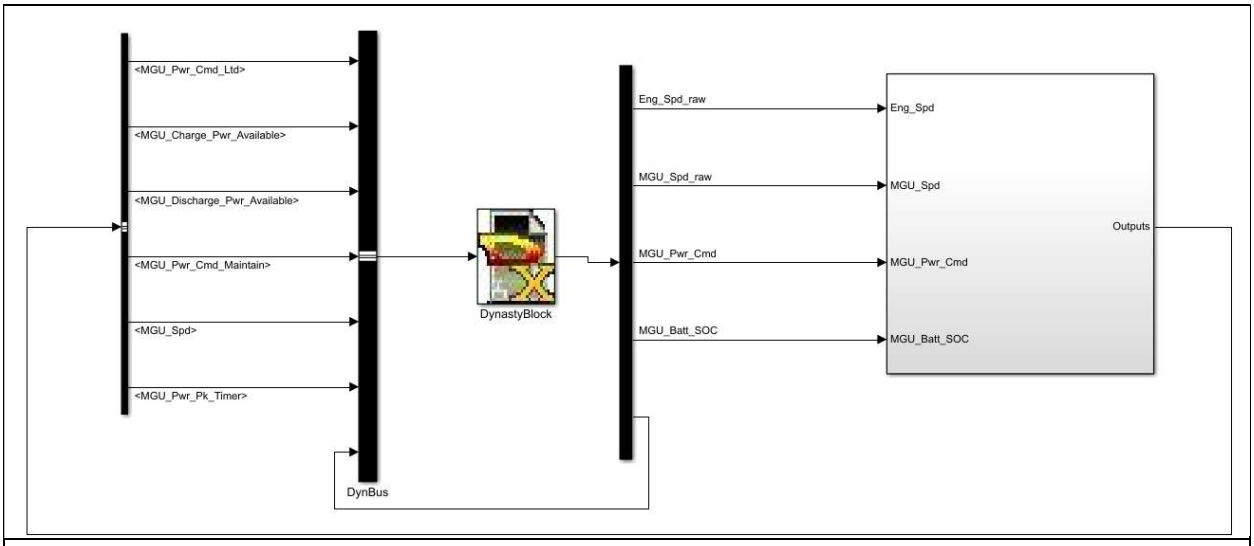

Figure 80: MGU Simulink model setup for DYNASTY Co-simulation

Figure 81: 48V MGU

3.2.8. Aftertreatment Development

SOPO ID #	Item Title	Item Description	Start Date	End Date	Status
Task 1.10	**Aftertreatment Development**	Aftertreatment re-design for reduced pressure drop. Harness the thermal management building blocks (like VVA) to enable selective catalytic reduction with > 98% conversion efficiency	3/1/2019	6/30/2020	100% Complete

The H2D2 program had a target to lower backpressure (BP) by 50% compared to that of the relevant current production engines. This was driven by the desire to extract as much waste heat through the SuperTurbo turbo compounding function, but this target of 50% was relaxed to ~30-35% during project execution due to the combined air and aftertreatment system need to drive EGR. The Caterpillar simulation tool, DYNASTY, allowed for modeling of various combinations of aftertreatment components as well as minimum (fresh) and maximum (aged) pressure drops across the DPF. Significant updates to the DYNASTY kinetic libraries, with a focus on most accurate pressure drop prediction, were completed throughout the aftertreatment development efforts. After extensive research using this simulation and supplier information, a complete aftertreatment system consisting of a DOC, DPF, mixer, SCR and AMOX was selected.

The decision was to have DOC on DPF (also called DOCF) in the final recommended aftertreatment system. The DOCF replaces the need for a separate DOC and DPF because this unified component has oxidation catalyst (PGM) coated over the DPF framework. This minimizes the backpressure while maintaining conversion requirements. Although no Caterpillar DOCF experimental data existed at the time of aftertreatment concept selection, the simulation results shared by the supplier provided enough confidence in this technology. Traditionally, the DPF framework consisted of square-shaped channels with alternate channels blocked from inlet or outlet. For this DOCF, a hexagonal-shaped channel framework was chosen because it exhibits a ~17% lower backpressure compared to traditional square channels. It should be noted that the DOCF concept has not yet been widely researched in industry. Because the concept fits the requirements of H2D2 so well, Caterpillar can take advantage of this as an opportunity to further explore the technology and how it could be used in the future.

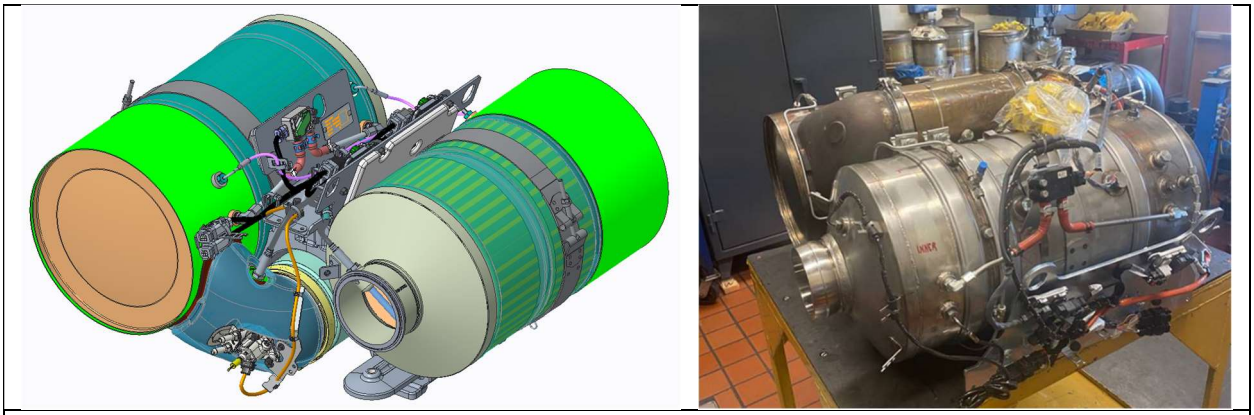

Figure 82: CAD CEM and Procured CEM

The existing Caterpillar 13L class production engine (C13B) had a 5” mixer, but it was found by the team that using 6” mixer will lower backpressure even further. Additionally, the production aftertreatment system had a compact CEM (Caterpillar Emissions Module) design but, for H2D2, a cross-cut CEM design with DEF dosing after the filters was finalized. This design will slightly improve pressure

drop numbers and will also minimize platinum migration impact over DEF dosing. Avoiding potential platinum migration is extremely valuable in this situation because platinum migration characteristics for DOCF are not yet understood. The final concept aftertreatment system design can be seen in Figure 82.

The C13B SCR technology is Gen III Cu-zeolite catalyst with 600 cpsi, but for H2D2, Gen IV 400 cpsi was recommended. The Gen IV SCR is found to be highly active so that the length of SCR and SCR/AMOX can be reduced from 12 to 10 inches. The reduction in length and lower cpsi will further minimize the pressure drop. To match the SCR, the same supplier's AMOX technology has been chosen for the final catalyst component in the system.

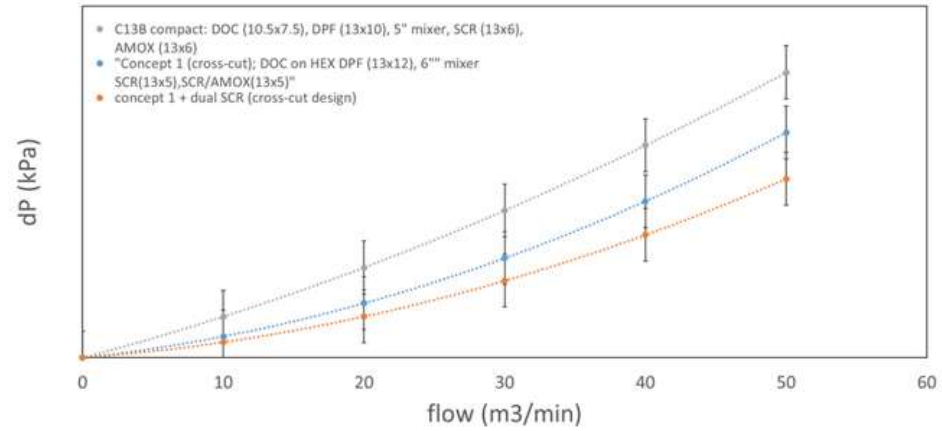

Figure 83: Mid-restriction curves: Pressure difference across CEM (kPa) as a function of volumetric flow.

Hybrid Concept Engine Aftertreatment Specification (High-Level)

- Hexagonal DOC on DPF
- Urea Dosing Injector
- 6" diameter urea mixer
- 4th Generation SCR, 400cpsi, 13"x5" (1st brick),
- 13"x5" (2nd brick ½ SCR, ½ AMOX)

3.2.9. Fuel System Development

SOPO ID #	Item Title	Item Description	Start Date	End Date	Status
Task 1.11	**Fuel System Development**	Procurement and evaluation of common-rail fuel system capable of > 250MPa peak injection pressure and digital rate shaping	6/1/2019	12/31/2020	100% Complete – On target

Caterpillar and vendors collaborated for the next generation common-rail fuel system for this concept engine system. This fuel system was fully incorporated into the engine design and combustion system development and prototype injectors were prepared for single cylinder test engine (SCTE) and for the 13L phase 1 engine testing. Specification of standard nozzle parameters (flow, spray angle, hole number, etc.) and prototype ordering was completed for matching to the piston design efforts in the **Piston Designs and Thermal Barrier Coatings** section.

In addition to the standard nozzle configurations, Group Hole Nozzle or Clustered Nozzle investigations were completed. Five different preliminary Group Hole Nozzle prototype injectors were tested in the SCTE during the first business period of the project. Figure 84 shows the tradeoff emissions and efficiency curves with the T4F piston. Emissions and fuel consumption levels are useful here for combustion hardware relative comparisons only, as the SCTE is not the same size and not directly correlated to the 13L concept engine. A clear efficiency and soot improvement can be seen with the "130-130" pink Group Hole Nozzle which is a 14-hole parallel configuration where there are 7 groups of parallel holes at a 130° spray umbrella angle. The result indicated a benefit and warranted inclusion in the H2D2 demonstration engine.

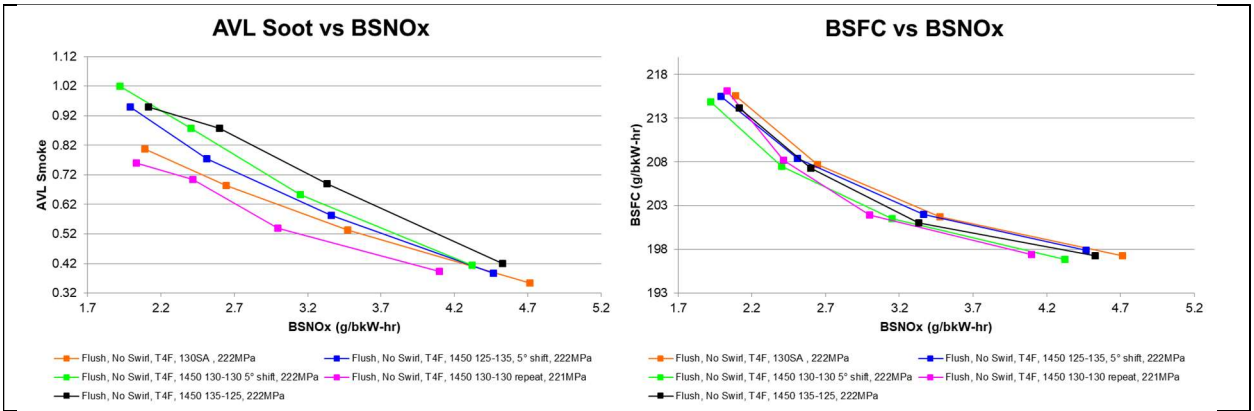

Figure 84: SCTE Group Hole Nozzle emissions and fuel consumption tradeoff curve results for 1800rpm, 231g/min (1700kPa IMEPn) fueling, 20% EGR and 220MPa rail pressure.

Combustion CFD simulation models for Group Hole Nozzles were developed and executed with the intention of confirming and refining the direction of the SCTE results. Figure 85 presents the CFD simulation results of the experiments in Figure 84, but with a different piston. Hiroyasu soot modeling was selected for computational efficiency, and the CFD produces similar Group Hole Nozzle trends to the experiments despite the piston difference.

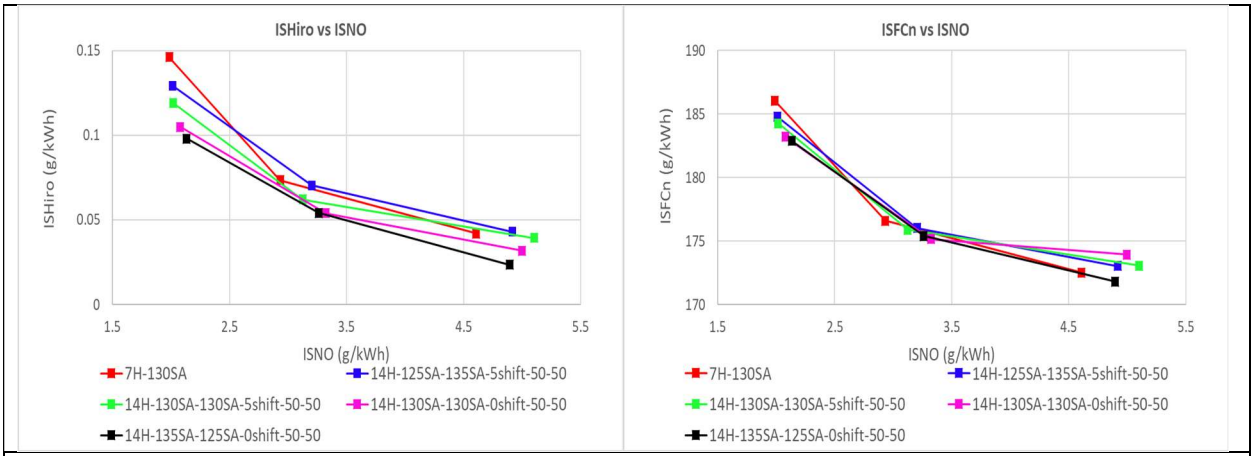

Figure 85: CFD prediction of Group Hole Nozzle emissions and fuel consumption tradeoff curve results for 1800rpm, 231g/min (1700kPa IMEPn) fueling, 20% EGR and 220MPa rail pressure.

The CFD models were further exercised to define spray targeting angles and parameters of the grouped hole and flow split nozzles. CFD Indicated specific fuel consumption (efficiency) and in-cylinder heat transfer trade-off plots are shown in Figure 86 for a rated power condition. Heat release rates are plotted in Figure 87. Some of the nozzles achieve a better NOx-efficiency tradeoff and are worth pursuing all else being equal. Large differences in in-cylinder heat transfer are predicted with the nozzles that have the lower-flowing holes in between the main higher-flowing holes. This heat transfer reduction is valuable from an efficiency standpoint, but more so from a durability, temperature limit, and thermomechanical fatigue standpoint (Go/No-Go #2 implications).

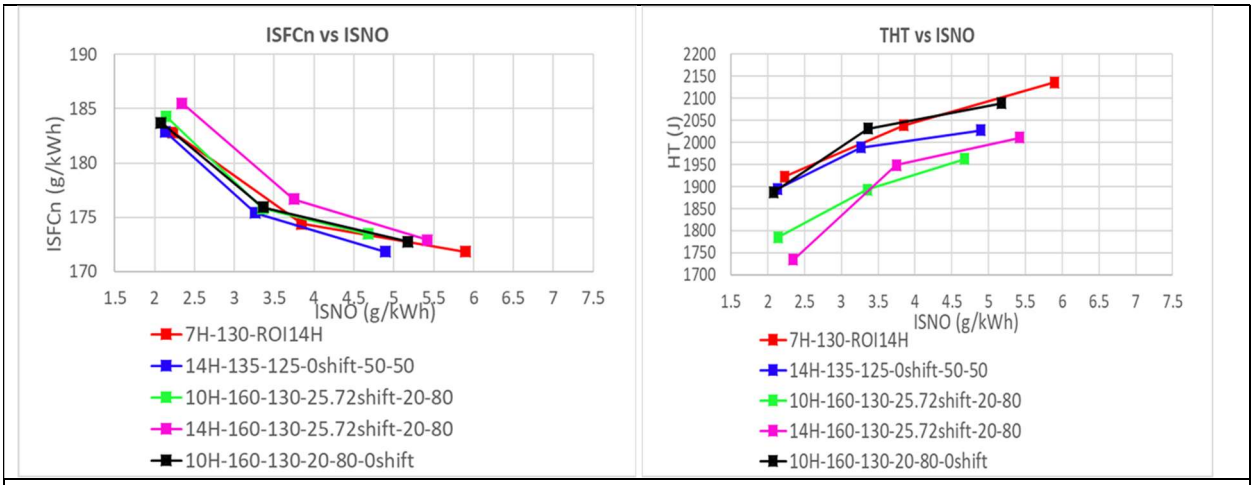

Figure 86: CFD prediction of Group Hole Nozzle NOx, heat transfer, and fuel consumption tradeoff curve results for 1800rpm, 231g/min (1700kPa IMEPn) fueling, 20% EGR and 220MPa rail pressure.

Figure 88 depicts the Group Hole Nozzle (GHN) and flow split nozzle concepts and how they visually look within the nozzle design and the spray pattern. Table 6 describes the main parameters defining the nozzle differences and specifications. Procurement and manufacturing of these injectors and nozzles was completed and included within the 13L phase 2 concept engine validation testing. However, timeline considerations forced a down-selected priority set of the following three configurations:

- Baseline 7H
- 14H Parallel GHN

- 10H 160/130 Off-Center

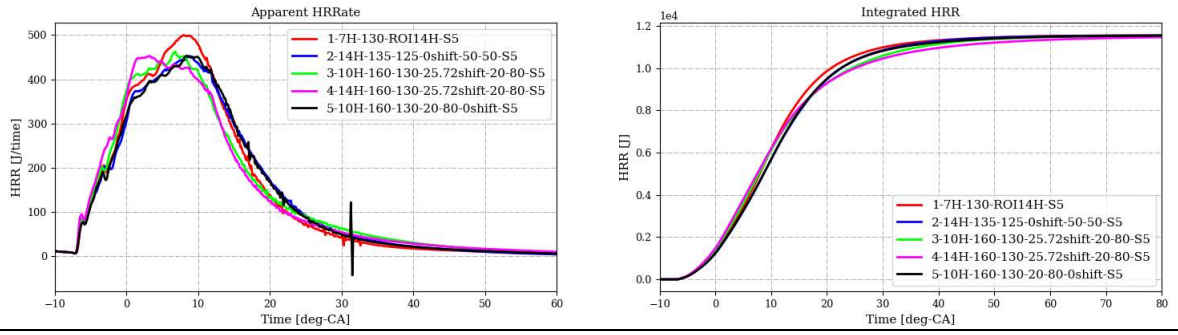

Figure 87: Apparent heat release rates and integrated heat releases from Figure 86

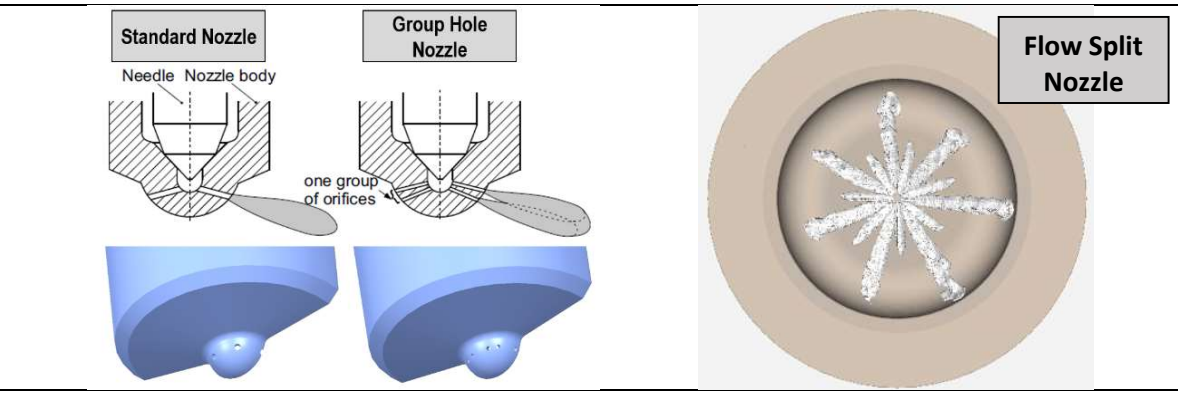

Figure 88: Schematics of nozzle layouts of the GHN concept (left) and a CFD iso-volume showing the general flow split nozzle concept (right).

Table 6: Group Hole and Flow Split Nozzles Selected for Procurement

	Baseline 7H	14H Parallel GHN	10H 160/130 Off-Center	14H 160/130 Centered	10H 160/130 Aligned
Top row: # of spray holes	7	7	5	7	5
Top row: Spray cone angle (psi * 2)	130°	130°	160°	160°	160°
Top row: Flow Split		50%	20%	20%	20%
Bottom row: # of spray holes	n/a	7	5	7	5
Bottom row: Spray cone angle (psi * 2)	n/a	130°	130°	130°	130°
Bottom row: Flow Split	n/a	50%	80%	80%	80%
Top to Bottom row: Alignment angle	n/a	0°	25.72°	25.72°	0°

3.3. Hybrid Engine System Build & Integration

SOPO ID #	Item Title	Item Description	Start Date	End Date	Status
Task 2.12	**Hybrid Engine System Build & Integration**	System virtual assembly, engine procurement, minor and major subsystem procurement and assembly fit-up.	4/1/2020	12/31/2021	100% Complete

3.3.1. Machine Integration Virtual Validation

The hybrid engine system was assembled into the 3 key machines and an analysis was completed to determine the feasibility of space available for the newly designed systems as well as compatibility of several motor generator units (MGU). This work supported the Go/No-Go #1 Decision in the beginning of this report.

Primary Issues:

- Any transmission mounting design changes were difficult and significant
- There was limited space between the transmission and the cooling package
- The engine PTO locations were being used by hydraulic pumps, reducing the availability of HVH250 locations
- 988K torque converter housing flange did not match 13X flywheel housing
    - SAE#1 vs. CAT ¾

Secondary Issues:

- Piping required re-routing for air and coolant lines
- Electrical wiring required re-routing or additions
- There were bracket design changes or additions

High Speed Flywheel:

- There was limited space available for mounting. However, it did not need to be near engine and could be packaged outside the powertrain bay

SuperTurbo:

- Gear / belt system is needed to connect to right hand side front PTO

Motor Generator Units of Selected Concept Layout:

3 High Voltage Hairpin (HVH) motor-generator units (MGU), HVH120-080-4P, HVH250, and HVH410, were selected from Remy (BorgWarner) to be used as prime candidates for the hybrid concept 2a and packaging study. The variable FEAD development of concept 2a has the high-speed flywheel (HSFW) attached to a HVH250 in all applications, with the option to use a second HVH250 or a HVH410 mounted to the engine-side at some location. The 48V HVH120 will replace the current alternator and will always be used. A decision was made between the HVH410 and the HVH250 with planetary gears with the information below from the packaging analysis, and the level of ability to attach the MGUs to the flywheel housing and transmissions.

HVH410 Summary:

- The input shaft was small and would need a coupling to flywheel
- The output shaft was too small and would need a coupling to transmission / torque converter

- Direct drive from the engine will be too much for the off the shelf MGU to handle
- None of the transmission gears matched the HVH410 internal output gear

HVH410 Mounting - Front of the crankshaft / damper:

- A bracket needed to be designed to support the MGU
  - The bracket will need to be attached to the engine and not the frame
- A coupler needed to be designed to match the input shaft on the MGU to the front damper
- The MGU interfered with the cooling package on all 3 machines.
- Extensive design changes were needed to accommodate the MGU.

HVH410 Mounting - Main engine flywheel:

- Off the shelf HVH410 cannot handle the torque from the engine
- A redesign for higher through-torque is required to reopen this as a possibility
- Additionally, there is a possibility of pushing the HVH410 toward the engine flywheel by reducing the flywheel thickness to maintain the same total inertia

HVH250 Mounting - Side of Engine:

- The MGU interferes with the fuel pump on one side
- There are 2 spots available on backside of the PTO
  - This space is taken up by hydraulic pumps in almost every machine
  - Point load increases on the PTO during retarding can cause reductions in rear crank bearing film thickness. This could limit the retarding power capability.
- Planetary gears needed to match the engine speed – space issue
- Space near the current starter location could be used – some interference with frame
- A new flywheel housing with a relocated or added PTO location

HVH120:

- Attached to 2nd level pulley plane on damper
- A/C compressor also can be moved to 2nd level pulley

Changes needed to install HVH410:

- 745C
  - Engine isolator mounts shifted toward rear of machine. Plate to follow
  - ATTAC cooling bracket / hood hinge bracket
  - ATTAC shifted forward (Interferes with grill)
  - Sway bar above ATTAC
- 390F
  - New front engine mount design
  - Engine isolator mounts shifted toward right side of machine
  - Entire cooling package shifted toward left side of machine
  - Fan shroud reduced
- 988K
  - Heat shield and bracketry shifted toward rear of machine
  - Cooling package shifted toward rear of machine

Table 7 attempts to summarize the options of the hybrid system that work or will need machine design modifications if a machine-level system is pursued. An "X" indicates non-feasible without the changes listed in the discussion above. A "✓" indicates feasible with little to no changes using the present designs

and or off the shelf components. It is clear that the small 48V HVH120 MGU is the most feasible as it is the smallest and least intrusive. It is also clear that the HSFW (coupled to a HVH250 MGU) can be packaged somewhere in each machine. The SuperTurbo has a clear installation path on 2 of the 3 machines as it is already closely located to the engine.

Table 7: Hybrid System Packaging & Integration Summary Matrix			
	Machine		
System	745C	390F	988K
HVH410 – Flywheel Mount	X	X	X
HVH410 – Front Crank Mount	Interference with cooling	Interference with cooling	Interference with cooling
HVH250 – Flywheel PTO Mount	X	Interference with frame	X
HVH250 – Lower Flywheel Housing Mount	X	X	Interference with frame
HVH120 – Alternator Replacement	✓	✓	✓
High Speed Flywheel Space Available	Pursue outside engine bay	✓	✓
High Speed Flywheel Location	Near Engine	Near Battery	Near Engine
Super Turbo Space Available	Interference with frame	✓	✓
Super Turbo Piping	Reverse of Current	Similar to Current	Reverse of Current
Fuel Filter	Remote Mounting	Remote Mounting	Remote or On-Engine
Oil Pan Orientation	Rear of Engine	Interference - Central	Rear of Engine

The following figures show a small representative subset of the CAD geometry and how it looks, fits, interferes, and packages into the three key machines.

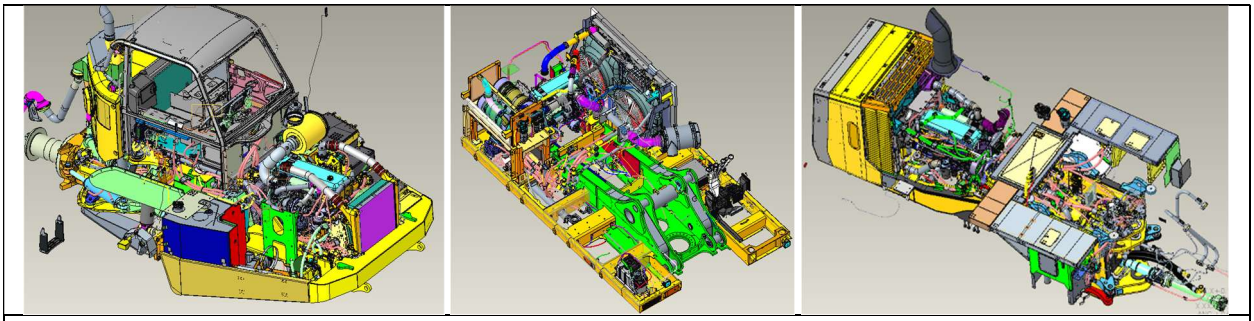

Figure 89: Packaging CAD assemblies for 745 AT, 390F, and 988K machines from left to right

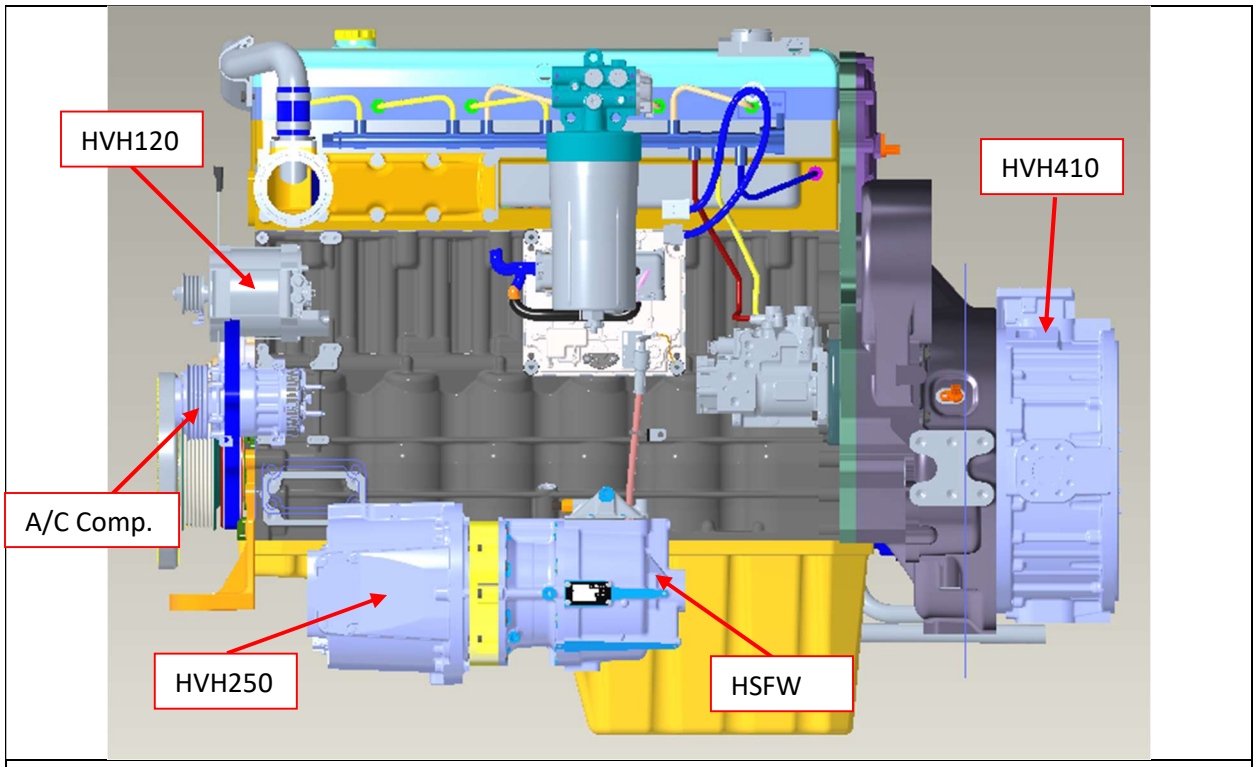

Figure 90: HSFW CAD with the HSFW-MGU floating next to the engine, the HVH410 in the rear-engine P2 position, and the 48V HVH120 on the 2nd level plane FEAD.

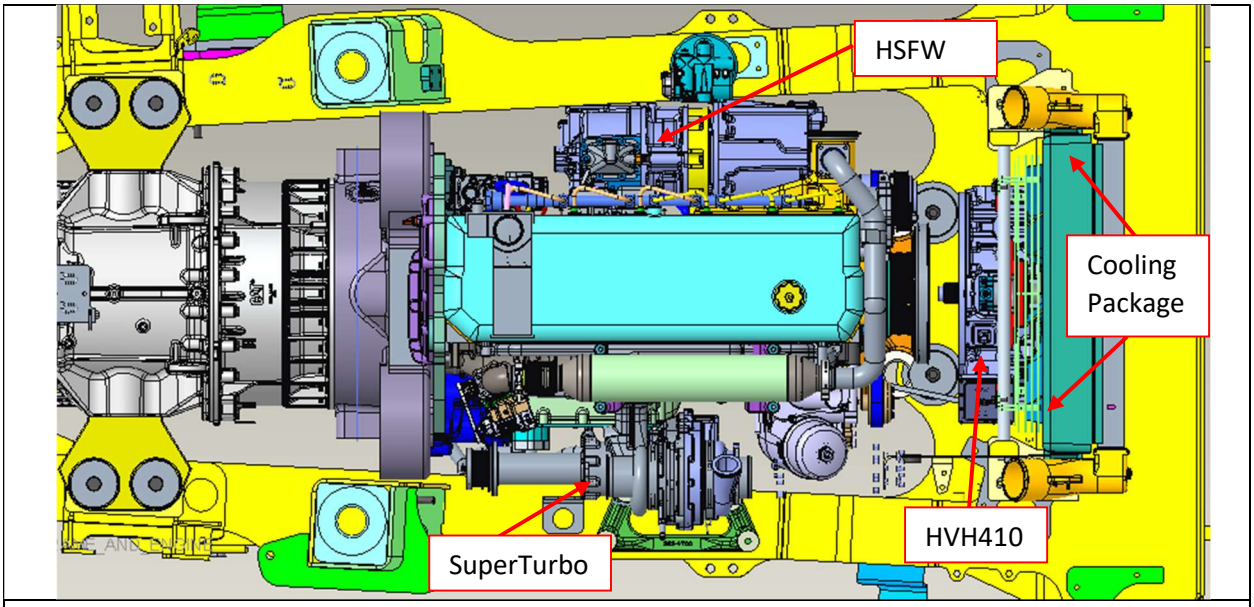

Figure 91: 745 AT with the HVH410 in the front position showing cooling package interference.

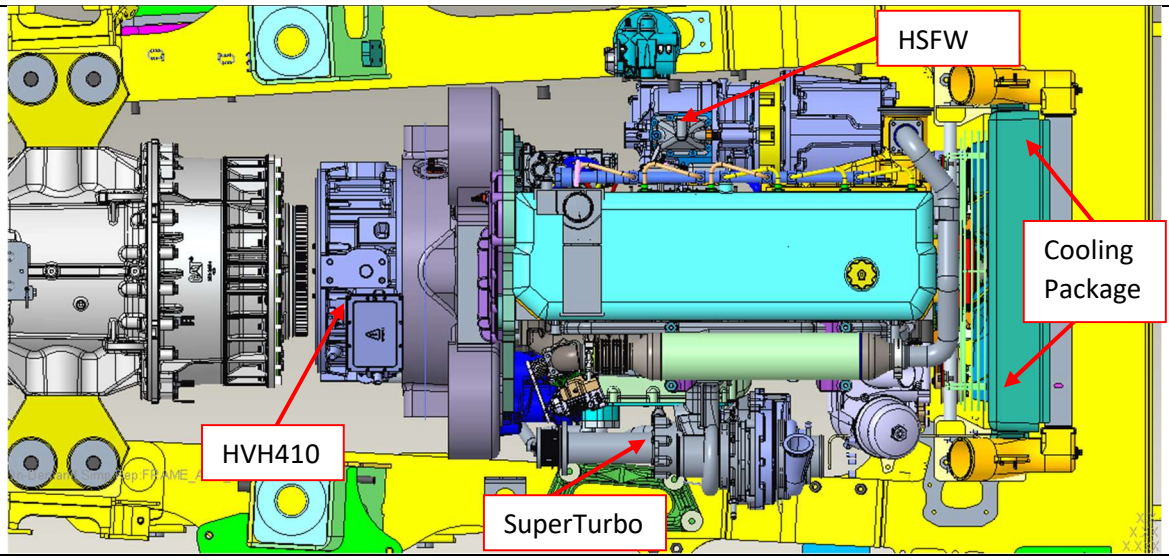

Figure 92: 745 AT with the HVH410 in the rear P2 position showing engine-cooling package interference.

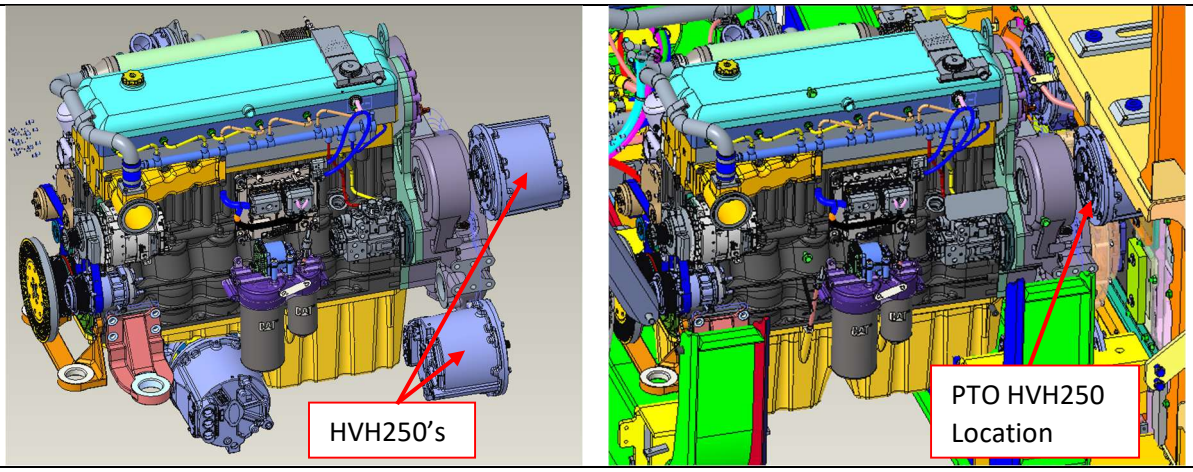

Figure 93: 390F with the HVH250 on the left-side rear PTO location

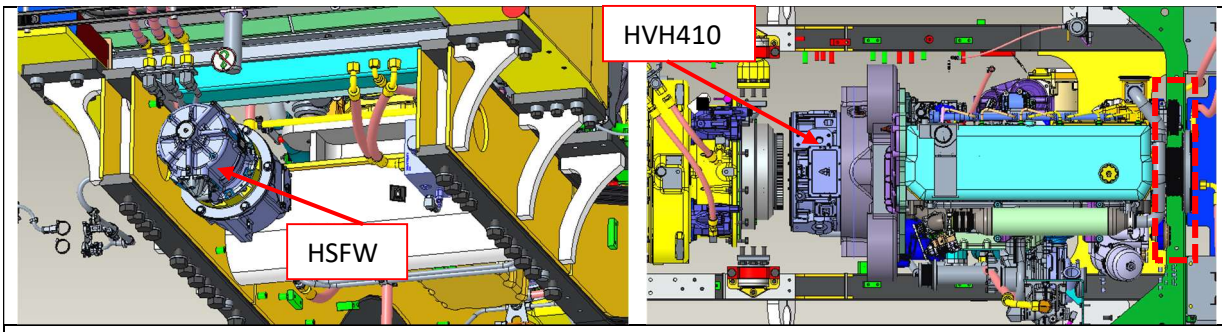

Figure 94: 988K with the HSFW under the cooling package (left) and the HVH410 in the P2 position with interference of the engine front with heat shields (right)

3.3.2. Test Cell Virtual Assembly

Test cell facility virtual installations were completed for the hybrid system only validation testing phase as well as the concept engine only and full system level installation. The completed virtual design of the hybrid only validation system and test cell setup is depicted in Figure 95. The CAD model comparison to the actual setup is shown in Figure 96. Piping and wiring were done as needed to complete the setup. Several benefits were derived from completing a virtual installation before a real-life build. Proper planning and layout contribute to a successful installation along with understanding system requirements such as cooling, electrical, exhaust, and mounting systems to reduce vibration.

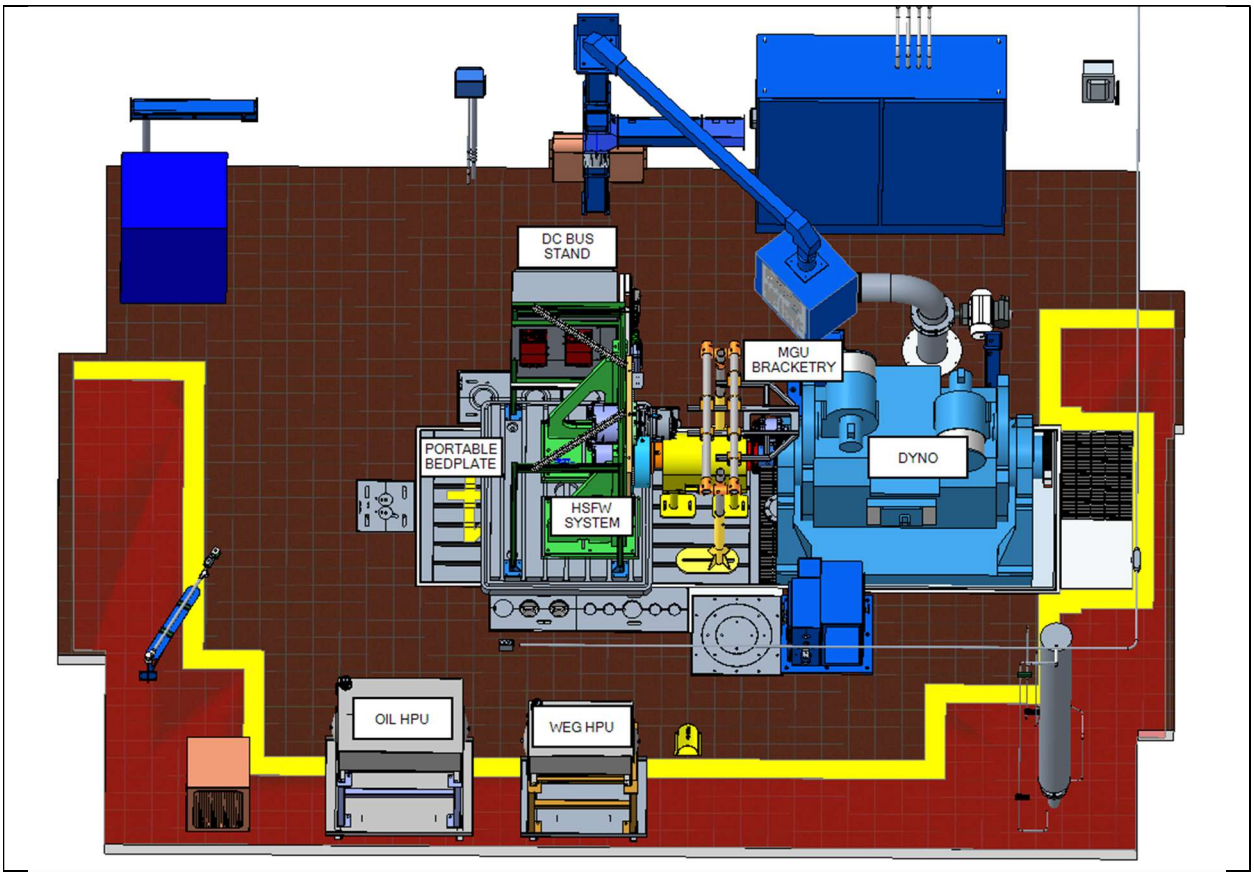

Figure 95: Layout of Hybrid-Only System Checkout Test Cell 104

The non-engine shakedown testing effort planned before the engine-connected testing was to debug and validate the hybrid performance and controls. The partial build and shakedown were completed and included everything except the core engine and the SuperTurbo: HSFW, HSFW electric drive MGU's and invertors, 48V MGU and battery emulator.

Figure 96: Hybrid-Only System Build Pictures & CAD Comparison

3.3.3. Concept Engine Build and Installation

The removal of the hybrid-only system had to occur first and then the installation of the H2D2 engine-only system into test cell 104 could take place. The core H2D2 concept Phase 2 engine build had no major issues of note. Installation continued for the first week of December 2021 which was followed by onsite visits to the Caterpillar Technical Center from SuperTurbo engineers for debugging and setup.

The mechanical setup of the SuperTurbo went without major issue and the Caterpillar team was trained by the SuperTurbo team on adjustment, operation, and calibration. Pictures of the test cell 104 installation of the engine and SuperTurbo in Figure 97 show a complete testing configuration with all necessary connections between SuperTurbo and engine made through the accessory traction fluid cart, i.e. coolant, shop air, sensors, and CAN connection.

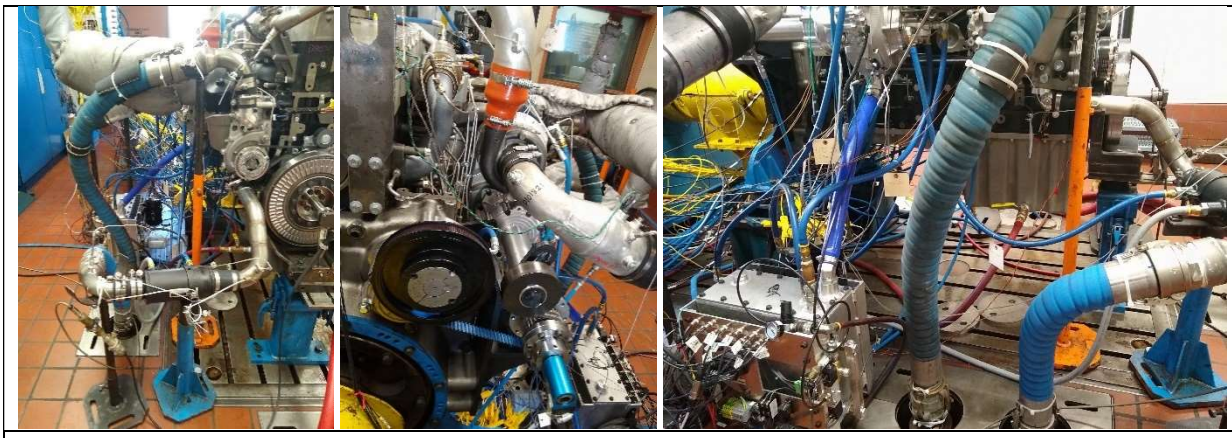

Figure 97: SuperTurbo Phase 2 Engine installation into test cell 104

Complete Engine and Hybrid System Build and Installation

The full hybrid system install was delayed. The bedplate with hybrid components was modified to work with adapter tubing to secure the floating bedplate to the main test cell bedplate, reducing vibration and allowing for shaft component alignment between the front engine damper and high-speed flywheel system as shown in Figure 98.

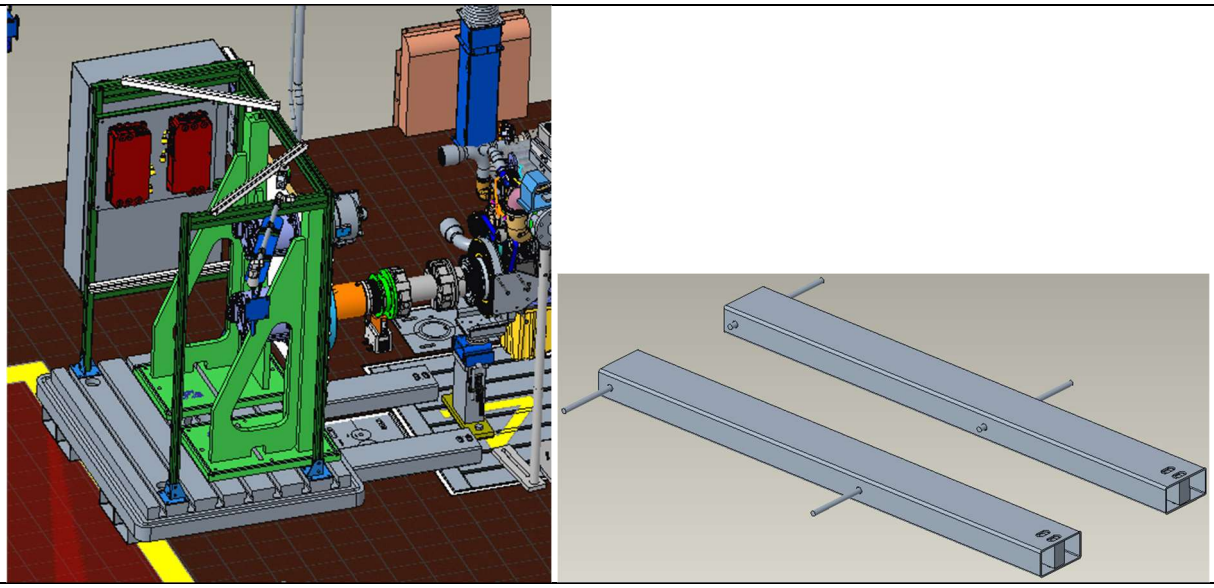

Figure 98: Hybrid Components Floating Bedplate Fixtured to Main Bedplate

The original encoder setup that determines crank angle at the front of the crankshaft was not feasible as the hybrid system will have a driveshaft running off the front of the crankshaft. Understanding cylinder pressure and crank angle is critical for successful performance development, so a rear-mounted encoder was added between the dyno and the engine to solve this issue as seen in Figure 99.

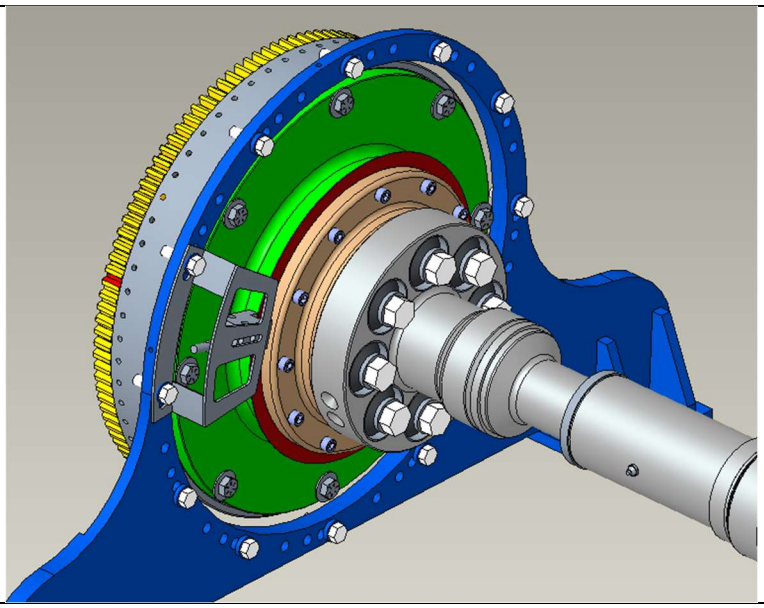

Figure 99: Rear crankshaft position encoder with flywheel adapter plates installed

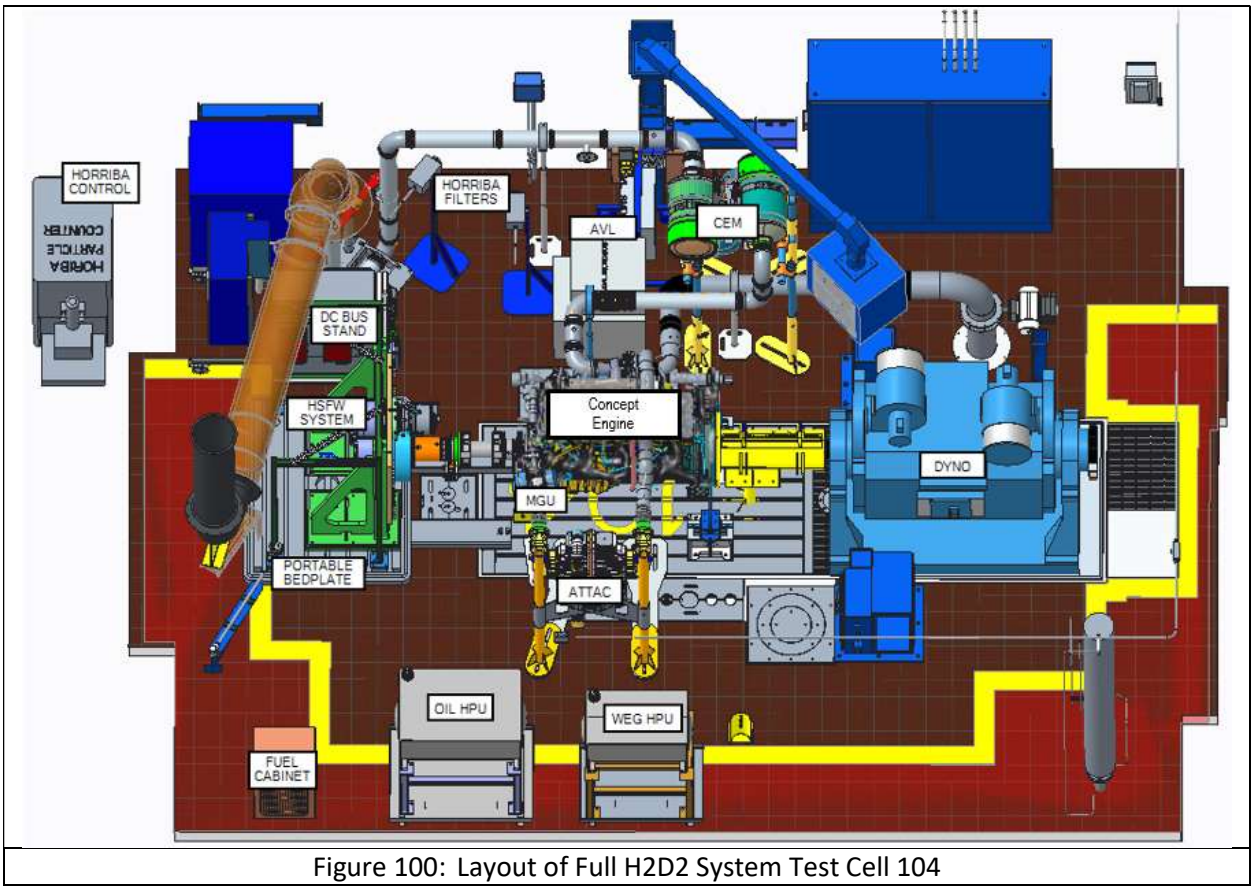

Figure 100: Layout of Full H2D2 System Test Cell 104

The complete Virtual Engine Installation (VEI) with exhaust system, piping, filters, CEM, oil pumps, hybrid HSFW, cooling system, and guarding in place is shown in Figure 100. This final design proved difficult as the test cell is smaller than most at the facility and there has not been a floating bedplate with the heavy mass outside of the normal test bedplate tested before. Vibration was damped with rubber

mats underneath the adapter plates and floating bedplate. Limited space did cause issues with maintenance and maneuverability in the cell. Overall, the design was robust and led to a successful installation.

3.3.4. Thermal Barrier Coated Components

The procurement of pistons with Thermal Barrier Coating (TBC) was revised due to supplier timelines, however two sets of pistons were received. The TBC pistons were evaluated in conjunction with the TBC head and combustion system in the last phase of the testing period, and one set continued all the way through to the final validation transient testing.

The TBC cylinder head was specified and successfully manufactured and procured. Figure 101 shows the physical prototype cylinder head and highlights the region (white color) where the TBC was applied. This TBC Cylinder head ran the duration of the validation testing.

Engine valves with TBC coating were successfully manufactured and completed. These TBC valves were evaluated during a single cylinder combustion system hardware sorting in the middle of the validation testing but were not put into the engine build due to time and variable constraints. Testing was completed on a rig to show the wear from heat and test durability of the coating.

Figure 101: TBC Cylinder Head Successfully Manufactured

3.3.5. Front Facing Exhaust Manifold

A bespoke designed forward-facing exhaust center section was needed to accommodate the switch from using the front engine drive for the SuperTurbo to the rear. The front-facing exhaust manifold center section was made of the same material as the rear facing exhaust and passed durability frequency response analysis and FEA on the first round.

Figure 102: Front facing exhaust manifold

3.3.6. Oil Gallery Solenoid

A solenoid was installed in place of the mechanical priority valve in the main oil gallery. To accomplish the transition, machining had to be done to the block, but the threads remained the same. The solenoid allowed for full authority control of the oil flow to the piston cooling jets.

Figure 103: Solenoid unpackaged and installed into engine block

3.4. Hybrid Engine System Validation

SOPO ID #	Item Title	Item Description	Start Date	End Date	Status
Task 3.13	**Hybrid Engine System Validation**	Engine Debug, Baseline Engine Testing, Hybrid Engine System Installation, and Hybrid Engine System Validation	9/30/2021	9/30/2022	100% Complete

The main subtasks of the Hybrid Engine System Validation Task 3.13 were the following items:

- Hybrid-Only Debug and Testing (incremental to original scope)
- Engine Debug
- Baseline Engine Testing (Engine-Only)
- Hybrid Engine System Installation
- Hybrid Engine System Validation

The following validation tests were able to be successfully completed within the project and the no-cost time extension Q16:

- Hybrid-Only System:
    - Mapping of devices and driveline losses
    - L3 and L4 controls calibration
    - Power and charge/discharge rate capability confirmation
- Engine-Only:
    - Steady-state performance and emissions mapping over the entire speed/load region
    - Motored friction curve measurement
    - Constant Speed Load Acceptance (CSLA) test
    - NRTC cycles for Tier 4 Final Emissions capability verification – ***Passed T4F Emissions***
    - 6 key machine cycles (out of the originally simulated 19)
- Full Hybrid System:
    - Motored friction curve measurement
    - NRTC cycles for the 3 key applications – ***only hybrid assisting strategy***
    - 6 key machine cycles (out of the originally simulated 19) – ***only hybrid assisting strategy***

3.4.1. Hybrid-Only Validation

Hybrid-only debug and validation testing was completed successfully. The hybrid L3/L4 controls were calibrated, and losses were mapped and used to update the controls and simulation models. The high-speed flywheel (HSFW) and 48V MGU hybrid systems performance and capability were confirmed. The HSFW system achieved a peak of 110 kW discharging and -130 kW charging power with a peak discharge rate of 12,000 Nm/sec at the engine input. The 48V MGU system achieved a peak of 20 kW discharging and -25 kW charging power with a peak discharge rate of 1366 Nm/sec at the engine input. Temporal plots of the various hybrid device and control parameters show the performance through a series of progressive load and charge/discharge steps, Figure 104, and Figure 105. The hybrid-only setup and performance validation allowed for easier full system integration and validation in the final testing phase.

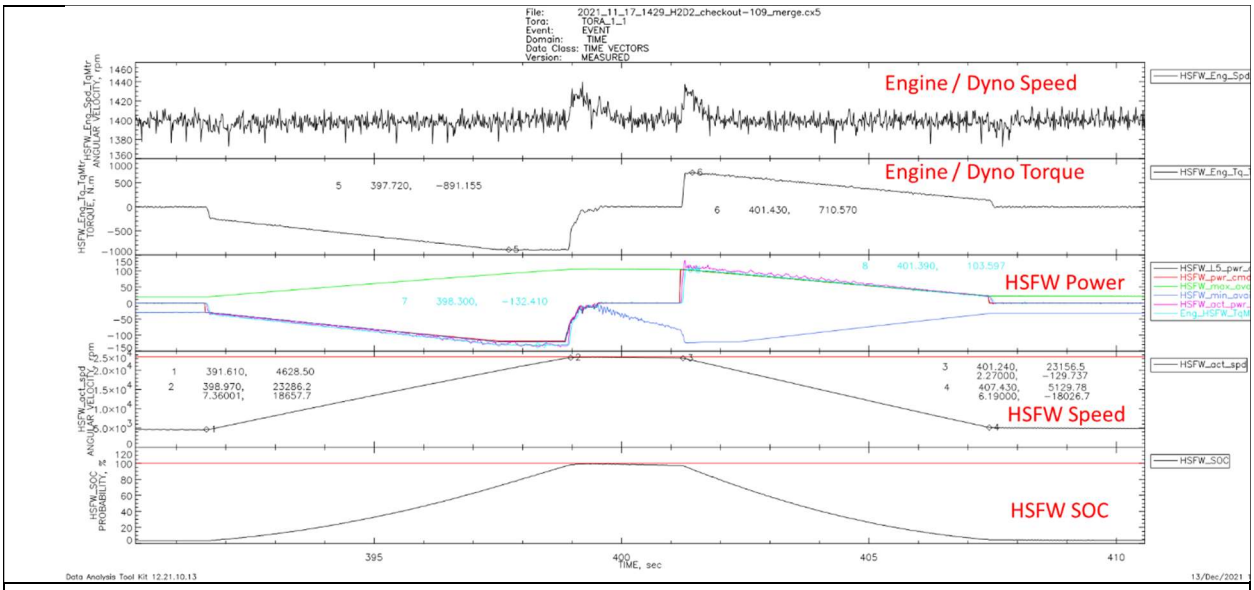

Figure 104: HSFW Charge and Discharge

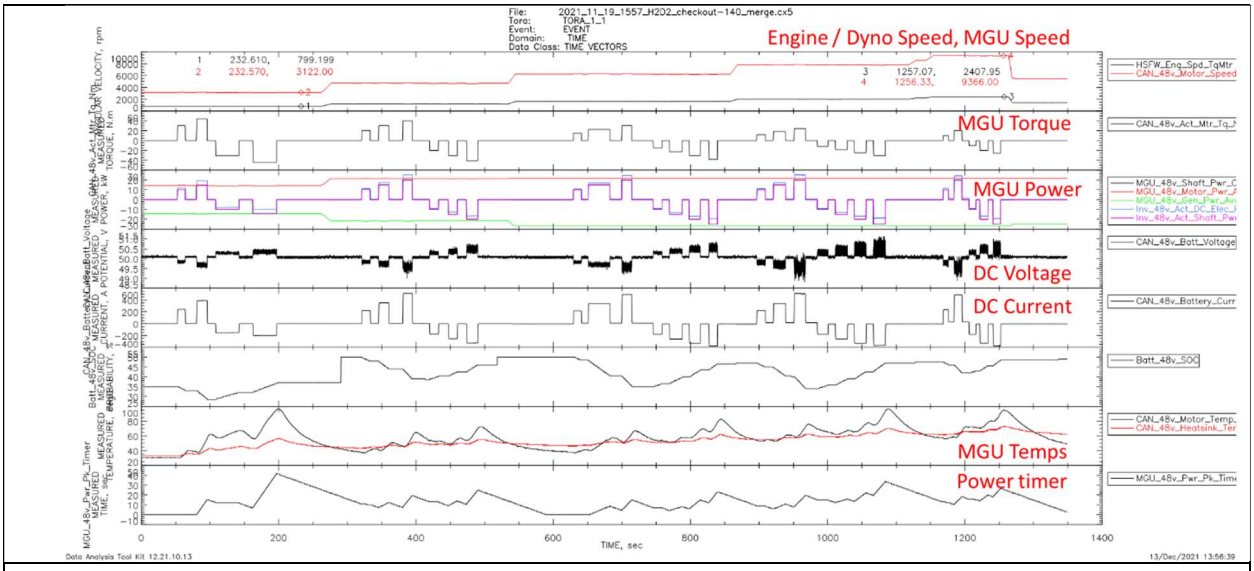

Figure 105: 48v MGU Charge and Discharge

The validation data acquired in Figure 104 and Figure 105 went into the DYNASTY system plant modeling through a correlation effort which resulted in good to excellent agreement between the test data and the simulation prediction. Figure 106 shows overplots between the validation data and simulation prediction after the model correlation and updating of loss submodels. The HSFW speed prediction can be seen to track very well with the data and indicates the electric drive MGU and hybrid drivetrain efficiency and losses were captured with a high degree of accuracy. Additionally, the no-load coast down of the HSFW was correlated to within ~2% error and adds to system modeling accuracy confidence. This was important as the full DYNASTY hybrid system model was relied on to supplement the quantification of the hybrid system performance and efficiency over transient application cycles.

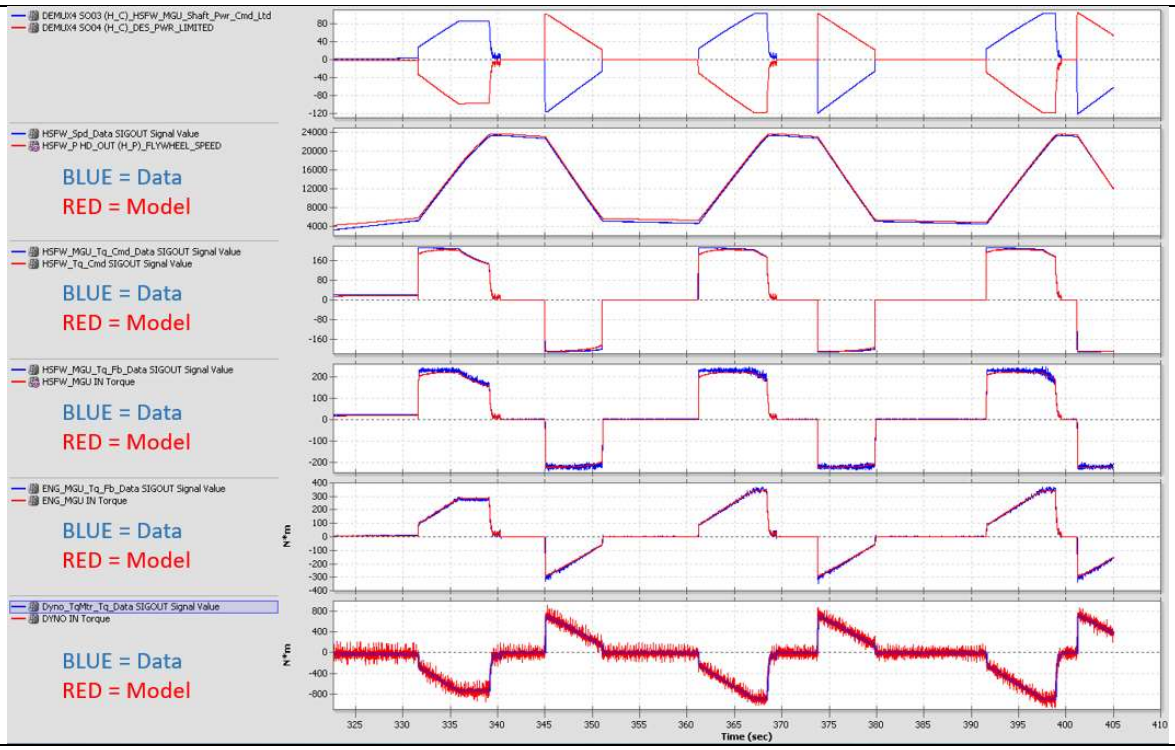

Figure 106: Full Power and Speed Charge and Discharge Plant Model Validation

3.4.2. Engine-Only Validation

Engine-Only steady-state validation testing occurred over the entire operation region of the powersystem and encompassed the three machine application lug curves as shown in Figure 106. The lug curves of the applications can be seen along with a composite lug curve representing the maximum torque envelope. Steady-state test points are called out along with simulation points for reference, indicating good alignment between the validation, simulation, and calibration efforts. Data was also acquired along the lug curves themselves, for torque and fuel limit calibration and accurate mapping to enable the transient certification-level effort when measuring cycle emissions through standardized processing methods.

Figure 108 presents the final calibrated intake manifold absolute pressure (IMAP) and IMAP error relative to the simulation running the offline optimized calibration. A monotonic increase in IMAP can be seen as moving up and to the right, as engine power increases. The IMAP level dictates the level of balance between supercharging and turbocompounding from the SuperTurbo, as discussed in prior report sections, and it can be seen that the final calibration generally had <5 kPa of error relative to the initial calibration. Two locations of difference can be noted with high IMAP error and are the result adjustment decisions to achieve the desired EGR flow/control and to smooth the calibration space.

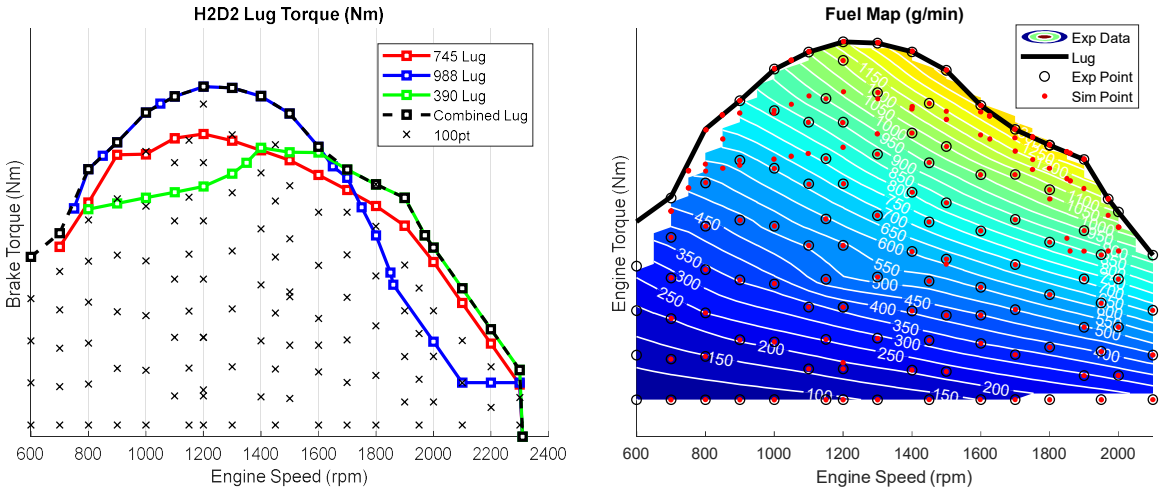

Figure 107: Lug curves, experimental and simulation data points for steady state validation

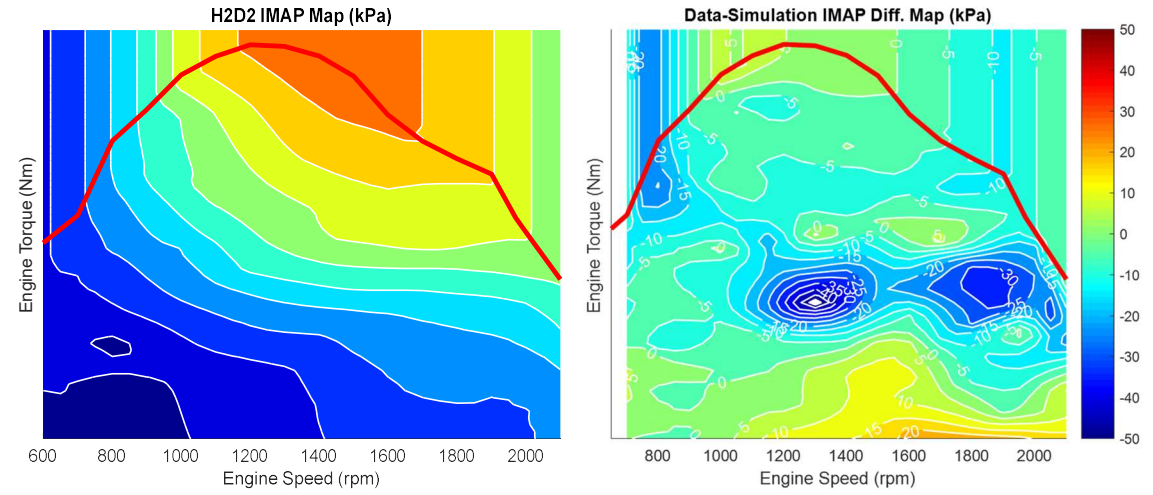

Figure 108: Final calibrated IMAP and error to the simulated IMAP

Moving to the combustion system, an example of the combustion sensitivity to SOI and rail pressure is shown in Figure 109 through Figure 111 for a 1800rpm full load operation point. The operating point is a critical point for the three machine applications and aligns to the operation histograms. High-quality cylinder pressure data shows the heat release rate differences over the SOI sweep and how the higher rail pressure increases the burn rates.

Plotting the combustion sensitivity data against NOx, the BSFC can be seen to be a better tradeoff for the baseline rail pressure, which is from the simulated/final calibration. This confirms the confidence that the combustion calibration is near optimum regarding efficiency and cylinder pressure limits for these critical high power operating modes. The developed combustion system was able to achieve the engine-out emissions (and therefore T4F tailpipe emissions levels as will be shown later) and indicated performance goals, as well as adhere to Caterpillar's durability constraints at this concept engine state of development. The final combustion system consisted of increased compression ratio, increased peak cylinder pressure, next generation common-rail fuel system with higher flowing fuel injectors, and thermal barrier coatings on the cylinder head and piston – as outlined in earlier report sections.

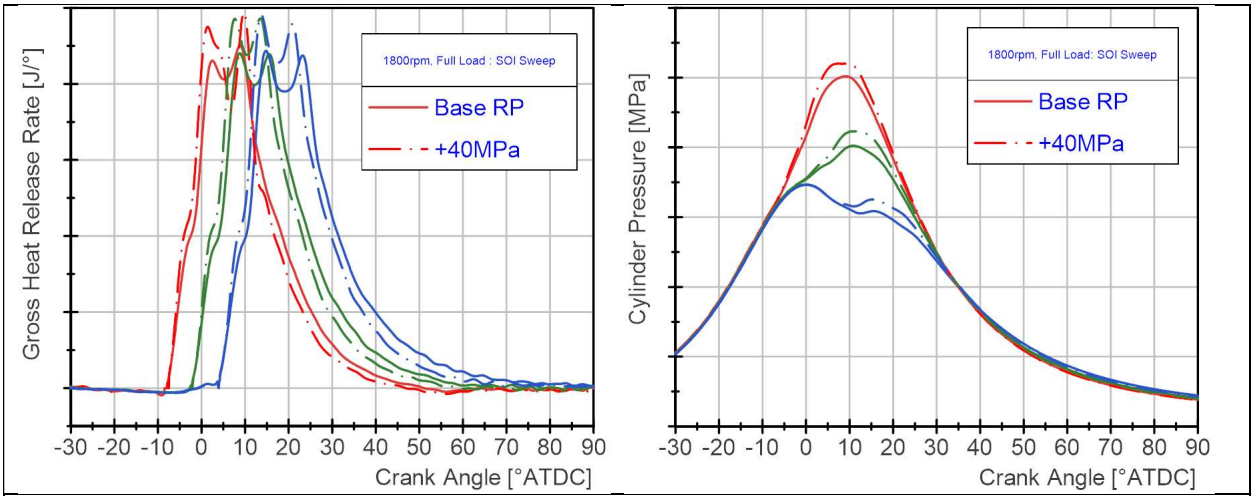

Figure 109: In-cylinder pressure and heat release rate injection timing sweep sensitivity data

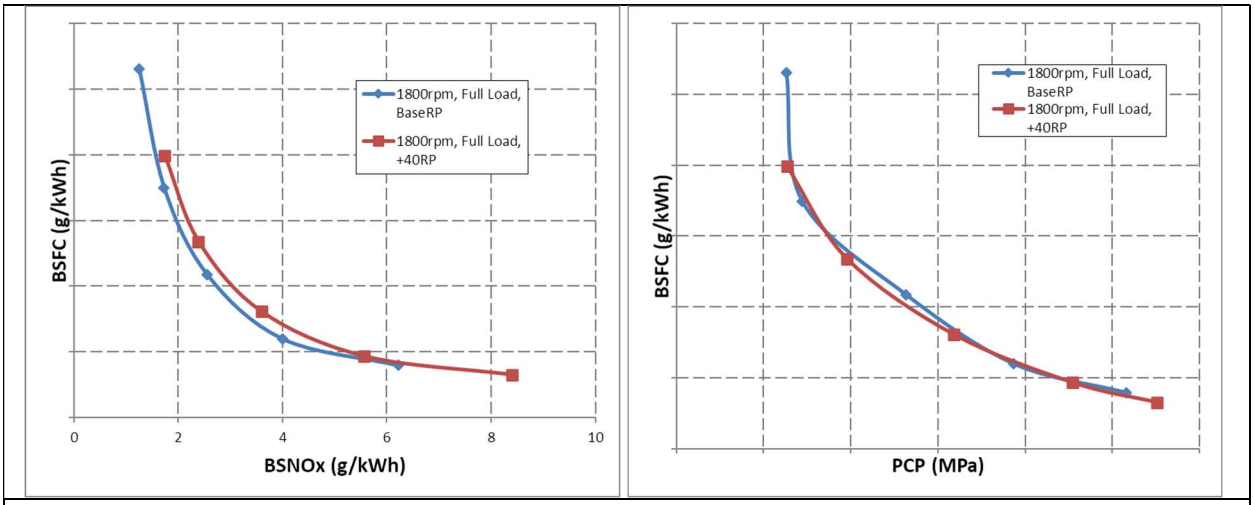

Figure 110: Efficiency and peak cylinder pressure sensitivity from the SOI and rail pressure sweep

Figure 111 plots the PMEP and pre-turbine exhaust temperature against the SuperTurbo MEP, which is calculated from a torque transducer measurement at the interface of the SuperTurbo driveshaft and engine PTO belt connection. A clear trade-off can be seen as combustion is retarded and exhaust temperatures increase. From the middle of the SOI point and retarded, the SuperTurbo MEP exceeds the PMEP of the engine, thereby recovering move energy via compounding than could otherwise be with a conventional turbocharger with high pressure EGR at these conditions.

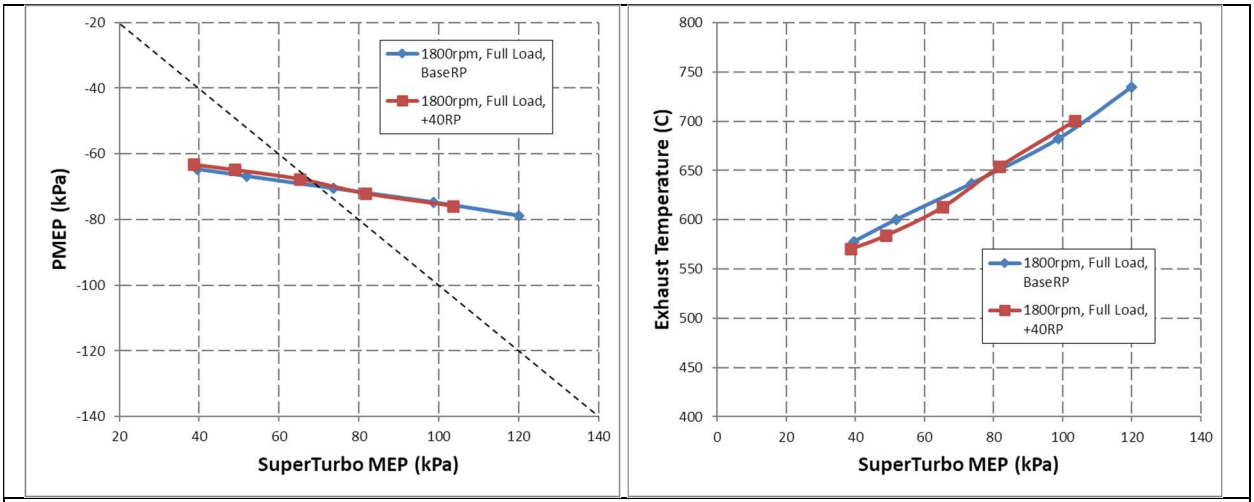

Figure 111: SuperTurbo compounding to PMEP sensitivity from the SOI and rail pressure sweep.

The full operation region calibration and resulting behavior of the combined air system is presented in the contour plots of Figure 112. The measured net SuperTurbo power at the PTO interface connection shows more negative (energy recovery via turbo compounding) power in the higher load and power regions toward the lug curve. Continuous levels peaking around 20kW of net compounding were achieved with the nominal design point of the 1.05 turbine flow nozzle. Also, high continuous levels were observed throughout testing with the other more restrictive nozzles, but the 1.05 nozzle was confirmed to be optimal for totally system efficiency. The combined PMEP+STMEP contour plot shows the resulting air system gain or loss, and the region of positive benefit can be seen to be around peak torque and power.

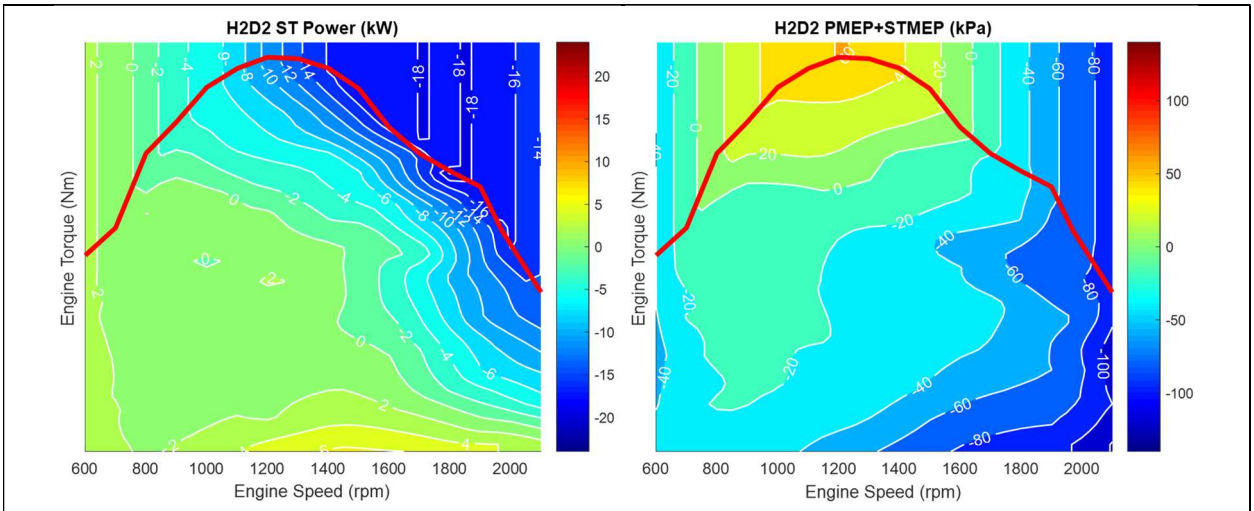

Figure 112: Final SuperTurbo power and combined air system MEP

To summarize the total combined efficiency assessment of the engine-only system, which includes all of the core engine, turbocompounding, and aftertreatment subsystems, percent difference comparisons to the reference C18 were made, Figure 113. The left contour plot shows the difference between the final validation test data and the DYNASTY Concept 13L engine-only simulation prediction prior to final correlation. There is a large region of ±2 difference, with the test data being more efficient (negative % diff) in the critical higher power and load regions. The areas of worst test efficiency and higher percent difference were found to be the very low load where the simulation typically struggles, and is attributed to differences in calibration, accuracy of combustion prediction, and accuracy of losses such as the SuperTurbo drive. The right contour plot illustrates where the total percent improvement in efficiency or

BSFC (negative) predominantly was found to occur, and an overplot of the 745 Articulated Truck NRTC cycle highlights strong alignment. The correlated and validated C18 simulation was used for the reference and is consistent with how the reporting was conducted throughout the project. Substantial 10-20% improvement ranges were validated from this testing, and final cycle results will be discussed in the following sections of the report.

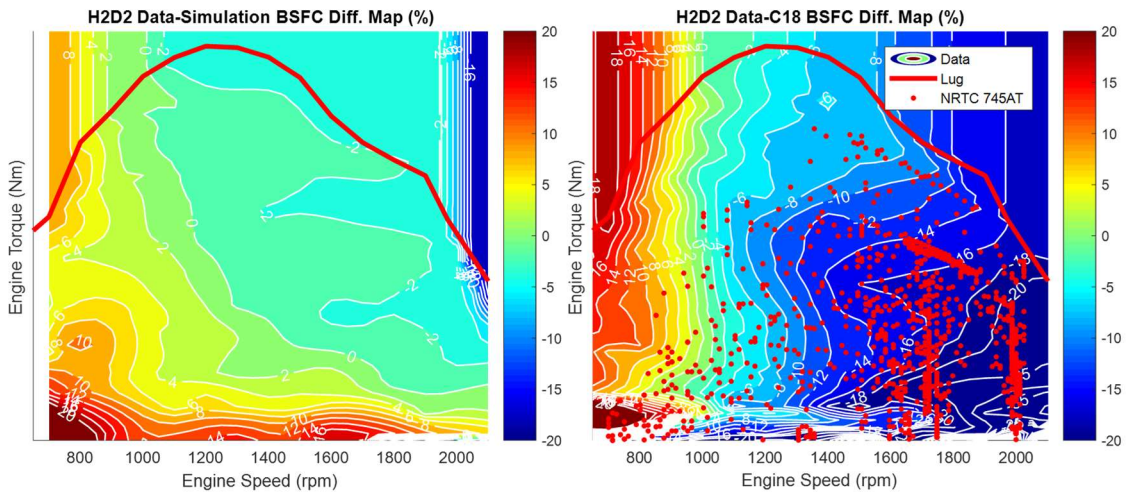

Figure 113: Left – H2D2 data to DYNASTY simulation percent difference in BSFC. Right – H2D2 data to original baseline C18 validated simulation percent difference in BSFC. Transient points from the 745 Articulated Truck NRTC are overlayed for alignment assessment.

To validate the transient load response of the engine-only H2D2 system, CSLA tests were completed. The test is conducted by warming the engine system up at a high load, then successively running no-load to full load steps from 800rpm to 1800rpm in 200rpm increments. Each load step is repeated three times while the transient engine performance metrics are recorded. Figure 114 shows two example CSLAs for 1200rpm and 1800rpm with plots of the system shaft torque, IMAP, and SuperTurbo power. Four conditions are overplotted with notations for the minimum AFR allowed from fuel limiting and one condition where close to zero SuperTurbo assisting power was prescribed. The supercharging assisting is easily observed and a large increase in IMAP rise was validated. Figure 115 plots some representative metrics from all of the CSLA validation data acquired, and refinement can be seen from balancing the transient calibration for response time, hardware limits, and soot emissions. The “final calibration” (yellow) was adopted for the remaining validation testing, but it should be noted that further improvements could still be achieved with more production-level fuel control calibration.

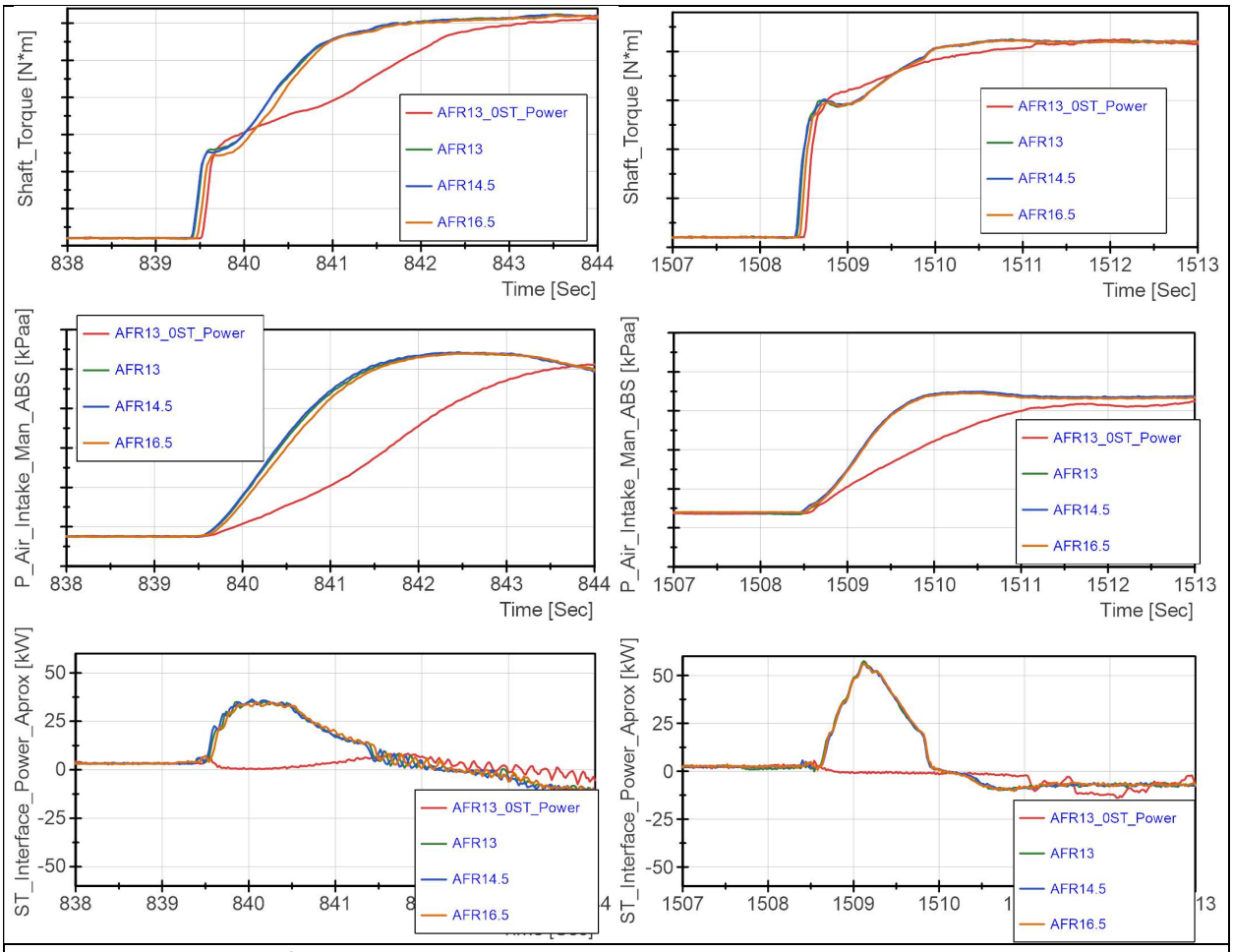

Figure 114: Left – 1200rpm CLSA transient data, Right – 1800rpm CSLA transient data

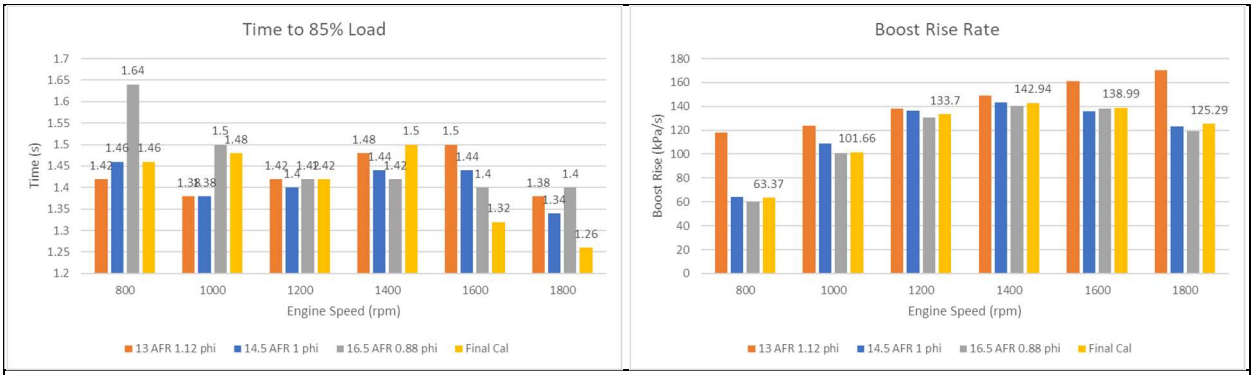

Figure 115: CLSA metrics of the time to 85% of the final load and the rate of boost rise

To give perspective to the performance achieved with the engine-only system, comparisons were made to a similar dataset with a state-of-the-art turbo with variable geometry turbine (VGT). The supercharging assistance of a driven turbo, like the SuperTurbo, is dominant at low engine speeds and Figure 116 illustrates the impact of being able to apply power directly to the turbine to build IMAP. Under these conditions the engine is fuel limited by a minimum AFR and can only make more load/power if more airflow/IMAP is generated. The difference in time to 85% load and boost/IMAP rise rate across the engine

speed range is plotted in Figure 117 – a drastic reduction in time to 85% load can be seen and the H2D2 system has near constant response times. This comparison conclusively validates the ability of the H2D2 engine-only system to achieve rapid load response toward the ability to work in a 30% downsized engine system application. The other hybrid elements (HSFW, MGU) supplement the immediate load/power request or "snap torque" and examples of this are shown later in Figure 123.

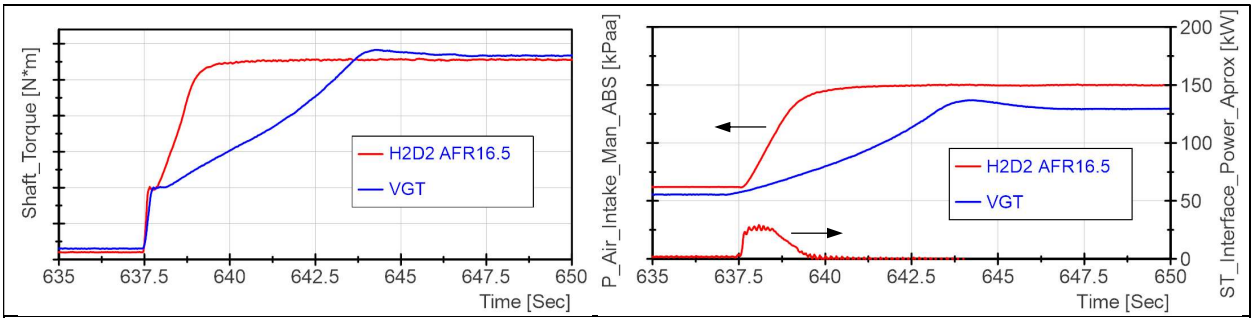

Figure 116: 1000rpm CSLA comparison between the final H2D2 calibration and a VGT dataset

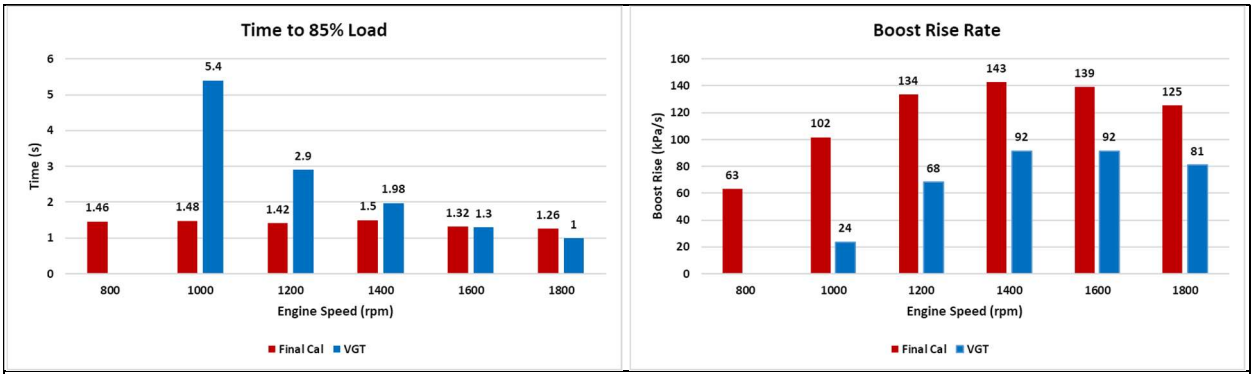

Figure 117: Comparison of CSLA metrics between the final H2D2 calibration and a VGT dataset

The final aftertreatment restriction, from measurements on an aftertreatment system very similar to the final design for the H2D2 project, was found to be lower than that used in the earlier simulation phases of the H2D2 project. The new AT restriction curve (grey) in Figure 118 was measured to be ~15% lower at the design exhaust flow point (peak exhaust flow for applications) than the originally predicted restriction curve (black – same as blue Concept 1 curve in Figure 83). Therefore, the total reduction from the baseline production 13L class engine was 35%, and this achieved the program goal. To round out the impact of this aftertreatment restriction, steady-state engine simulations were conducted to assess the impact of the final change in aftertreatment restriction on system performance/calibration to see if there was a need to re-calibrate or re-evaluate the turbine sizing. Based on the steady state simulations at high and mid loads, using the same calibration, the turbine mass flow had little change and the turbo compounding power increased because of decreased aftertreatment pressure drop. The turbocompounding power improvement was very small and within the margin to resize the turbine or re-do calibration.

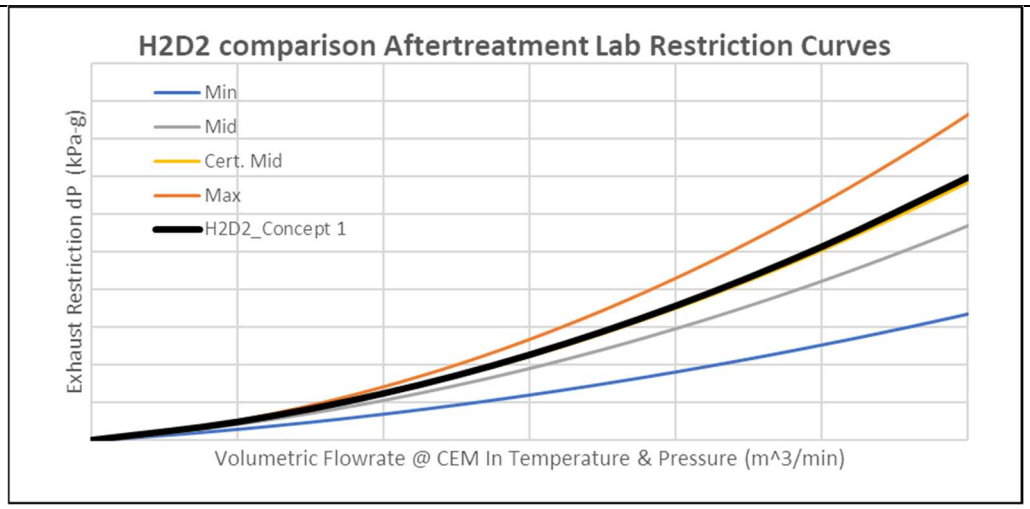

Figure 118: Comparison of final Aftertreatment restriction (grey) with predicted curve (black)

A subset of the engine-only validation testing area is the topic of friction reduction. Multiple sets of testing evaluations were able to be completed to quantify the concept engine friction, or at least the directional FMEP movement, Figure 119. Reductions were able to be measured from the base concept engine (base did not include all the friction reduction designs) with the base engine oil. This FMEP excludes the friction of running the SuperTurbo and represents the core engine, and the reduction maximum range was found to be between 13-15% for the data in Figure 119.

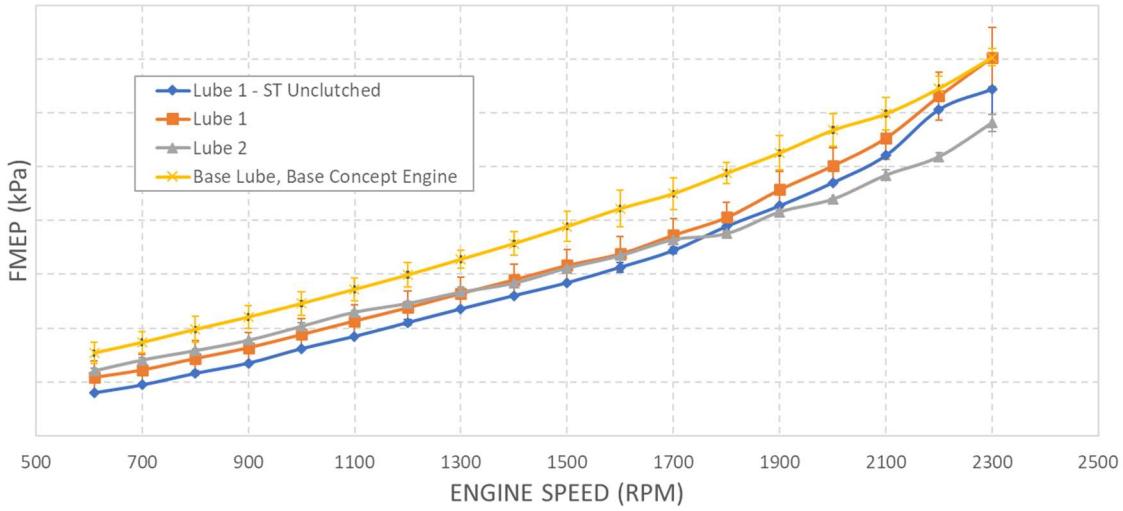

Figure 119: Motored friction tests of FMEP vs. engine speed for the concept engine

In order to satisfy the program requirement of meeting U.S. EPA Tier 4 Final off-road emissions the engine-only system was run through emissions certification-level testing for the 745AT rating. The 745AT rating was selected as it was the lowest power lug curve, with likely the most challenging periods of low exhaust temperature for NOx conversion in the aftertreatment system. The aftertreatment system from Figure 82 was de-greened prior to running the NRTC emissions certification cycles and example emissions traces with cycle integrated results are laid out in Figure 120. A cold NRTC and three hot NRTC cycles were run, and the composite results can be seen to meet the Tier 4 Final standards with acceptable development margin for this type of program. PM emission measurements for the cold cycle were incomplete, which is why no composite PM is listed. This test validation indicates that a full production

effort would be able to successfully meet Tier 4 Final emissions levels and achieve the Caterpillar requirements surrounding the off-road emissions tier. For the remainder of the testing the aftertreatment system was included, but the full certification-level of emissions testing and preparations were omitted to expedite performance and efficiency evaluations.

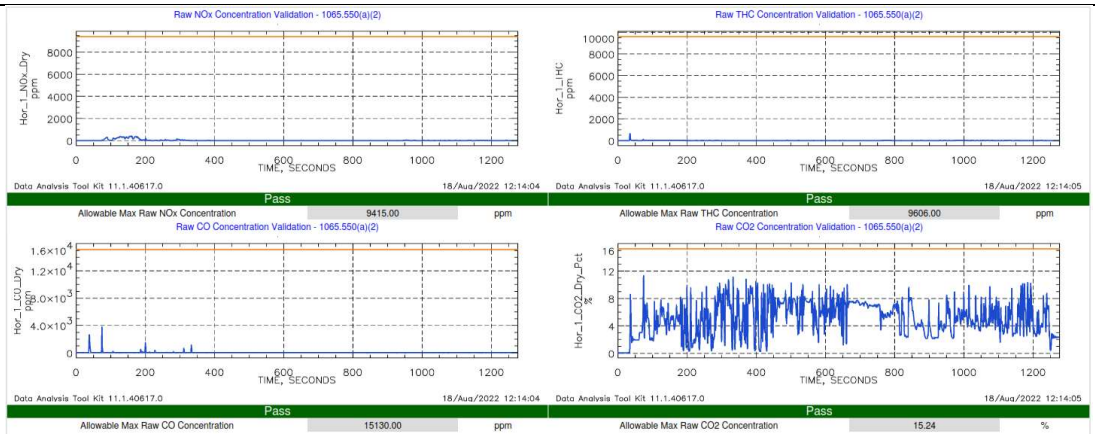

H2D2 NRTC Cold/Hot/Hot/Hot						
g/kWh	745 NRTC Cold	745 NRTC Hot 1	745 NRTC Hot 2	745 NRTC Hot 3	745 NRTC Composite	Standard
BSCO	0.229	0.1698	0.1602	0.1631	0.17083	3.5
BSHC	0.024	0.0074	0.0061	0.0062	0.00831	0.19
BSNOx	0.5108	0.3195	0.3234	0.3515	0.3494	0.4
BSPM	No Data	0.0091	0.0005	0.0008	NA	0.02

Figure 120: Hot NRTC 745AT emissions and a summary of the certification-level validation testing indicating T4F emissions capability of the concept engine and aftertreatment system - TI3262791

Table 8 lists the NRTC engine-only cycle efficiency, work, average power, and time for the three machine applications. The efficiency is normalized to a percent difference benefit from the C18 simulation, and the application average efficiency benefit was found to be 14.6%. The minimum application average benefit was 11.8% for the 988 large wheel loader and the maximum application average benefit was 16.1% for one the 390 hydraulic excavator. Generally, very good consistency in the efficiency was measured within a few tenths of a percent difference, except for the first 745AT NRTC HOT 1 cycle.

The six key machine cycle validation results listed in Table 9 were down selected from the full 19 machine cycles originally simulated to give a representative sample for validation testing. The application average was found to be 11.6% with a minimum of 8.5% for 745AT cycle 06 and a maximum of 13.8% for 390 cycle 10. The lower benefit of 11.6% for the machine cycles relative 14.6% for the NRTC is attributed to the different operating region and increased idle operation of the machine cycles. A combined application average between the NRTC and machine cycles was therefore found to be 13.1% fuel efficiency improvement. Two runs were also completed with a broad fuel injection SOI advance to get some sensitivity information.

Table 8: Engine-Only + Aftertreatment NRTC Testing Summary of Fuel Consumption Benefit – Normalizing Reference is the Validated C18 Simulation.				
H2D2 Engine-Only Test - Cycle	**Cycle BSFC Benefit - C18 SIM %Diff**	**Total Positive Cycle Work**	**Average Positive Cycle Power**	**Elapsed Time**
	[%]	[kWh]	[kW]	[s]
20 - NRTC (745AT) COLD	14.5%	47.8	138.9	1238
20 - NRTC (745AT) HOT 1	16.8%	48.5	140.9	1238
20 - NRTC (745AT) HOT 2	15.6%	47.8	139.0	1238
20 - NRTC (745AT) HOT 3	15.6%	47.9	139.2	1238
20 - NRTC (745AT) AVG	15.6%	48.0	139.5	1238
20 - NRTC (745AT) AVG HOT	16.0%	48.0	139.7	1238
21 - NRTC (390F) HOT 1	16.3%	50.5	147.0	1238
21 - NRTC (390F) HOT 2	16.1%	50.6	147.1	1238
21 - NRTC (390F) HOT 3	15.9%	50.6	147.1	1238
21 - NRTC (390F) AVG	16.1%	50.6	147.1	1238
22 - NRTC (988K\XE) HOT 1	11.9%	54.0	157.0	1238
22 - NRTC (988K\XE) HOT 2	11.7%	54.1	157.2	1238
22 - NRTC (988K\XE) HOT 3	11.8%	54.0	157.1	1238
22 - NRTC (988K\XE) AVG	11.8%	54.0	157.1	1238
Minimum	11.7%	47.8	138.9	1238
Maximum	16.8%	54.1	157.2	1238
Application Average	**14.6%**	50.9	147.9	1238

Table 9: Engine-Only + Aftertreatment Machine Application Cycle Testing Summary of Fuel Consumption Benefit – Normalizing Reference is the Validated C18 Simulation.				
H2D2 Engine-Only Test - Cycle	**Cycle BSFC Benefit - C18 SIM %Diff**	**Total Positive Cycle Work**	**Average Positive Cycle Power**	**Elapsed Time**
	[%]	[kWh]	[kW]	[s]
01 - 745	10.8%	14.1	162.8	311
01 - 745 Adv SOI Cal.	11.2%	14.0	162.5	311
05 - 745	11.8%	71.2	196.3	1305
06 - 745	8.5%	18.2	148.3	442
10 - 390X	13.8%	7.8	308.2	91
11 - 988K	10.2%	110.9	266.5	1498
19 - 988XE	9.9%	54.2	112.3	1737
19 - 988XE Adv SOI Cal.	10.7%	54.2	112.2	1737
Minimum	8.5%	7.8	112.2	91
Maximum	13.8%	110.9	308.2	1737
Application Average	**11.6%**	36.8	213.1	780

3.4.3. Full Hybrid System Validation

The full range of hybrid L5 control strategies were not able to be fully evaluated in test due to time, people, and cost constraints. The validation testing efforts occupied the full Q16 allowable time window through September 2022. Only a hybrid assisting strategy (best load response but with an expected efficiency loss) was able to be tested and conditions where engine braking occurred were not evaluated in test. This untested hybrid energy recovery impact on the system efficiency was quantified and captured with the highly correlated H2D2 System Level Model. Despite this testing shortcoming the team believes

that a large quantity of valuable validation testing was successfully completed, and the program validation milestone was successfully achieved.

Pictures of the final full H2D2 hybrid system test installation are presented in Figure 121 and document the complexity and capability of Caterpillar's powersystem facilities, resources, and personnel. Functional system operation and data acquisition was achieved, and a high degree of coordination had to be implemented between the hardware, facility devices, and emissions measurement systems.

Figure 121: Final H2D2 Full Hybrid System validation test installation which included the 13L concept engine, SuperTurbo, emissions aftertreatment catalysts, 48V MGU and battery emulator, HSFW electric drive, hybrid oil and coolant supply units, and numerous testing support systems.

Table 10 documents some of the H2D2 full hybrid system cycle results and gives an idea of the variation in the evaluated cycles in terms of power and energy. The BSFC percent difference to the engine-only cycle test results in Table 8 (NRTC – 14.6% vs. 13.9%) and Table 9 (11.6% vs. 9.2%) indicate that the full hybrid system running only in the assisting mode is not more efficient. As discussed previously, this is expected as, if no braking energy is recovered, the additional hybrid drive losses and HSFW charging will act solely as an increase in parasitic loss. The main benefit of an assist-only strategy would be relative to machine productivity as opposed to powersystem efficiency.

Table 10: Full Hybrid System (Without Braking Energy Recovery) Testing Summary of Fuel Consumption Benefit – Normalising Reference is the Validated C18 Simulation.				
H2D2 Full System Test - Cycle	**Cycle BSFC Benefit - C18 SIM %Diff**	**Total Positive Cycle Work**	**Average Positive Cycle Power**	**Elapsed Time**
	[%]	[kWh]	[kW]	[s]
01 - 745	6.5%*	13.6	175.3	310
05 - 745	11.0%	70.4	194.8	1305
06 - 745	8.9%	17.6	137.6	442
10 - 390X	9.5%*	7.8	305.7	91
11 - 988K	9.4%	105.8	268.2	1498
19 - 988XE	9.5%	55.0	113.2	1737
Minimum	6.5%	7.8	113.2	91
Maximum	11.0%	105.8	305.7	1737
Application Average	**9.2%**	40.7	221.9	798
20 - NRTC (745AT)	14.5%	48.1	146.2	1238
21 - NRTC (390F)	16.0%	50.3	152.9	1238
22 - NRTC (988K\XE)	11.4%	54.1	155.2	1238
Minimum	11.4%	48.1	146.2	1238
Maximum	16.0%	54.1	155.2	1238
NRTC Application Average	**13.9%**	50.9	151.4	1238

*** This data was lower than expected and attributed fuel flow measurement data quality**

The representative behavior of the full hybrid system when running over the transient cycles in the assisting mode are plotted in Figure 122 and Figure 123. Starting with Figure 122, a few of the key performance variables such as the various speeds and powers can be seen, and their general behavior can be understood over the entire NRTC for the 745 articulated truck. The cycle is fairly transient with many accelerations and changes in load/power. The hybrid device (SuperTurbo, HSFW, 48V MGU) power can be seen to be active throughout the cycle with times of higher frequency associated with times of more frequent transient power. In the assisting only mode, the hybrid device power is mostly positive on the graph, which indicates power flowing in the assisting direction. The HSFW (blue) line plot dips negative regularly and indicates time when the HSFW is recharging (speeding up) by using engine power. The HSFW speed behavior is seen in the third from the top plot, and it generally is a saw tooth behavior centered at ~18 krpm. This 18 krpm was set from the control strategy to enable high HSFW power availability for more powerful assists. Finally, the 48V battery state of charge (SOC) can be seen to only decrease throughout the cycle in the bottom plot due to the assist only mode and no attempt to recover engine braking energy (of which there is none in the NRTC). It should be noted that the SOC data in Figure 122 is using an emulated 2 kWh battery, while other full DYNASTY simulations used a 6 kWh battery. Also, the SuperTurbo torque transducer was failing or experiencing electrical interference during the hybrid runs and is the reason for times of nonphysical readings of high positive assisting power where there was turbocompounding negative power during the engine-only runs (e.g., time 625 to 750 seconds).

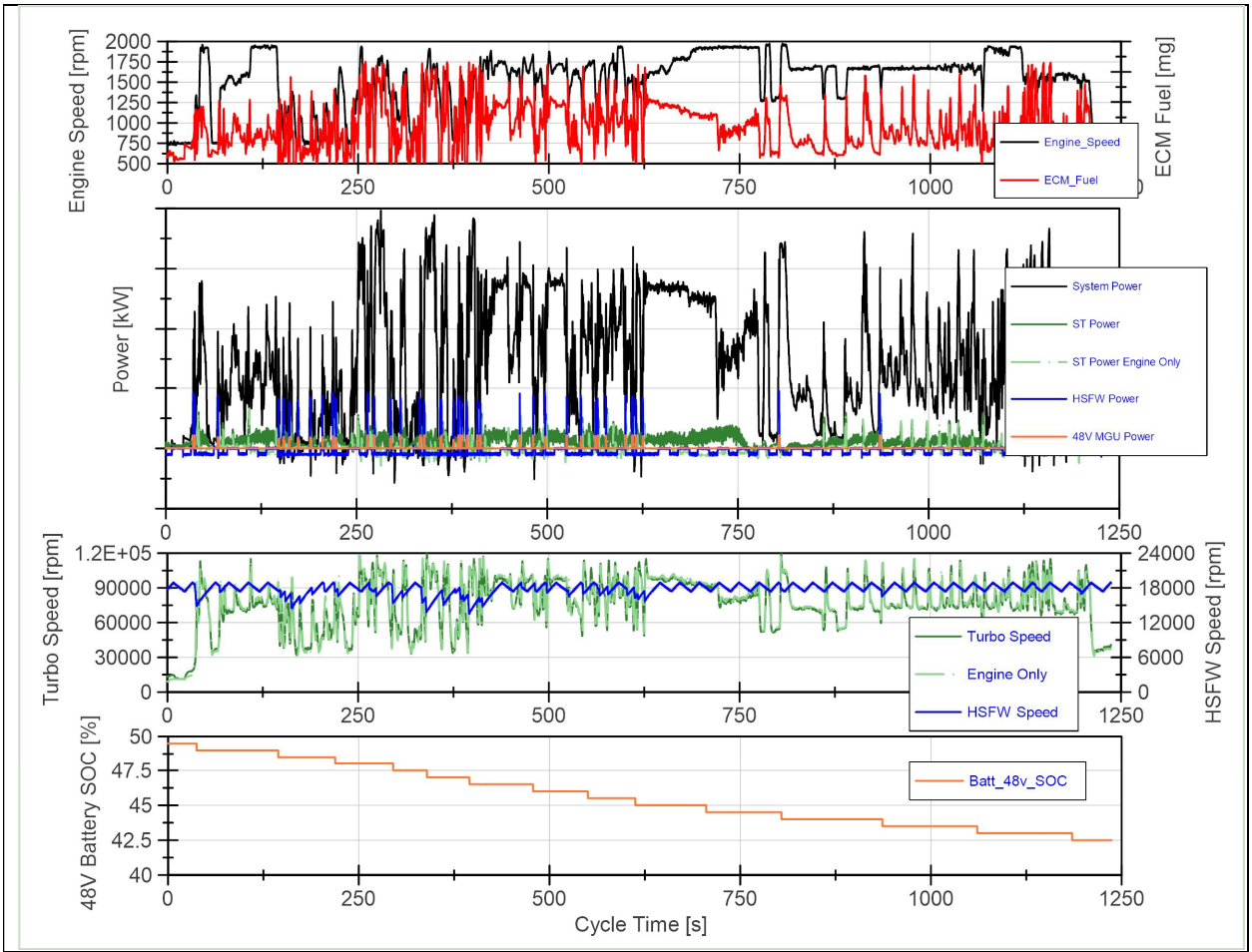

Figure 122: Transient plot of Hybrid Power from 745AT NRTC. Engine-Only data overlayed as dash-dot for comparison. Notes: Hybrid Assisting-Only strategy with 2 kWh battery for 48V MGU.

Turning to the zoomed in view in Figure 123, more detail on a few specific assisting events is illustrated. Here, the comparison to the engine-only NRTC cycle data can be compared by referencing the dash-dot lines, and the largest differences can be seen in the system total power. At time 339 seconds, a large load/power step is required and the full hybrid system triggers assisting by the HSFW, 48V MGU, and SuperTurbo. The system power is quickly brought up and greatly exceeds the "snap torque" behavior of the engine-only system. This is a good clear example of the desired behavior of the full hybrid system to enable a 30% engine downsizing. Changes in fueling, HSFW speed, and turbo speed can be seen in the corresponding line plots. The hill starting at ~332 seconds shows two distinct assisting events where the HSFW and 48V MGU are brought in and out in quick succession. This indicates an overshoot of the desired power and an undesired retrigger of the assisting. More refinement in the control strategy was found to be needed to avoid this type of behavior, and in Caterpillar's assessment this can be refined with more engineering time and adoption of hysteresis and proximity strategies within the current L5 controls architecture. Nevertheless, the full hybrid system was built and engineered to a robust enough level to run full transients, interrogate performance, update models with test validation data, and put forth a demonstration assessment of the concept.

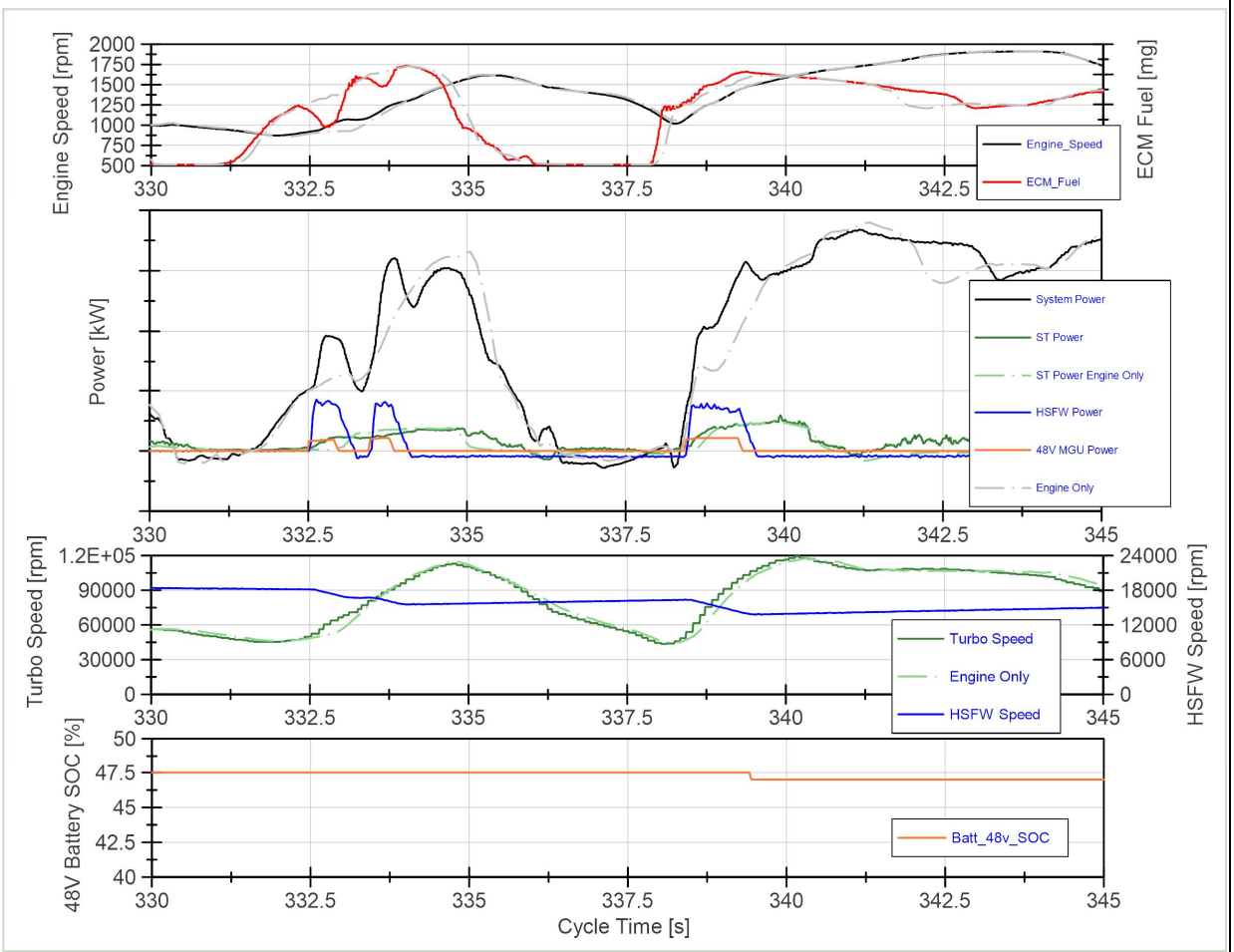

Figure 123: Zoomed in Transient PLOT of Hybrid Power from 745AT NRTC. Engine-Only data overlayed as dash-dot for comparison.

For the final assessment of the full hybrid system's capability and efficiency, when running with energy recovery and transient assisting, the validated DYNASTY system model was run for the six key machine cycles and three application NRTCs. This final efficiency accounting can be found the Hybrid Concept Definition section in Figure 25, and includes corrections for SOC over the cycle. The machine cycle application average benefit was found to increase by 0.6% to 12.2% (from 11.6% for the engine-only Table 9 results), while the NRTC application average benefic was found to increase by 0.7% to 15.3% (from the 14.6% for the engine-only Table 8 results). These final measurements and assessments of efficiency benefits for the full hybrid system and engine-only system were used as primary input to the technoeconomic analysis.

3.4.4. Validation Testing Delays and Hardware Failures

Throughout the engine and hybrid validation numerous engine-only testing difficulties and failures occurred. The following documents the testing problems encountered:

- Coolant system failure stemming from intermittent thermostat ceasing - Figure 124:
  - The root cause was not identified quickly and caused three separate testing delays before being fixed. The root cause was a bad prototype thermostat housing design, and the solution was to fully block open the thermostats.

- Failed PTO gear which drives the SuperTurbo belt and driveshaft assembly - Figure 124:
    - This occurred in January 2022 and completely shut down the testing with a removal of the engine from the test cell. The PTO failed at the bolted spline shaft adapter due to excessive friction and heat. The root cause was determined to be inadequate clearance between the PTO gear hub the flywheel housing. The housing was removed, machined, and a copper thrust washer was added with additional clearance. The PTO gear ran successfully to the completion of the test.
- Failed valvetrain rocker rollers and subsequently failed camshaft lobes - Figure 124:
    - This occurred concurrently with the failed PTO gear and therefore no additional time was lost. The root cause was identified as an issue with the rocker roller pin manufacturing and spare valvetrain parts were installed until permanently corrected parts could be received. New rocker rollers and camshafts were eventually installed to correct this.
- EGR control and estimation inaccuracies within the core engine software:
    - The accurate estimation of EGR flow on this concept engine was found to be more difficult than expected, and refinement work was required. Models and algorithms from the phase 1 concept engine did not translate to final phase 2 engine with the anticipated accuracy. The root cause of the difficulty stemmed from air system changes brought about by the SuperTurbo on phase 2 but not on phase 1.
- SuperTurbo Unit #1 clutch and driveshaft bearing failure:
    - This failure occurred during steady-state baseline measurement activities and the root cause was determined to be excess thrust loads in the SuperTurbo drive system. The backup SuperTurbo Unit #2 was shipped with increased bearing sizes and installed.
- A total of **64 calendar days** of delay can be attributed to these prototype engine hardware and software failures and problems

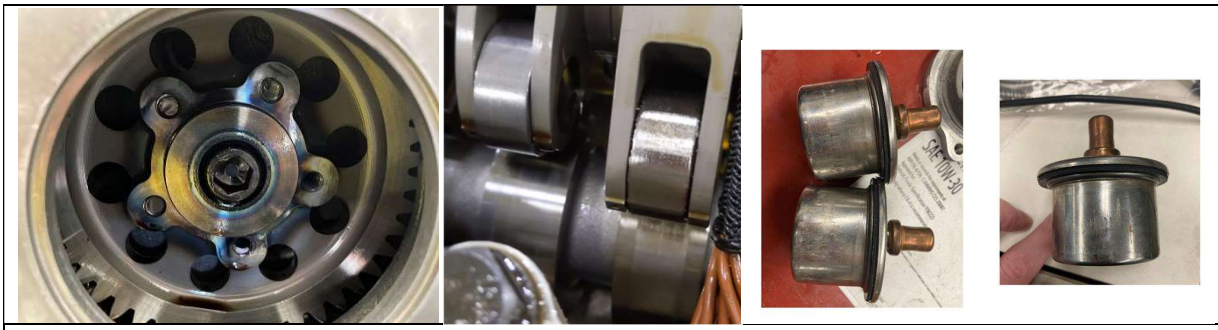

Figure 124: Failed PTO 5-bolt spline shaft (Left), valvetrain roller/cam failure (middle), thermostat scoring/ceasing (right)

The above hardware failures can be attributed to an incredibly high amount of new content with this concept engine system and the resulting timeline delays triggered a three month no-cost time extension to the program. Unfortunately, the difficulties continued into the no-cost time extension phase with the final hardware failures noted below.

- Piston/Ring/Liner (PRL) failure due to misaligned oil cooling jets
    - This was a major failure which required the engine to be removed completely from the test cell and the main core engine rebuilt. New pistons, rings, liners, valves, valve seats, and cooling jets were required. The root cause of the misaligned cooling jets was corrected.

- Aftertreatment DEF lines melted during high temperature aging due to installation location and insulation wrapping.
- The variable displacement oil pump failed and had to be replaced.
- The SuperTurbo Unit #2 had high rolling torque and was taken out of service with the root cause being a deteriorated driveshaft coupler. The rebuilt Unit #1 was shipped to Caterpillar and installed on the engine.
    - The root cause of the Unit #2 coupler failure was determined to be inadequate cooling, and design changes for a higher durometer coupler and increased air venting were made. These changes did not make it immediately into the rebuilt Unit #1, however.
- Unit #1 failed the driveshaft coupler only after 1 week of testing, due to a separate root cause of an overtightened radial screw compromising the hub threads. All corrective actions were completed on the Unit #2, shipped to Caterpillar, installed, and the Unit #2 ran successfully for the duration of the project.
    - It should be noted that the SuperTurbo hardware under test on H2D2 is now considered "legacy" hardware. Many of the hardware issues experienced during H2D2 testing have been designed out in the latest SuperTurbo generation; specifically, the torsional coupler has been removed from the newest designs, with no adverse consequences observed in SuperTurbo assessments to date.
- A total of another **53 calendar days** of delay can be attributed to these prototype engine hardware failures and problems within the no-cost time extension period

Figure 125: Failed Piston/Ring/Liner (Left), melted DEF lines and connector (Left-Middle), failed oil pump gear shaft (Right-middle), failed SuperTurbo internal driveshaft coupler (Right)

Despite the prototype hardware failures, Caterpillar and the project subrecipients were able to commit engineering, testing, personnel, and incremental financial resources to overcome these many hardware and early concept prototype challenges to complete the minimum validation testing required for the program, as documented in the earlier report sections.

4. Technoeconomic Analysis and Documentation

SOPO ID #	Item Title	Item Description	Start Date	End Date	Status
Task 3.14	**Technoeconomic Analysis and Documentation**	Hybrid system comparisons to the current diesel baseline, documentation of results, and Total Cost of Ownership analysis	4/01/2022	6/30/2022	100% Complete

Upon the completion of Task 3.13, the documentation and technoeconomic analysis was able to be performed utilizing the validation data and the subsequently validated simulations. The compilation of engine and powersystem cost, service, fuel consumption, and other relevant information was conducted for input into the analysis. Of course, this information is well known for the base diesel engine system, and this served as the normalizing reference.

The final Total Cost of Ownership (TCO) methodology contained the following input assumptions:

- 1500 hours/year machine application operation (745 AT, 988 K/XE, 390 F)
- Fuel and DEF consumption averages from the final test validated simulations for:
    - The NRTC for the three machine applications
    - And the six machine cycles validated in the testing
- Start/Stop fuel consumption reduction of 2% (middle of the 0.6-3.5% range in Table 1)
- 3.7% fuel reduction for Hybrid + Reduced Cooling (middle of the simulation prediction ranges in Table 1)
- 3% Inflation
- Low and High Fuel Prices
    - $4.50/gallon Diesel fuel, $7.00/gallon DEF
    - $6.00/gallon Diesel fuel, $9.00/gallon DEF
- Preventative Maintenance (PM) and overhaul costs
    - Lubrication, service events, service labor, major rebuilding parts, etc.
- Minimum and maximum CAPEX (Capital Expense)
    - Lower end of powertrain costs and profit margin
    - Upper end of powersystem costs and profit margin
- Residual powersystem value
- *No adjustment for the value of increased machine productivity due to a more responsive hybrid powersystem – this can be significant but is out of scope for the present project and analysis work given the powersystem' s goals of matching the 30% larger baseline diesel engine*

The four data series in Figure 126 successively add the fuel consumption benefits and cost differences when starting with the C18, then the H2D2 13L concept engine-only, then adding start/stop to the H2D2 13L concept engine, then adding the remaining hybrid elements to get the full H2D2 hybrid powersystem. Differences in first cost, or CAPEX, and fuel consumption drive the TCO payback period with respect to the baseline C18. Only the H2D2 Full Hybrid system indicates it will not pay back quickly (where quickly is considered less than 1.5 years). Fuel cost dominates these applications TCO given the size and duty cycle, so the large H2D2 efficiency improvements can clearly pay for themselves.

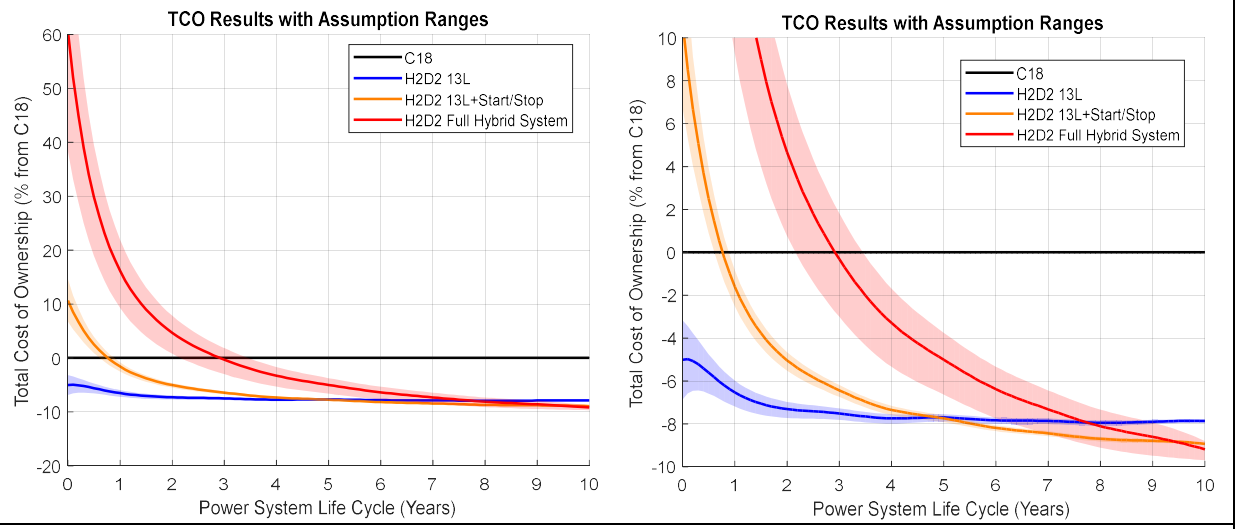

Figure 126: TCO results showing reductions (relative the C18 baseline) for the H2D2 13L, with start/stop, and with full hybrid system (HSFW and 48V MGU and start/stop)

The following are the key payback period and TCO percent difference key results with the data relative the C18 baseline summarized in Table 11:

- The H2D2 13L core engine has an immediate payback and would easily be adopted
- Adding start/stop quickly pays for itself in less than one year
  - On average it takes 4.9 years to payback relative the H2D2 13L engine-only system
- The full H2D2 Hybrid system has marginally acceptable payback periods near three years
  - On average it takes 7.8 years to payback relative the H2D2 13L engine-only system
- The full H2D2 Hybrid system has the greatest TCO reduction at the end of ten years

Table 11: Technoeconomic Analysis Key Results – C18 Baseline Reference

powersystem	Min. Payback (yrs.)	Ave. Payback (yrs.)	Max. Payback (yrs.)	Average 2 year TCO	Average 5 year TCO	Average 10 year TCO
H2D2 13L	Immediate	Immediate	Immediate	-7.3%	-7.7%	-7.9%
H2D2 13L + Start/Stop	0.61	0.77	0.88	-5.0%	-7.7%	-8.9%
H2D2 Full Hybrid System + Start/Stop	2.16	2.92	3.45	+4.7%	-5.0%	-9.2%

As an interesting comparison, an estimation of a full Battery Electric Vehicle (BEV) powersystem was made for these off-road applications. The BEV powersystems had the same assumptions as listed above for the TCO analysis, but with the following unique assumptions:

- 80% efficiency from electrical source input to powersystem mechanical output to account for battery charging/discharging, motor and inverter losses, and thermal management
  - No significant powersystem energy recovery opportunities assumed (consistent with the three H2D2 machine applications)
- Today's off-road cost ranges of robust, durable battery packs in the relevant size range
  - And a 5x lower midpoint cost for comparison
- Battery pack replacement at 15,000 hours with a yearly 5% decrease in cost from the present
- Battery pack sizing for approximately 3.0 hours of continuous application cycle operation

- 1.0, 1.5, and 2.0 electricity-to-diesel energy cost ratios based on $/kWh
  - The ratio for 2022 was 1.7 from the EIA's 2022 Annual Outlook with a decreasing trend to 1.35 by 2050[9]
  - Example: $4.50/gallon diesel fuel is ~$0.12/kWh based on the lower heating value and typical densities → a 1.5 ratio would equate to a delivered electricity cost to the BEV of $0.18/kWh in this analysis
- Reduced and less frequent service and preventative maintenance (e.g., no oil changes)

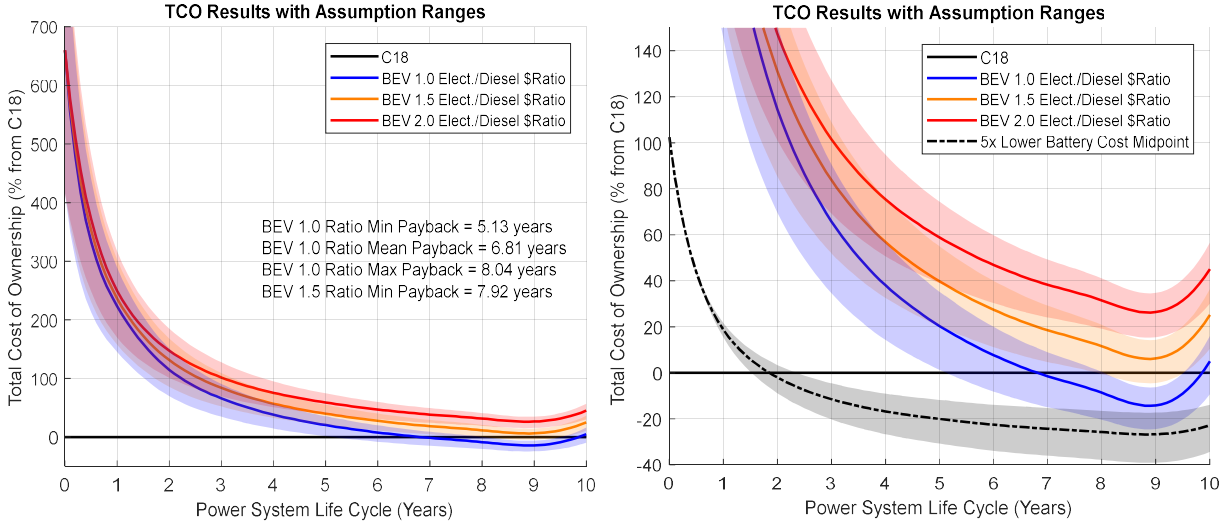

Figure 127: TCO results showing trends (relative the C18 baseline) for a 400kW BEV powersystem under different electricity-to-diesel energy cost ratios

The result of the TCO analysis in Figure **127** is quite interesting given the range of assumptions and large sensitivity to the electricity-to-diesel energy cost ratio. It is clear that if off-road battery pack costs, fuel, and electricity prices, stay relatively stable then a 400kW BEV does not make commercial and financial sense. A five times reduction of the midpoint of off-road battery pack current costs puts the payback at slightly less than two years, but still with a 100% increase in first cost. With current costs, only when the electricity-to-diesel energy cost ratio decreased toward unity do the payback periods approach a 5 year potential, and this is the minimum result stemming from the lower end of the CAPEX costs – which can be interpreted as a future with incrementally ever decreasing off-road battery pack costs. The 1.5 electricity-to-diesel energy cost ratio scenario may just slightly break even on TCO around 8.5 years, but then trends more expensive. All the BEV TCO results trend upward from 9 to 10 years due to the battery pack reaching the end of life and requirement replacement. This is a highly uncertain area, but it does illuminate a key TCO aspect for BEV powersystems.

The TCO of the BEV powersystem is frontloaded in the CAPEX expenditure of system, mainly the battery pack, and then pays for itself relative the diesel powersystems if the electricity costs are cheap enough relative the diesel fuel costs. Within the present hybrid powersystem program there is a clear immediate economic and greenhouse gas benefit to the investigated technologies, and it is recommended to appropriately adopt the H2D2 powersystem concepts prior to a full BEV system barring any drastic reduction in the electricity-to-diesel energy cost ratio.

It should also be acknowledged that a fuel cell based powersystem may be a better economic fit for these types of heavy duty applications, rather than a pure BEV solution. This is outside of the scope of

[9] EIA Annual Energy Outlook 2022, https://www.eia.gov/outlooks/aeo/

the immediate project and analysis, but clearly within the scope of powersystem manufacturers and the DOE. Additionally, if renewable energy costs can be reduced from today's $0.03-$0.05/kWh and achieve the DOE targets of $0.02/kWh, then this would aid in pushing the electric-to-diesel energy cost ratio in the beneficial direction for BEVs[10,11].

[10] https://www.eenews.net/articles/doe-heres-where-renewable-costs-are-heading/
[11] https://www.lazard.com/perspective/levelized-cost-of-energy-levelized-cost-of-storage-and-levelized-cost-of-hydrogen/

5. Conclusions and Summary

The following major conclusions were found throughout the analysis, design, and testing phases of the program:

- **Program Goal:** The developed hybrid powersystem was validated through test and simulation activities to have a range of efficiency improvement of 10.5-25.6% with a midpoint of 17.9% – which met the program goal of 17%±2 efficiency improvement.
    - Of the 17.9% powersystem efficiency improvement, the majority (13.1%) of the came from the core 13L concept engine, while the hybrid devices primarily supported fast transient load response required to downsize by 30% from the baseline 18L diesel engine. The limited efficiency improvement from the hybrid devices stemmed from the lack of energy regeneration or braking opportunity at the powersystem boundary (machine transmission or hydraulic system interface).
- **Program Goal:** Transient load response was validated through system simulation, engine-only testing, hybrid-only, and full system testing. On the order of ~1-1.5 second response times were measured uniformly from 800rpm to 1800rpm. The superior load response was achieved by the 13L concept engine through the ability of the SuperTurbo to rapidly build airflow/IMAP, and by the ability of the HSFW and MGU to supplement immediate block load deficiencies from 30% downsizing. The HSFW system was validated to achieve peak assisting of 110kW at 12,000 Nm/sec ramp rates.
- **Program Goal:** The powersystem was validated to be capable of meeting U.S. EPA Tier 4 Final off-road emissions through transient NRTC testing and was enabled by the developed low-restriction aftertreatment and engine combustion system. Tailpipe emissions measurements showed acceptable margins indicative of concept development on a de-greened aftertreatment engine system.
- A final hybrid concept was down-selected through rigorous system simulation and consisted of a driven turbocharger (SuperTurbo) mechanical connected to the engine rear geartrain, a high speed flywheel (HSFW) connected to the FEAD through an electric drive transmission, and a 48V motor generator unit (MGU) connected directly to the front-end accessory drive (FEAD). The mechanically connected SuperTurbo was selected over an electrical connection due to simplicity, easier control requirements, a higher technology development state, and no significant difference in application cycle efficiency. The electric drive transmission for the HSFW was selected over a mechanical CVT due to insufficient ratio rate response time, power capability, and the ability to have complete speed decoupling without range limitations.
- The durability of the concept 13L engine was validated through structural and Thermofluid simulations to be acceptable for continuous operation in the 30% downsized applications. Many aspects of the core engine were optimized toward this goal, driven by efficiency building blocks such as higher peak pressures, increased compression ratio, increased specific power, and reduced friction.
- The durability of the HSFW, MGU and their associated drive systems was validated through simulation and rig testing for 12,000 hours or beyond. Life limitations for the SuperTurbo CVT were identified with the present architecture, but with upgraded CVT materials acceptable life was predicted.
- The economic value of the investigated powersystem was assessed through a Total Cost of Ownership (TCO) analysis and found that the core engine would pay back immediately. Following

this the adoption of start/stop would pay back in less than one year and the full hybrid system in near three years. The economic benefit of a more responsive and therefore more productive powersystem than the baseline 18L engine was not included (as the program target was to match the 30% larger engine), but if assessed would decrease the payback periods further.

Section II – Program Financial Summary

The final spend against the DOE grant is shown Figure **128**.

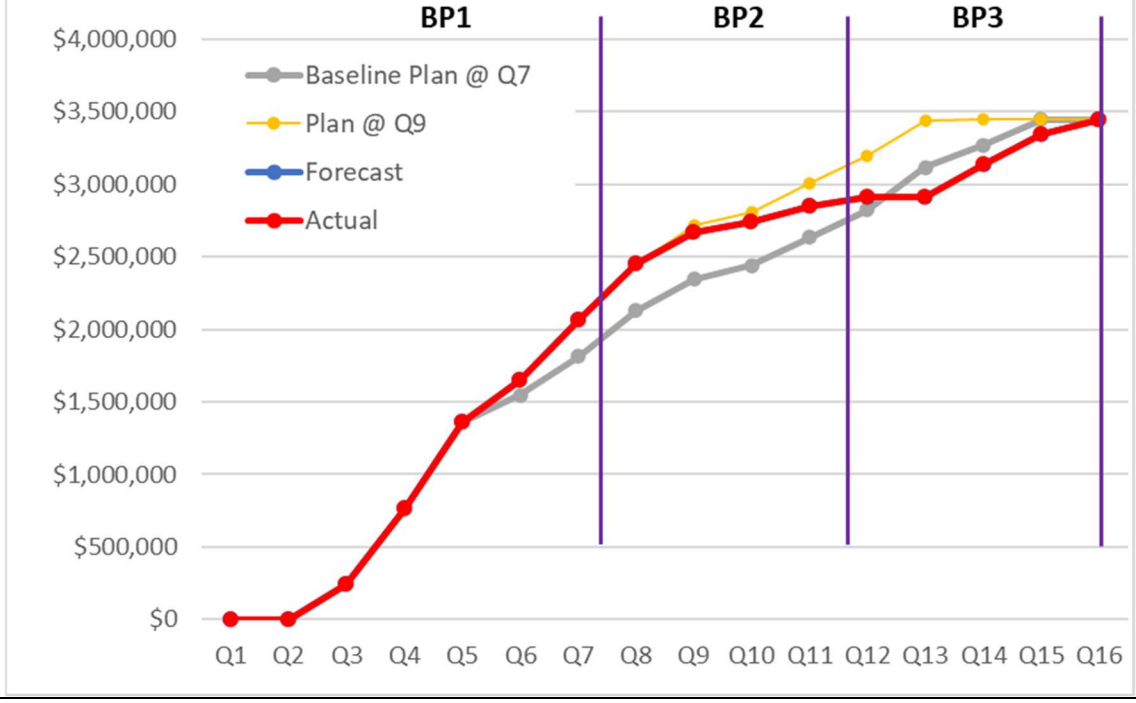

Figure 128: Actual (incurred) and forecasted spend against the DOE grant

In Q16, the government share of costs incurred was $3.441M (out of the total grant of $3.441M). This represents consumption of 100% of the total grant (up 2.7%-pts from Q15), and a 40.4% overall cost share by the DOE. The DOE's cost share declined from 46.4% to 40.4% by the end of the program, due primarily to the 3-month "no-cost" extension period (Jul 1 – Sep 30, 2022), during which the costs were borne by Caterpillar.

Section III – Patents and Publications

The following summarizes the patents and publications filed, thus far, under this program

1. Subject Invention:
   DOE S-Number or iEdison Invention Report Number/EIR Number: T-123430
   Corresponding Patent/Application Number(s): 11149679
   Inventor(s): Allen Chen, Aaron Heintz, Jason Van Farowe, Thomas Atwell, David Lueders
   Title: INTERNAL COMBUSTION ENGINE WITH TOP-DOWN COOLING

2. Subject Invention:
   DOE S-Number or iEdison Invention Report Number/EIR Number: T-123426
   Granted Patent Number: 11525385
   Inventor(s): Allen Chen, Aaron Heintz, Jason Van Farowe, Thomas Atwell, Scott Schuricht
   Title: DIVERTER FITTINGS FOR COOLING SYSTEMS OF AN ENGINE

3. Subject Invention:
   DOE S-Number or iEdison Invention Report Number/EIR Number: S-164530
   Corresponding Patent/Application Number(s): 11391223
   Inventor(s): Wade Robel, Spencer Huhn, Kevin Weiss, John McDonald, Jason Bloms
   Title: INCREASING BRAKING POWER AND EXHAUST GAS TEMPERATURE

4. Subject Invention:
   DOE S-Number or iEdison Invention Report Number/EIR Number: S-164844
   Corresponding Patent/Application Number(s): 11143137
   Inventor(s): Charlie Kim
   Title: ENGINE SYSTEM, COMBUSTION CONTROL SYSTEM, AND OPERATING METHOD WITH CLOSE-COUPLED EARLY PILOTS AND CYLINDER TEMPERATURE CONTROL

5. Subject Invention:
   DOE S-Number or iEdison Invention Report Number/EIR Number: T-121458
   Corresponding Patent/Application Number(s): 17/301651
   Inventor(s): Chad Koci, Jay Steffen, Fang Guo, Richard Kruiswyk, Gaurav Vasudeva, Robert McDavid, Timothy Bazyn
   Title: POWER SYSTEM FOR A MACHINE

6. Subject Invention:
   DOE S-Number or iEdison Invention Report Number/EIR Number: S-168822
   Corresponding Patent/Application Number(s): 17/127547
   Inventor(s): Fang Guo, Jay Steffen, Chad Koci, Richard Kruiswyk
   Title: HYBRID POWER SYSTEM CONTROL AND OPERATING STRATEGY BASED ON POWER SYSTEM STATE VECTOR CALCULATION

7. Subject Invention:
   DOE S-Number or iEdison Invention Report Number/EIR Number: S-164824
   Corresponding Patent/Application Number(s): 17/229446
   Inventor(s): Chad Koci, Yongli Qi, Jason Rasmussen, Daniel Sordelet
   Title: FUEL INJECTOR NOZZLE IN COMBINATION WITH THERMAL BARRIER COATING ON COMBUSTION CHAMBER SURFACE

8. Subject Invention:
   DOE S-Number or iEdison Invention Report Number/EIR Number: S-174874
   Corresponding Patent/Application Number(s): 17/848076

Inventor(s): Chad Koci, Kenth Svensson, Eric Wiebrecht, Venkatesan Veeriah, Suresh Chennagowni, Qingzhong Li
Title: SYSTEMS AND METHODS FOR THERMAL BARRIER COATINGS TO MODIFY ENGINE COMPONENT THERMAL CHARACTERISTICS

9. Subject Invention:
DOE S-Number or iEdison Invention Report Number/EIR Number: T-123432
Granted Patent Number: 11549459
Inventor(s): Allen Chen, Aaron Heintz, Jason Van Farowe, Thomas Atwell, David Lueders
Title: INTERNAL COMBUSTION ENGINE WITH DUAL-CHANNEL CYLINDER LINER COOLING

10. Koci, C., Steffen, J., Kruiswyk, R., Guo, F. et al., "A Hybrid Heavy-Duty Diesel powersystem for Off-Road Applications - Concept Definition," SAE Technical Paper 2021-01-0449, 2021, https://doi.org/10.4271/2021-01-0449.

11. Koci, C., Svensson, K., Martin, G., Kim, C., et al., “Optical Imaging for Understanding of Thermal Barrier Coated Piston Engine Performance,” presented at THIESEL 2022 Conference on Thermo- and Fluid Dynamics of Clean propulsion Powerplants 2022, Spain, September 13-16, 2022.